GDAŃSK UNIVERSITY OF TECHNOLOGY

INSTITUTE OF NAVAL ARCHITECTURE

Polish Maritime Research

No 4 (120) 2023
Vol. 30

ADDRESS OF PUBLISHER & EDITOR'S OFFICE:

GDAŃSK UNIVERSITY OF TECHNOLOGY

Institute
of Naval Architecture
G. Narutowicza 11/12
80-233 Gdańsk, POLAND

Price:
single issue: 25 PLN

Prices for abroad
single issue:
- in Europe EURO 15
- overseas USD 20

WEB:
pg.edu.pl/pmr

e-mail : pmr@pg.edu.pl

ISSN 1233-2585

CONTENS

ADDRESS OF PUBLISHER & EDITOR'S OFFICE:

GDAŃSK UNIVERSITY OF TECHNOLOGY

Institute of Naval Architecture
G. Narutowicza 11/12
80-233 Gdańsk, POLAND

Editorial

POLISH MARITIME RESEARCH is the scientific journal with a worldwide circulation. This journal is published quarterly (four times a year) by Gdansk University of Technology (GUT). On September, 1994, the first issue of POLISH MARITIME RESEARCH was published. The main objective of this journal is to present original research, innovative scientific ideas, and significant findings and application in the field of :

Naval Architecture, Ocean Engineering and Underwater Technology,

The scope of the journal covers selected issues related to all phases of product lifecycle and corresponding technologies for offshore floating and fixed structures and their components.

All researchers are invited to submit their original papers for peer review and publications related to methods of the design; production and manufacturing; maintenance and operational processes of such technical items as:

- all types of vessels and their equipment,
- fixed and floating offshore units and their components,
- autonomous underwater vehicle (AUV) and remotely operated vehicle (ROV).

We welcome submissions from these fields in the following technical topics:

- ship hydrodynamics: buoyancy and stability; ship resistance and propulsion, etc.,
- structural integrity of ship and offshore unit structures: materials; welding; fatigue and fracture, etc.,
- marine equipment: ship and offshore unit power plants: overboarding equipment; etc.

sciendo

POLISH MARITIME RESEARCH 1 (117) 2023 Vol. 30; pp. 4-16
10.2478/pomr-2023-0053

COMPUTER-AIDED SYSTEM FOR LAYOUT OF FIRE HYDRANTS ON BOARDS DESIGNED VESSEL USING THE PARTICLE SWARM OPTIMIZATION ALGORITHM

Piotr Gomułka
[1] Damen Engineering Gdansk, Gdansk
[2] Gdansk University of Technology, Gdansk, Poland

* Corresponding author: *piotr.gomulka@pg.edu.pl (Piotr Gomułka)*

ABSTRACT

The functional layout of fire safety equipment in technical spaces of ships is a time-consuming process. When designing a ship fire protection system, the designer must manually position each system component in such a way as to meet the requirements of regulations arising from the technical specification, various legal regulations of maritime conventions and classification societies of the vessel to be designed. Layout of fire hydrants assisted by a computer that is based on pre-defined criteria and various constraints could significantly support the designer in working easier and faster. This paper presents a prototype computer-aided design system that enables optimal placement of fire hydrants using the metaheuristic Particle Swarm Optimization (PSO) algorithm. This algorithm was used in Rhinoceros 3D software with its Grasshopper plugin for visualizing the arrangement of fire safety equipment. Various solution arrangements compared with the fire hydrant placement in real ships are illustrated by a case study. Demonstrating how design work can be facilitated and what potential benefits can be achieved are presented as well.

Keywords: ship, fire hydrant, design, layout, particle swarm optimization

INTRODUCTION

The placement of fire protection equipment in ship technical rooms is an extremely important and time-consuming part of the ship design. One of the important components of this equipment is the fire hydrant, and its rational or optimal placement on board ships should reduce the degree of fire hazard. The proper placement of fire hydrants requires designers to conduct a preliminary analysis of the fire hazards that may occur on the ship's board. This should be preceded by familiarization with the applicable regulations, such as the SOLAS Convention[1], the FFS Resolution[2] , classification society rules, and standards that specify requirements for the designed fire protection installation, as well as the technical specification of the vessel. Then, based on legal and technical requirements and hazard analysis, the designer begins to layout hydrants on a ship's board, including determining their minimum number and location to ensure maximum effectiveness of the fire protection system. This takes into account factors such as the type of hydrants, water flow and pressure, and ease of access to hydrants. In existing ship design practice, the designer manually positions each fire hydrant to meet the imposed requirements based on his experience and knowledge, use a database of similar design solutions, and also follow the guidelines of installed equipment manufacturers. As a rule,

[1] The International Convention for the Safety of Life at Sea (SOLAS)– an international maritime treaty that sets minimum safety standards for ships, including requirements for design, construction, equipment, and operation.

[2] The Fire Safety Systems (FSS) Code – an international standard that provides guidelines for the design, installation, and maintenance of fire safety systems on board ships.

the manufacturers specify, for example, the necessary service or operator space, the location of connecting cooperating installations, or impose the order of their installation. The last step is calculations or simulations regarding the hydraulics of the system performed to ensure that each hydrant will have adequate water flow and pressure and that the entire fire protection system will work effectively in the event of a fire occurrence.

This paper presents a prototype computer-aided design system that enables optimal placement of fire hydrants using the metaheuristic Particle Swarm Optimization (PSO) algorithm. The PSO algorithm is embedded in Rhinoceros 3D software with its Grasshopper plugin for visualizing the arrangement of fire protection equipment. The Grasshopper program is a visual scripting environment for Rhinoceros 3D software that is very popular in ship design offices. Users can both build and use a library of existing parametric algorithms to modify, analyze, or create 3D models from scratch. They are also able to automate design processes without the need for writing software code.

Various solution arrangements compared with the fire hydrant placement in real ships are illustrated by a case study. Demonstrating how design work can be facilitated and what potential benefits can be achieved are presented as well.

LITERATURE REVIEW

In the subject literature, there are many concepts and solutions for object placement in any enclosed space. For example, in [1], the authors presented three approaches to automating the object placement process: rule-based, genetic algorithms, and artificial neural networks. They also discuss ways to improve the quality of automatic object placement by taking into account the specificities of space and user preferences. The authors of the article referenced in [2] described a new approach to automatic object positioning in three-dimensional spaces. The method described there is based on the use of constraints that allow for precise control of the object placement process in space. They present a mathematical model that allows for the formal definition of constraints and their application in the object positioning process. In the publication [3], the authors provide an overview of problems related to object location that have applications in various fields, including transport network planning, store location, warehouse, and medical centers. On the other hand, the possibilities of using tools based on various variants of *p-median* and *p-center* algorithms to solve transport network planning problems, store and distribution center location are described in [4]. The paper [5] employs uncertainty theory to address the location problem of emergency service facilities under uncertainty. Using the inverse uncertainty distribution, the uncertain location set covering model was transformed into an equivalent deterministic location model. This paper first studies the uncertainty distribution of the covered demand that is associated with the covering constraint confidence level α. In addition, the authors model the maximal covering location problem in an uncertain environment using different modeling ideas, namely, the (α, β)-maximal covering location model and the α-chance maximal covering location model. It is also proven that the (α, β)-maximal covering location model can be transformed into an equivalent deterministic location model, and then, it can be solved. They also point out that there exists an equivalence relation between the (α, β)-maximal covering location model and the α-chance maximal covering location model, which leads to a method for solving the α-chance maximal covering location model. Finally, the ideas of uncertain models are illustrated by a case study.

There are also a number of studies presenting solutions for facilitating the placement of equipment or installations in ship technical rooms. For example, criteria for evaluating the placement of equipment in the ship engine room and analysis methods that allow for choosing the best option in terms of safety, energy efficiency, and costs are presented in [6]. On the other hand, methods and technologies that improve access to equipment in the engine machinery room in terms of maintenance cost planning and effective maintenance strategy implementation are presented in [7]. The study [8] concerns the integration of computer-aided and knowledge base systems in designing ship machinery equipment and installations. The authors describe how integrating these two systems allows for better optimization and increases the efficiency of the design process that ensures greater device reliability or facilitating their operation. In [9], the authors focus on issues related to the design of ship pipeline systems. For example, they discuss pipeline layout design criteria, taking into account aspects related to the difficult working conditions, such as vibration or corrosion.

Despite the numerous articles on this topic, simple engineering decision support systems enabling the generation of alternative layouts of equipment, including the placement of fire safety equipment on board ships, have not been presented. This is confirmed, among others, by authors of [10], stating that this issue is not well researched in terms of general solutions. They propose to solve that problem using the a modified iterative-deepening search method. It is the iterative-exploration method that uses a classical greedy algorithm by means of it is possible to show the possibility of preliminary placement of fire safety equipment.

Our approach is based on developing a prototype computer-aided design system that enables optimal placement of fire hydrants using the metaheuristic Particle Swarm Optimization (PSO) algorithm.

CONCEPT OF COMPUTER-AIDED DESIGN SYSTEM THAT ENABLES OPTIMAL PLACEMENT OF FIRE HYDRANTS

PSO algorithm as a means of supporting the placement of fire hydrants on ship decks

To solve the problem of optimal layout of fire hydrants on the shipboard, one type of meta-heuristic algorithm, i.e., the PSO algorithm, was used in the developed computer-aided system. It has been found to be particularly effective in optimizing problems related to closed spaces because it can efficiently explore and exploit the search space. Closed spaces, such as those found structural optimization problems, often have complex constraints and interactions between variables that can make classical optimization methods difficult to apply [11]. However, the PSO algorithm is able to navigate these complex search spaces by simultaneously exploring the search space and exploring promising regions of the search space.

Additionally, the PSO algorithm is capable of handling non-linear and non-convex optimization problems, which are often encountered in closed-space optimization problems. By using a swarm of particles, the PSO can avoid getting stuck in local optima and instead converge to a global optimum solution. However, the effectiveness of the algorithm depends on various factors such as the complexity of the problem, the size of the space, and the number of design variables involved. Therefore, it is important to carefully evaluate the suitability of the PSO algorithm for a specific application related to closed spaces before implementation.

However, it should be noted that PSO, as a member of the metaheuristic methods family, only provides a way to create an appropriate heuristic algorithm. In turn, such an algorithm enables the obtainment of a solution for which it is possible to prove how close it is to the optimal solution, i.e., it is a quasi-optimal solution. From the point of view of engineering practice and ship design offices, such a solution is fully acceptable.

As previously mentioned, the PSO algorithm is built into the Grasshopper application and is an integral component of it. The useful features of the Grasshopper application were used to create a tool that assists designers in properly placing fire hydrants. By defining sets of design rules and constraints that determine the placement of these hydrants, an algorithm was chosen that is suitable for the complexity of the computational problem.

Meta-heuristic algorithms, while not guaranteeing the discovery of global optimal solutions, can provide results close to optimal in a reasonable amount of time. This seems to be a favorable solution for placing fire hydrants on a shipboard. Meta-heuristics are often inspired by natural processes, such as swarm interactions (particle swarm optimization, ant colony optimization), generational evolution (genetic algorithms, genetic programming, evolutionary programming), as well as physical phenomena (e.g., simulated annealing). Among the existing optimization tools in the Grasshopper environment, frequently used ones include Galapagos [12], [13], Goat [14], Silvereye [15], Opossum [16], Dodo [17], and Nelder Mead [18]. However, choosing the best one is a very difficult and ambiguous task. In the subject literature, both simulation studies have shown the superiority of individual algorithms [14], [15] and works that suggested that no single algorithm was dominant for the considered optimization problems [14]. Therefore, a clear assessment of the usefulness of the tool depends on the optimization problem and comparative methods that measure the efficiency of algorithms (e.g., convergence time, stability, resistance to getting stuck in local optima).

In this study, the goal is not to compare individual algorithms in terms of their speed or effectiveness but to demonstrate that the use of simple optimization tools in the placement of fire protection system components can bring noticeable benefits to the designer (reducing design time), shipyards (lowering installation costs), and ultimately ship-owners, who will be responsible for maintaining the selected installation components. Based on the criteria of ease of implementation with the system responsible for placing the fire protection system components, as well as the simplicity of its operation and use, the PSO algorithm was used, which works by using the "Silvereye" plugin.

At its core, the PSO involves a population of candidate solutions, called particles, moving around in a search space and adjusting their position based on their own best-known position and the best-known position of their neighbors. Mathematically, the position of each particle in the search space is represented by a vector x, and its velocity is represented by a vector v. The objective function that needs to be optimized is denoted as $f(x)$. The PSO algorithm iteratively updates the position and velocity of particles until a termination criterion is met, such as a maximum number of iterations or a target objective function value. The mathematical model of the PSO algorithm has been found in many studies, e.g., in [19], [20], and [21].

To develop a prototype computer-aided design system that enables optimal placement of fire hydrants on ship-boards, we should formulate an optimization problem. To formulate it using the PSO algorithm in Grasshopper, we can follow these two steps:

– define the problem by defining the constraints, the objective functions, and the design variables that can be adjusted to optimize the objective functions,
– use a PSO algorithm implementation in Grasshopper using the "Silvereye" plugin.

Constraints

To ensure optimal placement of hydrants on board a designed ship, a designer support system should take into account the following constraints:

– space constraints; the available space on the ship deck is limited by the size and shape of the ship,
– legal regulations; they dictate the minimum number and placement of hydrants on ship decks,
– significance of compartments; areas on the ship where fire is most likely or the risk is negligible.

Space constraints

The developed system that enables optimal placement of hydrants has to take into account the physical limitation of the vessel's hull and the shape of the defined spaces. The shape of the hull can take on various forms, depending on the level of detail and complexity of the model. In Rhino Core software for design and modelling, it can be represented by:

– curves of various types, such as NURBS (Non-Uniform Rational B-Splines), Bezier, interpolating, spline,
– surface models, such as NURBS, which are one of the basic types of surfaces supported by Rhino Core, allowing for precise definition of the shape of the hull using control points and curves,
– mesh surface models,
– hybrid modeling,
– models imported from external CAD file formats, including IGES (Initial Graphics Exchange Specification), STEP (Standard for the Exchange of Product model data), SAT (Standard ACIS Text), and others; the hull can be designed in another program and imported into Rhino Core, where further work on the project can be carried out.

In the developed system, each of the ship rooms was created using closed curves (polylines), representing the outline of a particular space. The outlines assembled together form a flat projection on each of the analyzed vessel's decks, as shown in Figure 1. Such outlines can also be based, for example, on the general plan of the vessel made in a CAD program.

where:
p_i is the i-th control point,
W_i is the weight coefficient of the i-th control point, determining the influence of each of the control points on the curve,
B_i^n is the i-th degree Bernstein polynomial expressed by the formula:

$$B_i^n(t) = \begin{cases} \binom{n}{i} t^i (1-t)^{n-i} & for\ \ i = 0, \dots, n \\ 0 & for\ \ i < 0, i > n \end{cases} \tag{2}$$

Legal regulations

According to the SOLAS convention, the number and placement of hydrants should be such that at least two water streams, not originating from the same hydrant, one of which should be supplied by a single length of hose, can reach any part of the ship accessible to passengers or crew during ship navigation. Fire hoses should be long enough to cover any compartment by a water stream where their use may be required. Fire hoses should be at least 10 meters long, but no more than: 15 meters in engine rooms, 20 meters in other compartments and on open decks, and 25 meters on open decks of ships with a maximum width exceeding 30 meters.

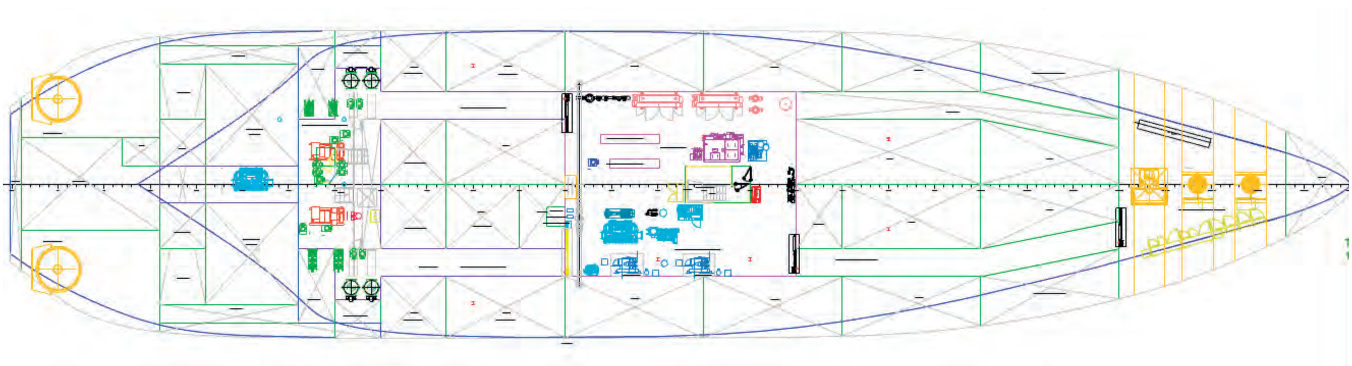

Fig. 1. Example top view projection of ship rooms created using closed curves

In the developed system, the range of the fire hose creates a circle with a radius equal to the length of the hose defined in the SOLAS convention. It should be noted that this is a certain simplification, as the actual range of the fire hose may be slightly smaller in the case of complicated compartment configuration and the need for its bends. In the developed system, the hose length can be easily defined and adjusted to any additional constraints or requirements, e.g., imposed by state authority regulations, which is illustrated in Figure 2.

Fire hydrants should be located within the ship's geometrical representation, and any obstacles on the vessel (e.g., pillars, reinforcements) must be taken into account and should not create any collisions. In rooms, hydrants are usually located near walls, typically near communication routes or evacuation exits. In our approach, it was assumed that fire hydrants would be located on a closed curve, forming the outline of the selected room. Any point markers on the curve can represent the graphic representation of a hydrant. B-spline curves are used to interpolate a curve defined by knot points. They are a chain of Bezier curves. Any point on a polynomial curve in real coordinates is determined by the following equation:

$$p(t) = \frac{\sum_{i=0}^{n} w_i \cdot p_i \cdot B_i^n(t)}{\sum_{i=0}^{n} w_i \cdot B_i^n(t)} \quad for\ t \in (0,1) \tag{1}$$

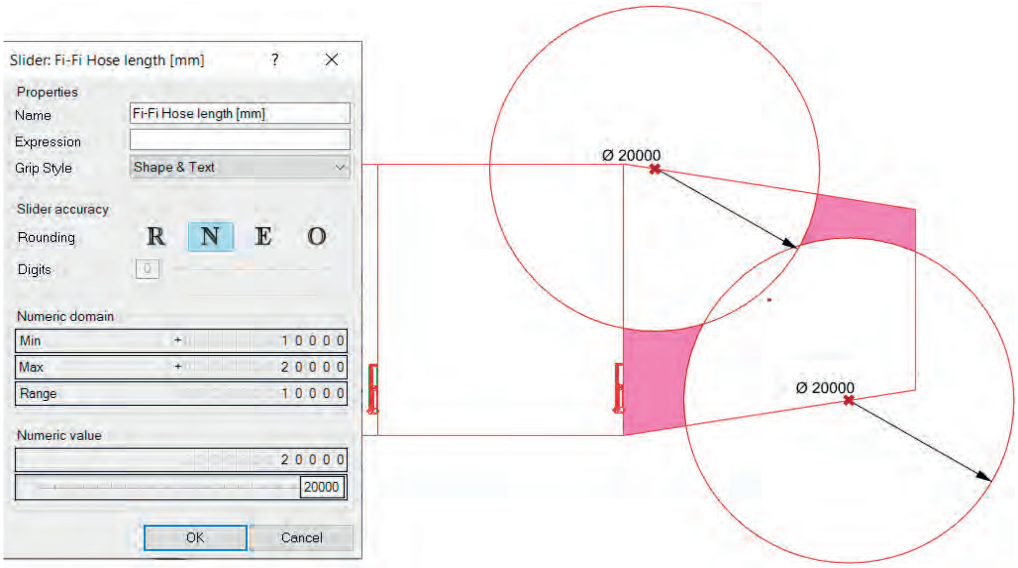

Fig. 2. Possible parameterization options for the length of a fire hose according to the SOLAS convention

Significance of compartments

The SOLAS Convention has distinguished different classes of bulkheads based on their ability to withstand fire and smoke on the endangered side. These bulkheads are classified as A, B, and C classes and create thermal and structural boundaries on the vessel. Spaces are separated by the appropriate class of bulkhead (either bulkheads or decks) depending on the level of fire risk. Details specifying the fire sealing standards to be applied to specific bulkheads between neighboring compartments can be found in SOLAS II-2 Part C. The following types of spaces are most relevant in terms of fire hydrant distribution:

– machinery space category A, which is classically considered the area with the highest fire risk and requires the highest safety standards – fire hoses with a length of not less than 10 [m] and not more than 15 [m] must be used,
– machinery spaces, which include both the previously mentioned machinery space category A and other spaces containing propulsion machinery, boilers, fuel units, steam and internal combustion engines, generators, and main electrical equipment, etc. – fire hoses with a length of not less than 10 [m] and not more than 15 [m] must be used,
– areas on the ship where the probability of fire is slight are usually considered places where the risk of fire is small and negligible, usually with limited human such as voids, cofferdams, tanks, chain lockers, fixed gas fire-extinguishing system storage rooms, and others – in this given case, there is no need to install a fire hydrant,
– other spaces and open decks – fire hoses with a length of not less than 10 [m] and not more than 20 [m] must be used.

In the developed system, each type of space is assigned to a specific drawing layer (Fig. 3). The number of layers and their assigned properties can be changed as desired. For example, machinery spaces of category A can be assigned to layer 1, while other machinery spaces can be assigned to layer 2. Spaces with low fire risk, such as voids or cofferdams, can be assigned to layer 3. Other spaces and open decks, where fire hoses are required, can be assigned to layer 4. By using different layers, the design team can easily distinguish between different types of rooms and apply different design criteria or safety measures accordingly.

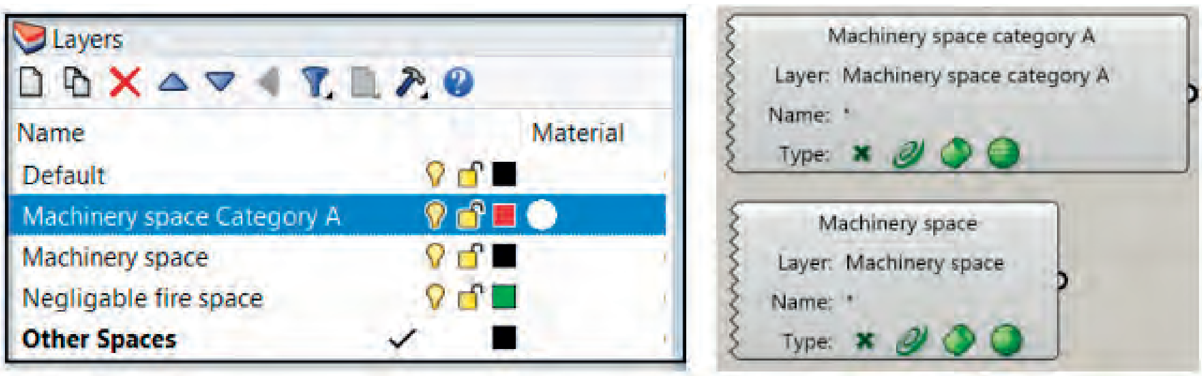

Fig. 3. Possible parameterization options for the length of a fire hose according to the SOLAS convention

Objective functions

In the case of optimizing the placement of fire hydrants, the objective function determines how well our system works from the perspective of the optimization criterion(s) chosen by the designers. They can prioritize each of these criteria, and then, the objective function will determine how well we meet these requirements. In the case of a few criteria selected, the objective function can be defined as a weighted sum of each criterion, where the weights are set by the designer.

In ship design practice, a number of alternative criteria for the rational placement of fire hydrants on shipboards can be found. Here are the most commonly encountered:

– maximization of the coverage of extinguished surfaces,
– minimization of power consumption to increase fire safety system efficiency,
– minimization of risk by optimal placement of hydrants in areas most vulnerable to fire,
– maximization of accessibility to hydrants,
– minimization of response time by optimal placement of hydrants that allow for fast and effective intervention,
– minimization of the number of hydrants to minimize costs and maintain system simplicity,
– minimization of response time, which assumes minimizing the time needed to reach the most fire-prone areas on the ship,
– minimization of the distance between hydrants to minimize costs.

It is obvious that the choice of criterion/criteria depends on many factors. The most important of these include the type of ship (cargo, passenger, etc.) and the size associated with it, as well as the preferences of the ship's owner or future ship operator.

In the developed system, the objective functions can be defined by four criteria, which are most preferred by the ship contractor, namely:

– the criterion of maximum coverage of the extinguished surface (or alternatively: minimizing the areas without reach of fire hoses),
– the criterion of minimal overlap of water streams,
– the criterion of minimum power demand for fire pump engines,
– the criterion of minimum distance from evacuation exits.

In all the cases of the objective function considered next, the design variables are the coordinates of the location of the hydrants *x* and *y*, which are distributed in the two-dimensional space determined by space conistraints, considering their position close to a closed curve forming the outline of the selected room. These coordinates are the centers of circles, whose radii are the lengths of fire hoses determined by the restrictions presented in the legal regulations and significance of compartments, respectively.

In addition, the designer arbitrarily determines the number of hydrants placed on each deck or room of the ship. At the current stage of system development, the determination of the number of hydrants is done iteratively, i.e., the designer takes any number of hydrants and then runs simulations looking for the best match. If a solution is found – the number and distribution of hydrants are stored. Then, another simulation is carried out reducing the number of hydrants in the next step (manually) until the *n-th* simulation finds a satisfactory solution.

In the case of the first criterion, which is the maximization of the coverage area of fire extinguishing, the area of such a zone depends on: the number of hydrants, the location of hydrants, the length of fire hoses connected to hydrants, and the configuration (shape) of the extinguished room. The measure of effectiveness in this case is to have a distribution of hydrants that ensures the most efficient fire protection. This can be expressed by the degree of coverage of the extinguished area, also defined as the area within the range of the fire hose. The larger the uncovered area, where there is no range of action of the fire hoses, the lower the effectiveness of the fire protection system.

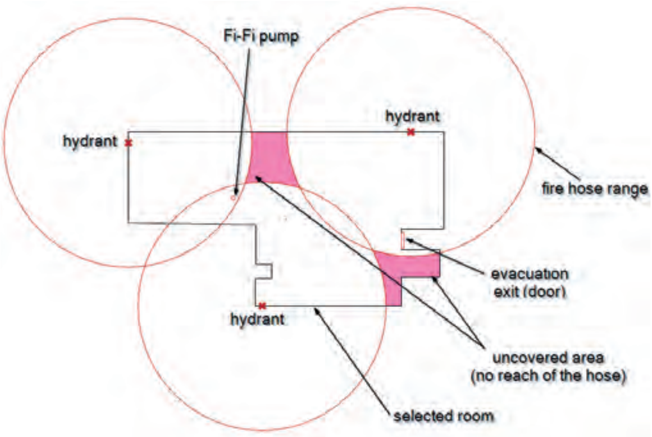

Fig. 4. Layout of hydrants with a demonstration of hose coverage in a selected room, taking into account the location of the fire pump, doors, and the area not covered by the installation

One possible way to present the distribution of hydrants and the coverage area of hoses in a selected room is to use a floor plan or a map of the room (Fig. 4). The hydrants can be marked with symbols or icons, and the coverage area of hoses can be presented as circles around each hydrant, showing the maximum distance the hoses can reach from each hydrant. The pump room and other important features such as doors and windows can also be marked on the floor plan. To illustrate the effectiveness of the fire protection system, the areas that are not covered by the hoses can be highlighted, indicating the potential areas where the fire could spread if the system is not sufficient. This can help to identify any potential weaknesses in the fire protection system and inform the decision-making process in optimizing the placement of hydrants and fire hoses for maximum coverage.

The developed system utilizes an algorithm that employs the region union and region difference functions to compare specified surfaces, calculate their difference, and determine their total area. The region union function is used to combine geometric regions represented as sets of points in two-dimensional space that can take different shapes, e.g., polygons. This function performs the operation of sum of sets, which can be mathematically described as:

$R_1 \cup R_2 \cup \ldots \cup R_n = \{x : x \in R_1 \text{ or } x \in R_2 \ldots \text{ or } x \in R_n\}$. This means that the sum of the sets $R_1 \cup R \cup \ldots \cup R_n$ contains those elements x that belong to the set R_1 ($x \in R_1$) or belong to the set R_2 ($x \in R2$) ... or belong to the set R_n ($x \in R_n$). The set of points of the resultant area A is equal to the sum of the individual sets $R_1, R_2, \ldots, R_n$ and $A = R_1 \cup R_2 \cup \ldots \cup R_n$ (n is the number of areas). Any point that belongs to at least one of these areas will also belong to the resultant area A. When the region union function runs, the program checks which areas intersect and then combines them to form a unified area. If the regions have common boundaries, these boundaries will be included in the resulting union region. The region difference function is used to calculate the difference between two geometric areas. It creates the resulting region, which is the result of subtracting one region from the other. The mathematical description of the function is as follows: $A = R_1 - R_2$. This means that the difference of the sets R_1 and R_2 consists of those elements x that belong to the set R_1 ($x \in R_1$) but do not belong to the set R_2 ($x \notin R2$). Mathematically, this means that the resulting area A is equal to the difference between the set of points R_1 and the set of points R_2. A point belonging to R_1 and not belonging to R_2 will also belong to the resulting area A. The goal of the algorithm is to find the smallest total area A_a of the zones not covered by the range of the hoses. Then, the objective function takes the following form:

$$f_1(x) = \sum_{a=1}^{n} A_a(x) \tag{3}$$

where:
$A_a(x)$ is the area of the region not covered by the reach of the fire hose.

Additionally, for better visualization, the custom preview function was used, which allows the user to quickly determine the areas not covered by the range of the fire protection system.

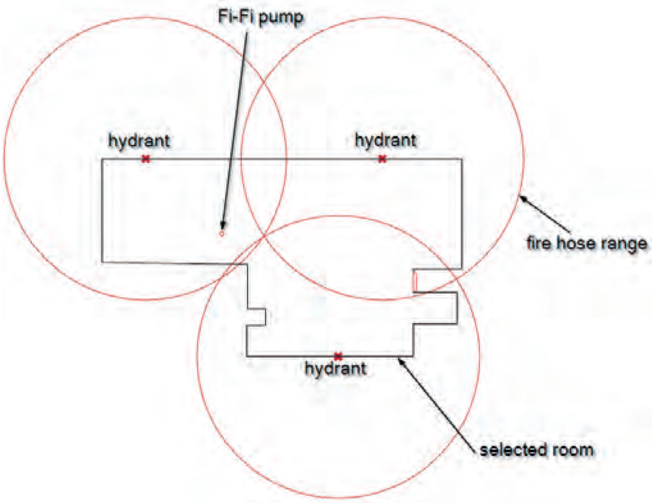

Fig. 5. Simulation results for criterion – maximization of the coverage area of extinguished surfaces

Figure 5 shows the results of a simulation in which the positions of three hydrants were changed. The algorithm placed the hydrants in such a way that the areas not covered by the hydrant range were as small as possible. In the case of the second criterion, which is the minimization of overlap of water streams, the algorithm works on the same principle as the one adopted in the first criterion. The difference, however, is that the areas protected by the fire hoses are compared, taking into account their common parts, i.e., overlapping areas B_a. In this criterion, the aim is to minimize the degree of mutual coverage of the hose ranges of their operation.

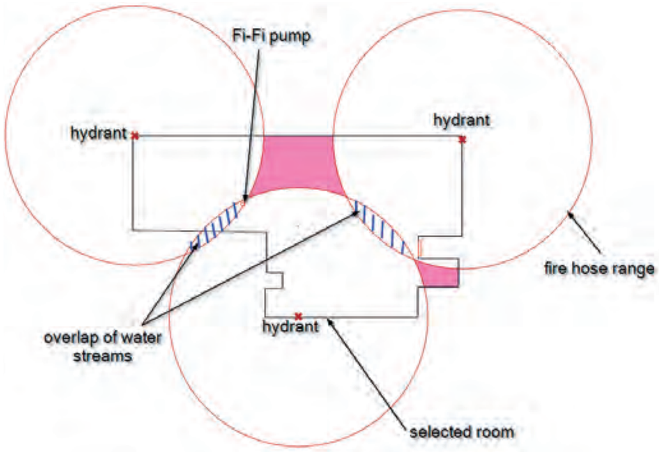

Fig. 6. Simulation results for criterion – minimization of overlap of water streams

In this case, the objective function takes the following form:

$$f_2(x) = \sum_{a=1}^{n} B_a(x) \tag{4}$$

where:
$B_a(x)$ is the area of the region of overlap of water streams.

Simulations were carried out by changing the positions of three hydrants. The algorithm placed the hydrants in such a way that the overlapping areas of the streams were as small as possible (Fig. 6).

The third criterion, which is the minimization of the power demand of the fire pump, depends on many factors, such as the length of the fire protection installation, the number of hydrants required for simultaneous supply, and the pressure of the fire extinguishing agent required in the fire protection installation. A longer pipeline contributes to greater pressure loss in the fire protection installation. This means that to achieve the required flow at the end point of the installation, the fire pump must generate higher pressure compared to a shorter pipeline. The pressure drop in the pipeline is proportional to the length of the pipeline and the flow velocity. The simplified mathematical equation of Darcy-Weisbach defines, among other things, the relationship between the length of the pipeline in a hydraulic system and the pressure drop in the system as follows [22]:

$$\Delta p = \lambda \frac{L}{D} \frac{\rho u^2}{2} \tag{5}$$

where:
Δp is the pressure drop [Pa],
λ is the resistance coefficient dependent, among others, on Reynolds number and relative roughness of the pipe [-],
L is the length of the pipeline [m],
D is the diameter of the pipeline [m],
ρ is the density of the fluid [kg/m^3],
u is the velocity of the fluid [m/s].

It should be noted that the power of the pump is directly proportional to the flow rate and pressure drop and inversely proportional to hydraulic efficiency. This means that there is a linear relationship between the length of the installation and the demand for the driving power of the fire pump. The power of the fire pump can be expressed by the following equation:

$$P = \frac{Q \cdot \Delta p}{(\eta \cdot \rho)} \tag{6}$$

where:
P is the power of the pump [W],
Q is the pump flow rate [m^3/s],
η is the hydraulic efficiency of the pump [-].

The solution to the proposed optimization criterion will, therefore, be to find the minimum of the objective function, which is the distance between each fire hydrant and the fire pump, with a previously defined location on the ship:

$$f_3(x) = \sum_{a=1}^{n} D_{a,p}(x) \tag{7}$$

and:
$\mathrm{D_{a,p}} = \sqrt{|\mathrm{x_a} - \mathrm{x_p}|^2 + |\mathrm{y_a} - \mathrm{y_p}|^2}$ for a planar system (XY),
$\mathrm{D_{a,p}} = \sqrt{|\mathrm{x_a} - \mathrm{x_p}|^2 + |\mathrm{y_a} - \mathrm{y_p}|^2 + |\mathrm{z_a} - \mathrm{z_p}|^2}$ for a spatial system (XYZ),

where:
$\mathrm{x_a}$, $\mathrm{x_p}$, $\mathrm{y_a}$, $\mathrm{y_p}$, $\mathrm{z_a}$, $\mathrm{z_p}$ are the geometric coordinates of hydrant "a" and pump "p",
$\mathrm{D_{a,p}}$ is the shortest distance between hydrant "*a*" and pump "*p*", *n* is the number of hydrants.

a) b)

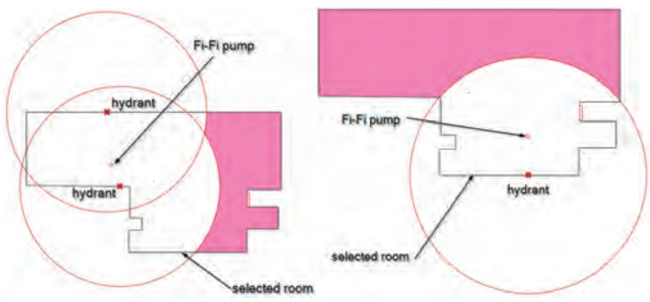

Fig. 7. Simulation results for criterion – minimization of the power demand of the fire pump: a) with two hydrants, b) with one hydrant

Figure 7 shows the results of a simulation that illustrates the power requirements for a given area depending on the number of hydrants installed.

In the case of the fourth criterion, i.e., the minimum distance from evacuation exits, the algorithm works in a similar way as described in criterion 3, with the difference that it takes into account the distance not from the fire pump, but from the evacuation exit. The objective function then takes the following form:

$$f_4(x) = \sum_{a=1}^{n} D_{a,we}(x) \tag{8}$$

and:
$\mathrm{D_{a,we}} = \sqrt{|\mathrm{x_a} - \mathrm{x_{we}}|^2 + |\mathrm{y_a} - \mathrm{y_{we}}|^2}$ – for a planar system (XY),
$\mathrm{D_{a,we}} = \sqrt{|\mathrm{x_a} - \mathrm{x_{we}}|^2 + |\mathrm{y_a} - \mathrm{y_{we}}|^2 + |\mathrm{z_a} - \mathrm{z_{we}}|^2}$ – for a spatial system (XYZ),

where:
x_a, x_{we}, y_a, y_{we}, z_a, z_{we}, are the geometric coordinates of hydrant "*a*" and evacuation exit "*we*",
$D_{a,we}$ is the shortest distance between hydrant "*a*" and evacuation exit "*we*".

a) b)

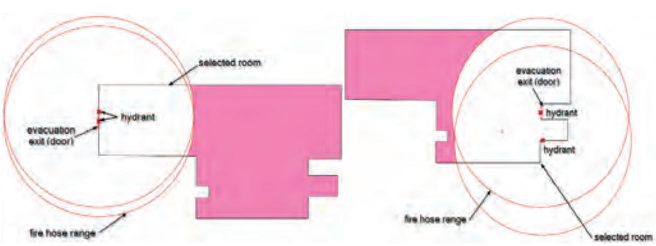

Fig. 8 Simulation results for criterion – minimum distance from evacuation exits: a) the evacuation exit is on the left side of the room, b) the evacuation exit is on the right side of the room

Two simulations were conducted, changing the location of the evacuation exits (Fig. 8). In Figure 8a, the evacuation exit is on the left side of the room, while in Figure 8b, it is on the right. The simulation parameters as well as the number of hydrants in both cases are the same. The algorithm placed the hydrants in the vicinity of the evacuation exits, which confirms the fulfilled assumption of placing the hydrants as close to them as possible.

It is obvious that the designer would like to take into account several of the mentioned optimization criteria simultaneously. In this case, these criteria should be merged into one representative objective function. There are many known methods for reducing classical multi-criteria optimization to single-criteria ones, such as the hierarchical optimization method, the method of constrained criteria, and the global criterion method.

In our approach, a relatively simple and often used weighted criteria method was applied. This method combines two criteria into a single objective function using a weighted sum. The substitute objective function would be a linear combination of the two criteria, where each criterion is multiplied by a weight factor that reflects its relative importance. The weights can be determined by the designer based on recognized priorities, for example, the type of a ship or ship-owner preference. In our approach, the total value of the substitute objective function, which represents the established criteria, should be minimized:

$$F_{sub}(x) = min \sum_{i=1}^{k} w_i \cdot f_i(x) \tag{9}$$

where:
k is the number of objective functions,
$f_i(x)$ is the value of the i-th objective function,
w_i are the weights of the objective function such that $w \in [0,1]$ and $\sum_{i=1}^{k} w_i = 1$.

As a rule, the substitute objective function can be subject to different criteria and may require normalization under certain circumstances. Normalization is the process of scaling or transforming data to bring it into a specific range or format. This is particularly important when dealing with multiple objectives or when the objective function has different units or magnitudes. This can be done using various techniques, but in this study, min-max normalization was applied. A detailed description of such a method utilized by the authors can be found in [23].

Weights are assigned to each of the objective functions, reflecting their relative importance to the overall evaluation of the solution. Various methods can be used to determine these weights, such as the analytical hierarchical process (AHP) method. Once the weights for each criterion have been determined, the weighted sum of the criteria for each solution was calculated, allowing the results to be compared on the basis of a single indicator and ultimately selecting the solution with the highest value.

The result of one such two-criteria simulation: maximizing the coverage of extinguished surfaces and minimizing the distance to evacuation exits is presented on Figure 9.

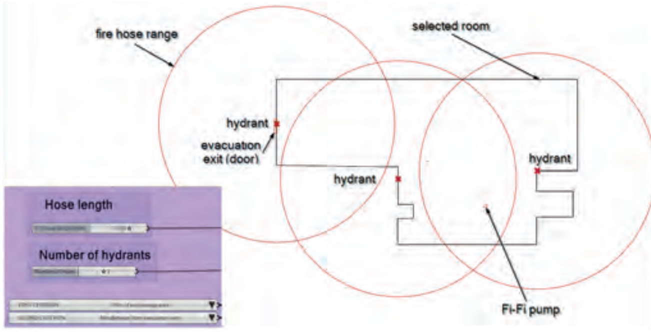

Fig. 9. Simulation results for two criteria – maximizing the coverage of extinguished surfaces and minimizing the distance to evacuation exits

It was assumed that the most relevant of the four criteria considered was the one that affects the degree of coverage of the room. The simulation showed that the extinguished surfaces were fully covered and the distance from the emergency exit also appeared to be optimal.

RESULTS AND DISCUSSION

As previously mentioned, the main goal of the developed system, i.e., the computer-aided system for the layout of fire hydrants on board designed vessels, is to reduce the designer's working time. It is difficult to estimate the working time of a designer who places hydrants on a ship's board using the classical method. On the one hand, the designer's working time depends on their knowledge, skills, and experience, for example expressing itself through routines, such as storing subject-specific regulations in his memory. On the other hand, this time depends on the type of ship and the constraints that exist in it, such as the scope of regulations that depend on the type of ship. In addition, designers may also be involved in other design work.

From the experience of one of the co-authors of this study as a lead engineer in a ship design office, the time required to complete the arrangement drawing is about 30 to 40 hours of design work. Assuming that nearly half of the time is taken up by the analysis of the placement of hydrants, and the rest is the pure drawing part, it is safe to say that potentially up to a dozen hours of work can be saved.

To evaluate the effectiveness of the developed system three different types of ships were considered. On board considered ships, hydrants were placed using the classical manual method and their layout was compared to the layout proposed by the developed system. These were ships of different types, namely:
– Fishery Researche Vessel (Fig. 10),
– Wind Platform Vessel (Fig. 11),
– Multi Role Auxiliay Vessel (Fig. 12).

It was assumed that the classical method of hydrant placement meets all the requirements (constraints) that were set before the designer. Figures 10, 11, and 12 show top view projections of selected rooms on the mentioned ships. In this case, specific details of the designed vessels were deliberately not provided to protect the intellectual property of ship-owners and the design office. Arrangements of individual technical rooms were modified, but the location and distribution of fire protection equipment remained unchanged. The placement of fire hydrants obtained using the classical method is marked using markers in the form of red circles, whereas the placement obtained using the developed system was overlaid on each projection using markers in the form of blue crosses.

In this case study, the values of individual weights of the objective function were determined based on one of the authors' experiences working in a ship design office, taking into account the type of vessel being designed. The example values of weights for individual partial objective functions have been presented in the captions of Figures 10, 11, and 12.

In particular, when formulating the substitute objective function, the following criteria were taken into account: maximizing the coverage of extinguished surfaces and minimizing the distance to evacuation exits for all considered vessels, i.e., the Fishery Research Vessel (Fig. 10), the Wind Platform Vessel (Fig. 11), and the Multi Role Auxiliary Vessel (Fig. 12).

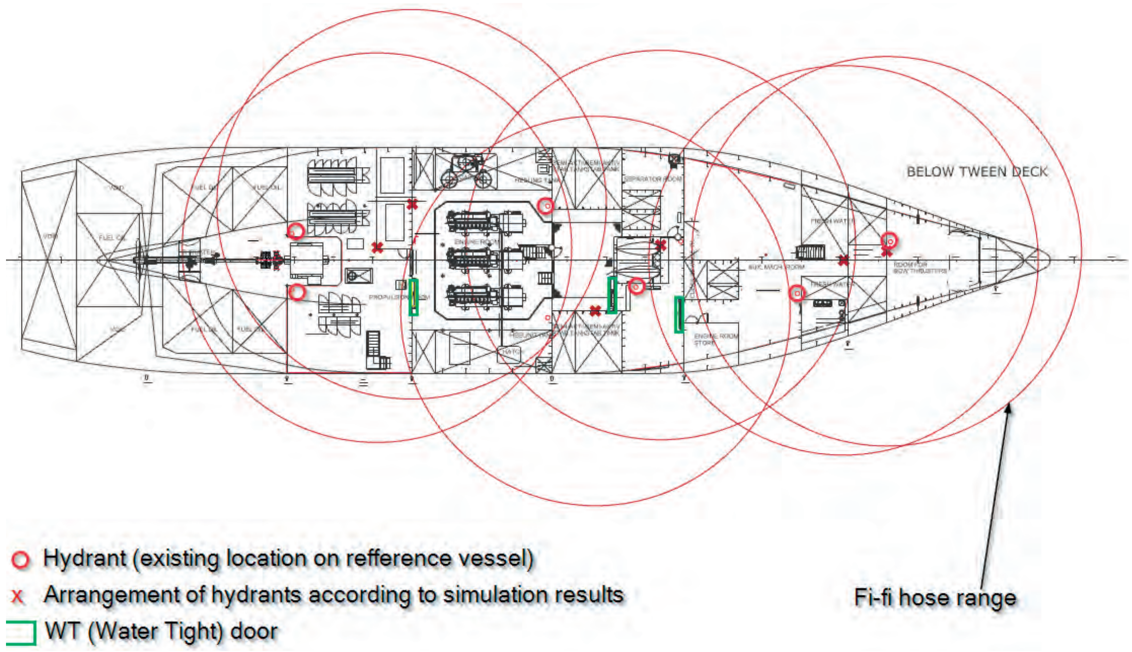

Fig. 10. Comparison of the actual arrangement of fire hydrants on a fishing vessel with their simulated distribution based on two selected criteria: maximizing the degree of coverage of extinguished areas and minimizing the distance from evacuation exits with weights $w_1 = 0{,}6$ and $w_4 = 0{,}4$ respectively

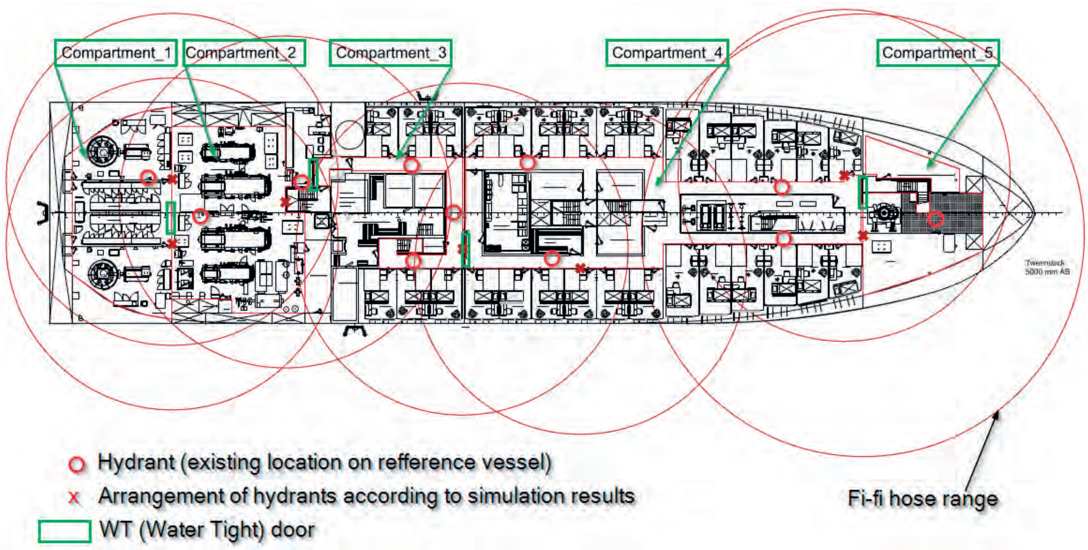

Fig. 11 Comparison of the actual arrangement of fire hydrants on a vessel servicing wind platforms with their simulated distribution based on two selected criteria: maximizing the degree of coverage of extinguished areas and minimizing the distance from evacuation exits with weights $w_1 = 0{,}6$ and $w_4 = 0{,}4$ respectively

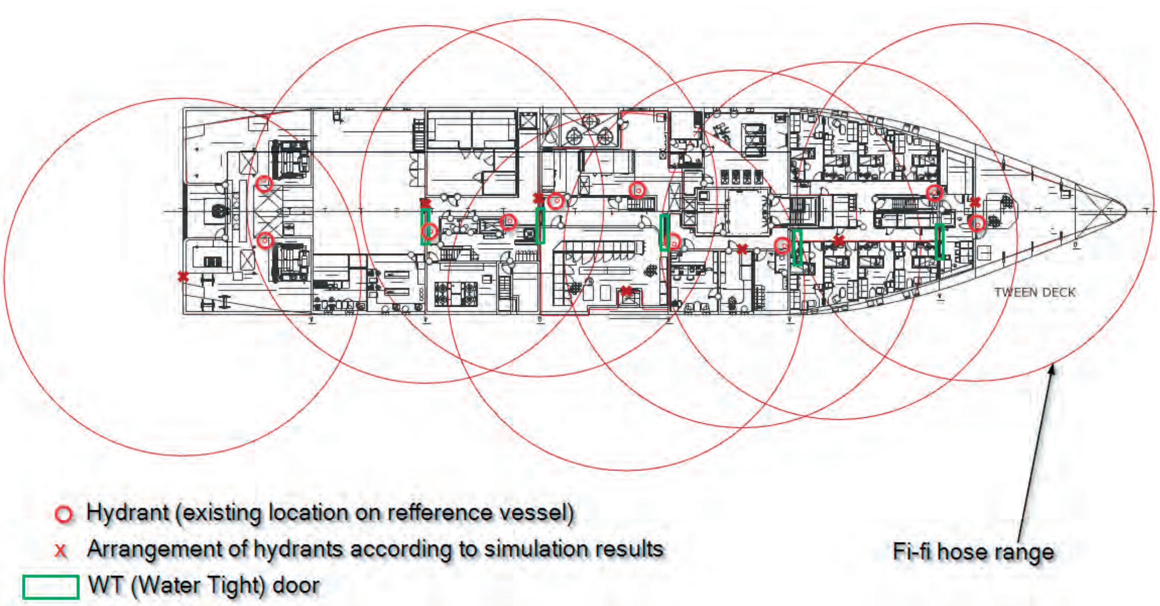

Fig. 12. Comparison of the actual arrangement of fire hydrants on a multi-purpose support vessel with their simulated distribution based on two selected criteria: maximizing the degree of coverage of extinguished areas and minimizing the distance from evacuation exits with weights w_1 = 0,6 and w_4 = 0,4 respectively

Based on the comparative analysis of the individual solutions regarding the arrangement of fire hydrants on the decks of various ships, the following can be concluded:

– both the layout of the fire hydrants obtained using the classical method and the one obtained using the developed system meet all the imposed requirements (constraints),
– the layout of the fire hydrants obtained using the developed system enables faster access by the firefighting team to the hydrants, thanks to the criterion of minimizing the distance from evacuation exits as a component of the substitute objective function, which significantly increases the level of protection against fire hazards on the ship.

Considering that the main goal of the developed system is to reduce the workload of the designer, the above-mentioned benefits are an additional but very significant element of the feasibility of the developed system. So, the basic question remains – how quickly can a solution related to the arrangement of fire hydrants be obtained using the developed system?

In order to answer the question above, a series of simulations were conducted using a computer with typical parameters for computers used in ship design offices. The results of the simulation duration for the Wind Platform Vessel are shown in Table 1. Similar simulations were conducted for the remaining three ships. Using the PSO algorithm, the number of iterations, speed, and number of particles (individuals) in the search space were varied. The type of analyzed vessel seemingly had an impact on the algorithm's speed, but this was solely due to the size of the graphic file that served as the source of the analyzed unit's general plan. The size of the graphic file depends on various factors, such as the number of graphic elements, resolution, number of layers, styles, and blocks contained in the file. The more graphic elements and details, the larger the file size, and consequently, the computer's computational power required for processing and displaying graphics in real-time becomes greater.

Tab. 1. Simulation duration for the Wind Platform Vessel, used for wind platform servicing, based on the criteria of maximizing the coverage degree of extinguished surfaces and minimizing the distance to evacuation exits

	number of hydrants					
	9	**12**	**15**	**18**	**25**	**50**
Max. speed = 0.1 Iterations: 20	11 [s]	11 [s]	11 [s]	12[s]	14 [s]	15 [s]
Max. speed = 0.2 Iterations: 20	11 [s]	11 [s]	11 [s]	12[s]	14 [s]	15 [s]
Max. speed =` 0.3 Iterations: 20	11 [s]	11 [s]	12 [s]	12[s]	14 [s]	15 [s]
Max. speed = 0.5 Iterations: 20	11 [s]	11 [s]	11 [s]	12[s]	13 [s]	15 [s]
Max. speed = 1 Iterations: 20	11 [s]	11 [s]	11 [s]	12[s]	14 [s]	15 [s]
Max. speed = 0.1 Iterations: 40	21 [s]	22 [s]	22 [s]	22 [s]	24 [s]	29 [s]
Max. speed = 0.2 Iterations: 40	21 [s]	21 [s]	22 [s]	23 [s]	24 [s]	28 [s]
Max. speed = 0.3 Iterations: 40	21 [s]	22 [s]	22 [s]	23 [s]	24 [s]	28 [s]
Max. speed = 0.5 Iterations: 40	21 [s]	21 [s]	22 [s]	22 [s]	24 [s]	29 [s]
Max. speed = 1 Iterations: 40	21 [s]	22 [s]	22 [s]	22 [s]	24 [s]	29 [s]

Changing the algorithm parameter of particle speed in the search space did not affect the algorithm's runtime. Increasing the number of hydrants used in the simulation (from 9 up to a maximum of 50) significantly increased the algorithm's runtime. The swarm size, determined by the number of particles (individuals) included in it, also had a significant impact on the algorithm's speed. In the extreme case, the time required to perform several dozen iterations was about 3 minutes, which compared to the time spent on placing hydrants in a classical way, seems to be an undeniable advantage of the applied method.

CONCLUSIONS

The proposed method is an attempt to support ship system designers using one of the methods of artificial intelligence, namely the PSO algorithm, which simulates the behavior of a particle swarm moving in a search space for the best solution to a problem, such as placement of fire hydrants on a ship's boards. The most important conclusions can be formulated as follows:

- the proposed method reduces the time-consuming process of firefighting equipment layout on a ship's boards while also easily implementing the general plan of the designed vessel in the Rhino environment,
- the use of metaheuristic optimization algorithms such as PSO can provide solutions in a relatively short time, ranging from a few seconds to several minutes, which is significantly shorter than the time required for manual design of hydrant placement, making the developed system much more efficient,
- as a result of optimal placement of fire hydrants based on selected criteria, additional benefits arise in the form of increased safety (faster access by firefighting teams to hydrants) and resource economy (reduced amount of water required to extinguish a fire or decreased electricity expenditure to power fire pumps).

Further research

The developed system is based on four different criteria for the optimal placement of fire hydrants; however, its further development seems reasonable. Directions for further research in the field of hydrant placement system using the PSO algorithm may include:

- optimization of the process of finding the minimum number of hydrants to reduce the cost of the ship's fire safety system while ensuring fire safety requirements,
- supplementing the developed system with additional optimization criteria depending on the specificity of the designed vessels, such as installation costs,
- using other metaheuristic optimization algorithms, such as genetic algorithms or ant colony algorithms, to compare the effectiveness of different algorithms in the context of hydrant placement.

REFERENCES

1. R. J. Cant and C. S. Langensiepen, "Methods for Automated Object Placement in Virtual Scenes," in *11th International Conference on Computer Modelling and Simulation, UKSim 2009*, 2009. doi: 10.1109/UKSIM.2009.69.
2. K. Xu, J. Stewart, and E. Fiume, "Constraint-based automatic placement for scene composition," in *Proceedings – Graphics Interface*, 2002.
3. R. Z. Farahani, N. Asgari, N. Heidari, M. Hosseininia, and M. Goh, "Covering problems in facility location: A review," *Computers and Industrial Engineering*, vol. 62, no. 1. 2012. doi: 10.1016/j.cie.2011.08.020.
4. S. Dantrakul, C. Likasiri, and R. Pongvuthithum, "Applied p-median and p-center algorithms for facility location problems," *Expert Syst Appl*, vol. 41, no. 8, 2014, doi: 10.1016/j.eswa.2013.11.046.
5. B. Zhang, J. Peng, and S. Li, "Covering location problem of emergency service facilities in an uncertain environment," *Appl Math Model*, vol. 51, 2017, doi: 10.1016/j.apm.2017.06.043.
6. S. Y. Kim, B. Y. Moon, and S. C. Shin, "Evaluation criterion of machinery arrangement design in a ship engine room," *Journal of Ship Production*, vol. 25, no. 3, 2009, doi: 10.5957/jsp.2009.25.3.117.
7. P. Gualeni, F. Perrera, M. Raimondo, and T. Vairo, "Accessibility for maintenance in the engine room: development and application of a prediction tool for operational costs estimation," *Ship Technology Research*, 2022, doi: 10.1080/09377255.2021.2020949.
8. J. K. Lee, K. H. Lee, N. S. Park, Y. U. Jang, J. Y. Bae, and H. S. Shim, "Integration of knowledge-base and CAD system for the machinery layout design of ships," in *Proceedings of the ASME Design Engineering Technical Conference*, 1996. doi: 10.1115/96-DETC/DAC-1070.
9. A. R. Chaudhuri and U. P. Thakur, "Design criteria of piping system for ships," *Journal of the Institution of Engineers (India), Part MR: Marine Engineering Division*, vol. 81, no. 1, 2000.
10. B. C. Lee, Y. Choi, and H. Chung, "Firefighting equipment arrangement optimization for an offshore platform considering travel distances," *J Mar Sci Eng*, vol. 9, no. 5, 2021, doi: 10.3390/jmse9050503.
11. X. Liu, B. Sun, Z. D. Xu, and X. Liu, "An adaptive Particle Swarm Optimization algorithm for fire source identification of the utility tunnel fire," *Fire Saf J*, vol. 126, 2021, doi: 10.1016/j.firesaf.2021.103486.

12. K. S. Lee, K. J. Han, and J. W. Lee, "Feasibility study on parametric optimization of daylighting in building shading design," *Sustainability (Switzerland)*, vol. 8, no. 12, 2016, doi: 10.3390/su8121220.

13. D. Rutten, "Galapagos: On the logic and limitations of generic solvers," *Architectural Design*, vol. 83, no. 2, 2013, doi: 10.1002/ad.1568.

14. C. Waibel, T. Wortmann, R. Evins, and J. Carmeliet, "Building energy optimization: An extensive benchmark of global search algorithms," *Energy Build*, vol. 187, 2019, doi: 10.1016/j.enbuild.2019.01.048.

15. J. M. Cichocka, A. Migalska, W. N. Browne, and E. Rodriguez, "SILVEREYE – The implementation of particle swarm optimization algorithm in a design optimization tool," in *Communications in Computer and Information Science*, 2017. doi: 10.1007/978-981-10-5197-5_9.

16. T. Wortmann, "Opossum – Introducing and Evaluating a Model-based Optimization Tool for Grasshopper," in *Proceedings of the 22nd Conference on Computer Aided Architectural Design Research in Asia (CAADRIA)*, 2022. doi: 10.52842/conf.caadria.2017.283.

17. I. Anton and D. TĂnase, "Informed Geometries. Parametric Modelling and Energy Analysis in Early Stages of Design," in *Energy Procedia*, 2016. doi: 10.1016/j.egypro.2015.12.269.

18. J. C. Lagarias, J. A. Reeds, M. H. Wright, and P. E. Wright, "Convergence properties of the Nelder-Mead simplex method in low dimensions," *SIAM Journal on Optimization*, vol. 9, no. 1, 1998, doi: 10.1137/S1052623496303470.

19. J. Kennedy and R. Eberhart, "Particle Swarm Optimization, Proceedings of IEEE International Conference on Neural Networks Vol. IV: 1942–1948.," Neural Networks.

20. L. M. Hiot *et al.*, *Handbook of Swarm Intelligence*, vol. 8. 2010.

21. S. Bhattacharyya and P. Dutta, *Handbook of research on swarm intelligence in engineering*. 2015. doi: 10.4018/978-1-4666-8291-7.

22. G. O. Brown, "The history of the Darcy-Weisbach equation for pipe flow resistance," in *Proceedings of the Environmental and Water Resources History*, 2002. doi: 10.1061/40650(2003)4.

23. K. Rudzki, P. Gomulka, and A. T. Hoang, "Optimization Model to Manage Ship Fuel Consumption and Navigation Time," *Polish Maritime Research*, vol. 29, no. 3, 2022, doi: 10.2478/pomr-2022-0034.

POLISH MARITIME RESEARCH 1 (117) 2023 Vol. 30; pp. 17-23
10.2478/pomr-2023-0054

RETROFITTING THE BOW OF A GENERAL CARGO VESSEL ANDEVALUATING ENERGY EFFICIENCY OPERATIONAL INDEX

Yordan Denev
Technical University of Varna, Bulgaria

* Corresponding author: *y.denev@tu-varna.bg (Yordan Denev)*

ABSTRACT

This report examines the feasibility and impact of retrofitting the bulbous bow on a general cargo ship, in terms of the energy efficiency operational index (EEOI), in the areas of Western Europe and the Eastern Mediterranean. Three ship forms were developed and analysed: with a bulbous bow, without a bulbous bow, and with a modified bulbous bow. The goal in developing the ship forms and conducting the analysis was to achieve minimal differences in the ship's characteristics with the same volumetric displacement, aided by PolyCAD software. A route was selected between two ports: Varna and Rotterdam. The labour intensity of the bulbous bow retrofitting process was evaluated and approximate values of labours costs and cost for the task were determined. The results obtained for resistance during ship motion, EEOI, and fuel consumption reductions, or increases, were compared against the retrofitting values. The return cost of retrofitting is evaluated and measured in terms of fuel saved.

Keywords: retrofitting, bulbous bow, energy efficiency design index, return costs

INTRODUCTION

In recent years, the International Maritime Organization (IMO) introduced requirements for reducing emissions to the environment. The IMO strategy aims to reduce freight rate carbon emissions by 40% by 2030, compared with 2008, and up to 70% by 2050 [1]. On January 1 2023, new regulations took effect, relating a ship's Energy Efficiency Existing Ship Index (EEXI) calculations to energy efficiency and initiating the annual operational carbon intensity indicator (CII) [2].

Taking the International Maritime Organization regulations into account, ship owners are required to take measures to improve the energy efficiency of their fleet as part of the global effort. Some of the measures to improve the energy efficiency of ships consist of methods to reduce the ship's resistance, use renewable energy, converting conventional diesel engines to operate on liquefied natural gas, modifying the bow design, or simply changing the configuration of the bulbous bow.

Retrofitting bulbous bows is an interesting process, not only for large container vessels, but also for other types of merchant ships. Force technology is carried out in the retrofitting of the bulbous bow of multipurpose vessels with 9100 DWT. The result is a 17.5% resistance saving [3].

A numerical analysis of retrofitting a bulbous bow for a modern container ship, operating with a slow-steaming profile, was presented in [4]. The retrofit analysis served as an illustrative example of a design process that relies on high-fidelity CFD simulations and surrogate modeling. The bulbous bow design candidates were generated by parametrically modifying the original bow geometry. These alternative designs were assessed using the open-source CFD toolbox Open FOAM, and the resulting effective power predictions were used to rank each design throughout the entire operating profile. Moreover, the impacts of the different bulbous bow designs on wave-making resistance and propeller performance were thoroughly examined. Surrogate models were then employed to explore the parameterized design space and establish a sequence of design exploration and exploitation cycles in the retrofit analysis, aiming to achieve an enhanced bow shape as the ultimate objective.

An assessment of the design and operational energy efficiency index of a group of container ships from Class A13, A15, and A19 was conducted in [5]. It transpired that, based on these indicators, the best performer was the container ship from Class A19, while Class A13 would need to reduce its speed by 45% to meet the requirements for lowering index values. The possibility of using a liquefied natural gas engine for the Class A19 ship could enhance its energy efficiency, resulting in savings of approximately $27 million [5].

A possible solution for reducing harmful emissions into the atmosphere is a hybrid propulsion system. Applied to a container ship of Class A19, respective reductions of NOx, SOx, and CO_2, by 52.0%, 63.7%, and 30.4%, were achieved, compared to a conventional system. Additionally, it is a more efficient option concerning environmental regulations, with an energy cost of $0.07/kWh and profitability of $21.9/ton [6].

The implementation of a double-hull bulb on the bow of a fishing vessel with a non-optimized hull directly impacted its operational efficiency. Following the modernization of the shape and towing tests, a reduction in resistance of approximately 10% was observed [7].

An evaluation of the resistance of a tanker during beam seas was conducted in [8]. Through simulation, the maximum and minimum wave angles were identified, at which the additional resistance reached its maximum and minimum values. These were 180 and 150 degrees for the maximum angle and 130 degrees for the minimum angle, taking into account that the degrees of freedom also directly influenced this effect.

In [9], a new type of bulbous form for ships, with a Froude number ranging from 0.4 to 0.5, was introduced, significantly differing from the conventional ones. This bulb shape reduced wave generation at high speeds but was sensitive to precise mounting position and velocity. The tests were conducted in a towing tank and software simulations were undertaken for a ship with a Froude number of about 0.45.

The aim of this study was to analyze the economic effect of retrofitting a ship's hull to improve the EEOI. Alongside all the efforts to improve the energy efficiency of existing ships, an economic analysis of the benefits must also be carried out, since such actions are costly and time-consuming, because the ship is not in operation. Retrofitting the bow of a ship is directly linked to the ship's stay in dry dock. From a technological perspective, such a task may not be overly complex, but the economic analysis is more challenging. Therefore, the article presents and analyses the benefits and return on investment in retrofitting the bow of a general cargo ship.

METHODOLOGY AND SECTION MODELLING

The methodology and section modelling are related to modernisation process descriptions in different stages of the calculations.

ENERGY EFFICIENCY OPERATIONAL INDICATOR EVALUATION

The IMO guidelines [10] define the methodology for the calculation of the Energy Efficiency Operational Indicator (EEOI) based on voyage parameters and the type of main engine fuel. EEOI is defined individually for cargo ships and bulk carriers in a wide deadweight range [11] but it can be calculated by the following equation [1]:

$$EEOI = \frac{\sum FC * Ccarbon}{\sum mi * D}, \frac{tCO_2}{tnm} \quad (1)$$

where *Fc* is the specific fuel consumption (g/kWh), *Ccarbon* is the fuel mass to CO_2 mass conversion factor for fuel, *mi* is the cargo carried (t), and *D* is the distance in nautical miles to the cargo carried or work done (nm).

Proper evaluation of the retrofitting effect on the energy efficiency operational index has to calculate the fuel cost before and after retrofitting. Fuel cost is calculated by:

$$Fuel\ cost = FC * Vs * Cfuel * D, \$ \quad (2)$$

where *Fc* is the specific fuel consumption (l/h), *Vs* is the ship service speed (kn), *Cfuel* is the fuel per $/l, and *D* is the distance in nautical miles to cargo carried or work done (nm).

WEIGHT OF SHIP HULL

The weight of the ship's hull is determined at the construction design stage and modernisation is based on working drawings and construction models. Mathematically, the weight can be explained by the followed expression:

$$W_{hull} = W_{main\ hull} + W_{BHD} + \cdots \dots \dots \dots \dots \dots .Wi \quad (3)$$

where *Wmain* hull is the weight of the ship's main hull (t), *WBHD* is the weight of transverse bulkheads in the ship's main hull (t), and *Wi* is all of the other constructions in the ship's hull (t).

MODERNISATION COST CALCULATION

Modernisation costs include the cost of billable hours for retrofitting and hull fabrication costs. The billable hours for fabricating and retrofitting parts of the ship's hull are calculated with the simple equation:

$$MH = W_{hull} * MH_{steel}, mh \quad (4)$$

where *Whull* is the weight of the ship's hull (t) and *MHsteel* are the billable hours per ton of steel construction (mh/t).

Hull fabrication costs closely depend on the steel price and the weight of modernised hull parts, see Eq. (5).

$$HFC = W_{hull} * Csteel, \$ \quad (5)$$

where *HFC* is the hull modernisation cost ($), *Whull* is the weight of the ship's hull (t), and *Csteel* is the final steel price in the country ($/t).

HULL MODELLING

The hull form was generated by PolyCAD software. To assess the effect of the modification of the ship's bow, the resistance was calculated using the Holtrop and Mennen method, for speeds ranging from 0-17 knots. The advantage of the software is the possibility of recalculating ship characteristics in the event of some form of change. After retrofitting, a small difference in mass displacement appeared.

MODEL VALIDATION AND VERIFICATION

In this type of analysis, it is important for the calculations to be within a range of 5% tolerance, which is assumed for engineering calculations. Otherwise, if there is more than 5% tolerance, the impact on the characteristics is significant. The retrofitting process consisted of modernising the forward ship hull's form without making changes to the ship's main dimensions.

The change in the geometry of the bow was achieved by mounting a bulb with a specific geometry that corresponds to the original ship's form. In this case, in order to ensure a constant displacement of water, changes were made to the coefficients of the shape, specifically the prismatic coefficient (Cp) and, consequently, the block coefficient (Cb). The coefficient of the mid-ship section remained the same for all shapes. Differences in Cb were within 2.5%, and differences in Cp were in the range 0.7-2.5%; higher differences in Cw coefficients were in the range 1.8-3.5%. The maximum difference in mass displacement was 0.46 t.

In the evaluation of the model shape, a mesh with rectangular and triangular elements was used. Each type of element was used in different areas of the ship's hull. For example, in the bow and stern regions where the hull shape has complex curvature in two directions, triangular mesh elements were used, while rectangular elements were used in the remaining areas. The transition elements between rectangular and triangular elements were rhomboidal. The grid spacing was 0.2 m with a key nudge of 0.002 m; the number of elements is shown in Fig. 1.

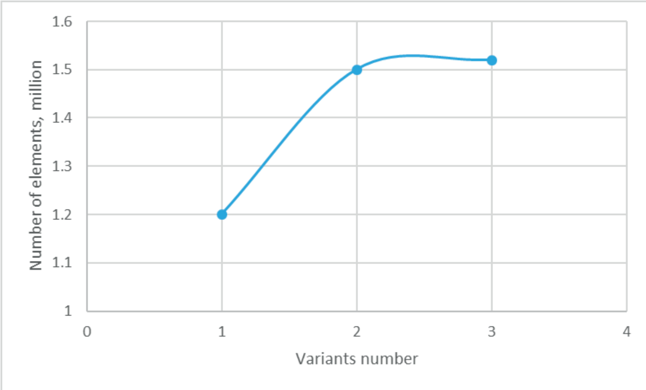

Fig. 1. Diagram of mesh independence

HULL FORM GENERATION

The main dimensions of the ship were L=120.62 m, B= 16.00 m, D= 9.03 m, and d= 6.67 m. The ship had a double bottom and double side, single deck and one hold, with a 116 TEU container capacity. The hold length was about 84.5m, with a double sided width of 1.3 m per side and a maximum hold breadth of 13.4 m. The service speed was 15 kn and the main engine type was a '5S35ME' with main engine power of 4350 kW. Three different forms with similar hull coefficients are shown in Table 1. The original hull form was without a bulbous bow (VAR1), while the other two had bulbous bows, where the dimensions of the bulb were different.

Tab. 1. Hull form coefficients

	VAR1	VAR2	VAR3
Cb	0.78	0.76	0.76
Cp	0.78	0.77	0.76
Cm	0.99	0.99	0.99
Cw	0.90	0.89	0.87
Δ, m^3	10518.34	10518.64	10518.80

The analysed ship was a general cargo ship with one hold of 7000 tDW. The location of the collision bulkhead was at 7% of Lpp, while the engine room bulkhead was at 23% Lpp, see Fig. 2 to Fig. 4.

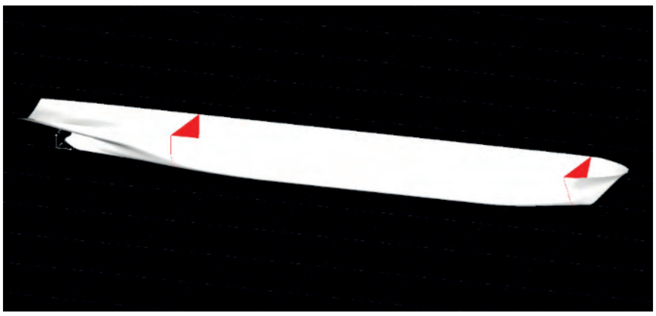

Fig. 2. Variant one (original hull form) without bulbous bow

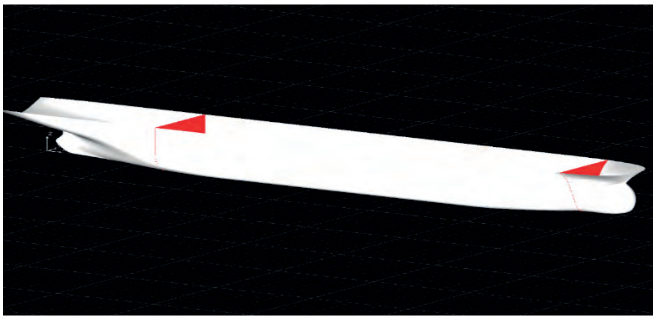

Fig. 3. Hull form variant VAR2 with bulbous bow

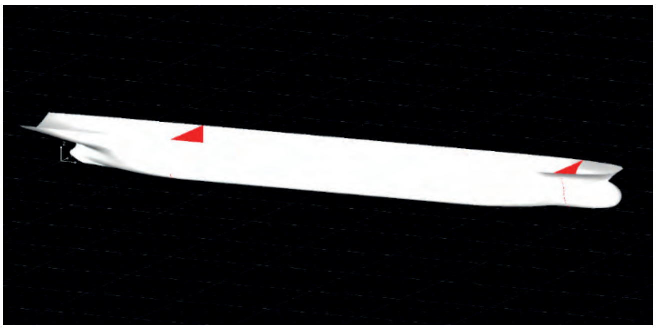

Fig. 4. Hull form variant VAR3 with modified bulbous bow

Retrofitting the forward part of the ship's hull with a bulbous bow decreases the total resistance by about 18% for a service speed of 15 knots (Fig. 5), decreasing the necessary main engine power and reducing carbon dioxide in the atmosphere.

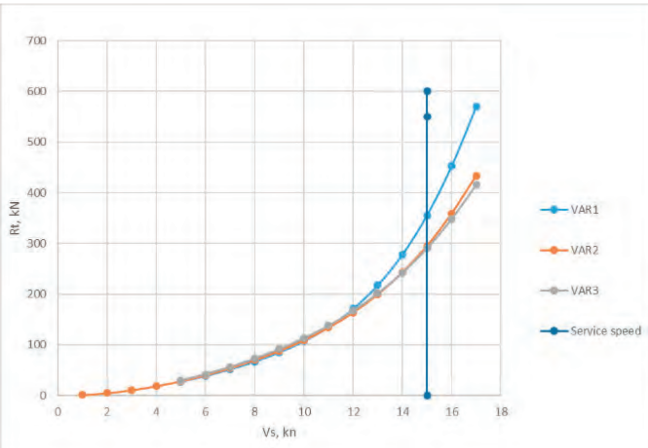

Fig. 5. Total resistance of ship hulls

After the established positive effect of the modification of the ship's bow, it was necessary to determine whether, and to what extent, it led to an improvement in the energy efficiency index of the ship, as well as the return on investment, in terms of resources and time invested in the modification for regular voyage distances.

VOYAGE PARAMETERS

Voyage parameters were selected in accordance with shipping trends and the transportation of goods between the Black Sea and Western European ports. The distance from the port of Varna to the port of Rotterdam is 3940 nm, as shown in Fig. 6.

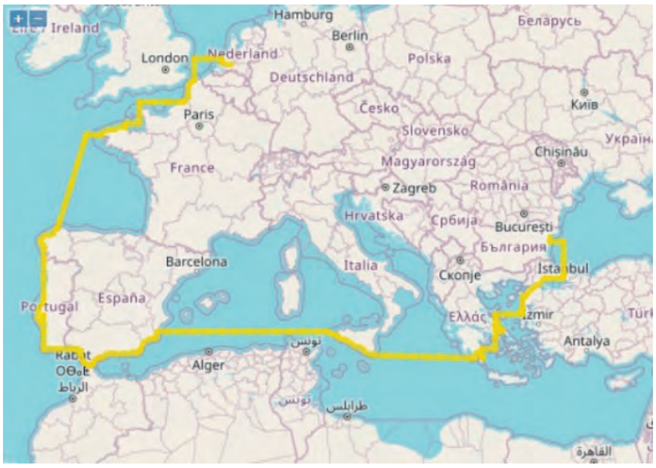

Fig. 6. Voyage distance map

The distance of 3940 nm was travelled in 11 days, at an operational speed of 15 kn in good weather conditions. The ship's main engine was a '5S35ME' type, with the specific fuel consumption and fuel costs shown in Fig. 7. The maximum consumption occurred with the first hull form, which is without a bulbous bow, and the minimum occurred with a modified bulbous bow.

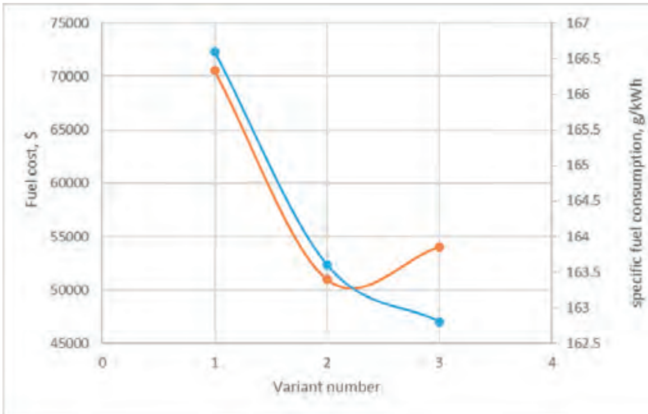

Fig. 7. Voyage fuel cost and specific fuel consumption

Considering the main engine-specific consumption, ship service speed, distance between ports, and marine diesel prices, the fuel cost for one voyage was calculated using the CEAS engine calculator (specific for different engine powers) and is presented in Fig. 6. Average marine diesel oil costs 0.42 €/liter, which corresponds to 546.5 $/mt of very low sulfur fuel oil (according to prices from July 19, 2023) [12].

Despite the fact that the specific fuel consumption for the second variant of the ship's hull form is the lowest, it does not result in the lowest overall fuel cost when evaluating the total fuel expenses. This is due to the fact that the difference in specific fuel consumption between the second and third variants is only 0.8 g/kWh in favor of the second one, which does not make a significant impact on the end result, as the resistance that needs to be overcome with the second hull form is higher than the third one.

ENERGY EFFICIENCY OPERATIONAL INDEX EVALUATION BASED ON VOYAGE PARAMETERS

EEOI is an indicator for evaluating ship energy efficiency and CO_2 emissions to the environment during a ship's operation and through her life cycle. Using the equation for EEOI offered in [10], for generated ship hulls, indexes are calculated considering voyage parameters and actual ship conditions. For a voyage from the port of Varna to the port of Rotterdam with a speed of 15 kn, a distance of about 3940 nm, a deadweight of about 7000 t, and a fuel carbon content of 0.86 for light fuel oil [13], the EEOI calculated by Eq. (1) is presented in Fig. 8.

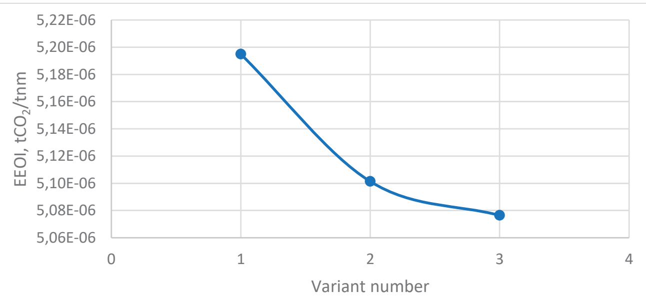

Fig. 8. Energy Efficiency Operational Index for hull forms

After retrofitting the forward part of the ship hull, EEOI is improved, which leads to a reduction of CO_2 emissions. The reduction measured (as a percentage) is about 4% for ship hull variant VAR2 and about 3% for hull variant VAR3. The retrofitting effect is not so high but, related to the ship dimensions, it is satisfactory.

CAPITAL EXPENDITURE FOR RETROFITTING AND RETURN COSTS

The effects of forward part retrofitting will be clearer after calculating capital expenditure, return costs, and time for return costs. To study this effect, it is necessary to calculate the hull steel weight, billable hours for its fabrication, and their differences for different forms. After production calculations, the return cost and time are calculated.

Ship steel hull weight estimation can be evaluated by the mathematical equations presented in [14] but they are not appropriate in this case, because hull weight is calculated in relation to weight displacement. In the case study, the volumetric and weight displacement are the same for all forms, and computer model development is used for hull weight evaluation. The results are shown in Table 2.

Tab. 2. Ship hull weights

	VAR1	VAR2	VAR3
WEIGHT HULL, T	835.1	852.0	894.0
Bulb area, m^2	0.00	10.30	9.03
Bulb length, m	0.00	2.00	3.00
Bulb radius, m	0.00	1.50	2.00

The difference in hull weights, after retrofitting, is about 17 t of steel construction for variant VAR2 and 59 t of steel construction for variant VAR3. Differences of such magnitude do not affect the ship's carrying capacity since, during the conceptual design stages, a 1% reserve displacement is provided; the results are shown in Fig. 9.

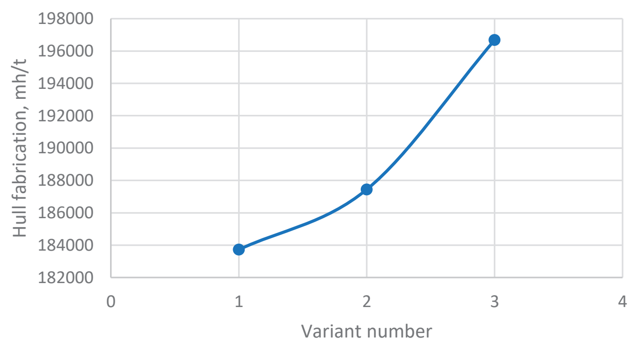

Fig. 9. Billable hours for steel hull fabrication

The thickness of hull plating in all variants is 16 mm, which, according to [15], is necessary for 220 mh per ton of steel construction. This means that, with increasing hull weight, the billable-hours for fabrication and costs increase too. The Chinese steel price is 500 $/t [16], while the USA steel price is 680 $/t [17]. The steel price in Bulgaria is about 450$/t. For the purpose of this study, the price of steel in Bulgaria is averaged to 600 $/t, including the cost of work, cost of transportation, cost of blasting and painting, and the cost of cutting in Bulgaria (Table 3).

Tab. 3. Hull cost for different variants

	VAR1	VAR2	VAR3
Hull Fabrication Cost, $	501,060	511,200	536,400

The difference in hull cost price between variant VAR2 and variant VAR1 (the original) is about $10,000, which is about €9000, and equal to about 41 t of very low sulphur fuel oil. For a voyage from the port of Varna to the port of Rotterdam, the fuel price is about €60,000, which means that, after forward hull part retrofitting and EEOI improvement, the return cost is very fast, i.e. after the second voyage after retrofitting.

CONCLUSIONS

This paper studied the possibilities and effects of retrofitting the forward part of a ship's hull designed without a bulbous bow. To evaluate these effects, three ship hull forms were developed. The original form was without a bulbous bow, while the other two had a bulbous bow.

Calculations of resistance and engine power were carried out using the Holtrop and Mennen method and the hull form was generated by PolyCAD software. In new form generation, the volumetric displacement of the original ship hull was preserved for the newly generated forms. There were small changes in the block and prismatic coefficients.

After forward hull part retrofitting, the total resistance was reduced by about 18%, which lead to a necessary engine power reduction. To study the numerical retrofitting effects, a ship voyage between the port of Varna and the port of Rotterdam was selected, with a distance of 3940 nm. The specific fuel consumption for all designed forms were found and it should be noted that variant VAR3 has a minimum specific fuel consumption, but the fuel cost for the voyage is not minimal because the necessary power is higher.

Hull shape variant VAR3 is optimal for EEOI but not optimal for retrofitting or building costs. The capex cost is about $35,000 higher than variant VAR1 (the original) and about $25,000 higher than variant VAR2. The difference in fuel cost between variant VAR3 and variant VAR2 is about $3800 per voyage, while the difference between VAR1 and VAR3 is $16,500, and between VAR1 and VAR2 it is about $20,000.

Retrofitting of the forward part of the ship hull is more reasonably carried out using variant VAR3, with a modified bulbous bow, so that the EEOI is at its lowest and approximately 35 t of very low sulphur fuel oil is saved. Capex costs are higher and equal to 64 t of very low sulphur fuel oil, which means that, after the second voyages, the capex cost will be returned.

DECLARATION OF COMPETING INTERESTS

The author declare that they have no known competing financial interests or personal relationships that could have appeared to influence the work reported in this paper.

REFERENCES

1. Dimerco, 'IMO 2023 Regulations: Definition and Implications' [online], available https://dimerco.com/imo-2023-regulations/

2. IMO, 'Rules on ship carbon intensity and rating system enter into force' [online, viewed 18.06.2023], available from https://www.imo.org/en/MediaCentre/PressBriefings/pages/CII-and-EEXI-entry-into-force.aspx

3. F. Technology, 'Retrofitting a new bulbous bow' [online, viewed 02.07.2023] available https://forcetechnology.com/da/cases/retrofitting-af-en-ny-bulb

4. G. Filip, H. K. Dae, S. Sahu, J. de Kat, and M. Kevin, 'Bulbous Bow Retrofit of a Containership Using an Open Source Computational Fluid Dynamics (CFD) Toolbox.' Paper presented at the SNAME Maritime Convention, Houston, Texas, USA, October 2014. doi: https://doi.org/10.5957/SMC-2014-T58

5. A.R. Nader and S.S. Ibrahim, 'Enhancing energy efficiency for new generations of containerized shipping', Ocean Engineering, Volume 215, 2020, 107887, ISSN 0029-8018, https://doi.org/10.1016/j.oceaneng.2020.107887.

6. A.R. Nader and S.S. Ibrahim, 'Hybrid/dual fuel propulsion systems towards decarbonization: Case study container ship Ocean Engineering, Volume 281, 2023, 114962, ISSN 0029-8018, https://doi.org/10.1016/j.oceaneng.2023.114962.

7. H.R. Díaz-Ojeda, F. Pérez-Arribas, and T.R. Stephen, 'The influence of dihedral bulbous bows on the resistance of small fishing vessels: A numerical study', Ocean Engineering, Volume 281, 2023, 114661, ISSN 0029-8018, https://doi.org/10.1016/j.oceaneng.2023.114661.

8. H.J. Cho, S.H. Lee, D. Oh, and J.K.J. Paik, 'A numerical study on the added resistance and motion of a ship in bow quartering waves using a soft spring system', Ocean Engineering, Volume 280, 2023, 114620, ISSN 0029-8018, https://doi.org/10.1016/j.oceaneng.2023.114620.

9. Z. Liu, W. Liu, Q. Chen, F. Luo, and S. Zhai, 'Resistance reduction technology research of high speed ships based on a new type of bow appendage', Ocean Engineering, Volume 206, 2020, 107246, ISSN 0029-8018, https://doi.org/10.1016/j.oceaneng.2020.107246.

10. International Maritime Organization, 'Guidelines for Voluntary Use of the Ship Energy Efficiency Operational Indicator (EEOI)', 2009.

11. J. Boekhoff, 'Understand your shipping emissions' [online, viewed 08.07.2023] available from https://www.carbonchain.com/blog/understand-your-shipping-emissions

12. 'Ship & Bunker, Rotterdam bunker price' [online, available 08.07.2023] available from https://shipandbunker.com/prices/emea/nwe/nl-rtm-rotterdam

13. 'Classification Society, Appendix- calculation of energy efficiency operational indicator based on operational data' [online viewed 01.07.2023] available from https://

www.imorules.com/GUID-EF0096C9-A807-4C9C-A5EF-1B0DDE4C01A3.html

14. A. Papanikolaou, ‘Ship Design- Methodology of Preliminary Design, 2014, Springer Dordrecht, https://doi.org/10.1007/978-94-017-8751-2;

15. G. Butler, ‘Guide to Ship Repair Estimates’, Oxford, 2000, Butterworth-Heinemann, Elsevier ISBN 0 7506 4834 1

16. ‘Made in China’ [online] available https://www.made-in-china.com/products-search/hot-china-products/Shipbuilding_Plate_Price.html

17. ‘Steel Pipes and fittings, Shipbuilding steel price’ [online viewed 12.07.2023] available from https://www.sambhavpipes.com/shipbuilding-steel-plate.html

sciendo

POLISH MARITIME RESEARCH 4 (120) 2023 Vol. 30; pp. 24-30
10.2478/pomr-2023-0055

USE OF THE AHP METHOD FOR PREFERENCE DETERMINATION IN YACHT DESIGN

Jan Sierzputowski *
Artur Karczewski
Przemysław Krata
Gdansk University of Technology, Institute of Naval Architecture, Gdansk, Poland

* Corresponding author: *jan.sierzputowski@pg.edu.pl (J. Sierzputowski)*

ABSTRACT

A sailing yacht is a human-centred product, the design of which revolves primarily around the wants and desires of the future owner. In most cases, these preferences are not measurable, such as a personal aesthetic feeling, or a need for comfort, speed, safety etc. The aims of this paper are to demonstrate that these preferences can be classified and represented numerically, and to show that they are correlated with the type of yacht owned. As a case study, the owner's preferences for deck equipment are considered. These are determined by pairwise comparisons of the importance rankings for features previously defined by yacht owners, following the analytic hierarchy process (AHP) method. As a result, a quantitative representation of these preferences is established, and they are shown to be correlated with the type of yacht. The findings of the current study show that the yacht owners' preferences can be represented numerically, leading to a utilitarian conclusion that concerns the support and even some degree of automation of the design process.

Keywords: Yacht Design, AHP Method, Yacht User Preferences, Sailing Yacht, Human-Centred Design

INTRODUCTION

As a technical object, a yacht needs to be designed and built to withstand rough sea conditions, to ensure safety and convenience to people on board, and to provide pleasure, or possibly even the perception of luxury resulting from spending time in a unique way. As a recreational vehicle, it needs to meet the expectations of users with a wide range of comfort levels. The achievable speed of a yacht is also a significant feature, since racing forms part of the lifestyle of numerous sailors. Whatever the exact purpose, a yacht can be recognised as a human-centred object. This aspect, although clearly more prominent for a yacht than for other watercraft, is to some extent similar for many types of vessels. The main design objectives may vary depending on the type of vessel, meaning that the optimal solution depends on the specific purpose of the ship. Nevertheless, all ships must be safe at sea, economically efficient, and generally perform well within their scope of application. Although the definitions of these requirements are tailored to the purpose, the main thrust of the designer's efforts remains very similar [1].

The scientific literature in the field of ocean engineering is mainly focused on maritime transport, its impact on the environment, and ways to optimise it, with the goals of safety and health; it therefore includes issues related to improving the efficiency of ships, for example by increasing the speed, capacity, lifespan and human safety while lowering pollution, costs, risks and accidents [2], [3]. The vast majority of research on motor yachts addresses the optimisation of the hull shape and the automation of the design process [4], [5].

For a sailing yacht, the aspects most often studied are its behaviour in waves [6] and the prediction of its speed under sail [7]. Other areas of interest are the aero- and hydrodynamics of the yacht [8], the behaviour of the sails [9], and the performance of the yacht under different sail settings [10]. Existing articles have also considered masts and rigging, for example the overall strength and performance of standing rigging [11], and the optimisation of the rigging structure design process [12]. Although the human factor is considered in several of the research papers mentioned above, the main purpose of the researchers has been to improve the yacht as a technical object.

Yachts are made for people, and designers therefore prefer a human-centred approach. Human comfort on board is discussed in scientific publications in terms of ergonomic guidelines [13], [14] or with regard to the design of the interior and exterior of a yacht [15]. The term „human factor" is considered mainly in association with safety [16], [17], and rarely in relation to the conceptual design of the interior of the yacht [18]. Although the authors of the latter reference discuss the importance of knowing the customer's needs and requirements, this is not suitable for an automated design process and only applies to one-off production. The design process itself has been considered in several articles, ranging from different design approaches and ways of communicating with the customer [19], through design optimisation [20], to the entire approach to yacht design [21] which involves gathering information on the client's preferences in the initial phase of the project. Baranowski in [22], focuses on modifying a sailing yacht to accommodate disabled individuals. This process entails gaining a deep understanding of the requirements of such individuals and implementing tailored solutions on the yacht. However, it must be noted that this scenario is rare and does not extend to the production of yachts on a larger scale.

The design process is related to the selection of the best solution for a given project, although this is usually the "best" only in certain respects, such as cost or a low risk of failure, and the choice may be made using multi-criteria decision-making (MCDM) methods [23]. However, there is a noticeable lack of studies of the selection of deck equipment for a yacht in relation to the preferences of yacht owners, in other words studies that take into account a variety of different aspects of yacht operation, such as comfort, performance, cost, durability, and aesthetics. These are subject to the individual feelings of the owner, and due consideration has not yet been paid to this subject. Deck equipment should also be considered as a link between the sailor and the sail, which can act in both directions.

Questions arise as to whether it is possible to objectively examine and classify the preferences of sailing yacht owners and present them numerically, whether there are any correlations between yachts and their owner's preferences, and whether these correlations could be used in the yacht design process.

To answer these questions, the analytic hierarchy process (AHP) method, a tool that facilitates decision making, is applied in this study. The aim of this method is to make the right decision, rather than to indicate certain preferences or to find any correlations between these and other features. However, one of the steps of this method requires experts to determine the weights of the features affecting the decision-making process. These weights reflect the preferences of the experts. In the case considered here, they will be determined by the owners of sailing yachts through a survey created based on the instructions given by the developer of this method. The opinions of shipowners on the use of their yachts, for example sailing them, operating them and maintaining them in good condition, will be considered here, with deck equipment and rigging forming the main focus of the study.

The ability to determining users' preferences in a measurable, numerical way could significantly speed up the design process. The designer could then rely on these numbers to improve their design. Costs related to the replacement of failed elements, which in shipyard conditions can reach up to 40% of the value of the entire construction [24], would also decrease.

The rest of this paper is organised as follows. In the next section, the AHP method used in the study is explained, and the study preparation process is presented. The subsequent section presents the obtained results and a discussion, while the last section presents the conclusion.

IDENTIFICATION OF THE END-USER'S PREFERENCE PATTERNS

As the central idea behind this research is to identify and quantify the typical patterns of preferences of yacht end-users, the AHP method was adopted, since there are many examples of its use in solving a variety of problems where it is impossible to quantify the decision variables. This method was deemed suitable to determine the subjective ratings provided by owners of yachts.

Analytic hierarchy process

The AHP method is a multi-criteria decision support method (multiple-criteria decision analysis, MCDA) that was proposed by Saaty in the 1970s [25]. Methods of this type are used when the number of decision variables (i.e. the factors influencing the final decision) exceeds human analytical capabilities; in other words, when there are too many variables for the human mind to be able to grasp them all at once, especially if there are contradictory features [26]. The AHP is an effective method for dealing with complex problems of this type [27]. It helps decision makers set priorities between alternatives, sub-criteria and criteria in the decision-making process, and to make the best decision in a given context [23], [28]–[30]. The method is used to structure the problem, starting from the goal to be achieved as a result of making a decision, through the criteria affecting the choice, and ending with the possible options.

Fig. 1. The AHP hierarchy pyramid

The algorithm for the AHP method consists of several consecutive steps:

1. Determining the decision problem;
2. Developing a decision model using a hierarchical structure;
3. Comparing criteria in pairs using a fundamental scale of comparison;
4. Determining priorities and their interpretation;
5. Dealing with inconsistent answers;
6. Group decision making (aggregation of results);
7. Making a decision;
8. Analysing the effects of the decision;

This process is widely discussed in the scientific literature in relation to many different decision-making problems, including those relevant to the maritime industry, and will not be further explored in this article. For more information, please see the sources.

APPLICATION OF THE AHP METHOD IN THIS STUDY

Experts

The purpose of using the AHP method is to make the right decision, rather than to indicate certain preferences of the experts or to find any correlations between these preferences and other features. This study focuses on the opinions of yacht owners on the use of their yachts, i.e. sailing them, operating them, and maintaining them in good condition. The experts in this study are therefore all owners of sailing yachts who are responsible for their maintenance and are their main end-users.

Decision-making goal

The decision-making goal should be formulated in such a way that the experts' answers reflect their personal preferences in relation to the use of their yachts. If a decision were to be made, it should affect the quality of operation of a yacht from the point of view of the user (yacht owner). Since the direct link between the sailor and the yacht is the deck equipment and rigging, these should be the focus. Thus, the decision-making goal in this case is the selection of the optimal deck equipment for a particular sailing yacht.

Hierarchical structure of a decision problem

Tab. 1. Features of the deck equipment

Criteria	Description
Price of the accessory	Preferred value: low price.
Durability	Resistance, failure-free operation, durability, strength, ease of repair of the equipment. Preferred value: high durability.
Efficiency	Functionality, ease and convenience of use (efficiency is a general characteristic that allows one to say that one element is better than another in terms of use). Preferred value: high efficiency.
Weight of the accessory	Preferred value: low weight.
Aesthetics of the accessory	Colour, shape, attractiveness, matching the appearance of the yacht, overall visual and aesthetic impression of the accessory. Preferred value: high level of aesthetics.

- Decision goal: Selection of the optimal deck equipment for a given sailing yacht.
- Criteria influencing the decision: Based on the author's experience of sailing and professional work in the selection and sale of deck equipment, the criteria in Table 1 were identified.
- Selectable options: Groups of accessories should be identified, such as winches, staysail furlers, masts, standing and running rigging, cleats, jammers, etc. Individual products should then be associated with these groups, and solutions with different parameters should be found (e.g. Winch 1, Winch 2, Winch 3, etc.). Since the purpose of this study was to examine the preferences of users rather than to select equipment, this step was omitted.

The overall hierarchy is shown in the form of a diagram in Fig. 2.

In this case, there is one goal involving five equipment features (N = 5) that influence decision making, and 15 options (M = 15) with different parameters for each feature that classify them higher or lower. The options are not considered here.

Obtaining experts' judgements

To collect the individual judgements from the owners of a wide range of sailing yachts, a survey was created and posted in several social media groups that included yacht owners.

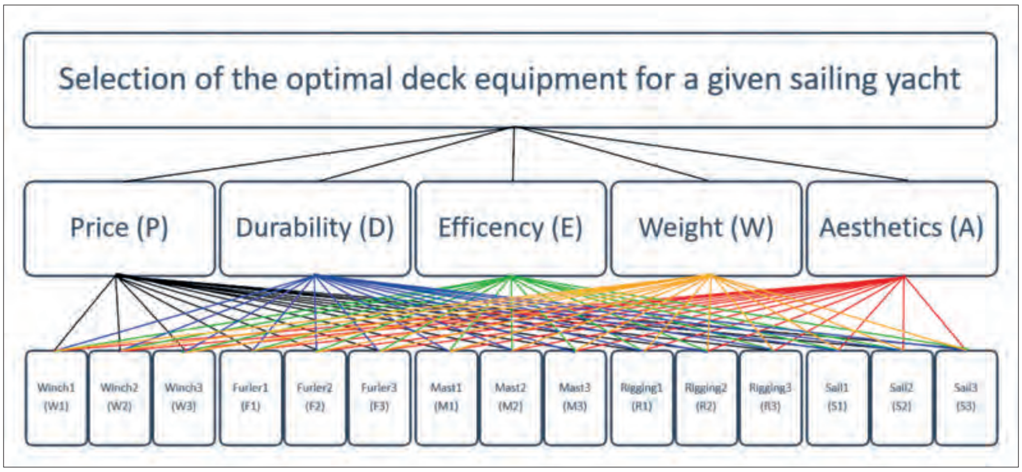

Fig. 2 Hierarchy structure tree of sailing yacht deck equipment applying the AHP method

It was also sent directly to a few yacht owners known to the authors.

The survey asked experts to compare the features listed in Table 1, in pairs. As there were five features, 10 comparisons were needed to cover all possible combinations. The respondents were asked to decide which of the two features was more important than the other, and to what extent, based on a rating scale from one to nine [25]. The scale was limited to odd numbers only (1, 3, 5, 7, 9) to make the comparison easier for the respondents. Furthermore, to check whether the preferences formed some kind of pattern, respondents were asked to provide additional information about the yacht they owned and which formed the subject of the pairwise comparison, such as the brand, hull type, main dimensions and purpose of the yacht. They were also asked to provide brief information on their sailing aspirations and age.

RESULTS

Experts' answers

A total of 48 responses were obtained from the experts, the vast majority of whom were owners of tourist/cruising yachts. The numbers of respondents for each type of yacht are presented in Table 2 below. The judgements are shown in the table in Appendix 1.

Tab. 2. Number of respondents by type of yacht owned

Yacht type owned by the respondent	Number of respondents
Racing/cruising yachts	2
Racing yachts	2
Expedition yachts	5
Seagoing cruising yachts	24
Inland/coastal cruising yachts	15

DETERMINATION OF YACHT OWNERS' PRIORITIES

To establish a priority ranking, each method mentioned in reference [26] was studied, and the outcome with the lowest consistency ratio (CR) value [25] was selected to ensure that the answers did not contradict each other. These priorities were determined for each respondent. Due to the number of responses involved, only a selection of results are shown in Table 3.

Tab. 3. Calculated individual priorities

No	Price	Mass	Efficiency	Durability	Aesthetics	CR
1	33.62%	15.19%	17.69%	26.07%	7.43%	0.1697
2	18.32%	4.76%	13.41%	52.95%	10.56%	0.1605
3	3.61%	14.29%	22.50%	50.89%	8.71%	0.2698
...						
11	16.40%	19.47%	19.47%	25.19%	19.47%	0.0339
12	26.91%	23.20%	8.61%	29.47%	11.80%	0.4303
...						

Verification

According to Saaty [25], a CR of greater than 0.1 indicates inconsistency, and the answer should be rejected. Unfortunately, an overwhelming majority of the answers to our survey were inconsistent (CR > 0.1, highlighted in red in Table 3). To investigate these discrepancies, a control participant with the highest CR was consulted, who reported that the priority weights determined by the AHP method on the basis of his answers were as he expected; in other words, he considered them subjectively correct. He also did not identify any substantive errors in the construction of the questionnaire.

Correcting respondents' answers

As the questionnaire was found to be intelligible and the priority ranking of the results was considered correct, the WAM method [31] was implemented to improve the CR.

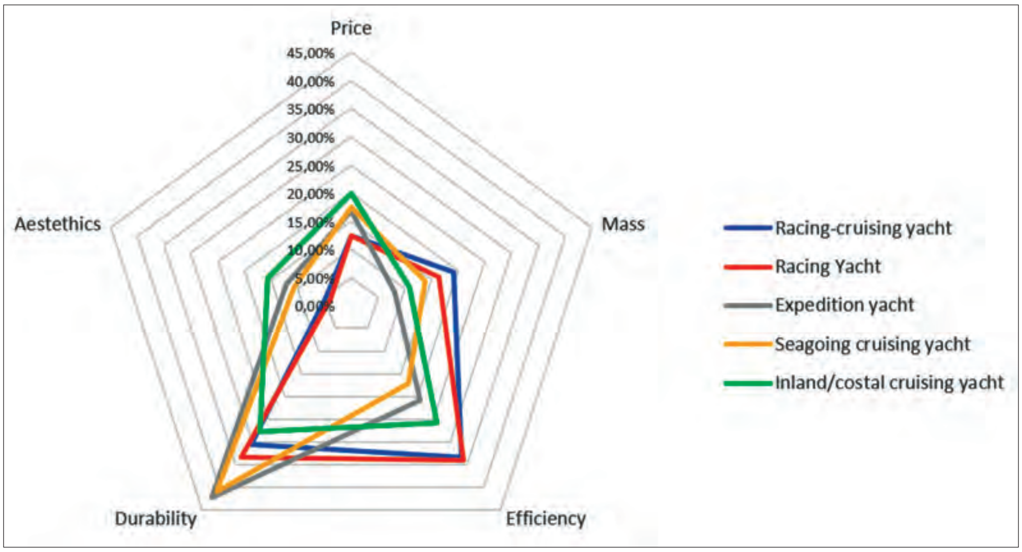

Fig. 3 Yacht owners' preferences, determined based on aggregated consistent individual judgements by yacht type

Tab. 4. *Preferences of sailing yacht owners*

Yacht type	Price	Mass	Efficiency	Durability	Aesthetics	CR
Racing/cruising yacht	12.45%	19.15%	33.23%	30.43%	4.75%	0.049
Racing yacht	12.41%	16.45%	33.90%	33.45%	3.78%	0.036
Expedition yacht	16.79%	8.03%	20.75%	42.22%	12.21%	0.026
Seagoing cruising yacht	17.46%	13.87%	17.18%	40.81%	10.68%	0.011
Inland/coastal cruising yacht	19.92%	10.90%	25.85%	27.71%	15.62%	0.005

Tab. 5. *Preferences of sailing yacht owners aggregated before CR improvement*

Yacht type	Price	Mass	Efficiency	Durability	Aesthetics	CR
Racing/cruising yacht	11.93%	17.76%	33.11%	33.03%	4.16%	0.084
Racing yacht	17.60%	15.56%	31.41%	32.24%	3.20%	0.314
Expedition yacht	16.85%	7.80%	20.31%	43.69%	11.35%	0.061
Seagoing cruising yacht	17.39%	13.53%	16.31%	42.34%	10.43%	0.045
Inland/coastal cruising yacht	19.79%	11.01%	25.01%	28.65%	15.53%	0.022

The individual judgements were corrected, and new priorities and CR values were calculated. The new results are shown in the table in Appendix 2.

Group aggregation results

After aggregating the results according to the values specific to each yacht (such as the overall length (LOA), breadth (B), displacement (D), etc.), according to the factors of slenderness, comfort, etc., it was concluded that the purpose of the yacht had the greatest correlation with the priorities. The individual judgements were divided into groups related to the type of yacht owned, and then aggregated using the geometric mean method [32]. As a result, the percentage degree of importance was obtained for each of the features of the deck equipment, depending on the type of yacht. The results are shown in Fig. 3 and Table 4.

In order to explore the impact of improving the respondents' answers on the relevance of the results, inconsistent judgments were also aggregated for comparison. It was found that the aggregation method using the geometric mean had a positive impact on the final CR, which was greater than 0.10 only for the group of racing yachts. The results obtained from this process were very similar to those of the improved answers, as shown in Fig. 4 and Table 5.

DISCUSSION

The use of a nine-point rating scale and a pairwise comparison of features seems to be a good method for determining priorities among yacht owners. The results showed that durability was the most important feature for expedition and seagoing cruising yachts, whereas the efficiency and mass of an accessory were the most important aspects for racing and racing/cruising yachts. The owners of inland/coastal cruising yachts had the most balanced priorities (regardless of the mass of an accessory) and valued aesthetics most highly.

The use of the AHP method imposes certain limitations on the results. The method used to conduct the study, the number of respondents, their questionable proficiency in the

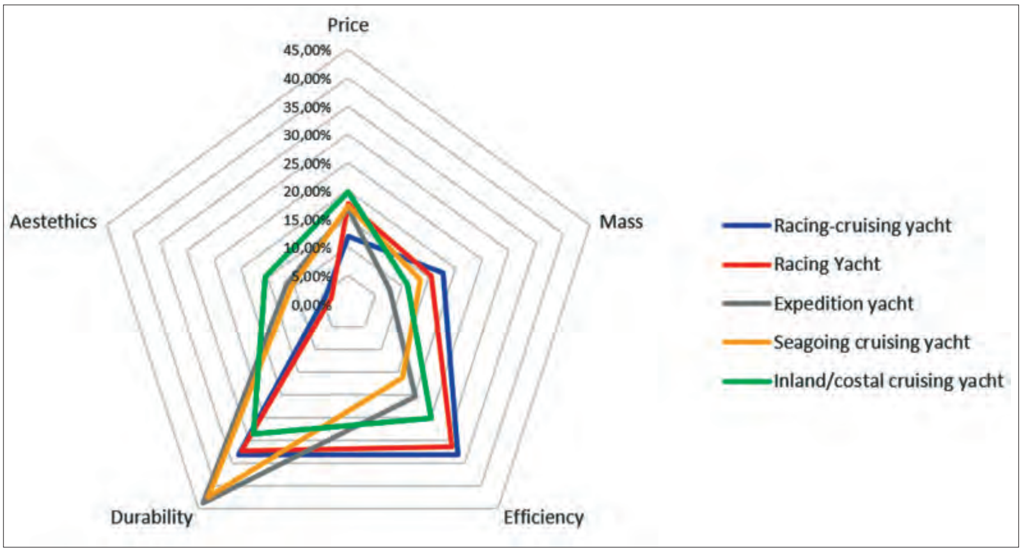

Fig. 4 Yacht owners' preferences determined based on aggregated inconsistent individual judgements by yacht type before CR improvement

field under study and the consistency of the matrix of their answers differ significantly from the recommendations made by the developer of the AHP, which may cast doubt on the results obtained in this work. However, as indicated by the control respondents, the prioritisation of their responses was in line with their expectations, even if the CR was greatly inflated. Furthermore, a comparison showed that the improvements to the CR had a negligible effect on the final results in terms of the priorities. The biggest error was found in the priority of the price reported by racing yacht owners, which reached 5%, whereas the error in the efficiency was 2.5% and the variability in all the other priorities was less than 1%. This error was due to the small number of respondents in this group (two people) and the fact that one of them gave very inconsistent answers.

Most of the inconsistent answers that required correction came from the owners of tourist yachts. Some of them pointed to the extreme advantage of feature 1 over feature 2, feature 2 over feature 3, and feature 3 over feature 1. As if all features were equally important to them. It can therefore be concluded that people engaged in hobby, tourist and recreational sailing do not have extensive expert knowledge of the field of equipment selection, and are not aware of the frequent need to compromise. Much less extreme responses were received from the owners of racing and expedition yachts, although only two responses were received from racing yacht owners, one of which was very inconsistent.

Research has shown that the preferences of yacht owners in terms of equipment vary depending on the purpose of the yacht. The purpose also affects their sailing aspirations; for example, an owner may take advantage of the qualities of an expedition yacht to go on long voyages. This, in turn, affects the owner's experience and expert knowledge.

The results obtained here indicate that the AHP method can be used as a priority setting tool. However, the question to be answered differs from the one that will be posed in the method as a decision problem, meaning that it needs to be very carefully thought out.

CONCLUSION

The aims of this study were to examine, classify and numerically rank the preferences of sailing yacht owners, and to explore whether these preferences depended on the type of yacht owned. The AHP method was applied to the research problem, and it was shown that these preferences were correlated with the purpose of the yacht owned by the respondent. A scheme for the numerical representation of these intangibles was presented, and may be valuable in the yacht design process, as these data are much more comprehensible and can be processed by a computer in this form.

The research results show that a group of people who own similar vessels have similar preferences and expectations towards their yachts and the related equipment. It can therefore be concluded that when designing a new yacht, properly determining the preferences of the future owner will lead to a more precise determination of the yacht's purpose. This, in turn, leads to a more accurate determination of the required nautical qualities, yacht size, equipment etc. When these preferences are expressed as numerical values, they can be used to automate the selection of certain elements, which can significantly improve the design process.

Since a relatively small group of yacht owners was involved in this study, it would be advisable to carry out further work with larger groups. Data collected from a much larger number of respondents might allow their preferences to be classified according to other factors, such as the sailing area or the size of the yacht. The use of these data in the design process is therefore the next step for future work. The classification of equipment components according to the features presented here, and assigning them to particular types of yacht, would be possible avenues to explore.

REFERENCES

1. G. Di Bucchianico and A. Vallicelli, "User-centered approach for sailing yacht design," in *Human Factors and Ergonomics in Consumer Product Design*, vol. 2, W. Karwowski, M. Soares, and N. Stanton, Eds., 2011, pp. 445–463.

2. S. Tavakoli, D. Khojasteh, M. Haghani, and S. Hirdaris, "A review on the progress and research directions of ocean engineering," *Ocean Engineering*, vol. 272, p. 113617, Mar. 2023, doi: 10.1016/j.oceaneng.2023.113617.

3. T. Song, T. Tan, and G. Han, „Research on preventive maintenance strategies and systems for in-service ship equipment," *Polish Maritime Research*, vol. 29, no. 1, pp. 85–96, Mar. 2022, doi: 10.2478/pomr-2022-0009.

4. A. Mancuso, A. Saporito, and D. Tumino, "Parametric hull design with rational Bézier curves," in *Lecture Notes in Mechanical Engineering*, Springer Science and Business Media Deutschland GmbH, 2021, pp. 221–227 doi: 10.1007/978-3-030-70566-4_36.

5. S. Khan, E. Gunpinar, K. M. Dogan, B. Sener, and P. Kaklis, "ModiYacht: Intelligent CAD tool for parametric, generative, attributive and interactive modelling of yacht hull forms," in *SNAME 14th International Marine Design Conference, IMDC 2022*, Society of Naval Architects and Marine Engineers, 2022, doi: 10.5957/IMDC-2022-311.

6. J. R. Binns and P. A. Brandner, "Dynamic interaction of breaking waves and inverted sailing yachts: Explaining the efficacy of mast height retention relative to vertical centre of gravity," *Ocean Engineering*, vol. 35, no. 17–18, pp. 1759–1768, Dec. 2008, doi: 10.1016/j.oceaneng.2008.08.013.

7. G. Guelfi and E. Canepa, "New development in 6-DOF algorithms for sailing yacht velocity prediction program and new insight in appendages force modelling," Master's Degree in Nautical Engineering, 2013.

8. C. A. Marchaj, *Aero-Hydrodynamics of Sailing*. Adlard Coles Nautical, 2000.

9. B. Augier, P. Bot, F. Hauville, and M. Durand, “Dynamic behaviour of a flexible yacht sail plan,” *Ocean Engineering*, vol. 66, pp. 32–43, 2013, doi: 10.1016/j.oceaneng.2013.03.017.

10. T. Matulja, L. Jedretić, and M. Hadjina, “Influence analysis of deck equipment positioning on performances in sailing,” pp. 101–109.

11. C. M. Rizzo and D. Boote, “Scantling of mast and rigging of sail boats: A few hints from a test case to develop improved design procedures,” 2010.

12. M. Pawłusik, R. Szłapczyński, and A. Karczewski, “Optimising rig design for sailing yachts with evolutionary multi-objective algorithm,” *Polish Maritime Research*, vol. 27, no. 4, pp. 36–49, Dec. 2020, doi: 10.2478/pomr-2020-0064.

13. W. Karwowski, M. M. Soares, and N. A. Stanton, “Human factors and ergonomics in consumer product design uses and applications,” CRC Press. 2011.

14. N. Kalkan, “Human factors and ergonomic considerations for super-fast boat design,” 2015. [Online]. Available: http://mybroadband.co.za/photos/showfull.

15. S. Ö. Felek, “Parametric sailing yacht exterior and interior design,” 2020, doi: 10.14744/tasarimkuram.2019.30085.

16. D. Harris, S. Mccartan, B. Verheijden, H. Groningen, and M. Lundh, “European Boat Design Innovation Group: The marine design manifesto. Human factors in safety management systems view project next generation civil flight deck concepts view project,” 2014. [Online]. Available: https://www.researchgate.net/publication/280065046.

17. M. Bilski, “Selected Human Factors in Marina Design,” *Procedia Manuf.*, vol. 3, pp. 1646–1653, 2015, doi: 10.1016/j.promfg.2015.07.482.

18. T. Bosma, “A human factor’s approach to mega yacht concept design,” Master of Philosophy, University of Strathclyde, Glasgow, 2013.

19. R. Gill, “Approaches to design,” *Des. Stud.*, vol. 1, no. 3, pp. 141–145, Jan. 1980, doi: 10.1016/0142-694X(80)90020-4.

20. P. von Buelow, ‘Using Evolutionary algorithms to aid designer of architectural structures,” in *Creative Evolutionary Systems*, Elsevier, 2002, pp. 315–336. doi: 10.1016/B978-155860673-9/50050-1.

21. L. Larson, R. E. Eliasson, and M. Orych, *Podstawy Projektowania Jachtów*, 4th ed., vol. 1. Warszawa: Almapress, 2014.

22. B. Branowski, M. Zabłocki, P. Kurczewski, and A. Walczak, „Selected issues in universal design of yachts for people with disabilities,” *Polish Maritime Research*, vol. 28, no. 3, pp. 4–15, Sep. 2021, doi: 10.2478/pomr-2021-0030.

23. E. Miszewska, M. Niedostatkiewicz, and R. Wisniewski, “The selection of anchoring system for floating houses by means of AHP method,” *Buildings*, vol. 10, no. 4, Apr. 2020, doi: 10.3390/BUILDINGS10040075.

24. M. Naujok, *Boat Interior Construction: A Bestselling Guide to DIY Interior Boatbuilding*, 2nd ed., vol. 1. Adlard Coles Nautical, 2002.

25. T. L. Saaty, *The Analytic Hierarchy Process: Planning, Priority Setting, Resource Allocation (Decision Making Series)*, vol. 1. McGraw-Hill, 1980.

26. W. C. H. Beck, A. Prusak, and P. Stefanów, “Budowa i analiza modeli decyzyjnych krok po kroku AHP-analityczny proces hierarchiczny,” 2014.

27. G. Khatwani and A. K. Kar, “Improving the cosine consistency index for the analytic hierarchy process for solving multi-criteria decision making problems,” *Applied Computing and Informatics*, vol. 13, no. 2, pp. 118–129, Jul. 2017, doi: 10.1016/j.aci.2016.05.001.

28. A. Jozaghi et al., “A comparative study of the AHP and TOPSIS techniques for dam site selection using GIS: A case study of Sistan and Baluchestan Province, Iran,” *Geosciences (Switzerland)*, vol. 8, no. 12, Dec. 2018, doi: 10.3390/geosciences8120494.

29. F. de Felice and A. Petrillo, “Absolute measurement with analytic hierarchy process: A case study for Italian racecourse,” *International Journal of Applied Decision Sciences*, vol. 6, no. 3, p. 209, 2013, doi: 10.1504/IJADS.2013.054931.

30. F. de Felice and A. Petrillo, “Multicriteria approach for process modelling in strategic environmental management planning,” *International Journal of Simulation and Process Modelling*, vol. 8, no. 1, p. 6, 2013, doi: 10.1504/IJSPM.2013.055190.

31. J. Benítez, X. Delgado-Galván, J. Izquierdo, and R. Pérez-García, “Improving consistency in AHP decision-making processes,” *Appl. Math. Comput.*, vol. 219, no. 5, pp. 2432–2441, Nov. 2012, doi: 10.1016/j.amc.2012.08.079.

32. J. Krejčí and J. Stoklasa, “Aggregation in the analytic hierarchy process: Why weighted geometric mean should be used instead of weighted arithmetic mean,” *Expert Syst. Appl.*, vol. 114, pp. 97–106, Dec. 2018, doi: 10.1016/j.eswa.2018.06.060.

POLISH MARITIME RESEARCH 4 (120) 2023 Vol. 30; pp. 31-42
10.2478/pomr-2023-0056

OPTIMAL UV QUANTITY FOR A BALLAST WATER TREATMENT SYSTEM FOR COMPLIANCE WITH IMO STANDARDS

Nguyen Dinh Thach
Phan Van Hung *
Faculty of Navigation, Vietnam Maritime University, Haiphong, Viet Nam

* Corresponding author: *phanvanhung@vimaru.edu.vn (Phan Van Hung)*

ABSTRACT

Ballast water management is an effective measure to ensure that organisms, bacteria and viruses do not migrate with the ballast water to other areas. In 2004, the International Maritime Organization adopted the International Convention on the Control and Management of Ballast Water and Ship Sediments, which regulates issues related to ballast water management. Many technologies have been researched and developed, and of these, the use of UV rays in combination with filter membranes has been shown to have many advantages and to meet the requirements of the Convention. However, the use of UV furnaces in ballast water treatment systems requires a very large capacity, involving the use of many high-power UV lamps. This not only consumes large amounts of electrical energy, but is also expensive. It is therefore necessary to find an optimal algorithm to enable the UV radiation for the UV controller in the ballast water sterilisation process to be controlled in a reasonable and effective manner. This controller helps to prolong the life of the UV lamp, reduce power consumption and ensure effective sterilisation. This paper presents a UV control algorithm and a controller for a UV furnace for a ballast water treatment system installed on a ship. The results of tests on vessels illustrate the effect of the proposed UV controller.

Keywords: UV Quantity Controller, Ship, Ballast Water Management, Viable Organisms Threat, Marine Environment.

NOMENCLATURE

$UV_{Dose}(k)$	– is the amount of UV at the current point
$UV_{Dose}(k-1)$	– is the amount of UV at the previous point
τ	– is the amount of water entering and leaving this region
V_a	– is the amount of water injected in one cycle τ
UV^a_{dose}	– is the amount of UV available in the amount of water injected into the V_j area
$V_b = V_j - V_a$	– is the amount of water remaining in volume V_j at time k–1
$UV^b_{dose}=UV^j_{dose}(k-1)$	– is the amount of UV in volume V_j at time k–1
T	– is the sampling time for the controller
dUV	– is the difference between two values dUV1 and dUV2
$U''(k)$	– is the value at the present time
$U''(k-1)$	– is the value at the time of the previous product

INTRODUCTION

Ships use ballast water to ensure stability and manoeuverability. This water is taken in and discharged as needed to counterbalance the hull stress caused by rough sea conditions, loading and unloading operations, or changes in fuel and water levels. In addition, ballast water helps to control the trim of the vessel, thereby ensuring it maintains the appropriate balance and posture during its voyage [1]–[5]. However, this water may harbour a diverse range of organisms, such as phytoplankton, zooplankton, bacteria, viruses, and macrofauna. The unintentional transfer of potentially invasive alien species (of which there are around 7,000 to 10,000 different types, including marine microbes, plants, and animals) occurs worldwide on a daily basis, leading to economic losses of tens of billions of US dollars annually [6]–[10]. The International Maritime Organization (IMO) [11] has identified numerous undesirable and invasive species associated with ballast water operations. The introduction of non-indigenous species through ballast water discharge can inflict severe consequences on local ecosystems, as invasive species have the potential to outcompete native species for resources, leading to significant alterations in the structure and function of an ecosystem [12]–[22]. Moreover, they have the capacity to introduce diseases and parasites, which can pose a threat to native species and disrupt the delicate balance of the food web. Certain invasive species can even modify water chemistry, potentially leading to eutrophication and the proliferation of harmful algal blooms. The impacts of ballast water discharge on aquatic ecosystems can also have significant economic repercussions. The introduction of invasive species can inflict damage on both commercial and recreational fisheries, diminishing their yields and affecting the livelihoods of those who depend on them. Furthermore, invasive species can cause harm to infrastructure and property, resulting in increased maintenance costs and decreased property values. The expenses associated with controlling and eradicating invasive species can be substantial, and their effects may persist for many years [6], [7], [19],[13], [23]–[29].

The Ballast Water Management Convention (Ballast Water Management Convention, 2004) was adopted by an IMO Diplomatic Conference in February 2004, and finally came into force globally on 8 September 2017. This convention requires ships to effectively treat their ballast water to remove or neutralise aquatic organisms and pathogens before discharging it into new locations. Its aim is to prevent the spread of invasive species and potentially harmful pathogens. Ships operating under this convention may be subjected to port state control in any port or offshore terminal of a party to the Ballast Water Management Convention; this inspection process may involve verifying the presence of a valid certificate and an approved ballast water management plan on board, checking the ballast water record book, and possibly conducting ballast water sampling in accordance with the guidelines for ballast water sampling (G2) to meet standards D1 and D2.

Ballast water management systems (D3) must be approved by the administration, and must adhere to the IMO guidelines. In 2016, revised guidelines for the approval of ballast water management systems (G8) were adopted, and were later transformed into a draft mandatory code for the approval of ballast water management systems (BWMSs), with particular reference to the procedure for approval of BWMSs that use active substances (G9).

All ships are required to comply with the D2 standard by 8th September 2024, and must ensure that their BWMSs meet the required criteria to protect marine ecosystems from potential invasive species and pathogens [11], [30]. Some essential water quality parameters necessary for effective marine environment management include physico-chemical factors such as temperature, colour, turbidity, salinity, dissolved oxygen, conductivity, suspended solids, and radioactivity. Monitoring and understanding these parameters are crucial to ensure the proper and sustainable management of the marine ecosystem [16], [31]–[34].

Several ballast water treatment systems or combinations of systems have been developed and put into practical use to ensure compliance with the standards set by the BWM Convention. It is worth mentioning that ballast water treatment systems that utilise UV rays in conjunction with a membrane filter are highly regarded for their efficient microbial treatment capability and cost-effectiveness [35]–[39].

Ballast water treatment systems using UV reactors often employ multiple high-power UV lamps within a single reactor. To ensure effective bactericidal results, precise control over the UV reactor is necessary, which involves maintaining a consistent UV lamp dose that adheres to the specified standard. In practice, the dose of UV radiation relies on two critical factors: the flow rate of water passing through the reactor, and the intensity of UV radiation within the UV reactor itself [29],[36], [37], [39],[40]. Identifying these factors and devising a control method for the UV reactor is a crucial area of research that requires careful study and implementation. At present, the ballast water treatment systems of many global brands employ a basic ON/OFF control measure for the UV reactor, although some continuously run the reactor at full capacity regardless of variations in water flow. As a result, the UV dose becomes unstable, leading to inefficient energy consumption and a shorter lifespan for the UV lamps. This article focuses on formulating and establishing optimal control equations for the UV reactor, with the aim of addressing the aforementioned drawbacks and improve the performance of systems such as these [37],[38],[29],[41]-[43].

CONTROL ALGORITHM FOR A UV FURNACE CONTROLLER

UV QUANTITY MODEL

The ballast water of the vessel has zero UV when it enters the UV furnace. During the process of flowing through the furnace, the ballast water is treated with UV rays, so the amount of UV gradually increases and until the desired amount is reached at the outlet. The distribution of the amount of UV over the length of the furnace is illustrated in Figure 1. The lower the flow rate of the water, the higher the UV level at the outlet, or the steeper the characteristic of the UV quantity according to the furnace location.

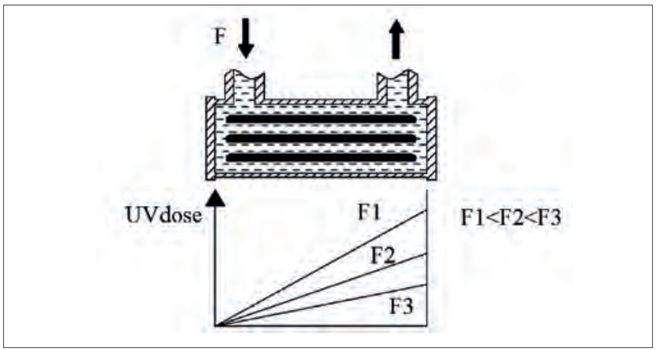

Fig. 1. Distributions of UV in the furnace when treating ballast water

To calculate the amount of UV involved, we divide the UV furnace into equal parts V_1, V_2, …, V_n. If these are small enough, the amount of UV at all points in each one of these parts can be considered constant. That is, the amount of UV in the hypothetical furnace is approximately distributed in each volume fraction V_j as shown in Figure 2.

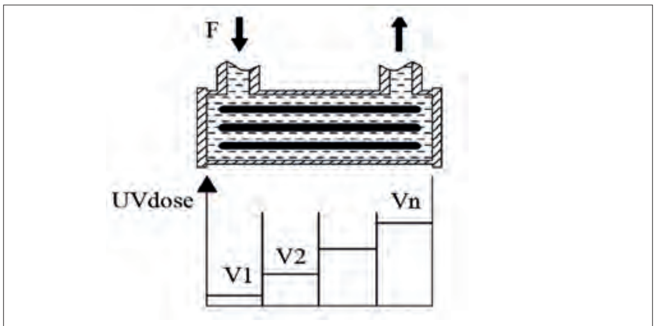

Fig. 2. Distribution of UV in the furnace according to the hypothesis

A PLC is a computing device based on a microcontroller, and the signals from the PLC are digital ones. Calculations with application operations for real-time control are performed by the PLC over a certain period of time called the calculation cycle τ. If the current time period of the PLC is the kth cycle (Figure 3), then the previous computation times are k–1, k–2, etc. and the subsequent computation times are k+1, k+2, etc.

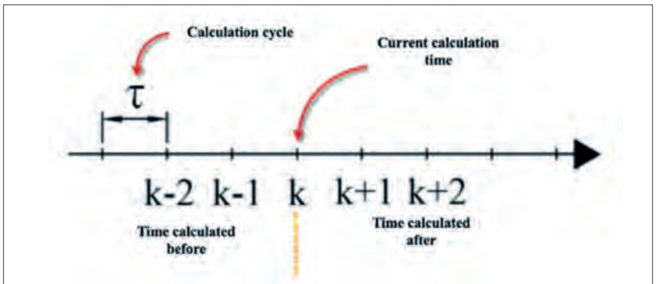

Fig. 3. Calculation periods for the PLC

As the PLC performs calculations with a period τ, we consider the variation in the amount of UV between two consecutive time points. If $UV_{Dose}(k)$ is the amount of UV at the current point, then $UV_{Dose}(k-1)$ is the amount at the previous point.

For a section V_j of the UV furnace (Figure 4), the amount of water entering and leaving this region in each calculation cycle τ is $V_a = F \cdot \tau$ (litres). In one cycle τ, the amount of UV received by the ultraviolet lamp is $i \cdot \tau$. The amount of UV in section V_j at time k $\left(UV^j_{dose}(k)\right)$ can then be approximated as follows:

$$UV^j_{dose}(k) = \frac{UV^j_{dose} \cdot V_a + UV^b_{dose} \cdot V_b}{V_j} + i \cdot \tau \quad (1)$$

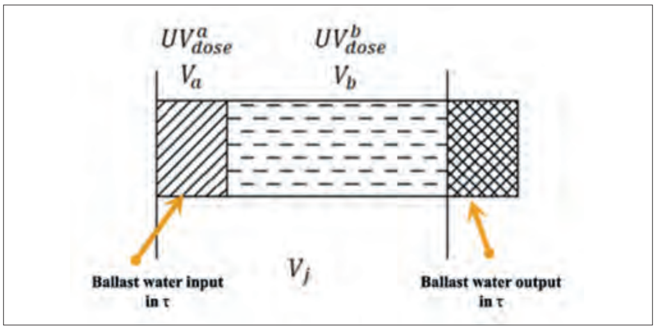

Fig. 4. Calculation of the amount of UV in a section V_j of the furnace

Transforming Eq. (1) gives:

$$UV^j_{dose}(k) = \frac{UV^a_{dose} \cdot F \cdot \tau + UV^j_{dose}(k-1) \cdot (V_j - F \cdot \tau)}{V_j} + i \cdot \tau \quad (2)$$

$$UV^j_{dose}(k) = UV^j_{dose}(k-1) \cdot \left(1 - \frac{F \cdot \tau}{V_j}\right) + UV^a_{dose} \cdot \frac{F \cdot \tau}{V_j} + i \cdot \tau \quad (3)$$

The amount of water pumped out of part V_j of the furnace in this time period τ will have a UV content equal to the amount of UV in part V_j at the previous time $UV^j_{dose}(k-1)$.

To ensure the correctness of Eq. (3), the calculation time τ and the volume of each part V_j must be chosen so that each time the PLC is updated, the amount of water flowing into each volume V_j does not exceed this volume. In other words, the condition $F_{max.\tau} < V_j$ ensures the accuracy of the UV calculation in Eq. (3).

For systems using PLCs, the calculation period is generally taken as 0.1 s. With a design rated flow rate of 55 litres per second, the maximum design flow for the furnace is 70 litres per second. Thus, the volume of each division $V_j > 70 \cdot 0.1 = 7$ litres. Thus, a UV oven with volume 78 litres can be divided into 10 parts at most. The smaller the component parts, the higher the accuracy, but the larger the computational volume; thus, we need to choose the lowest feasible volume with an acceptable calculation error.

In this study, we carry out a simulation where the amount of UV is calculated according to Eq. (3) for a number of divisions ranging from three to 10. Since the construction of the model is the same for each number of divisions, we only present an illustration for a model with five parts. Using Eq. (3), a mathematical model of the amount of UV at time k can be constructed as shown in Figure 5, where the UV furnace is divided into five equal parts, V1 to V5.

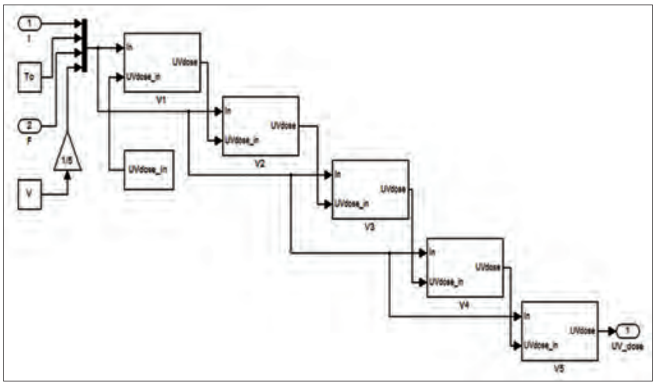

Fig. 5. Example of a model constructed to calculate the amount of UV in the furnace

To calculate the amount of UV at time k, we need to know the amount of UV at time k−1. The model in Figure 6 uses a memory block to save the value at the previous calculation time. In other words, if the input to the memory block is the value of $UV_{dose}(k)$, the output is the value of $UV_{dose}(k-1)$.

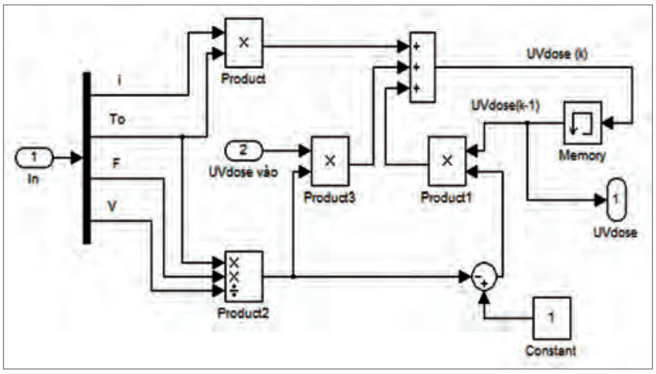

Fig. 6. Details of the calculation in block V_j

CONSTRUCTING THE CONTROL ALGORITHM

The entire UV furnace space is divided into five parts, V_1, V_2, …, V_5, and the amount of UV in each part is defined in Eq. (3). V_1 receives ballast water from outside the furnace, while V_5 contains the amount of water coming out of the furnace after treatment. The variables of the fuzzy control structure are defined as shown in Figure 7.

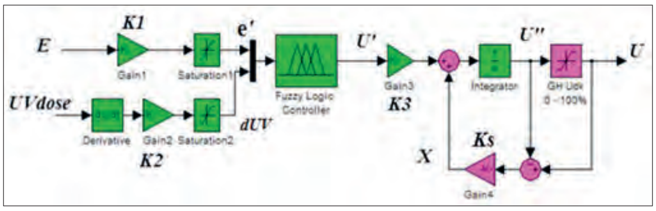

Fig. 7. Variables used by the fuzzy controller structure for the UV furnace

The two values e′ and dUV are determined as follows:

$$e' = \begin{cases} 1 & if\ E \cdot K_1 > 1 \\ E \cdot K_1 & if\ -1 \le E \cdot K_1 \le 1 \\ -1 & if\ E \cdot K_1 < 1 \end{cases} \tag{4}$$

$$e' = \begin{cases} 1 & if\ \Delta U_{dose} \cdot K_2/T > 1 \\ \Delta U_{dose} \cdot K_2/T & if\ -1 \le \Delta U_{dose} \cdot K_2/T \le 1 \\ -1 & if\ \Delta U_{dose} \cdot K_2/T < -1 \end{cases} \tag{5}$$

The output signal of the fuzzy controller U′ for varying values of the two inputs e′ and dUV can be calculated in many ways, for example based on the shape of the membership function, based on a transformation matrix, or by using an output signal table.

For PLC devices, constructing membership functions for the input and output variables requires considerable system resources and long computation times, which can affect the controllability of the PLC; hence, to calculate the value of the fuzzy control output U′ we use a table lookup method, as follows.

Step 1: Tabulate the output value U′ according to the input e′and dUV

From the fuzzy controller results obtained from the simulation using Matlab software, we enter some representative values in the ranges of the input variables e′ and dUV. The simulation then gives the output values U′ shown in Table 1.

Tab. 1. Output value U′ for varying values of input e′ and dUV

U′		dUV										
		−1	−0.8	−0.6	−0.4	−0.2	0	0.2	0.4	0.6	0.8	1
e′	1	0.5	0.5	0.5	0.5	0.5	0.5	0.3	0.15	0.05	0.02	0
	0.8	0.5	0.5	0.5	0.5	0.46	0.38	0.22	0.1	0.03	0	−0.4
	0.6	0.5	0.5	0.5	0.5	0.4	0.2	0.1	0.03	0	−0.1	−0.1
	0.4	0.5	0.5	0.5	0.36	0.23	0.1	0.03	0	−0.1	−0.4	−0.6
	0.2	0.5	0.44	0.36	0.2	0.1	0.03	0	−0.1	−0.3	−0.7	−0.9
	0	0.5	0.38	0.2	0.1	0.03	0	−0.1	−0.3	−0.8	−0.9	−1
	−0.2	0.3	0.22	0.1	0.04	0	−01	−0.4	−0.7	−0.9	−1	−1
	0.4	0.15	0.1	0.03	0	−0.1	−0.3	−0.7	−0.9	−1	−1	−1
	−0.6	0.05	0.03	0	−0.1	−0.3	−0.8	−0.9	−1	−1	−1	−1
	−0.8	0.02	0	−0.1	−0.4	−0.7	−0.9	−1	−1	−1	−1	−1
	1	0	−0.1	−0.1	−0.6	−0.9	−1	−1	−1	−1	−1	−1

Step 2: Determine the value of the fuzzy controller output U′

There are two cases in regard to the values of e′ and dUV at the input.

Case 1: The values of e′ and dUV match those in the table, in which case looking up the value from the table is simple. The value of the control output U′ is exactly the same as the value in the table.

Case 2: The values of e′ and dUV do not coincide with any value in the table, and their values are between two values in the table. Suppose e′ is between two values e'_1 and e'_2, and dUV is between two values dUV_1 and dUV_2. Then, as e′ and dUV each have two values, there are four cells in Table 2 below.

Tab. 2. Calculation of the value of U′

U′		dUV	
		dUV_1	dUV_2
e′	e'_1	A_1	B_1
	e'_2	A_2	B_2

To construct a formula for the lookup table of U′ values, we first derive a formula to determine the value of y_K corresponding to the value of x_k, knowing that the point $K(x_K, y_K)$ lies between two points $M(x_1, y_1)$ and $N(x_2, y_2)$, as shown in Figure 8. The equation for the line MN has the form:

$$\frac{y-y_2}{y_1-y_2} = \frac{x-x_2}{x_1-x_2} <-> y = \frac{y_1-y_2}{x_1-x_2} \cdot (x-x_2) + y_2 \tag{6}$$

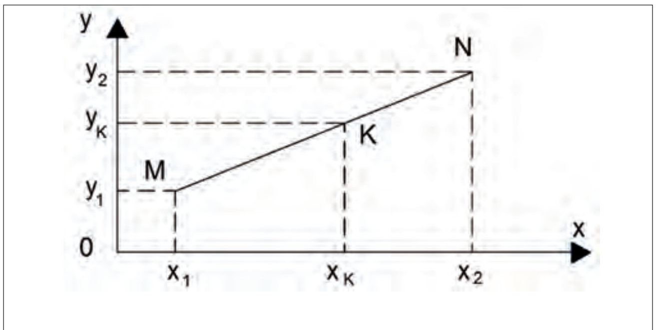

Fig. 8. Determining the value of yK in a segment MN

The value of y_k is then determined from the value of x_k using Eq. (7):

$$y_K = \frac{y_1-y_2}{x_1-x_2} \cdot (x_K-x_2) + y_2 \tag{7}$$

The method used to determine the control output value U′ is illustrated in Figure 9. We apply Eq. (7) to calculate the value of U_1 for segment A_1A_2 and U_2 for segment B_1B_2 depending on the value of e′, as follows:

$$U_1 = \frac{A_1-A_2}{e'_1-e'_2} \cdot (e'_1 - e'_2) + A_2$$
$$U_2 = \frac{B_1-B_2}{e'_1-e'_2} \cdot (e'_1 - e'_2) + B_2 \tag{8}$$

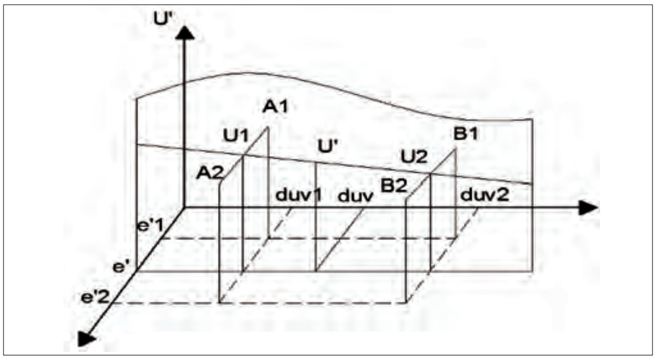

Fig. 9. Method used to determine the value of the control output U′ from the lookup table

We apply Eq. (7) to calculate the value of U′ on segment U_1U_2 in dUV as follows:

$$U' = \frac{U_1-U_2}{dUV_1-dUV_2} \cdot (dUV - dUV_2) + U_2 \tag{9}$$

Here, we consider an example where we determine the value of U′ for two inputs, e′ = 0.1 and dUV = −0.35. In this case, e′will lie between two values $e'_1 = 0.2$ and $e'_2 = 0$, and dUV between two values $dUV_1 = -0.4$, $dUV_2 = -0.2$. We can use the lookup table to get four values, A_1, A_2, B_1, and B_2, as shown in Figure 10.

$$U_1 = \frac{A_1-A_2}{e_1-e_2} \cdot (E'-e_2) + A_2 = \frac{0.2-0.1}{0.2-0} \cdot (0.1-0) + 0.1 = 0.15$$
$$U_2 = \frac{B_1-B_2}{e_1-e_2} \cdot (E'-e_2) + B_2 = \frac{0.1-0.03}{0.2-0} \cdot (0.1-0) + 0.03 = 0.065$$
$$U' = \frac{U_1-U_2}{dUV_1-dUV_2} \cdot (dUV-dUV_2) + U_2 = \frac{0.15-0.065}{-0.4+0.2} \cdot (-0.35+0.2) + 0.065 = 0.129$$

U'		dUV										
		-1	-0.8	-0.6	-0.4	-0.2	0	0.2	0.4	0.6	0.8	1
e	1	0.5	0.5	0.5	0.5	0.5	0.5	0.3	0.15	0.05	0.02	0
	0.8	0.5	0.5	0.5	0.5	0.46	0.38	0.22	0.1	0.03	0	-0.4
	0.6	0.5	0.5	0.5	0.5	0.4	0.2	0.1	0.03	0	-0.1	-0.1
	0.4	0.5	0.5	0.5	0.36	0.23	0.1	0.03	0	-0.1	-0.4	-0.6
	0.2	0.5	0.44	0.36	0.2	0.1	0.03	0	-0.1	-0.3	-0.7	-0.9
	0	0.5	0.38	0.2	0.1	0.03	0	-0.1	-0.3	-0.8	-0.9	-1
	-0.2	0.3	0.22	0.1	0.04	0	-0.1	-0.4	-0.7	-0.9	-1	-1
	-0.4	0.15	0.1	0.03	0	-0.1	-0.3	-0.7	-0.9	-1	-1	-1
	-0.6	0.05	0.03	0	-0.1	-0.3	-0.8	-0.9	-1	-1	-1	-1
	-0.8	0.02	0	-0.1	-0.4	-0.7	-0.9	-1	-1	-1	-1	-1
	-1	0	-0.1	-0.1	-0.6	-0.9	-1	-1	-1	-1	-1	-1

Fig. 10. Lookup table of output values U′

To determine the output signal U, it is necessary to calculate the value of the output U″. Based on the control structure in Figure 7, we have:

$$U''(s) = \frac{1}{s} \cdot \left(K_3 \cdot U'(s) + X(s)\right) \tag{10}$$

where $X(s) = K_s\left(U(s) - U''(s)\right)$ is the value of the anti-saturation integral. We convert Eq. (10) to the Z domain using the Tustin method:

$$s = \frac{2}{T} \cdot \frac{z-1}{z+1} \tag{11}$$

to get Eq. (12) in the Z domain:

$$U''(z) = \frac{T}{2} \cdot \frac{z+1}{z-1} \cdot \left(K_3 U'(z) + X(z)\right)$$

$$\left(1-\frac{1}{z}\right)\cdot U''(z)=\frac{T}{2}\cdot\left(1+\frac{1}{z}\right)\cdot\left(K_3\cdot U'(z)+X(z)\right) \quad (12)$$

To implement Eq. (12) in the PLC, we transform it into a differential equation as follows.

$$U''(k)-U''(k-1)=$$
$$\frac{T}{2}\cdot\left(K_3\cdot U'(k)+K_3\cdot U'(k-1)+X(k)+X(k-1)\right)$$

$$U''(k)=U''(k-1)+\frac{T}{2}\cdot$$
$$\left(K_3\cdot U'(k)+K_3\cdot U'(k-1)+X(k)+X(k-1)\right)$$

$$U''(k)=U''(k-1)+\frac{T}{2}\cdot$$
$$\left(K_3\cdot U'(k)+K_3\cdot U'(k-1)+X(k-1)\right)+\frac{T}{2}\cdot X(k) \quad (13)$$

If we set $F=U''(k-1)+\frac{T}{2}\cdot\left(K_3\cdot U'(k)+K_3\cdot U'(k-1)+X(k-1)\right)$, then

$$U''(k)=F+\frac{T}{2}\cdot X(k) \quad (14)$$

To calculate U″(k), we consider three cases:
Case 1: $U''(k)\in[0,1]$

Then $X(k)=k_s\cdot\left(U(k)-U''(k)\right)=0$. From Eq. (14), we have:

$$U''(k)=F \quad (15)$$

Case 2: $U''(k)>1$

Then $X(k)=k_s\cdot\left(1-U''(k)\right)$, and from Eq. (14) we get:

$$U''(k)=\frac{2}{2+k_s\cdot T}\left(F+\frac{T}{2}\cdot k_s\right) \quad (16)$$

Case 3: $U''(k)<0$

Then $X(k)=k_s\cdot\left(0-U''(k)\right)$, and from Eq. (14), we get:

$$U''(k)=\frac{2F}{2+k_s\cdot T} \quad (17)$$

The controller output after the limiting step is determined by the following system of equations:

$$U(k)=\begin{cases}1 & khi\ \ U''(k)>1\\ U''(k) & khi\ \ 0\le U''(k)\le 1\\ 0 & khi\ \ U''(k)<0\end{cases} \quad (18)$$

The algorithm for calculating the value of the fuzzy controller in the PLC for the UV furnace is summarised in Figure 11.

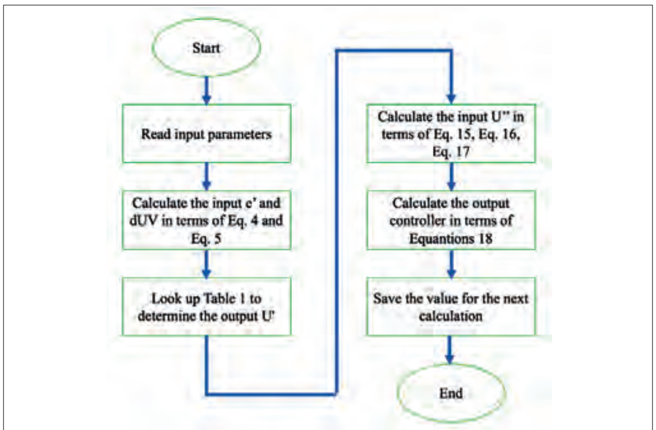

Fig. 11. Algorithm for calculating the output value of the fuzzy control

DEVELOPMENT OF THE UV QUANTITY CONTROLLER

The basic components of a fuzzy controller are the fuzzy stage, the composition rule, and the defuzzification stage. Since basic fuzzy controllers are only capable of processing current signals, these are called static fuzzy controllers. To extend their application to dynamic control problems, the necessary kinematics are added to the basic fuzzy controller to provide it with the derivative or integral value of the signal. When used with these kinematics, the basic fuzzy controller is called a dynamic fuzzy controller.

For the ballast water treatment UV reactor, this is a nonlinear object. This nonlinearity is expressed in the relationship between the flow rate F and the amount of UV, and between the UV lamp control signal (U_{dk}) and the UV intensity. The relationship between UV_{dose} and the flow F is described in general terms by the system of equations in (13) and (14). These systems are difficult to control with PIDs, and experiments are required to determine the accuracy of the controller. In this case, other controllers are often used (for example based on fuzzy control, neural control, or adaptive control) for the system. In the present paper, we build a fuzzy controller, as this has certain outstanding features: (i) the control is based on the operator's experience; (ii) there no need for an object model to set up the controller; and (iii) it can be applied to industrial control devices such as PLCs or microprocessors [43].

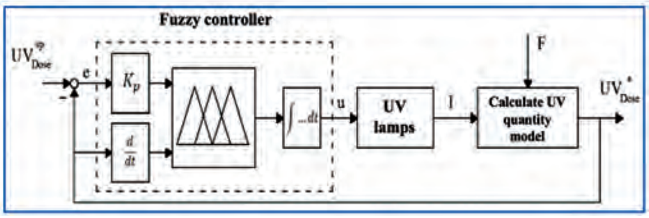

Fig. 12. Structure fuzzy controller for UV reactor

The fuzzy control structure for the UV reactor is shown in Figure 12. In this structure, the controller has two inputs and one output signal. The output signal of the controller is in the range [0,1], corresponding to a UV intensity of the lamp of between zero and I_{max}.

The two inputs of the fuzzy controller are: wrong order between the UV amount set and the UV amount of water treated in the reactor. Rate of variation of UV content of ballast water.

To facilitate the construction of the model and the signal processing step, all of the input values to the fuzzy controller are converted to standard values between –1 and 1. To do this, we need to pass additional inputs in the form of the coefficients K_1 and K_2, as shown in Figure 13.

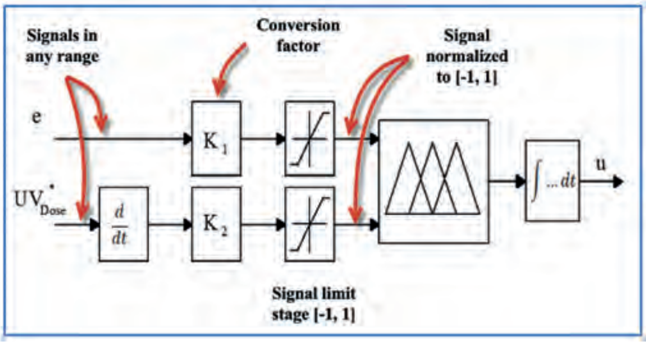

Fig. 13. Fuzzy control structure with additional inputs in the form of value conversion factors

We then determine the conversion factor K_1 for the control error input e. The coefficient K_1 is used to convert the range of the deviation e from $[-e_0, e_0]$ to the range $[-1, 1]$ for input into the fuzzy controller. The range $[-e_0, e_0]$ should be chosen so that for the smallest value of the limit e_0, the change in e is greatest in this interval.

To ensure the good operation and impact of the bias $e_0 = \frac{UV^{dm}_{dose}}{10}$, the coefficient K_1 is determined using Eq. (19):

$$K_1 = \frac{1}{e_0} = \frac{10}{UV^{dm}_{dose}} = \frac{10}{200} = 0.05 \tag{19}$$

We determine the conversion factor K_2 for the variable rate input UV_{dose} as follows. K_2 is used to convert the range of values for the rate of change dUV_{dose}/dt from $[-dUV_0, dUV_0]$ to the range $[-1,1]$ to feed into the fuzzy controller. Based on the simulated response of the rate of change of UV in the reactor, the rate of change of UV_{dose} at the fastest time has the value $dUV_{dose}/dt = 10$. Thus, the dUV_{dose}/dt variable takes values in the range $[-10, 10]$, or in other words, the coefficient $K_2 = 1/10 = 0.1$.

The construction of the fuzzy controller was first carried out in Matlab to simulate and verify the operation before applying it to real objects. Simulation can help to shorten the equipment testing time, reduce costs and allow us to gain experience in controlling the system. Here, we used a Sugeno fuzzy controller [46] with two inputs (the signal bias e and the variable dUV_{dose}/dt) and one output (Output 1). This controller was implemented in Matlab with the Fuzzy Toolbox, as shown in Figure 14. The next step was to build linguistic variables for the inputs/outputs and to create membership functions corresponding to these linguistic variables for each input/output. To simplify the process of building the membership function for the input linguistic variables, we define linguistic values as shown in Table 3.

Tab. 3. Linguistic variables for signal input

Linguistic variable	Meaning	Value
GN	Great negative	–1
LN	Large negative	–0.6
SN	Small negative	–0.3
ZE	Zero	0
SP	Small positive	0.1
LP	Large positive	0.3
GP	Great positive	0.5

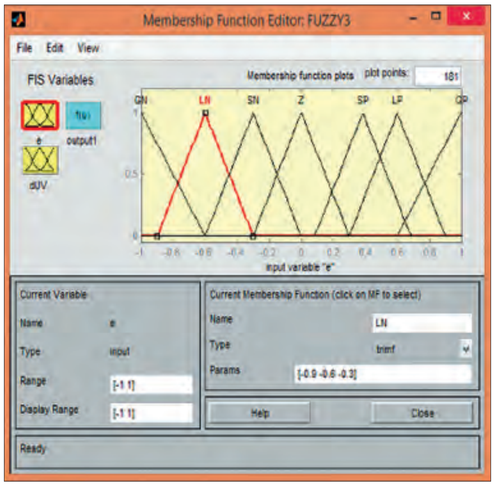

Fig. 14. Fuzzy controller toolbox with the membership function of the input bias UV

After building the membership function for the inputs, we constructed the membership function for the outputs. From the UV intensity response characteristics of the system, we know that the rate of increase in the UV intensity is limited by the response of the lamp, meaning that this is a factor that cannot be further increased. The rate of reduction in UV intensity is also high. We therefore created an asymmetric controller characteristic in which the control signal used to increase the UV intensity changed more slowly than the rate of decrease in the UV intensity of the reactor. This meant that the control characteristic could eliminate the problem whereby the system response cannot keep up with the changing speed of the control, which affects the output quality of the system. To build the output signal, we used language variables for the output with the values shown in Table 3.

When the two inputs (e, dUV_{dose}/dt) and the fuzzy rule had been built, the controller was able to completely determine the explicit value of the output U_{dk} according to the values of the input. The relationship between U′ and the two input signals (e, dUV_{dose}/dt) is shown graphically in Figure 10. In this feature, Output 1 of the controller varies in the range $[-1, 0.5]$. With these characteristics, the controller will have a slower increase rate of 1/2 than the decrease rate of the signal. As mentioned above, this deviation in the rate of increase/decrease is found purely based on practical experience, and depends on the rates of increase and decrease in the UV intensity in the reactor being asymmetric. This surface is also the basis for building algorithms for fuzzy controllers on PLC.

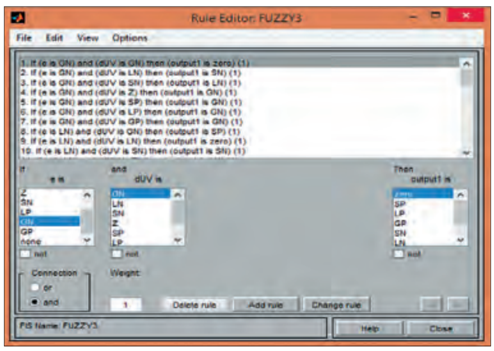

Fig. 15. Developing the fuzzy rule in Matlab software

Tab. 4. Fuzzy rule for controller

Output 1		dUV_{dose}/dt						
		GN	LN	SN	Z	SP	LP	GP
e	GN	Z	SN	LN	GN	GN	GN	GN
	LN	SP	Z	SN	LN	GN	GN	GN
	SN	LP	SP	Z	SN	LN	GN	GN
	Z	GP	LP	SP	Z	SN	LN	GN
	SP	GP	GP	LP	SP	Z	SN	LN
	LP	GP	GP	GP	LP	SP	Z	SN
	GP	GP	GP	GP	GP	LP	SP	Z

With the proposed control structure, after building the component models, we get the simulation model shown in Figure 11 and Table 3, where the input is in the range [−1,1], and the controller output after the integral is in the range [0%,100%].

EVALUATION OF BIOCHEMICAL EFFICIENCY DURING TESTING OF BALLAST WATER TREATMENT SYSTEM ACCORDING TO IMO STANDARD G8

CONFIGURATION FOR ON-BOARD TESTING

The IMO G8 provision pertains to the testing of ballast water treatment systems on board vessels. According to these regulations, testing of a ballast water treatment system requires the installation of such a system on a ship where the normal ballast operations are carried out. This means that the ballast system of the ship should be fully operational in the usual manner.

To conduct tests on the proposed ballast water treatment system, a specific procedure was followed. The ballast water treatment system was installed on the ship, and was configured as shown in Figure 16. This configuration diagram served as a guide for the proper installation and arrangement of the system components to ensure that it functioned as intended. This setup allowed for the systematic testing and evaluation of the system's performance under real-world conditions, and ensured that it met the requirements and standards set out in the IMO G8 regulations.

ONBOARD TEST PROCEDURE

In accordance with the requirements outlined in G8, shipboard testing of ballast water treatment systems is a comprehensive process that is conducted over a minimum duration of six months. During this testing period, there are specific criteria that must be met, and a series of test cycles need to be completed successfully. Each test cycle comprises several distinct steps, which ensure a thorough evaluation of the performance of the treatment system, as follows:

- Pumping ballast water into the control tank: The initial step of the test cycle involves pumping ballast water into a designated control tank on the ship. This control tank serves as a reference point for monitoring the quality and condition of the ballast water before it undergoes treatment.
- Pumping ballast water into the ballast tanks for treatment: After filling the control tank, the next step is to pump ballast water from this tank into the ship's ballast tanks, which form part of the treatment system. It is at this point that the ballast water will be subjected to the treatment process designed to eliminate or reduce the concentration of aquatic organisms.
- Draining the ballast water from the control tank: Once the ballast water has been transferred to the tanks of the treatment system, the control tank is emptied or drained. This step is essential for maintaining consistency in the testing process, as it allows for comparison between treated and untreated water samples.
- Discharging ballast water from treated ballast tanks: Following the treatment process, the treated ballast water is discharged from the tanks. In this step, the effectiveness of the treatment system is evaluated in terms of rendering the ballast water compliant with environmental regulations, particularly concerning the control of invasive species and pathogens.

To meet the IMO G8 requirements, it is crucial that this sequence of work steps is repeated continuously for at least six months. The testing process must also yield a minimum of three consecutive successful test cycles to demonstrate the consistent and reliable performance of the ballast water treatment system for various operating conditions and environmental factors. This stringent testing protocol helps ensure that ships' BWMSs meet international standards for environmental protection.

BALLAST WATER SAMPLING AND ANALYSIS DURING TESTING

(1) Number of samples in one test cycle

Three input water samples are taken during the process of pumping ballast water into the counter-egg tank (taken at the beginning, middle and end of the process).

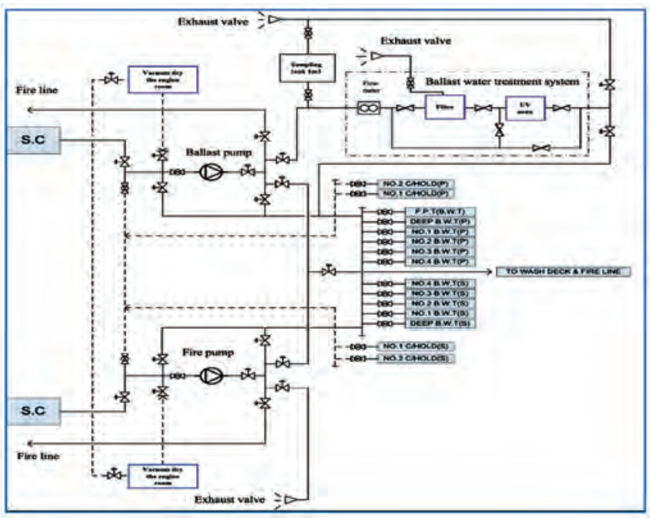

Fig. 16. Diagram showing an example of a test configuration for a ballast water treatment system on a ship

Three samples are taken from the discharge line during the process of discharging the ballast water from the egg tank (taken at the beginning, middle and end stages). A total of nine samples are taken from the discharge line during the process of discharging the ballast water from the treated ballast tank (three samples in the first stage, three in the middle stage, and three in the final stage).

(2) Test criteria for samples

For each sample, the following criteria need to be met:

Environmental parameters: temperature, salinity (PSU), TSS (mg/l), DOC (mg/l) and POC (mg/l);

Number of living organisms: 50 μm/m^3;

Number of living organisms: 10–50 μm/1 ml;

Vibrio cholerae (cholera): cfu/100 ml;

Escherichia coli group (intestinal bacilli): cfu/100 ml;

Intestinal enterococci group: cfu/100 ml;

Heterotrophic bacteria: cfu/1 ml.

(3) Criteria for a successful test cycle

Step 1: Inlet water requirement

The input water must satisfy the following criteria:

Number of living organisms with size ≥ 50μm: 100/m^3;

Number of living organisms 10–50 μm in size: 100/1 ml

Step 2: Requirements for water samples during discharge of the ballast water from the control tank

Number of living organisms 50 μm in size: 10/m^3;

Number of living organisms 10–50μm in size: 10/1 ml

Step 3: The requirements for water samples during the discharge of ballast water from the treated ballast tank are considered to comply with the D2 discharge standard (IMO BWM Convention).

EXPERIMENTAL RESULTS AND DISCUSSION

On-board testing of the ballast water treatment system was completed over a test period exceeding six months. Testing was carried out in accordance with the IMO Guidelines for the Approval of Ballast Water Treatment Systems (G8). The collection and analysis of ballast water samples was carried out by the Institute of Marine Environment and Resources under the supervision of the Vietnam Register. The test results for the ballast water treatment system according to IMO's G8 standard are presented in Table 5, where the average value of a parameter for three samples is recorded in the corresponding cell in the results.

The test results in Table 5 show that the input parameters for the water were in accordance with the requirements of the IMO. The parameters for the ballast water discharge from the reference tank are also in accordance with the requirements of IMO, and the parameters of the treated water from the ballast tank met the IMO standard D2.

The measurement results corresponding to the actual amounts of UV when operating on board under different conditions show that the controller works well, and the parameters of the system are suitable at the design value. The Vietnam Institute of Marine Environment and Resources has confirmed that various samples of ballast water after treatment from the commissioning testing conducted with the subject BWMS are considered to comply with D2 discharge standard (IMO BWM Convention).

CONCLUSION

Ballast water management is a vital measure to ensure that organisms, bacteria, and viruses do not spread to new areas when discharging ballast, in accordance with the International Convention on the Control and Management of Ballast Water and Ship Sediments established in 2004, which regulates ballast water management issues. The UV reactor used in a ballast water treatment system often requires multiple high-power UV lamps within a single unit, due to its large capacity. These high-power UV lamps consume significant electrical energy, and impose high costs.

Efficiently controlling UV radiation during the water disinfection process is therefore essential to extend the lifespan of UV lamps, reduce energy consumption, and ensure effective antimicrobial treatment. This research has focused on developing optimal equations 19 (and Eqs. (4)–(18)) and a controller for a UV reactor in a ballast water treatment system (Figs. 11–13) installed on a ship. Experimental results from five ships have been presented to demonstrate the efficiency achieved by the proposed UV controller. When the proposed control algorithm is applied, the UV lamp shines at the appropriate intensity to meet the ballast water treatment requirements, rather than continuously operating at high intensity. This results in significant energy savings compared to a system without a UV

Tab. 5. Measured values

Name of ship	Treatment rated capacity (m^3/h)	IMO standard		Sampling period
		Viable organisms ≥50μm (org/m^3): <10	Viable organisms 10-50μm (org/ml): <10	
ANBIEN BAY	500	4	6.8	10h50–14h00, 02/06/2022
TTC PIONEER	200	No live organisms detected	7.8	11h10–12h15, 06/06/2022
ROYAL 89	100	6	4.5	09h50–10h40, 15/08/2022
TRACY	150	1	2.9	15h00–15h30, 20/09/2022
AN THINH PHU 08	100	1	0.2	08h00–09h00, 14/10/2022
THAI BINH 35	50	1	1.7	11h30–12h10, 02/11/2022

controller. Furthermore, operating at low intensity rather than continuously at high intensity can help prolong the life of the UV lamp.

The development of effective treatment approaches such as these can enhance ballast water management, thus mitigating the negative impacts of invasive species on marine environments, economies, and human well-being.

ACKNOWLEDGMENTS

The authors would like to thank their colleagues at Vietnam Maritime University, Vietnam Register, Institute of Marine Environment and Resources, and the shipping companies for their assistance in this work. We also appreciate the constructive suggestions from the anonymous reviewers, which were invaluable in improving the quality of the manuscript.

REFERENCES

1. G. Altug, S. Gurun, M. Cardak, P. S. Ciftci, and S. Kalkan, "The occurrence of pathogenic bacteria in some ships' ballast water incoming from various marine regions to the Sea of Marmara, Turkey," *Mar. Environ. Res.*, vol. 81, pp. 35–42, Oct. 2012, doi: 10.1016/j.marenvres.2012.08.005.

2. L. J. Aridgides, M. A. Doblin, T. Berke, F. C. Dobbs, D. O. Matson, and L. A. Drake, "Multiplex PCR allows simultaneous detection of pathogens in ships' ballast water," *Mar. Pollut Bull.*, vol. 48, no. 11, pp. 1096–1101, Jun. 2004, doi: 10.1016/j.marpolbul.2003.12.017.

3. J. Chen, Y. Lin, J. Zhou Huo, M. Xia Zhang, and Z. Shang Ji, "Optimization of ship's subdivision arrangement for offshore sequential ballast water exchange using a non-dominated sorting genetic algorithm," *Ocean Engineering*, vol. 37, no. 11, pp. 978–988, Aug. 2010, doi: 10.1016/j.oceaneng.2010.03.012.

4. I. Staffell and P. Balcombe, "How to decarbonise international shipping: options for fuels, technologies and policies," *Energy Convers. Manag.*, [Online]. Available: https://www.academia.edu/38669854/How_to_decarbonise_international_shipping_options_for_fuels_technologies_and_policies

5. P. Van Hung, K.-S. Kim, L. Q. Tien, and N. M. Cuong, "Distribution of oil spill response capability through considering probable incident, environmental sensitivity and geographical weather in Vietnamese waters," *Journal of International Maritime Safety, Environmental Affairs, and Shipping*, vol. 2, no. 1, pp. 31–41, Nov. 2018, doi: 10.1080/25725084.2018.1511240.

6. G. Drillet et al., "Improvement in compliance of ships' ballast water discharges during commissioning tests," *Mar. Pollut. Bull.*, vol. 191, p. 114911, Jun. 2023, doi: 10.1016/j.marpolbul.2023.114911.

7. P. E. Neill and M. Arim, "Human Health Link to Invasive Species," in *Encyclopedia of Environmental Health*, pp. 570–578, 2019, doi: 10.1016/B978-0-12-409548-9.11731-2.

8. S. Gollasch, C. L. Hewitt, S. Bailey, and M. David, "Introductions and transfers of species by ballast water in the Adriatic Sea," *Mar. Pollut. Bull.*, vol. 147, pp. 8–15, Oct. 2019, doi: 10.1016/j.marpolbul.2018.08.054.

9. O. Vidjak *et al.*, "Zooplankton in Adriatic port environments: Indigenous communities and non-indigenous species," *Mar. Pollut. Bull.*, vol. 147, pp. 133–149, Oct. 2019, doi: 10.1016/j.marpolbul.2018.06.055.

10. P. Van Hung, K.-S. Kim, and M. Lee, "Cooperative response to marine hazardous and noxious substances and oil spill incidents in the ASEAN region," *Australian Journal of Maritime & Ocean Affairs*, vol. 11, no. 1, pp. 61–72, Jan. 2019, doi: 10.1080/18366503.2018.1559524.

11. IMO, International Maritime Organization [IMO], 2004. International Convention for the Control and Management of Ships' Ballast Water and Sediments. International Maritime Organization, London. [Online]. Available: http://www.imo.org/en/About/Conventions/List ofConventions/Pages/International- Convention-for-the-Control-and-Management-of-Ships%27-Ballast-Water-and-Sediments-(BWM).aspx

12. G. Elidolu, S. I. Sezer, E. Akyuz, O. Arslan, and Y. Arslanoglu, "Operational risk assessment of ballasting and de-ballasting on-board tanker ship under FMECA extended evidential reasoning (ER) and rule-based Bayesian network (RBN) approach," *Reliab. Eng. Syst. Saf.*, vol. 231, p. 108975, Mar. 2023, doi: 10.1016/j.ress.2022.108975.

13. D. K. Gray, I. C. Duggan, and H. J. Macisaac, "Can sodium hypochlorite reduce the risk of species introductions from diapausing invertebrate eggs in non-ballasted ships?," *Mar. Pollut. Bull.*, vol. 52, no. 6, pp. 689–695, Jun. 2006, doi: 10.1016/j.marpolbul.2005.11.001.

14. P. P. Sangave, A. Mukherjee, and A. Pandit, "Ballast water treatment using hydrodynamic cavitation," Nov. 2014. [Online]. Available: https://www.semanticscholar.org/paper/Ballast-Water-Treatment-Using-Hydrodynamic-Sangave-Mukherjee/ ca3f5edcc2a28ba175b1a4c0093b70b49bb2a334

15. S. Rahman, "Implementation of ballast water management plan in ships through ballast water exchange system," *Procedia Eng.*, vol. 194, pp. 323–329, Jan. 2017, doi: 10.1016/j.proeng.2017.08.152.

16. E. Tsolaki and E. Diamadopoulos, "Technologies for ballast water treatment: A review," *Journal of Chemical Technology & Biotechnology*, vol. 85, no. 1, pp. 19–32, Jan. 2010, doi: 10.1002/jctb.2276.

17. S. A. Bailey and H. Rajakaruna, "Optimizing methods to estimate zooplankton concentration based on generalized patterns of patchiness inside ballast tanks and ballast water discharges," *Ecol. Evol.*, vol. 7, no. 22, pp. 9689–9698, Nov. 2017, doi: 10.1002/ece3.3498.

18. C. Grob and B. G. Pollet, "Regrowth in ship's ballast water tanks: Think again!" *Mar. Pollut. Bull.*, vol. 109, no. 1, pp. 46–48, Aug. 2016, doi: 10.1016/j.marpolbul.2016.04.061.

19. V. Rață and L. Rusu, "Ballast water pollution risk assessment in the Black Sea," in *Mechanical Testing and Diagnosis*, Jan. 2021, pp. 35–40. doi: 10.35219/mtd.2020.4.05.

20. E. Briski *et al.*, "Combining ballast water exchange and treatment to maximize prevention of species introductions to freshwater ecosystems," *Environ. Sci. Technol.*, vol. 49, no. 16, pp. 9566–9573, Aug. 2015, doi: 10.1021/acs.est.5b01795.

21. A. Travizi *et al.*, "Macrozoobenthos in the Adriatic Sea ports: Soft-bottom communities with an overview of non-indigenous species," *Mar. Pollut. Bull.*, vol. 147, pp. 159–170, Oct. 2019, doi: 10.1016/j.marpolbul.2019.01.016.

22. P. Mozetič *et al.*, "Phytoplankton diversity in Adriatic ports: Lessons from the port baseline survey for the management of harmful algal species," *Mar. Pollut. Bull.*, vol. 147, pp. 117–132, Oct. 2019, doi: 10.1016/j.marpolbul.2017.12.029.

23. J.-H. Park, Y.-B. Sim, S.-Y. Kang, and S.-H. Kim, "Inactivation of indicating microorganisms in ballast water using chlorine dioxide," *Ecology and Resilient Infrastructure*, vol. 5, no. 3, pp. 111–117, Sep. 2018, doi: 10.17820/ERI.2018.5.3.111.

24. T. McCollin, G. Quilez-Badia, K. D. Josefsen, M. E. Gill, E. Mesbahi, and C. L. J. Frid, "Ship board testing of a deoxygenation ballast water treatment," *Mar. Pollut. Bull.*, vol. 54, no. 8, pp. 1170–1178, Aug. 2007, doi: 10.1016/j.marpolbul.2007.04.013.

25. L. A. Drake, M. A. Doblin, and F. C. Dobbs, "Potential microbial bioinvasions via ships' ballast water, sediment, and biofilm," *Mar. Pollut. Bull.*, vol. 55, no. 7, pp. 333–341, Jan. 2007, doi: 10.1016/j.marpolbul.2006.11.007.

26. S. Vodyanitskaya et al., "Methods of decontamination of ship ballast water with polyguanidine disinfectant," International Journal of Infectious Diseases, vol. 79, p. 77, Feb. 2019, doi: 10.1016/j.ijid.2018.11.195.

27. E. Lakshmi, M. Priya, and V. S. Achari, "An overview on the treatment of ballast water in ships," *Ocean Coast Manag.*, vol. 199, p. 105296, Jan. 2021, doi: 10.1016/j.ocecoaman.2020.105296.

28. M. N. Tamburri, K. Wasson, and M. Matsuda, "Ballast water deoxygenation can prevent aquatic introductions while reducing ship corrosion," *Biol. Conserv.*, vol. 103, no. 3, pp. 331–341, Mar. 2002, doi: 10.1016/S0006-3207(01)00144-6.

29. J.-T. Baek, J.-H. Hong, M. Tayyab, D.-W. Kim, P. R. Jeon, and C.-H. Lee, "Continuous bubble reactor using carbon dioxide and its mixtures for ballast water treatment," *Water Res.*, vol. 154, pp. 316–326, 2019, doi: https://doi.org/10.1016/j.watres.2019.02.014.

30. IMO, "Globallast guidelines for development of a national ballast water management Strategy, 1997. Guidelines for preventing the introduction of unwanted organisms and pathogens from ships ballast waters and sediment discharges. Resolution A.868 (20)." 2004.

31. G. H. Briton, B. Yao, and G. Ado, "Evaluation of the Abidjan lagoon pollution," *Journal of Applied Sciences and Environmental Management*, vol. 11, no. 2, 2007, doi: 10.4314/jasem.v11i2.55030.

32. J. Liu, P. Wang, G. Liu, J. Dai, J. Xiao, and H. Liu, "Study of the characteristics of ballast bed resistance for different temperature and humidity conditions," *Constr. Build. Mater.*, vol. 266, p. 121115, Jan. 2021, doi: 10.1016/j.conbuildmat.2020.121115.

33. N. A. Salleh *et al.*, "Pathogenic hitchhiker diversity on international ships' ballast water at West Malaysia port," *Mar. Pollut. Bull.*, vol. 172, p. 112850, Nov. 2021, doi: 10.1016/j.marpolbul.2021.112850.

34. G. Romanelli *et al.*, "Ballast water management system: Assessment of chemical quality status of several ports in Adriatic Sea," *Mar. Pollut. Bull.*, vol. 147, pp. 86–97, Oct. 2019, doi: 10.1016/j.marpolbul.2017.12.030.

35. M. R. First and L. A. Drake, "Life after treatment: detecting living microorganisms following exposure to UV light and chlorine dioxide," *J. Appl. Phycol.*, vol. 26, no. 1, pp. 227–235, Feb. 2014, doi: 10.1007/s10811-013-0049-9.

36. Z. Manxia, L. Shengjie, T. Xiaojia, L. Xiang, and Z. Yimin, "Evaluation of micro-pore ceramic filtration and uv radiation combination on ballast water treatment," in *2010 International Conference on Digital Manufacturing & Automation*, pp. 670–673, Dec. 2010, doi: 10.1109/ICDMA.2010.374.

37. P. P. Stehouwer, A. Buma, and L. Peperzak, "A comparison of six different ballast water treatment systems based on UV radiation, electrochlorination and chlorine dioxide," *Environ. Technol.*, vol. 36, no. 16, pp. 2094–2104, Aug. 2015, doi: 10.1080/09593330.2015.1021858.

38. I. Rivas-Zaballos, L. Romero-Martínez, I. Moreno-Garrido, J. Moreno-Andrés, A. Acevedo-Merino, and E. Nebot, "UV-LEDs combined with persulfate salts as a method to inactivate microalgae in ballast water," *Journal of Water Process Engineering*, vol. 51, p. 103361, Feb. 2023, doi: 10.1016/j.jwpe.2022.103361.

39. J. Xiao, Y. Xu, L. Hu, and H. Wu, "Evaluating the treatment performance of filtration & real-time UV irradiation

processes for bacteria and pathogens in fresh ballast water," *Reg. Stud. Mar. Sci.*, vol. 63, p. 102971, 2023, doi: https://doi.org/10.1016/j.rsma.2023.102971.

40. N. F. Gray, "Chapter Thirty-Four - Ultraviolet disinfection," in *Microbiology of Waterborne Diseases (Second Edition)*, S. L. Percival, M. V Yates, D. W. Williams, R. M. Chalmers, and N. F. Gray, Eds., Second Edition. London: Academic Press, 2014, pp. 617–630. doi: https://doi.org/10.1016/B978-0-12-415846-7.00034-2.

41. Y. Wang, L. Zou, L. Ma, Z. Zhao, and J. Guo, "A survey on control for Takagi-Sugeno fuzzy systems subject to engineering-oriented complexities," *Systems Science & Control Engineering*, vol. 9, no. 1, pp. 334–349, 2021, doi: 10.1080/21642583.2021.1907259.

42. "DESMI to manufacture ballast water treatment system under licence," *Pump Industry Analyst*, vol. 2012, no. 8, pp. 12–13, 2012, doi: https://doi.org/10.1016/S1359-6128(12)70370-1.

43. B. Sayinli, Y. Dong, Y. Park, A. Bhatnagar, and M. Sillanpää, "Recent progress and challenges facing ballast water treatment – A review," *Chemosphere*, vol. 291, p. 132776, 2022, doi: https://doi.org/10.1016/j.chemosphere.2021.132776.

sciendo

POLISH MARITIME RESEARCH 1 (117) 2023 Vol. 30; pp. 43-53
10.2478/pomr-2023-0057

EFFECTS OF SWAY AND ROLL EXCITATIONS ON SLOSHING LOADS IN A KC-1 MEMBRANE LNG TANK

Se-yeol An[1]
Hyeon-won Jeong[1]
Ohyoung Kim[2]
W. Jaewoo Shim[1,*]
[1] Department of Chemical Engineering, Dankook University, Gyeonggi-do, 16890, South Korea
[2] School of Polymer Science and Engineering, Dankook University, Gyeonggi-do, 16890, South Korea

* Corresponding author: *wjshim@dankook.ac.kr (W. Jaewoo Shim)*

ABSTRACT

This study investigates the effects of sway and roll excitations on sloshing liquid loads in a tank, using Ansys Fluent software. The model considered in the study is a 1:50 scaled membrane-type tank, based on a KC-1 membrane LNG tank designed by Korea Gas Corporation (KOGAS). The volume of fluid (VOF) method is used to track the free surface inside the tank, and the standard k-ε model is applied to express the turbulent flow of the liquid. To explore the motion of the tank under excitation, a user-defined function (UDF) and a dynamic mesh technique are employed to control the external forces exerted on the tank through its motion. The results, in the form of time series data on the sloshing pressures in the tank under pure sway, roll, and coupled sway-roll, are analysed, with specific ranges for the excitation amplitudes and frequencies. We show that variations in excitation frequency and amplitude significantly influence the sloshing loads. Sloshing loads are found to intensify when the excitation frequency matches the tank's primary natural frequency, 1.0 ω'_1. Furthermore, with coupled sway-roll excitations, the sloshing loads are weakened when the sway and roll are in-phase and are intensified when these are out-of-phase. Fast Fourier transform analysis provides insights into the frequency domain, showing that the dominant frequency is 0.88 Hz and it is approximately equal to the tank's primary natural frequency, 1.0 ω'_1.

Keywords: KC-1 membrane LNG tank; Sloshing; Sway; Roll; Coupled sway-roll; Fast Fourier transform (FFT)

INTRODUCTION

The term 'sloshing' refers to unrestrained movements of the free surface of a liquid in a container, and occurs when a partially filled tank is exposed to external perturbations, which cause the free surface of the liquid to oscillate [1]. In the case of small perturbations, sloshing can be approximated as a linear superposition of different wave components [2]. However, it is important to note that sloshing flow represents a complex fluid motion. Under certain conditions, the pressure exerted on the inner walls of the tank that are in contact with the liquid can increase dramatically; this is because the unrestrained free surface tends to undergo significant excursions for even small movements of the tank [1]. Consequently, in severe cases, the loads generated by sloshing can lead to structural damage to the tank's inner walls. These issues are related to ensuring the safety of waterway transportation of liquefied natural gas (LNG) in LNG tankers. To address these concerns, it is important to predict the sloshing flow of a liquid loaded in a tank and the resulting pressure variations. Accurate predictions and an understanding of sloshing behaviour can help in devising measures to mitigate potential structural damage and enhance the safety of LNG transportation.

The motion of a tank floating on the sea has six degrees of freedom (6DOF), with external forces exerted on the tank that can include a single DOF, such as surge, sway, heave, pitch, roll, or yaw as well as multiple coupled DOFs [3]. As a result, many studies have been conducted to investigate sloshing within tanks subjected to multiple coupled excitations [2–5]. Chen and Wu [3] conducted a study of fluid sloshing in three-dimensional tanks filled to an arbitrary depth under various excitation frequencies and motion with multiple DOFs. They demonstrated that instability of sloshing occurs when the excitation frequency of the heave motion is twice as large as the fundamental natural frequency under coupled surge-sway-heave excitations. Hou et al. [2] studied liquid sloshing in a two-dimensional tank under single and multiple coupled external excitations, such as coupled sway-roll and coupled sway-roll-heave excitations. In their research, they showed that sloshing loads are intensified when the tank experiences multiple coupled excitations and that match the first order natural frequency of the tank. Wu et al. [4] conducted experiments to investigate the impact loads from liquid sloshing at low liquid loading rates under coupled roll-pitch excitations. They observed that when the excitation frequencies for roll and pitch are between 0.98 f_1 and 1.113 f_1, where f_1 represents the first-order natural frequency of a sloshing liquid in a rectangular tank, a roof-bursting phenomenon by the liquid occurred. In addition, they noted that the maximum impact pressure was observed at 1.09 f_1.

In summary, several studies have been conducted on sloshing in tanks under various liquid filling levels and ship motions. However, limited attention has been given to investigating sloshing phenomena under the influence of coupled sway-roll excitations, which represent one of the most extreme instances of sloshing-induced structural damage within the context of the 6DOF motion of a tank [5]. The largest sloshing loads occur in the range $0.1 \leq h/H \leq 0.5$ for the liquid filling height [5]. Hence, this study investigates sloshing in a tank filled to 50% with water under pure sway, pure roll, and coupled sway-roll excitations, to gain insights into the behaviour of the liquid and to understand the potential impacts on the structural integrity of the tank under these specific conditions.

The model considered in the study is a 1:50 scaled membrane-type tank based on the design of a 48,280 m^3 KC-1 membrane LNG tank designed by Korea Gas Corporation (KOGAS) [6]. To investigate the sloshing loads, the variations in the excitation frequency and amplitude are considered in order to observe the time-dependent sloshing pressure variations over a wide range of sway, roll, and coupled sway-roll excitations, using the Ansys Fluent computational fluid dynamics (CFD) software. MATLAB software is also used to perform a fast Fourier transform (FFT) analysis of the time series results for the sloshing pressures under coupled sway-roll excitations, to provide a quantitative analysis in the frequency domain.

COMPUTATIONAL MODELING

COMPUTATIONAL MODEL

In a sloshing analysis, the free surface of a liquid exhibits nonlinearity as the external forces increase, and one challenging aspect of sloshing analysis is the accurate tracking of the flow of this nonlinear free surface. To address this issue, Hirt and Nichols [7] introduced the volume of fluid (VOF) method, which represents the volume occupied by the liquid in each computational cell as a discrete function. This method provides a solution for effectively tracking the nonlinear free surface waves. Since its introduction, the VOF method has been widely used to track the free surface in sloshing analyses, and it is also adopted in the present study, using Ansys Fluent software. Eq. (1) gives the function that expresses the volume fraction of liquid occupying a cell.

$$\alpha(x, y, z) = \begin{cases} 0 \\ 0 \sim 1 \\ 1 \end{cases} \tag{1}$$

When the value of α is zero, this represents an empty state with no liquid in the cell, while values of α between zero and one represent a free surface that includes both liquid and gas. When the value of α is one, this indicates that only liquid is present in the cell. Fig. 1 shows the volume fractions of liquid in each of the cells based on the values of α.

Fig. 1. An example of the distribution of α values in cells [8]

GOVERNING EQUATIONS

In this study, a conventional numerical approach is employed to calculate the sloshing phenomenon of liquid in a tank. It is assumed that the fluid flow is incompressible, and the turbulent flow in the sloshing phenomenon is represented by the Reynolds-averaged Navier-Stokes (RANS) equation. The Reynolds stresses and the turbulent flow field in the RANS are calculated based on the standard k-ε model. The volume fraction for the two phases, liquid and gas, is calculated using the volume fraction equation in Eq. (2):

$$\frac{1}{\rho_q}\left[\frac{\partial}{\partial t}\left(\alpha_q\rho_q\right)+\nabla\cdot\left(\alpha_q\rho_q\bar{u}_q\right)=S_{\alpha_q}+\sum_{p=1}^{n}\left(\dot{m}_{pq}-\dot{m}_{qp}\right)\right] \tag{2}$$

where the variables $\dot{m}_{pq}$ and $\dot{m}_{qp}$ represent the mass transfer from phases p to q and from phases q to p , respectively [9, 10]. S_{α_q} is the source term for phase q in a cell [9, 10]. Eq. (3) is the governing equation for the momentum, as follows:

$$\frac{\partial}{\partial t}(\rho\vec{u})+\nabla\cdot(\rho\vec{u}\vec{u})=-\nabla p+\nabla\cdot(\bar{\bar{\tau}})+\rho\vec{g}+\vec{F} \tag{3}$$

where $\vec{u}$ denotes the velocity vector, ρ the density of the mixture, p the static pressure, and $\bar{\bar{\tau}}$ the stress tensor [11, 12]. $\rho\vec{g}$ and $\vec{F}$ represent the gravitational body force and external body force, respectively [11, 12]. The stress tensor, $\bar{\bar{\tau}}$, can be expressed as:

$$\bar{\bar{\tau}}=\mu(\nabla\vec{u}+\nabla\vec{u}^T) \tag{4}$$

where μ is the dynamic viscosity [11, 12].

EXCITATION FORCES

The tank can experience external perturbations including sway and roll excitations. Sway excitation induces a linear transverse (lateral or side-to-side) motion along the tank's transverse axis, whereas roll excitation induces a tilting rotation of the tank about its longitudinal axis, with the centre of the bottom of the tank acting as the centre of the coordinate system. If the sway and roll excitations are periodic, they can be represented in the form of sinusoidal waves, as shown below.

$$X=X_0 sin\ (\omega t) \tag{5}$$

$$\theta=\theta_0 sin\ (\omega t) \tag{6}$$

Eq. (5) is the mathematical expression for the sway excitation, while Eq. (6) is the mathematical expression for the roll excitation. Here, X and θ represent the lateral displacement and the rotational displacement, respectively. X_0 represents the amplitude of the lateral displacement, θ_0 represents the amplitude of the rotational displacement, and ω is the frequency of the excitations.

Fig. 2 shows the two-dimensional geometric parameters of a rectangular tank and a prismatic model tank. The rectangular tank is considered for the validation of modelling assumptions used in the computation, and the membrane-type tank with a prismatic shape is the model LNG tank used in the study.

To model the sway and roll excitations of the tank, the first natural frequency of the prismatic tank was used. The first natural frequency of the rectangular tank, ω_1, can be determined using Eq. (7), and its correlation with the first natural frequency of the prismatic tank, ω'_1, is expressed in Eq. (8) [13–15]:

$$\omega_1^2=\frac{\pi g}{B}tanh\left(\frac{\pi h}{B}\right) \tag{7}$$

$$\frac{{\omega'_1}^2}{{\omega_1}^2}=1-\frac{\left[B_1H_1^{-1}sinh\left(\frac{\pi H_1}{B}\right)-B_1H_1^{-1}sin^2\left(\frac{\pi B_1}{B}\right)\right]}{\pi sinh\left(\frac{2\pi h}{B}\right)} \tag{8}$$

In this study, Eq'ns. (5) to (8) are used to apply external excitations to the tank, in order to induce prescribed motions according to specific formulae. To accurately simulate the motion of the tank under these excitations, a user-defined function (UDF) and a dynamic mesh technique are employed to impose the external excitation effectively.

The investigation focused on the effects of different excitations on the sloshing loads in the tank, including single excitations (pure sway and pure roll) and multiple coupled excitations '(coupled sway-roll)'. In particular, the sloshing pressures in the tank are analysed when the excitation of roll

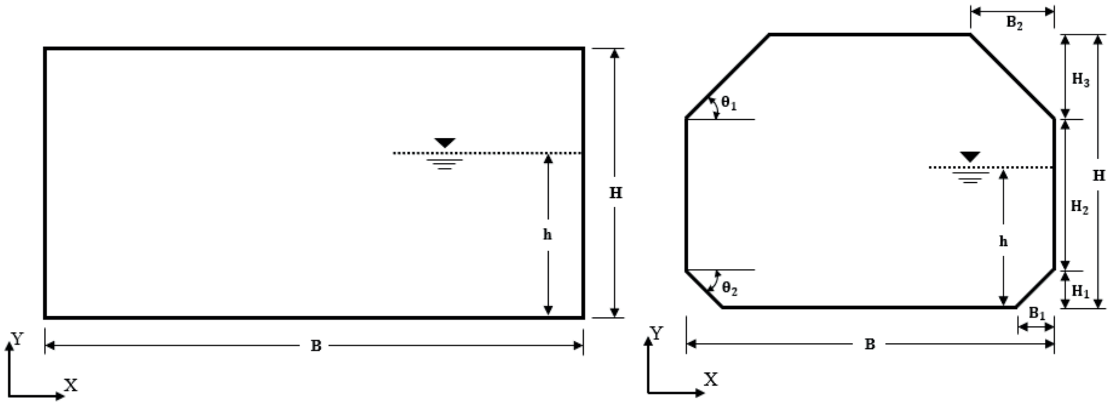

Fig. 2. Parameters for a two-dimensional rectangular tank (left) and a two-dimensional prismatic tank (right)

is coupled with the sway's in the same-phase (0°) and the opposite-phase (180°).

Fig. 3 shows the time-dependent lateral displacements of a tank subjected to a pure sway excitation having an amplitude of 0.015 m, while others are the time-dependent rotational displacements due to pure roll excitations with amplitudes of 1°, 3°, and 5° in the same-phase or the opposite-phase relative to the sway's. The frequency of the excitations was set to the first natural frequency of the tank, denoted as 1.0 ω_1'.

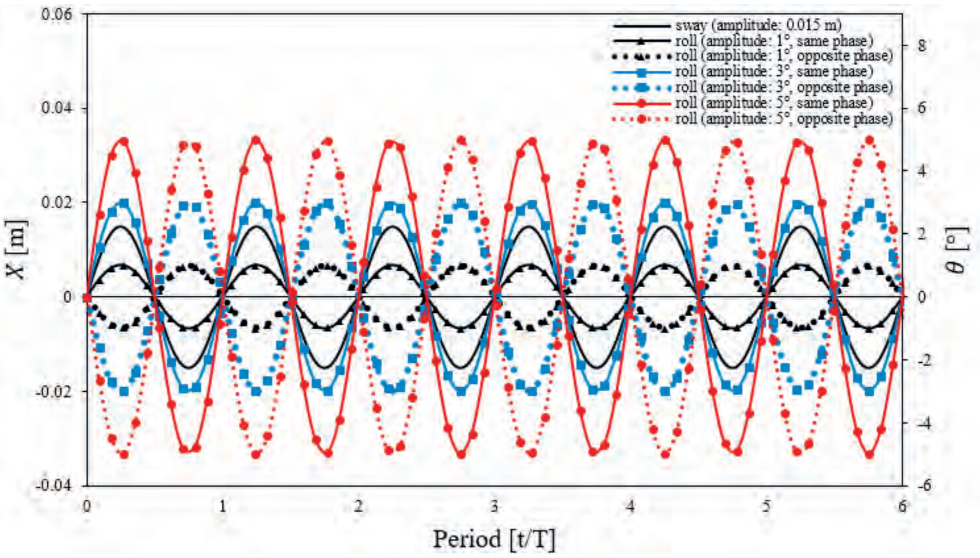

Fig. 3. Displacement of a tank due to pure sway and pure roll excitations. The roll excitation is in-phase or out-of-phase with the sway excitation

VALIDATION

To assess the validity of the modelling assumptions used for the numerical simulation, a comparison was conducted between the simulation results and experimental data obtained from a well-known prior study conducted by Hinatsu [16]. The experimental data selected for the comparison consisted of measurements of sloshing pressures in a rectangular tank under pure sway excitation. A schematic representation of the rectangular tank used in their experimental investigation is presented in Fig. 4. The tank had a base length of 1.2 m and height of 0.6 m. For the experiment, the tank was filled with water to 60% of its height from the floor, and the remaining spaces were filled with air. Subsequently, the tank was subjected to pure sway excitation characterised by an amplitude of 0.015 m and a period of 1.404 s. During the validation process, the simulation results were compared to the experimental data pertaining to the sloshing impact pressure at a specific location, denoted as P_1 at the tank wall (as indicated in Fig. 4). The primary objective of this comparison was to evaluate the degree of agreement between our simulation data and the experimental data regarding the sloshing impact pressures at the designated point.

In the numerical simulation, the fluid motion was modelled as an incompressible unsteady flow, with a no-slip condition assumed at the walls. To track the free surface, which represents the interface between the water and air, the VOF method was employed [7]. To express the turbulent flow of the liquid, the standard k-ε model was used [17]. To calculate the pressure on a computational mesh from the velocity components, the semi-implicit method for pressure-link equations (SIMPLE) algorithm was used, in which the momentum equations were coupled with an iterative procedure [18]. A compressive scheme was used to calculate the volume fraction for the interface capturing problem [19].

Fig. 4 illustrates the base case for the computational mesh used in the simulation of the rectangular tank, which was formed of a combination of triangular and rectangular grids. When excitation is applied to a tank, sloshing-induced liquid forces often impacts and shocks certain zones on the upper-left and upper-right walls of the tank, and on the roof. Furthermore, the motion of the liquid near the point of impact exhibits complex flow phenomena [20]. Thus, to accurately capture the complex flow behaviour of the liquid, smaller triangular grids (0.0025 m here in the base case) were employed near the anticipated impact zones on the walls [20, 21]. Larger rectangular grids (0.005 m in the base case) were used in the remaining regions to reduce the computational time while still maintaining reasonable accuracy. The entire mesh for the base case consisted of a total of 64,620 grid points. To assess the numerical accuracy of the results in terms of the sloshing loads in the tank with respect to the grid resolution, two cases were analysed: the base case and a coarse case of 32,132 grid points, half the number of the base case. It is important to note that in both cases, the number of grid points significantly exceeded those used in a validation process (7,200) performed by Rhee [12]. Furthermore, our study investigated the influence of the time step size on accuracy. Three time steps were compared: a base time step of 0.0005 s, a large time step of 0.001 s (twice that of the base case), and an extra-large time step of 0.002 s (twice that of the large case).

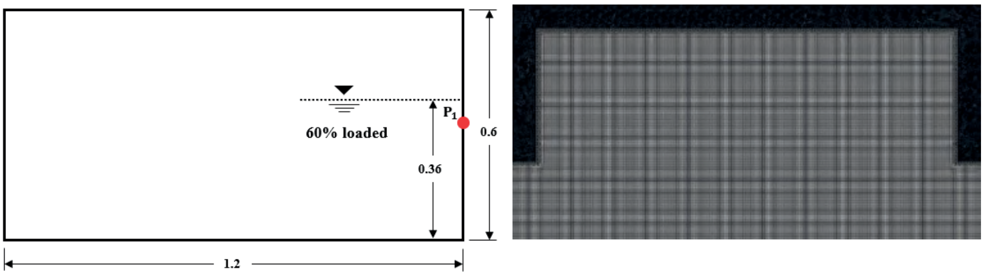

Fig. 4. Schematic of the rectangular tank used in the validation process (left) and the base case of the computational mesh for the tank (right) [Units: m]

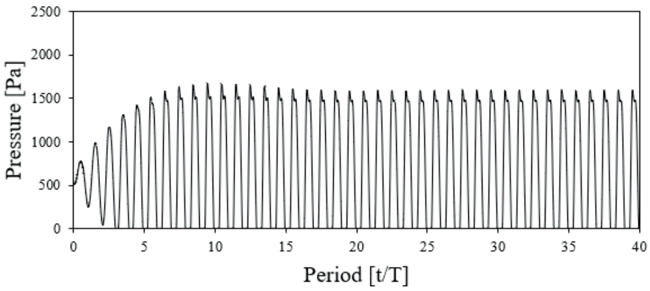

Fig. 5. Pressure history at point P_1 of the rectangular tank for the base cases of both the mesh and time step size

Tab. 1. Sensitivity of sloshing pressure at point P_1 of the rectangular tank to the number of grid points and the time step size between the 20th and 25th cycles

Mesh	Number of grid points	Average pressure [Pa]	ε [%]	$\varepsilon_{validation}$ [%]
Base	64,620	1,562.317	-	0.68
Coarse	32,132	1,577.064	0.94	1.63
Time step	**Size [s]**	**Average pressure [Pa]**	**ε [%]**	**$\varepsilon_{validation}$ [%]**
Base	0.0005	1,562.317	-	0.68
Large	0.001	1,519.703	2.73	2.06
Extra-large	0.002	1,424.312	8.83	8.21

Fig. 5 illustrates the variation in sloshing pressure at point P_1 of the rectangular tank, obtained from a simulation of the base cases for both the mesh and the time step size. The sloshing pressure initially rises, and then goes through a transient phase where it increases and subsequently decreases. After the 20th cycle, the pressure variations stabilise, and a steady-state region is reached.

Table 1 provides assessments of the simulation accuracy based on the number of grid points and the time step size. To evaluate the accuracy, the average values for the top 10% of sloshing pressure values at P_1 between the 20th and 25th cycles in the steady-state region were compared with the experimental values (comparable six cycles in steady-state region). To investigate the accuracy in terms of the number of grid points, the time step was set to the base case, whereas to investigate the accuracy in terms of the time step size, the mesh was set to the base case. The error between our simulation data and the experimental data is denoted as $\varepsilon_{validation}$, and the error relative to the simulation values for the base cases as ε.

The results for the accuracy with respect to the number of grid points showed that ε was 0.94% for the coarse case, and the values of $\varepsilon_{validation}$ for the base and coarse case were 0.68% and 1.63%, respectively. The values for the base case, with a larger number of grid points, were more consistent with the experimental values. The results for the accuracy with a varying time step size gave values for ε of 2.73% and 8.83% for the large and extra-large cases, respectively; the values of $\varepsilon_{validation}$ for the large and extra-large cases were 2.06% and 8.21%, respectively, while $\varepsilon_{validation}$ for the base case was 0.68%. This investigation revealed that reducing the time step size led to a decrease in the error. Fig. 6 shows a graph of the variations in sloshing impact pressure at point P_1, and compares the data obtained from the simulation of the base cases for both the mesh and time step size with the experimental data. The experimental data shown in the figure were obtained by Fourier decomposition of the raw experimental data [22]. The graph shows remarkable agreement between our computed data and the experimental data, thus confirming that the assumptions used in the simulation were appropriate, and the base cases for both the mesh and time step size were therefore adopted for the simulations in the remainder of the study. These results validate the reliability and accuracy of our numerical simulation in terms of capturing the sloshing behaviour of water in a tank under the specified conditions.

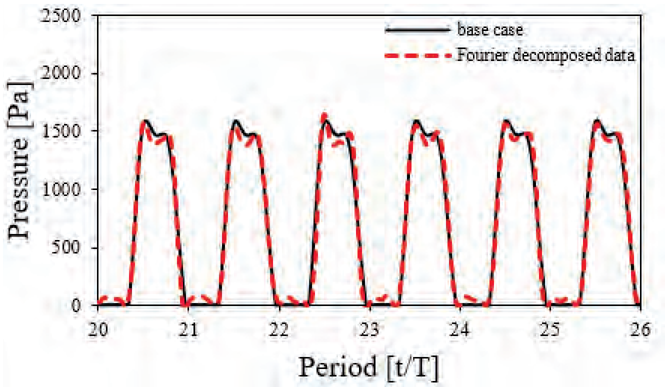

Fig. 6. Pressure history at P_1 of the rectangular tank between cycles 20 and 25: comparison of the base case simulation vs. the Fourier decomposition of experimental data [22]

RESULTS AND DISCUSSION

A simulation study was conducted using a prismatic model tank filled with 50% water, as shown in the schematic diagram in Fig. 7. The main objective of the investigation was to analyse the influence of the excitation frequency and amplitude on the sloshing pressure in the model tank under both sway and roll excitations, beyond the conditions used for the validation of the rectangular tank. To explore the effect of the excitation amplitude, three different sway amplitudes of 0.0075, 0.015, and 0.03 m were analysed. Similarly, three different roll amplitudes were examined: 1°, 3°, and 5°. In addition, the excitation was investigated at six different frequencies relative to the tank's primary natural frequency, ω'_1, with values of 0.8 ω'_1, 1.0 ω'_1, 1.2 ω'_1, 1.4 ω'_1, 1.6 ω'_1, and 1.8 ω'_1. To assess the sloshing pressure under various types of external excitation, the excitations were classified into four scenarios: pure sway, pure roll, and coupled sway-roll with both the same-phase and the opposite-phase. The study particularly focused on analysing the sloshing impact pressures at point P_1, as indicated on the tank wall in Fig. 7. In the same figure, the computational mesh used to simulate the tank is shown, to enable a visualisation of the detailed mesh structure used to capture the sloshing behaviour. In this study, we investigated the effects of sloshing on the tank under various excitation scenarios with a 50% liquid filling level, as this is a tank filling condition known for its severe sloshing-induced damage [5]. We conducted a total of 42 simulations, with 18 for pure sway, 18 for pure roll, and six for coupled sway-roll.

It was observed that an increase in the excitation amplitude led to an increase in the sloshing pressure. This was be attributed to the heightened excitation forces acting on the tank as the amplitude increases, which result in greater sloshing-induced forces. However, during pure rolls with frequencies of 0.8 ω'_1, 1.2 ω'_1, and 1.8 ω'_1, it was noted that the relationship between amplitude and pressure exhibited a nonlinear softening effect, leading to a reduced rate of increase in the sloshing pressure. In a study conducted by Akyildiz and Ünal [23] on sloshing pressure during pitch motion, they also found that sloshing pressure exhibited decreased sensitivity to amplitude, causing a reduction in the rate of pressure increase.

The impact of excitation frequency on sloshing pressure was also investigated. Fig. 8 shows that under pure sway excitation, the lowest pressure occurred at an excitation frequency of 1.6 ω'_1, whereas under pure roll excitation, the lowest pressure occurred at an excitation frequency of 1.4 ω'_1, under the same amplitude conditions. When the frequency of pure sway or roll was 1.0 ω'_1, the highest sloshing pressure was recorded under the same amplitude conditions. This behaviour was attributed to resonance, in which the frequency matches the tank's primary natural frequency, causing intense sloshing of the liquid. This resonance effect results in a significant increase in sloshing pressure, and in engineering design, it is important to avoid the conditions for resonance and their potential detrimental effects on the structural integrity of tanks [24, 25].

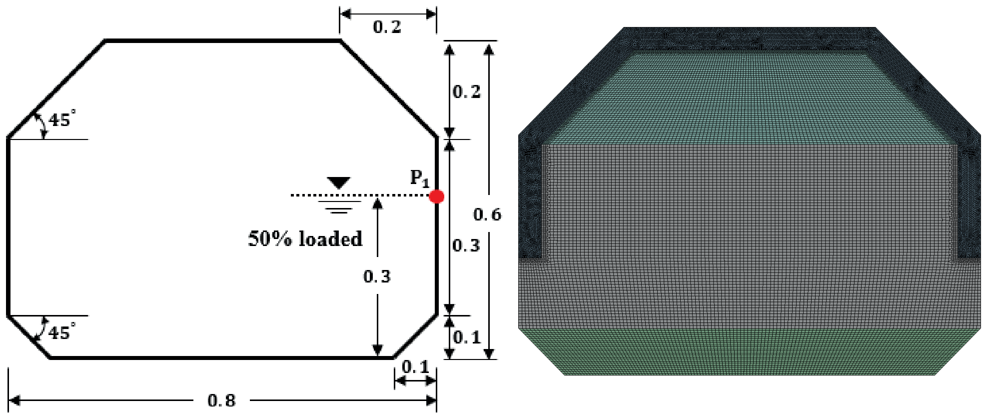

Fig. 7. Schematic of the prismatic model tank (left, actual LNG tank size: H = 29.71 m, H_1 = 4 m, H_2 = 16.507 m, H_3 = 9.203 m, B = 40.31 m, B_1 = 4 m, B_2 = 9.203 m, $\theta_1 = \theta_2$ = 45°) and the base case of the computational mesh used for the tank (right) [Units: m]

PURE SWAY AND PURE ROLL EXCITATIONS

Fig. 8 and Table 2 present the results for the sloshing pressure at point P_1 in the model tank, obtained under pure sway and pure roll excitation forces of various frequencies and amplitudes. The data include the average values of the top 10% sloshing pressures between the 16th and 21st cycles, after the transient phase.

Tab. 2. Average pressures at P_1 for the prismatic model tank under pure sway or roll excitations [Units: Pa]

Frequency	Pure sway			Pure roll		
	Amplitude			Amplitude		
	0.0075 m	0.015 m	0.03 m	1°	3°	5°
0.8 ω'_1	141.153	309.174	618.612	165.666	546.482	886.990
1.0 ω'_1	716.198	903.424	1219.392	666.429	981.332	1409.812
1.2 ω'_1	183.924	321.814	465.267	87.447	236.756	347.834
1.4 ω'_1	79.544	160.115	277.848	13.921	79.483	159.855
1.6 ω'_1	40.974	123.624	254.184	19.642	116.830	228.883
1.8 ω'_1	109.614	184.812	276.799	73.855	191.390	303.609

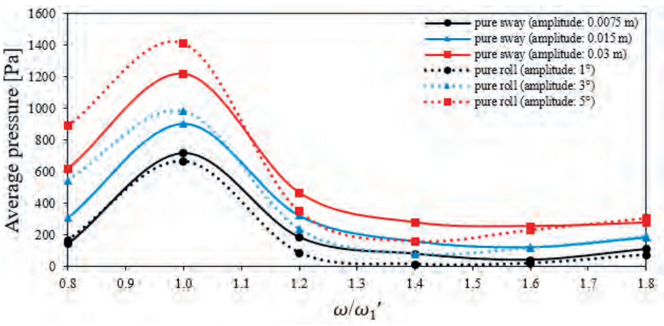

Fig. 8. Average pressures at P_1 for the prismatic model tank vs. excitation frequency of pure sway and pure roll

COUPLED SWAY-ROLL EXCITATIONS

We also investigated several cases of coupled sway-roll excitations for the model tank, which were divided into two types, with the opposite-phase or the same-phase. The opposite-phase cases were Case 1 (roll amplitude: 1°), Case 2 (roll amplitude: 3°), and Case 3 (roll amplitude: 5°), while the same-phase cases were Case 4 (roll amplitude: 1°), Case 5 (roll amplitude: 3°), and Case 6 (roll amplitude: 5°). In all cases, the amplitude of the sway excitation was fixed at 0.015 m, while the roll motion was varied, with amplitudes of 1°, 3°, and 5°. The frequency of the coupled excitations was set to 1.0 ω'_1.

Fig. 9 shows the variations in sloshing pressure between the 16th and 21st cycles for Cases 1–6, together with the results for the pure sway scenario (amplitude: 0.015 m). It is seen that in Cases 1–3 (coupled excitations with the opposite-phase), the sloshing pressures are in-phase, thus causing higher pressures compared to those for pure sway. Moreover, as the amplitude of the roll excitation increases, sloshing pressure also increases due to the intensified sloshing-induced forces under the coupled sway-roll excitations. The variation in sloshing pressures becomes more unstable with an increase in the roll amplitude, leading to complex pressure variations. This phenomenon arises when the amplitude surpasses a specific threshold, resulting in roof impact. As the amplitude increases, in Cases 2 and 3, the impact on the roof intensifies, leading to significant deviations from linear predictions and the emergence of intricate pressure variations [26].

In Cases 4 and 5, it was observed that the sloshing pressures in the tank were decreased compared to those under pure sway. This reduction pressure results from the cancellation of sloshing-induced forces under coupled sway-roll excitations, primarily due to the phase alignment of the tank's excitation. This phase alignment occurs in the direction where the sloshing-induced forces generated in the tank by each sway and roll cancel each other out. In addition, the magnitude of the roll amplitude plays an important role in influencing this pressure decrease. In Case 4, with small roll amplitude of 1°, the pressure variations are mostly in phase with pure sway, but this results in a lower sloshing pressure compared to pure sway. In Case 5, however, the increased roll amplitude causes a deviation and shift in the phase of the pressure variation, moving it out-of-phase, as shown in Fig. 9. A substantial phase shift occurred in Case 5 because the increased amplitude of the roll excitation influenced the sloshing motions more than the sway excitation. Case 5 exhibited the lowest sloshing pressures due to significant force cancellation, as indicated by the similarity between the average pressures for pure sway with an amplitude of 0.015 m and pure roll with an amplitude of 3° (see Table 2). Finally, Case 6 demonstrates that with a large roll amplitude of 5°, the roll excitation dominates the sloshing motion to the extent that the phase of pressure variations shifts to the opposite to that of pure sway, and also increases the pressure beyond the cancellation effect observed in Case 5.

Table 3 provides information on the maximum peak pressure during the initial 25s and the average values for the top 10% of sloshing pressures at point P_1 between the 16th and 21st cycles. Case 1 showed an increase of approximately 200 Pa in the maximum peak pressure compared to pure sway; although Cases 2 and 3 exhibited significantly higher maximum peak pressures compared to that of pure sway, the rise in the average pressures was not as significant as the increase in the maximum peak pressures. The dramatic increase in the maximum peak pressure (P_{max}) can be attributed to the instability of the pressure associated with the roof impact. In contrast, the maximum peak pressures and average pressures in both Cases 4 and 5 were lower than for pure sway. Case 6 showed higher pressures than for pure sway, as the cancellation of sloshing-induced forces was insignificant due to the unbalanced forces of the roll with a large amplitude of 5°, which imposed a phase shift toward the opposite of the sway motion.

The movements of the free surface of the liquid inside the tank under pure sway and in Cases 1–6 are presented in Fig. 10. It can be seen that under coupled sway-roll with the opposite-phase, the free surface flows became more complex with an increase in the amplitude of the roll. In contrast, when the sway and roll had the same-phase, sloshing did not exhibit significant oscillation compared to the opposite-phase cases (Cases 1–3). As a result, Case 5 (Fig 10(f)), with a roll amplitude of 3°, was the most stable, while Case 3 (Fig. 10(d)) exhibited the most unstable behaviour of the free surface.

Tab. 3. Maximum peak pressures and average pressures of the prismatic model tank for each scenario

Scenario	P_{max} [Pa]	Time [s]	Average pressure [Pa]
Pure sway	1,037.687	9.55	903.424
Case 1	1,237.384	7.28	1,007.630
Case 2	3,277.842	6.17	1,342.786
Case 3	3,961.499	11.80	1,548.946
Case 4	800.638	16.35	749.527
Case 5	568.884	18.01	537.824
Case 6	1,179.679	7.83	953.605

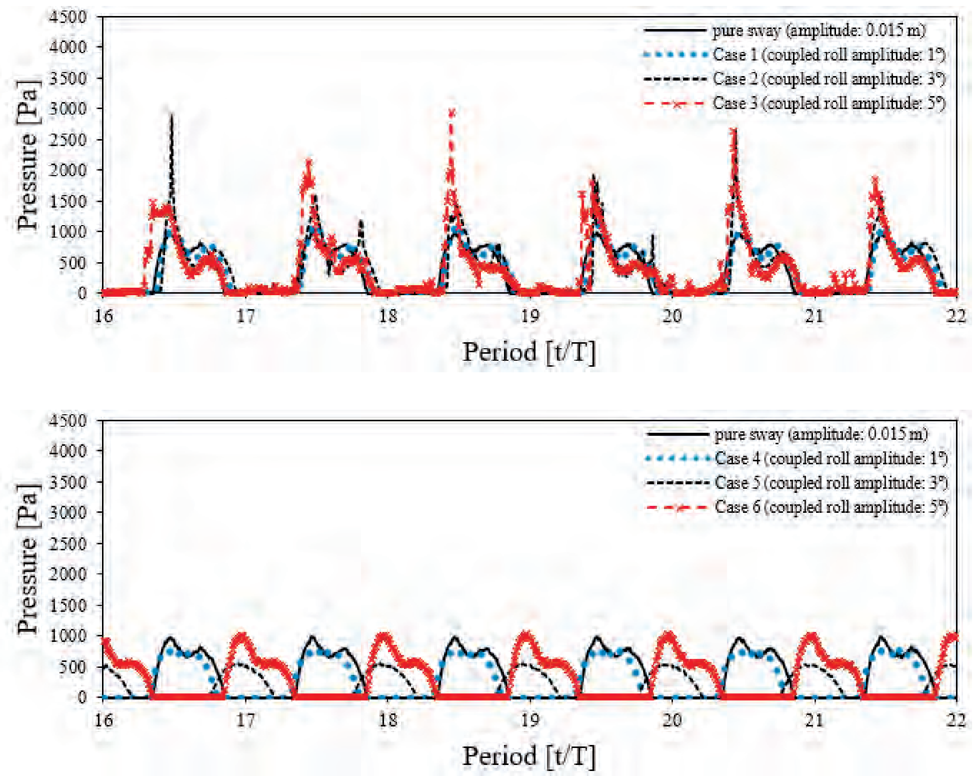

Fig. 9. Comparison of pressure variations at P_1 of the prismatic model tank (over cycles 16 to 21): top graph (pure sway, Cases 1, 2, and 3) and bottom graph (pure sway, Cases 4, 5, and 6)

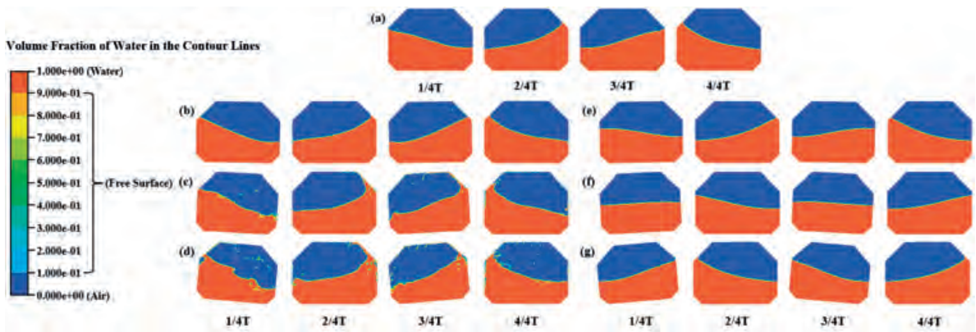

Fig. 10. Contours of the volume fraction of the prismatic model tank: (a) pure sway, (b) Case 1, (c) Case 2, (d) Case 3, (e) Case 4, (f) Case 5, (g) Case 6

FFT ANALYSIS

The sloshing pressure data obtained from 0–25 s were subjected to quantitative analysis using the FFT algorithm. This analysis focused on the time series data representing the sloshing pressures in the model tank under three scenarios: pure sway and coupled sway-roll excitations with both the same-phase and the opposite-phase. The results were examined in both the time domain and frequency domain, as shown in Fig. 11. Throughout the FFT analysis, we observed the presence of high-frequency noise exceeding 5 Hz in all cases. To mitigate this noise, a filtering technique based on the FFT algorithm with a cutoff frequency of 5 Hz was employed [27].

In all cases, the analysis revealed that the highest amplitude of pressure occurred at the dominant frequency of the frequency domain, 0.88 Hz, which was closely approximated to the primary natural frequency of the tank, 1.0 ω'_1 (= 0.884918 Hz). Other pressure peaks were also observed at frequencies corresponding to integer multiples of the dominant frequency, specifically at 1.76, 2.64, 3.52, and 4.40 Hz. This observation suggests that in addition to the dominant frequency, these integer multiples of the dominant frequencies can also affect sloshing behaviour significantly [28]. The amplitudes of pressure at these frequencies are presented in Table 4, and pressure histories and FFT spectra are shown in Fig. 11.

In Case 1, the pressure amplitude at the dominant frequency was larger than that for pure sway, whereas in Cases 2 and 3, the amplitudes were very similar to that for pure sway. However, the amplitudes at frequencies of 1.76 and 2.64 Hz increased compared to those of both pure sway and Case 1. In Case 3, the amplitudes were larger in the vicinity of 3.52 and 4.40 Hz (i.e., 3.48, 3.56, 4.24, 4.36, 4.44, and 4.52 Hz), rather than at the 3.52 and 4.40 Hz. Furthermore, in Cases 2 and 3, sawtooth-shaped amplitude spectra were observed, implying the occurrence of complex sloshing phenomena. These phenomena were attributed to the nonlinear characteristics associated with irregular wave crests and breaking waves [29]. Fig. 11(c) and (d) demonstrate the instability of the sloshing pressure due to roof impacts, contributing to a significant increase in the pressure amplitude at or near the integer multiples of the dominant frequency (i.e., 1.76, 2.64, 3.52, and 4.40 Hz). In Cases 4–6, the pressure amplitudes at the dominant frequency were smaller than that for pure sway. This result is attributed to the cancellation effect between sloshing-induced forces due to coupled sway-roll excitations with the same-phase. In Case 5, the pressure amplitude at the dominant frequency was the smallest, as the largest cancellation occurred compared to the other cases.

These FFT results revealed several phenomena. Firstly, for coupled sway-roll with the opposite-phase without roof impact, the amplitudes of pressure increased at the dominant frequency compare to that of pure sway. Secondly, for coupled sway-roll having the opposite-phase with roof impact, the amplitudes of pressure resulted in tallest peaks that are similar in magnitudes and comparable to that of pure sway at the dominant frequency; while at or near integer multiples of the dominant frequency, most of the pressure peaks increased compare to that of pure sway. Thirdly, when the excitations are coupled with the same-phase, the amplitude at the dominant frequency decreased compare to the sway's. Finally, it was confirmed that the amplitude at the dominant frequency decreased significantly when the sloshing-induced forces of sway and roll, coupled in the same-phase, were similar.

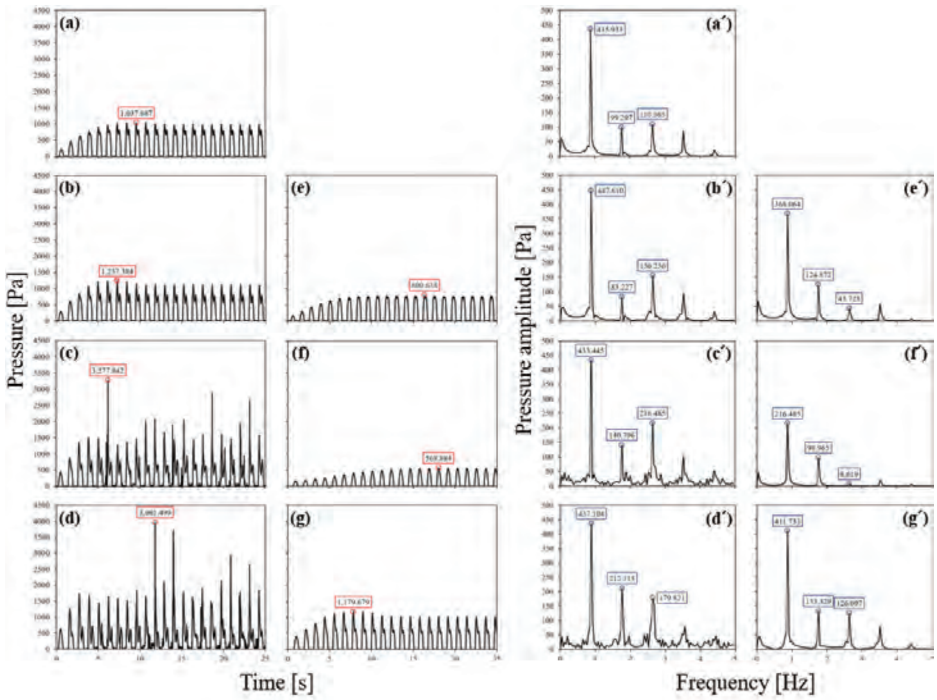

Fig. 11. Pressure histories (with P_{max}) and FFT spectra at P_1 of the prismatic model tank: pure sway - (a) and (a´); Case 1 - (b) and (b´); Case 2 - (c) and (c´); Case 3 - (d) and (d´); Case 4 - (e) and (e´); Case 5 - (f) and (f´); and Case 6 - (g) and (g´)

Tab. 4. Amplitudes of sloshing pressure signals in the prismatic model tank at frequencies under different scenarios

Scenario	Frequency [Hz]				
	0.88	1.76	2.64	3.52	4.40
Pure sway	435.933	99.297	110.365	86.362	22.177
Case 1	447.610	83.227	156.256	95.055	31.253
Case 2	433.445	140.796	216.485	100.433	52.718
Case 3	437.104	212.115	179.821	50.733	29.098
Case 4	368.064	124.872	43.728	59.307	7.711
Case 5	216.485	98.965	8.619	21.374	6.767
Case 6	411.733	133.329	126.097	79.448	18.885

CONCLUSION

In this study, we investigated the liquid sloshing loads exerted on the inner walls of a KC-1 membrane LNG tank under various excitation scenarios. These scenarios included single excitations (pure sway and pure roll) and coupled sway-roll excitations, both with the same-phase and the opposite-phase, across different ranges of excitation amplitudes and frequencies. The findings revealed that the intensity of liquid sloshing loads significantly increases when the resonance effect occurs. Moreover, we observed that under coupled sway-roll excitations with the same-phase, the sloshing loads become weaker than that for the case of pure sway, except when the force of the roll is substantially larger than the force of the sway, such that it overcomes the diminishing effect. Conversely, when applied with the opposite-phase, coupled sway-roll excitations strengthen and increase the sloshing loads substantially more than in the case of pure sway.

FFT analysis further identified that when the excitation frequency was 1.0 ω'_1, representing the first natural frequency of the tank, the sloshing pressure peaked predominantly at the dominant frequency, at 0.88 Hz, which is close to ω'_1 (= 0.884918 Hz). Interestingly, under coupled sway-roll excitations with the same-phase, the amplitude of sloshing pressure at the dominant frequency was significantly reduced compared to that of pure sway, contrasting with the cases with the opposite-phase, where it was increased. When coupled sway-roll excitations were in the opposite-phase with no roof impact conditions, the amplitude at the dominant frequency increased. However, in the presence of roof impact during sloshing, instabilities in the free surface manifest, resulting in a nearly constant amplitude at the dominant frequency in comparison to the sway's. Concurrently, the amplitudes of sloshing at or in proximity to other integer multiples of the dominant frequency exhibit predominant increase.

This study has demonstrated that a resonance effect in the context of the sloshing phenomenon in a KC-1 tank occurs when the natural frequency of the fluid sloshing inside the tank aligns with the frequency of the external forces acting on the tank. This alignment can lead to significant amplification of the sloshing motion, potentially resulting in instability, the risk of fluid spillage, or even structural damage. In addition, when the overall time series data for sloshing pressure were analysed, instances of roof impact were found to introduce instability into the pressure variations, making pressure predictions challenging. When the KC-1 tank is subjected to wave conditions involving both sway and roll excitation forces, there are measures that can be implemented to effectively mitigate the risk of substantial and unstable pressure surges. These measures include dampening or controlling the sloshing motion using baffles or dampers, promoting cancellation effects between the sloshing-induced forces stemming from each excitation, or adjusting the tank's natural frequency.

Further investigation will be necessary to explore the sloshing-induced forces in more diverse scenarios, including various types of multiple coupled excitations by manipulating the phases of the excitations with different filling heights. Moreover, it is important to expand the analysis domain from two dimensions to three, for a comprehensive understanding of the sloshing phenomenon.

ACKNOWLEDGEMENT

This research was supported by the research fund of Dankook University in 2021.

NOMENCLATURE

Denomination [units]

α	Volume fraction of liquid [-]
α_q	Volume fraction of phase q [-]
ρ	Density of the mixture [kg/m^3]
ρ_q	Density of phase q [kg/m^3]
$\vec{u}$	Velocity vector [m/s]
$\vec{u}_q$	Velocity vector of phase q [m/s]
S_{α_q}	Source term of phase q in a cell [kg/m^{3}s]
$\dot{m}_{pq}$	Mass transfer from phase p to phase q [kg/m^{3}s]
$\dot{m}_{qp}$	Mass transfer from phase q to phase p [kg/m^{3}s]
p	Static pressure [N/m^2]
$\bar{\bar{\tau}}$	Stress tensor [N/m^2]
$\vec{g}$	Acceleration of gravity [m/s^2]
$\vec{F}$	External body force [kg/m^{2}s^2]
μ	Dynamic viscosity [Pa s]
X	Horizontal displacement [m]
X_0	Amplitude of the sway excitation [m]
θ	Rotational displacement [°]
θ_0	Amplitude of the roll excitation [°]
ω	Frequency [rad s^{-1}]
t	Time [s]
H	Total height [m]
H_1	Height of the chamfered bottom corner [m]
H_2	Height excluding the corners [m]
H_3	Height of the chamfered upper corner [m]
B	Total breadth [m]
B_1	Breadth of the chamfered bottom corner [m]
B_2	Breadth of the chamfered upper corner [m]
θ_1	Angle of the chamfered upper corner [°]
θ_2	Angle of the chamfered bottom corner [°]
h	Height of the water filling [m]
ω_1	First natural frequency of the rectangular tank [rad s^{-1}]
ω_1'	First natural frequency of the prismatic tank [rad s^{-1}]
P_1	Internal pressure point in the rectangular tank and prismatic tank [Pa]
P_{max}	Maximum peak pressure [Pa]

REFERENCES

1. H. N. Abramson, "The dynamic behavior of liquids in moving containers, with applications to space vehicle technology," Department of Mechanical Sciences, Southwest Research Institute, Washington, D.C., NASA-SP-106, 1966.

2. L. Hou, F. Li, and C. Wu, "A numerical study of liquid sloshing in a two-dimensional tank under external excitations," *Journal of Marine Science and Application*, vol. 11, pp. 305-310, September 2012, doi: 10.1007/s11804-012-1137-y.

3. B. F. Chen and C. H. Wu, "Effects of excitation angle and coupled heave-surge-sway motion on fluid sloshing in a three-dimensional tank," *Journal of Marine Science and Technology*, vol. 16, pp. 22-50, December 2011, doi: 10.1007/s00773-010-0111-0.

4. W. Wu, C. Zhen, J. Lu, J. Tu, J. Zhang, Y. Yang, K. Zhu, and J. Duan, "Experimental study on characteristic of sloshing impact load in elastic tank with low and partial filling under rolling coupled pitching," *International Journal of Naval Architecture and Ocean Engineering*, vol. 12, pp. 178-183, 2020, doi: 10.1016/j.ijnaoe.2019.10.003.

5. B. Godderidge, S. R. Turnock, and M. Tan, "Evaluation of a rapid method for the simulation of sloshing in rectangular and octagonal containers at intermediate filling levels," *Computers & Fluids*, vol. 57, pp. 1-24, March 2012, doi: 10.1016/j.compfluid.2011.09.010.

6. H. Jeong and W. Jaewoo Shim, "Calculation of boil-off gas (BOG) generation of KC-1 membrane LNG tank with high density rigid polyurethane foam by numerical analysis," *Polish Maritime Research*, vol. 24, no. 1, pp. 100-114, April 2017, doi: 10.1515/pomr-2017-0012.

7. C. W. Hirt and B. D. Nichols, "Volume of fluid (VOF) method for the dynamics of free boundaries," *Journal of Computational Physics*, vol. 39, no. 1, pp. 201-225, January 1981, doi: 10.1016/0021-9991(81)90145-5.

8. J. Haider, "Numerical modelling of evaporation and condensation phenomena," Thesis, Institut für Raumfahrtsysteme, Universität Stuttgart, Lampoldshausen, 2013.

9. V. Singal, J. Bajaj, N. Awalgaonkar, and S. Tibdewal, "CFD analysis of a kerosene fuel tank to reduce liquid sloshing," *Procedia Engineering*, vol. 69, pp. 1365-1371, 2014, doi: 10.1016/j.proeng.2014.03.130.

10. A. B. Desamala, V. Vijayan, A. Dasari, A. K. Dasmahapatra, and T. K. Mandal, "Prediction of oil-water flow patterns, radial distribution of volume fraction, pressure and velocity during separated flows in horizontal pipe," *Journal of Hydrodynamics*, vol. 28, pp. 658-668, August 2016, doi: 10.1016/S1001-6058(16)60670-4.

11. M. L. Hosain, U. Sand, R. Bel Fdhila, "Numerical investigation of liquid sloshing in carrier ship fuel tanks," *IFAC-PapersOnLine*, vol. 51, no. 2, pp. 583-588, 2018, doi: 10.1016/j.ifacol.2018.03.098.

12. S. H. Rhee, "Unstructured grid based Reynolds-averaged Navier-Stokes method for liquid tank sloshing," *Journal of Fluids Engineering*, vol. 127, no. 3, pp. 572-582, 2005, doi: 10.1115/1.1906267.

13. O. M. Faltinsen and A. N. Timokha, "An adaptive multimodal approach to nonlinear sloshing in a rectangular tank," *Journal of Fluid Mechanics*, vol. 432, pp. 167-200, April 2001, doi: 10.1017/S0022112000003311.

14. O. M. Faltinsen and A. N. Timokha, "Analytically approximate natural sloshing modes and frequencies in two-dimensional tanks," *European Journal of Mechanics – B/Fluids*, vol. 47, pp. 176-187, September-October 2014, doi: 10.1016/j.euromechflu.2014.01.005.

15. N. Parthasarathty, H. Kim, Y. H. Choi, and Y. W. Lee, "A numerical study on sloshing impact loads in prismatic tanks under forced horizontal motion," *Journal of the Korean Society of Marine Engineering*, vol. 41, no. 2, pp. 150-155, 2017, doi: 10.5916/jkosme.2017.41.2.150.

16. M. Hinatsu, "Experiments of two-phase flows for the joint research," In: Proceedings of the SRI-TUHH mini-Workshop on Numerical Simulation of Two-Phase Flows, Ship Research Institute, Tokyo, Japan, pp. 12-19, 2001.

17. Y. H. Chen, Y. F. Yue, Y. Zhang, R. P. Li, and X. Xu, "Numerical investigation of vibration suppression for the combined device of non-Newtonian fluids coupled elastic baffle," *Journal of Applied Fluid Mechanics*, vol. 16, no. 3, pp. 591-602, 2023, doi: 10.47176/jafm.16.03.1311.

18. H. Jin, Y. Liu, H. Li, and Q. Fu, "Numerical analysis of the flow field in a sloshing tank with a horizontal perforated plate," *Journal of Ocean University of China*, vol. 16, no. 4, pp. 575-584, 2017, doi: 10.1007/s11802-017-3369-6.

19. O. Ubbink, "Numerical prediction of two fluid systems with sharp interfaces," Thesis, Department of Mechanical Engineering, London University, January 1997.

20. B. Godderidge, S. Turnock, C. Earl, and M. Tan, "The effect of fluid compressibility on the simulation of sloshing impacts," *Ocean Engineering*, vol. 36, no. 8, pp. 578-587, June 2009, doi: 10.1016/j.oceaneng.2009.02.004.

21. C. Hu and M. M. Kamra, "An unstructured mesh method for numerical simulation of violent sloshing flows," *Journal of Hydrodynamics*, vol. 32, no. 2, pp. 259-266, April 2020, doi: 10.1007/s42241-020-0019-z.

22. B. Godderidge, S. Turnock, M. Tan, and C. Earl, "An investigation of multiphase CFD modelling of a lateral sloshing tank," *Computers & Fluids*, vol. 38, no. 2, pp. 183-193, February 2009, doi: 10.1016/j.compfluid.2007.11.007.

23. H. Akyildiz and E. Ünal, "Experimental investigation of pressure distribution on a rectangular tank due to the liquid sloshing," *Ocean Engineering*, vol. 32, no. 11-12, pp. 1503-1516, 2005, doi: 10.1016/j.oceaneng.2004.11.006.

24. J. H. Jung, H. S. Yoon, and C. Y. Lee, "Effect of natural frequency modes on sloshing phenomenon in a rectangular tank," *International Journal of Naval Architecture and Ocean Engineering*, vol. 7, no. 3, pp. 580-594, May 2015, doi: 10.1515/ijnaoe-2015-0041.

25. S. Wu and Y. Ju, "Numerical study of the boil-off gas (BOG) generation characteristics in a type C independent liquefied natural gas (LNG) tank under sloshing excitation," *Energy*, vol. 223, no. 15, pp. 1-19, May 2021, doi: 10.1016/j.energy.2021.120001.

26. K. P. Thiagarajan, D. Rakshit, and N. Repalle, "The air-water sloshing problem: Fundamental analysis and parametric studies on excitation and fill levels," *Ocean Engineering*, vol. 38, no. 2-3, pp. 498-508, 2011, doi: 10.1016/j.oceaneng.2010.11.019.

27. H. Kim, P. Nanjundan, J. Jeon, and Y. W. Lee, "Numerical estimation on applying air-trapping mechanism to suppress sloshing loads in a prismatic tank," *Journal of Mechanical Science and Technology*, vol. 34, no. 7, pp. 2895-2902, 2020, doi: 10.1007/s12206-020-0621-6.

28. X. Yuan, Y. Su, and P. Xie, "Frequency characteristics of sloshing resonance in a three-dimensional shallow-water rectangular tank," *Journal of Marine Science and Engineering*, vol. 10, no. 11, pp. 1792-1804, November 2022, doi: 10.3390/jmse10111792.

29. H. Kim, M. K. Dey, N. Oshima, and Y. W. Lee, "Numerical study on sloshing characteristics with Reynolds number variation in a rectangular tank," *Computation*, vol. 6, no. 4, pp. 53-63, October 2018, doi: 10.3390/computation6040053.

POLISH MARITIME RESEARCH 4 (120) 2023 Vol. 30; pp. 54-60
10.2478/pomr-2023-0058

ANALYSIS OF THE ENVIRONMENTAL IMPACT OF THE HULL CONSTRUCTION OF A SMALL VESSEL BASED ON LCA

Jacek Nakielski
Gdansk University of Technology, Institute of Naval Architecture, Poland

* Corresponding author: *janak@pg.edu.pl (J.Nakielski)*

ABSTRACT

In recent years, issues related to the impact of human activity on the natural environment have become pressing, and the challenge of global warming necessitates immediate action. To support environmental protection efforts, it has become imperative to adopt a broader perspective when evaluating various products and systems. A valuable tool for such assessments is a life cycle assessment (LCA), which enables a comprehensive analysis of the entire life cycle of a product.
This paper presents a comparative analysis of the hull of a fast patrol craft, fabricated using three different materials: steel, aluminium, and composite materials. The LCA covers every stage from material production, through the construction and use of the hull, to its eventual disposal. A specific criterion was established to evaluate the impact of the hull on the environment, with clearly defined system boundaries.
In the final section, we draw some conclusions that underscore the importance of reusing construction materials. By emphasising this approach, ecological footprints can be minimised and a sustainable future can be created.

Keywords: LCA, hull, craft, recycling materials

INTRODUCTION

Over the past few decades, there has been a substantial increase in awareness of ecological issues and the urgent need for environmental protection. This heightened awareness has primarily been driven by the alarming surge in greenhouse gas emissions, which significantly contribute to Earth's changing climate [1]. Numerous actions are now being carried out to address this critical situation, including changes in approaches to natural resources, production processes, and the exploitation, disposal and recycling of materials.

To evaluate the environmental impact of a given product, the life cycle assessment (LCA) has emerged as a valuable method. This structured approach, which has been standardised by the ISO (International Organization for Standardization) [26], enables a comprehensive evaluation of the inputs and outputs of a product's environmental impact over its entire life cycle. An LCA typically has four main components: goal definition and boundary setting, analysis, impact assessment, and interpretation [3].

Due to the inherent complexity of a ship, conducting a thorough analysis is particularly challenging, and this especially true when interpreting the results. To streamline and enhance the effectiveness of the LCA method, it is advisable to break down the ship into subsystems (hull, engine room, equipment, etc.). A crucial aspect of this process is the selection of appropriate system boundaries, as this can significantly influence the outcomes and their subsequent interpretation [4].

In this paper, an analysis using LCA and life cycle cost analysis (LCCA) is applied to a luxury mono-hull motor yacht [5]. Four design configurations of the hull are considered, and it is shown that the lowest total life cycle cost is found for a configuration with an aluminium hull and carbon fibre composite hatches.

In a study by Wang et al. [6], an analysis based on an LCA was carried out for a hybrid ferry. LCA models were established using commercial software called GaBi (a portmanteau of two German words, Ganzheitliche Bilanzierung), and included various activities associated with the four phases of the ship's life, including steel processing and machinery installations in the shipyard; the operation of the engine and batteries on board; maintenance of the ship hull; and the scrapping of hull materials and machinery. Among other things, these authors presented an optimal strategy for coating of the hull.

For a better understanding of the LCA methodology, the reader is referred to [7]. This paper presents several examples of decisions made based on the LCA methodology; for example, the decision as to whether the hull of the new Greenpeace flagship "Rainbow Warrior III" was to be built from steel or aluminium was made by the Dutch company TNO.35 using the LCA methodology. Based on the results from the LCA, steel was chosen for the hull, while the superstructure and mast were built from aluminium.

METHOD

ENVIRONMENTAL IMPACT ASSESSMENT CATEGORY FOR THE HULL

When assessing the environmental impact of a particular object, the first step is to determine the factors that will define this impact. Today, one of the most widely used criterion for evaluation is the carbon footprint, which represents the total greenhouse gas emissions resulting from the production, operation, and disposal of the hull of a craft. Alternatively, the water footprint or the overall environmental footprint can be considered. In this article, however, energy consumption serves as the chosen category for evaluating the object's environmental impact.

Data on the energy consumption of various technological processes can be found in a diverse range of literature sources. Although the appropriateness of using energy as an environmental impact criterion is subject to debate, we note that energy exhibits a lower variability compared to other physical flows. This enhances its reliability as a measure for assessing the environmental influence of an object.

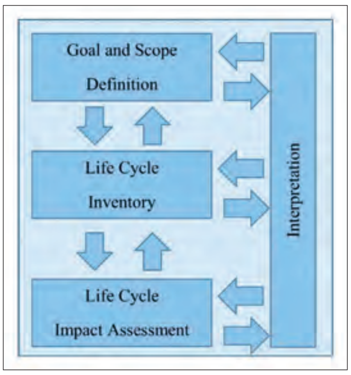

Fig. 1. Phases of an LCA according to ISO 14040:2006 Environmental management—Life cycle assessment—Principles and framework [2]

STUDY OBJECT

The hull of the fast patrol craft described in [8] was chosen as a subject for further analysis. The primary objective was to find the optimal shape of the hull for several different materials. Table 1 provides an overview of the fundamental parameters of the unit, while Figs. 2 and 3 present visual representations of hulls made of aluminium and composite (fibre-epoxy laminate), respectively.

For this study, three materials were considered for the hull: steel, aluminium, and glass-epoxy laminate. Of the characteristic parameters examined here, one of the key factors was the weight of the hull for each material, as shown in Table 2.

Tab. 1. Specifications of the 24 m high-speed patrol craft studied in this paper [8]

Basic parameter	Value	Units
Overall length	23.85	m
Length between perpendiculars	20.05	m
Overall breadth	5.10	m
Draft design waterline	0.97	m
Loaded displacement	48.20	tons
Light displacement	38.20	tons
Total power installed	1380	kW

Table 2 shows the weights of the hull when made of different materials.

Tab. 2. Mass of the hull of the 24 m high-speed patrol craft [8]

Material	Mass [kg]
Steel (NV40)	16,700
Aluminium (NV-5083)	8,700
Composite (fibre-reinforced epoxy)	7,700

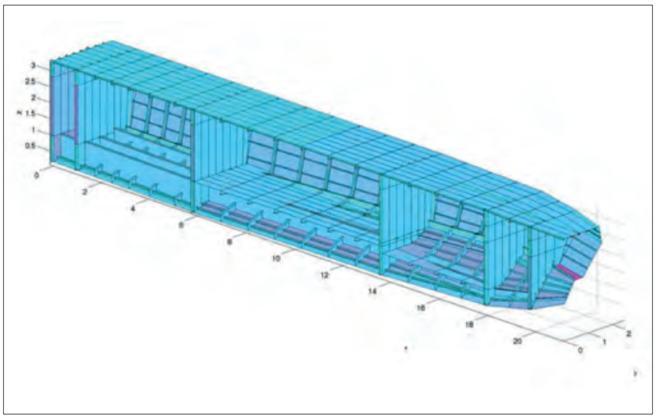

Fig. 2. Structure of the aluminium hull [8]

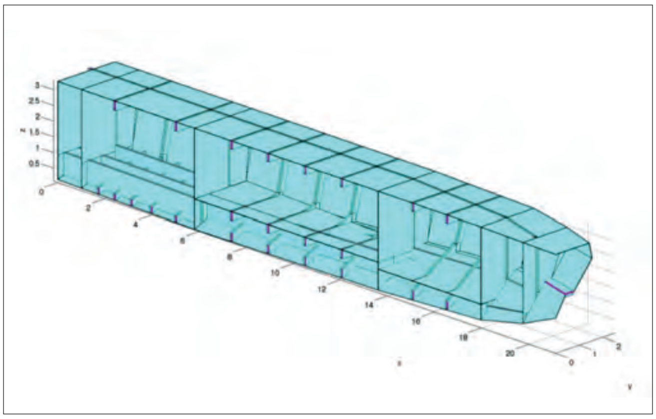

Fig. 3. Structure of the composite hull [8]

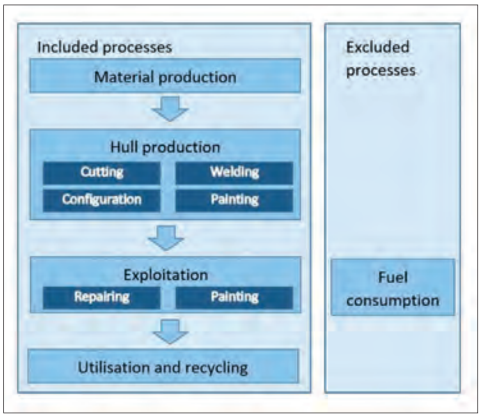

Fig. 4. Boundaries of the system [2]

BOUNDARIES OF THE SYSTEM

To conduct a comprehensive analysis based on LCA, it is vital to establish clear boundaries and definitions. In the analysis presented below, the boundaries have been precisely defined as follows [9]:

1. A „cradle-to-grave" approach is applied that considers the entire life cycle of the hull, encompassing the production of materials required for its construction, its operational phase (lasting 20 years), eventual disposal, and the potential for material reuse.
2. Characteristics of the hull that remain constant and do not vary depending on the material used have been excluded from the analysis.
3. The assumption is made that all materials and processes examined here are exclusively used to construct the hull, and are not employed elsewhere.
4. Fuel consumption has been excluded from the analysis, given that a lighter hull generally leads to reduced fuel consumption or requires a less powerful engine for propulsion.
5. The production of tools and other materials essential for the construction of the hull is not considered in this study.

Clearly defining these boundaries allows the analysis to be focused and relevant, and permits a more accurate evaluation of the hull's environmental impact based on the selected criteria. The boundaries of the system are illustrated in Fig. 4.

RESULTS

PRIMARY PRODUCTION OF MATERIALS

To determine the energy consumption over the entire life cycle of the hull, the initial step is to calculate the energy consumed in the production of each individual material. This analysis includes the primary production of the material, starting from the extraction procedure, and all necessary technological processes; the energy needed to obtain materials from recycling is also considered.

Table 3 presents a comprehensive summary of the results for the energy consumption during production of the materials used to construct the hull of the craft. These findings serve as a basis for a further evaluation of the hull's environmental impact using the LCA approach.

From the table above, it can be seen that the production of aluminium is the most energy-intensive process among the materials considered here: for instance, the energy consumption associated with the recycling of aluminium is comparable to the primary production of steel. However, for the construction of the same hull, approximately twice as much steel is needed compared to aluminium. The production of composite materials is also a highly energy-intensive process.

Tab. 3. Total energy required to produce the hull material [4], [10], [11], [12]

Process	Mass	Units	SEC	Units	Energy consumption	Unit
Steel production (primary steel)	16,700	kg	22.00	MJ/kg	367,400	MJ
Steel production (recycled steel)	16,700	kg	8.60	MJ/kg	143,620	MJ
Aluminium production (primary aluminium)	8,700	kg	220.0	MJ/kg	1,914,000	MJ
Aluminium production (recycled aluminium)	8,700	kg	20.0	MJ/kg	174,000	MJ
Production of glass-epoxy laminate	7,700	kg	70.0	MJ/kg	539,000	MJ
Production of glass-epoxy laminate						

Tab. 4. Energy consumed in the production of the steel hull

Process	Mass	Units	SEC	Units	Energy consumption	Unit
Cutting with an oxy-acetylene torch	262.00	m	0.25	MJ/m	65.50	MJ
MAG welding of transverse stiffeners	821.00	m	4.70	MJ/m	3,858.70	MJ
MAG welding of longitudinal stiffeners	821.00	m	5.50	MJ/m	4,515.50	MJ
MAG welding hull and deck plating	262.00	m	3.00	MJ/m	786.00	MJ
Painting – wetted surface area of the hull	148.00	m^2	38.00	MJ/m^2	5,624.00	MJ
Painting – unwetted surface area of the hull	77.84	m^2	25.00	MJ/m^2	1,946.00	MJ
Painting – deck area	99.74	m^2	25.00	MJ/m^2	2,493.50	MJ
Painting – surface of the inner part of the hull	508.71	m^2	10.00	MJ/m^2	5 087.6	MJ
				Total:	24,493.50	MJ
SEC - specific energy consumption						

Tab. 5. Energy consumed in the production of the aluminium hull

Process	Mass	Units	SEC	Units	Energy consumption	Unit
Water jet cutting	262.00	m	0.06	MJ/m	15.72	MJ
Friction stir welding – longitudinal stiffeners	630.00	m	1.20	MJ/m	756.00	MJ
Friction stir welding – transverse stiffeners	260.00	m	1.20	MJ/m	312.00	MJ
Friction stir welding – hull and deck plating	262.00	m	1.20	MJ/m	314.00	MJ
Painting – wetted surface area of the hull x	148.00	m^2	28.00	MJ/m^2	4,144.00	MJ
Painting – unwetted surface area of the hull x	77.84	m^2	15.00	MJ/m^2	1,167.60	MJ
Painting – deck area	99.74	m^2	15.00	MJ/m^2	1,496.10	MJ
Painting – surface of the inner part of the hull	554.95	m^2	10.00	MJ/m^2	5,549.52	MJ
				Total:	13,755.34	MJ
SEC - specific energy consumption						

Tab. 6. Energy consumed in the production of the composite hull

Process	Mass	Units	SEC	Units	Energy consumption	Unit
Plug	213.00	m^2	51.00	MJ/m^2	10,863.00	MJ
Steel supporting structure	213.00	m^2	10.00	MJ/m^2	2,130.00	MJ
Vacuum infusion process	213.00	m^2	7.00	MJ/m^2	1,491.00	MJ
Curing	213.00	m^2	430.00	MJ/m^2	91,590.00	MJ
Painting – wetted surface area of the hull	148.00	m^2	28.00	MJ/m^2	4,144.00	MJ
Painting – unwetted surface area of the hull	77.84	m^2	15.00	MJ/m^2	1,167.60	MJ
Painting – deck area	99.74	m^2	15.00	MJ/m^2	1,496.10	MJ
Painting – surface of the inner part of the hull	485.58	m^2	10.00	MJ/m^2	5,855.83	MJ
				Total:	117,737.53	MJ
SEC - specific energy consumption						

HULL CONSTRUCTION

To estimate the energy costs associated with the construction of the hull, including processes such as cutting, welding, vacuum infusion, hardening, and painting, specific parameters needed to be calculated, such as the weld lengths, mould surfaces, and surfaces to be painted. These calculations and estimates were made based on data from references [8] and [13].

We note that when constructing a hull using primary or recycled steel, the energy costs remain constant. Similarly, for an aluminium hull, the energy consumed during the production process is unchanged regardless of whether the aluminium used for production is from primary or recycled sources.

Table 4 summarises the individual processes related to the production of the steel hull.

A very similar combination of individual postproduction processes are also found for the construction of the aluminium hull (see Table 5).

The production technology used for the composite hull differs significantly from the steel and aluminium hulls. An important step in the production of the composite hull is the implementation of a „plug" used as the basis for the lamination process. For serial production, the plug can be reused, leading to reduced energy expenditure; however, for the purposes of this article, unit production is assumed.

The results for the energy balance for the entire production process, including material production and hull construction, are interesting. For primary steel, the hull construction process accounts for only 6.63% of the overall energy consumption at this stage, whereas for an aluminium hull, this value is only 0.72%. When the materials are obtained from recycling, these values rise to 39.09% for steel and 9.09% for aluminium. In contrast, for a hull made using composite technology, the percentage is 21.84%. Fig. 5 shows a graph of these values.

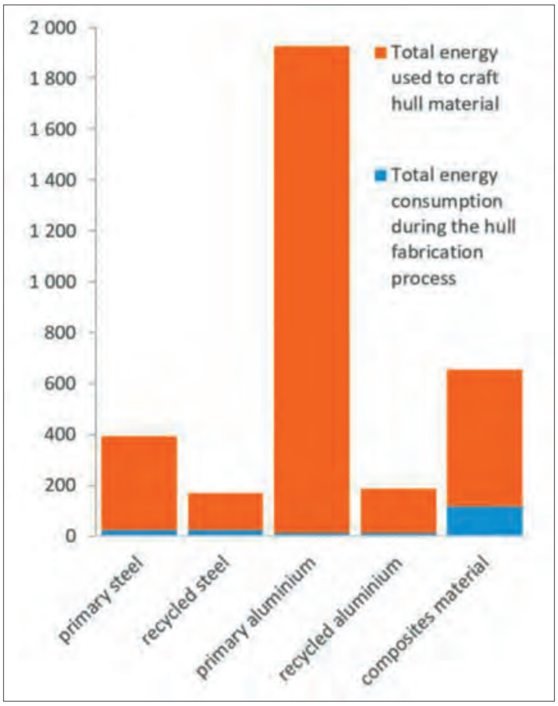

Fig. 5. Total energy consumed in producing the hull material and fabricating the hull

HULL USE

The next stage in the life cycle of the hull is its usage. In the scenario considered here, we assume that each year, 10% of the material of the hull will be replaced, regardless of the material or technology used for construction. Although other scenarios could be considered, we adopt a simplified approach for the sake of this analysis. In addition, we assume that the life expectancy of each hull is 20 years, though this assumption may be subject to question, as hulls often remain in service beyond two decades. The replacement process itself, together with the energy consumed during the production of the replacement material, makes up 10% of the energy required for the production of the original hull (in the case of the composite material hulls, energy costs related to the production of the plug are not included).

Another factor related to hull usage is maintenance, which mainly involves painting. Steel hulls are repainted every five years, while those made of other materials require annual repainting.

Table 7 provides a comprehensive overview of each type of hulls and the individual energy costs during use.

Tab. 7. Energy consumed during use

Process	Energy consumption	Units
Primary steel		
Total energy used to craft hull material	36,740.00	MJ
Total energy consumed in the hull fabrication process	922.57	MJ
Painting (every five years)	15,150.56	MJ
Total over 20 years	813,853.64	MJ
Secondary steel		
Total energy used to craft hull material	14,362.00	MJ
Total energy consumed in the hull fabrication process	922.57	MJ
Painting (every five years)	15,150.56	MJ
Total over 20 years	366,293.64	MJ
Primary aluminium		
Total energy used to craft hull material	191,400.00	MJ
Total energy consumed in the hull fabrication process	139.81	MJ
Painting (every year)	12,357.22	MJ
Total over 20 years	1,927,755.34	MJ
Secondary aluminium		
Total energy used to craft hull material	17,400.00	MJ
Total energy consumed in the hull fabrication process	139.81	MJ
Painting (every year)	12,357.22	MJ
Total over 20 years	597,940.64	MJ
Composite material		
Total energy used to craft hull material	52,813.70	MJ
Total energy consumed in the hull fabrication process	10,607.40	MJ
Painting (every year)	11,663.53	MJ
Total over 20 years	1,501,692.60	MJ

RECYCLING AND DISPOSAL

When considering the life cycle of the hull for a selected craft, the final element is disposal, as steel and aluminium hulls can be recycled. The disposal process involves cutting or dismembering the hull, which naturally consumes energy. However, steel and aluminium offer extensive possibilities for reuse, with up to 95% of the hull weight being recyclable according to [5]. In contrast,

Tab. 8. Recycling and disposal

Process	Mass	Units	SEC	Units	Energy consumption	Unit
Steel						
Cutting with an oxy-acetylene torch	846.00	m	0.25	MJ/m	211.50	MJ
Reuse of steel					–212 591.00	MJ
				Total:	–212 379.50	MJ
Aluminium						
Plasma cutting	846.00	m	0.86	MJ/m	727.56	MJ
Reuse of aluminium					–1 653 000.00	MJ
				Total:	–1 652 272.44	MJ
Composite material						
Shredding	7,700.00	kg	0.92	MJ/kg	7,084.00	MJ
Burning	770.00	kg	30.00	MJ/kg	–23,100.00	MJ
				Total:	–16,016.00	MJ
SEC - specific energy consumption						

only 5% of a composite hull can be recycled [5]. Research is under way to improve the recycling possibilities for composite materials [14, 15].

DISCUSSION

Table 9 and Fig. 6 show the total energy consumption for each type of material considered here. For recycled steel and aluminium, the environmental benefits from their reuse were not taken into account.

Tab. 9. Total energy consumption

Primary steel	Recycled steel	Primary aluminium	Primary aluminium	Composite material
993.25 GJ	534.50 GJ	4,353.42 GJ	786.42 GJ	2,142.41 GJ

The data show that building a hull from primary aluminium incurs the highest energy consumption, followed by a hull made of composite materials. The use of recycled materials significantly reduces the energy consumption, and this is particularly noticeable for aluminium. Although steel hulls are the heaviest, steel is found to be the most energy-efficient material. The energy cost for primary steel is only about 200 GJ higher than that of recycled aluminium. The difference in energy cost between primary and recycled aluminium is considerable, whereas the difference between virgin and recycled steel is relatively smaller. A hull made of recycled steel is 1.86 times less energy-consuming than a hull made of virgin steel; in contrast, the ratio for aluminium is 5.34.

Composite materials are relatively inefficient in terms of energy consumption, as the recycling of these materials is challenging. Intensive research is ongoing to make the recycling of composite materials more efficient.

CONCLUSION

In this study, a relatively simple model was considered with similar life cycle scenarios for hulls made of different materials. In future analyses, the life cycle scenarios for specific materials may be calculated with greater precision.

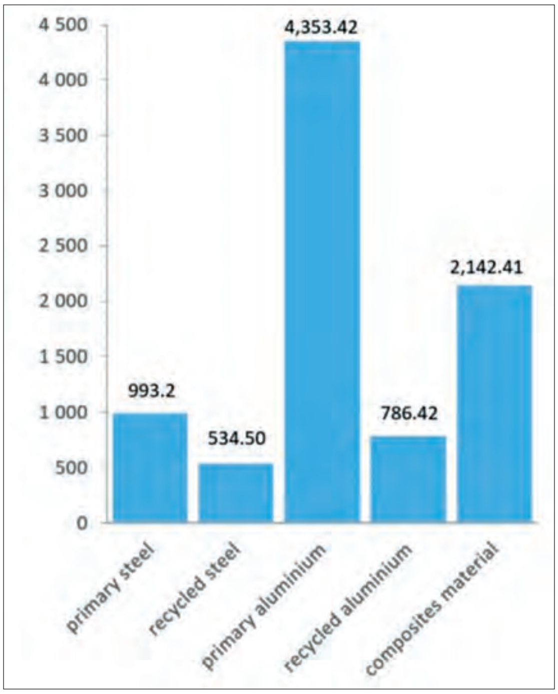

Fig. 6. Total energy consumption

Technological processes such as welding or gas cutting, which are based on electrical or chemical energy, are less energy-efficient than processes based on mechanical energy, such as welding and water jet cutting.

The analysis of the hull production focused on the processes themselves (cutting, welding, painting). However, the overall energy required to make the hull is higher than that considered here, because our analysis did not take into account factors such as transport, water consumption, electricity needed for lighting and ventilation, etc. A comparison of the ratio of the energy used in the production of the hull to the energy needed to produce the material (0.72% for aluminium, 6.63% for steel) need not take this additional energy into account, but in future research, the total energy cost of hull production, especially for recycled and composite materials, could be calculated to give more accurate results.

The production stage of the individual materials incurred the highest energy cost, meaning that the development of technologies to reduce energy consumption during production processes is crucial. It is also important to ensure that the energy used in the production of steel or aluminium comes from renewable sources.

The choice of hull material significantly influences both the energy costs and the environmental footprint. Analyses such as the one presented here can aid in making informed decisions at the design stage.

One key element of a strategy for reducing the cost of energy consumption, and hence the impact on the environment, is the reuse of materials. In the case considered here, this was particularly applicable to aluminium.

REFERENCES

1. J. Barreiro, S. Zaragoza, and V. Diaz-Casas, 'Review of ship energy efficiency', *Ocean Engineering*, Volume 257, 2022. doi: 10.1016/j.oceaneng.2022.111594.

2. ISO 14040:2006 Environmental management - Life cycle assessment - Principles and framework.

3. S.D. Chatzinikolaou and N.P. Ventikos, 'Assessing environmental impacts of ships from a life cycle perspective', in *2nd International Conference on Maritime Technology and Engineering, MARTECH 2014*, Lisbon, Portugal, 15-17 October 2014. doi.org/10.1201/b17494

4. L. Joosten, 'The Industrial Metabolism of Plastics. Analysis of Material Flows, Energy Consumption and CO_2 Emissions in the Lifecycle of Plastics', PhD [Dissertation], Utrecht University, 2001.

5. C. Favi, M. Germani, F. Campi, M. Mandolini, S. Manieri, M. Marconi, and A. Vita, 'Life cycle model and metrics in shipbuilding: How to use them in the preliminary design phases', in *25th CIRP Life Cycle Engineering (LCE) Conference*, Copenhagen, Denmark, 30 April – 2 May 2018. doi: 10.1016/j.procir.2017.11.071

6. H. Wang, E. Oguz, B. Jeong, and P. Zhou, 'Life cycle cost and environmental impact analysis of ship hull maintenance strategies for a short route hybrid ferry', *Ocean Engineering*, Volume 161, Pages 20-28, 2018. doi: 10.1016/j.oceaneng.2018.04.084

7. T. Pawlik, Ed., 'Ship life cycle assessment and management', City University of Applied Sciences and GAUSS GmbH, Bremen, Germany, 2011.

8. I. Stenius, A. Rosén, and J. Kuttenkeuler, 'On structural design of energy efficient small high-speed craft', KTH Centre for Naval Architecture, *Marine Structures*, Volume 24(1): Pages 43-59, 2010. doi: 0.1016/j.marstruc.2011.01.001

9. P. Borowiec, 'Life cycle assessment for selected vessel', MSc [Dissertation], Gdansk University of Technology, 2022.

10. S. V. Joshi, L. T. Drzal, A. K. Mohanty, and S. Arora, 'Are natural fiber composites environmentally superior to glass fiber reinforced composites?', *Composites Part A: Applied Science and Manufacturing*, Volume 35, Issue 3, Pages 371-376, 2004. doi: 10.1016/j.compositesa.2003.09.016

11. P. Michaelis, T. Jackson, and R. Clift, 'Exergy analysis of the life cycle of steel', *Energy* Volume 23, Issue 3, Pages 213-220, 1998. doi: 10.1016/S0360-5442(97)00081-9

12. G. Rombach and D. Liebig, 'A scenario to optimise the energy demand of aluminium production depending on the recycling quota', *Resources, Conservation and Recycling*, Volume 33, Issue 3, Pages 217-234, 2001. doi: 10.1016/S0921-3449(01)00086-6.

13. F. Nicolae, C. Popa, and H. Beizadea, 'Applications of life cycle assessment (LCA) in shipping industry', *14th International Multidisciplinary Scientific GeoConference & EXPO SGEM2014, Section Air Pollution and Climate Change*, Albena, Bulgaria, 17-26 Jun 2014. doi: 10.5593/sgem2014/b42/s19.038.

14. Jianqiao Wu, Ying Pan, Ziyi Ruan, Ziji Zhao, Jing Ai, Jinghai Ban, and Xianghai Jing, 'Carbon fiber-reinforced epoxy with 100% fiber recycling by transesterification reactions', *Frontiers in Materials Sec. Polymeric and Composite Materials*, Volume 9, 2022. doi: 10.3389/fmats.2022.1045372.

15. M. M. Rabby, M. Rahman, P. P. Das, V. Vadlamudi and R. Rassel, 'Carbon fibers recycling from degraded prepress and mechanical properties of recycled composite', *North America Society for the Advancement of Material and Process Engineering (SAMPE)*, Seattle, United States, 17 April 2023. doi: 10.33599/nasampe/s.23.0267.

sciendo

POLISH MARITIME RESEARCH 1 (117) 2023 Vol. 30; pp. 61-73
10.2478/pomr-2023-0059

EFFECTS OF PROPELLER FOULING ON THE HYDRODYNAMIC PERFORMANCE OF A MARINE PROPELLER

Ali Zinati
Department of Maritime Engineering, Amirkabir University of Technology, Tehran, Islamic Republic of Iran
Mohammad Javad Ketabdari
Department of Maritime Engineering, Amirkabir University of Technology, Tehran, Islamic Republic of Iran
Hamid Zeraatgar *
Faculty of Marine Technology, Amirkabir University of Technology, Tehran, Islamic Republic of Iran

* Corresponding author: *hamidz@aut.ac.ir (Hamid Zeraatgar)*

ABSTRACT

Propeller performance is typically considered under clean conditions, despite the fact that fouling is an inevitable phenomenon for propellers. The main objective of this study is to investigate the effects of roughness due to fouling on the performance of a propeller using a CFD simulation in conjunction with the roughness function model. A simulation of a clean propeller is verified for a five-blade propeller model using existing experimental results. A roughness function model is then suggested based on existing measured roughness data. The simulations are extended for the same propeller under varying severities of roughness. Initially, it is concluded that K_T and η_o gradually decrease with increasing fouling roughness, while K_Q increases, compared to smooth propeller. For instance, at J=1.2 for medium calcareous fouling, K_T is reduced by about 26%, K_Q increases by about 7.0%, and ηo decreases by 30.9%. In addition, for the rough propeller, the extra power required is defined as the specific sea margin (SSM) to compensate for the power loss. A slight roughness causes a large decrease in η_o. A propeller painted with foul-release paint and an unpainted propeller are found to require 2.7% SSM and 57.8% SSM over four years of service, respectively. Finally, the use of foul-release paints for propeller painting is strongly advised.

Keywords: Propeller performances, Blade roughness, Frictional resistance, CFD simulation, Fouling

INTRODUCTION

Nowadays, shipping is a more important means of transportation compared to land and aviation. World globalisation has increased shipping traffic, transportation, and the capacities of goods transporters, which has increased fuel consumption as a result. Ships are a contributor to greenhouse gas (GHG) emissions [1], and in recent years, increasing pressure has been placed on the marine industry to decrease GHG emissions through regulatory legislation. IMO (International Maritime Organization) indicated that efficiency improvements could be achieved through operational [2] and technological methods, as these could increase overall performance and decrease fuel consumption [3-10]. Temporary roughness, which refers to temporal changes in the hull and propeller surface roughness, is caused by fouling organisms during a period of service [8]. The increase in skin resistance due to fouling is responsible for a significant proportion of the total resistance, as a small amount of fouling can cause a significant increase in fuel consumption and air pollution.

The effects of roughness on hulls and propellers can be evaluated using the boundary layer similarity law or the CFD method. Both of these methods require a roughness function for the surface in question.

As mentioned at ITTC 2021 [11], there is a need to adopt or develop new methods to predict the roughness effects of marine biofouling and modern fouling-control coatings on ship hydrodynamics and propeller performance. For this reason, ITTC 2021 recommended that the roughness function should be determined or developed by researchers for different surface conditions [11].

Several roughness function models have been proposed that are appropriate for different surface conditions. Some of these consider antifouling coatings such as the Townsin [12], Demirel [13], Vargas [14], and Grigson of Colebrook types [15]. One roughness function model proposed by Song [16] was appropriate for polished surfaces with sandpaper 60 and 80. Another roughness function model for surfaces covered with closely packed sand grain roughness was proposed by Cebeci [17]. The effects of biofilm can be predicted using the roughness function model of Farkas [18]. However, research on roughness function models is still needed, as indicated by ITTC 2021 [11] for the prediction of the roughness effects of marine biofouling.

The impacts of hard fouling and biofilm on the performance of ships using the roughness function proposed by Grigson were studied by Farkas et al. [19, 20]. The impact of inhomogeneous roughness distribution on the frictional resistance of a plate was considered using the roughness function model in conjunction with a longitudinal roughness position [21].

The roughness effects of fouling conditions on the performance of some propellers have been investigated using CFD simulations. Kellett et al. [22] investigated the effect of biofouling on a real four-blade ship propeller at the model scale using the roughness function approach. Owen et al. [23] calculated the performance of a PPTC propeller under different fouling conditions using a previously developed roughness function. Song et al. [24, 25] investigated the roughness effect of barnacles with varying sizes and coverage of a KP505 propeller using a roughness function of the Grigson type. The impact of biofilm on propeller performance was studied by Farkas et al. [26-28]. These studies have indicated that biofilms significantly decrease propeller performance, and should therefore be given due importance.

CFD-based hydrodynamic analysis has been extensively employed in many areas of research. However, the literature review above indicates that CFD cannot represent the complex geometry of a rough surface such as a propeller. ITTC 2021 [11] recommended employing either the similarity law or CFD simulations in conjunction with the roughness function model in order to include roughness effects. The main objective of this study is to investigate the effects of roughness on propeller performance through the use of CFD simulation with a roughness function model. In addition, an attempt is made to introduce a new roughness function model. To achieve these aims, a five-blade propeller model is considered. The clean propeller is simulated and compared to existing experimental results for validation, and the simulations are then extended to represent several severities of roughness for the same propeller using the verified simulation setup. The results are analysed, and the extra power required to compensate for the power loss of the roughed propeller is formulated and estimated. The effects of painting propellers as a means to diminish the roughness are also considered. The novelty of this study is that it sheds light on the details of the propeller performance with respect to surface roughness and presents a new roughness function model.

EFFECTS OF ROUGHNESS ON THE BOUNDARY LAYER

A turbulent boundary layer is assumed to consist of two regions: an inner area and an outer area. The flow in the inner area is affected by the surface roughness, whereas the flow in the outer area is independent of the surface conditions.

The velocity profile for smooth walls in the log-law region of a turbulent boundary layer can be defined as follows:

$$U^+ = \frac{1}{\kappa} ln\,(y^+) + B \tag{1}$$

where y^+ is the non-dimensional normal distance from the wall, κ is the von Karman constant, and B is the smooth wall log-law intercept.

Roughness leads to a decrease in the log-law velocity profile, and the downward shift of the velocity profile for rough walls is known as the roughness function, ΔU^+. The log-law velocity profile for rough walls in the turbulent boundary layer is [25]:

$$U^+ = \frac{1}{\kappa} ln(y^+) + B - \Delta U^+ \tag{2}$$

Various parameters can be used to define roughness, but the most frequently used is the roughness height, k_s. The dimensionless form of the roughness height is the roughness Reynolds numberk_s^+, defined as $k_s^+ = k_s\, U_\tau/\nu$, where U_τ is the friction velocity.

The most common method of solving for the turbulent boundary layer flow near the wall is to implement a wall function approach using an appropriate roughness function model.

PROPULSION CHARACTERISTICS

For a propeller in open-water conditions, the thrust coefficient, K_T, torque coefficient, K_Q, and efficiency, η_0, are expressed in non-dimensional forms. When the propeller is fitted aft of the hull, the incoming flow is non-uniform, and the quasi-propulsive efficiency coefficient, η_D, is a function of the open-water efficiency, η_O, the relative rotative efficiency, η_R, and the hull efficiency, η_H, as follows:

$$\eta_D = \eta_O\, \eta_H\, \eta_R \tag{3}$$

NUMERICAL SIMULATION

In this section, the governing equations are introduced, the roughness function is presented, and the numerical simulations of smooth and roughed propellers are explained.

MATHEMATICAL FORMULATION

The governing equations in this context are those of mass and momentum conservation, which for compressible flows in the Cartesian coordinate system are as follows [23]:

$$\frac{\partial(\rho \bar{u}_i)}{\partial x_i} = 0 \tag{4}$$

$$\frac{\partial(\rho \bar{u}_i)}{\partial x_i} + \frac{\partial}{\partial x_i}\left(\rho \bar{u}_i \bar{u}_j + \rho \overline{u_i' u_j'}\right) = -\frac{\partial \bar{p}}{\partial x_i} + \frac{\partial \overline{\tau_{ij}}}{\partial x_j} \tag{5}$$

where ρ is the density, $\rho\overline{u_i' u_j'}$ is the Reynolds stress, $\bar{u}_i$ is the averaged Cartesian component velocity, and p is the mean pressure. $\overline{\tau_{ij}}$ are the mean viscous stress tensor components, as follows:

$$\overline{\tau_{ij}} = \mu\left(\frac{\partial \bar{u}_i}{\partial x_j} + \frac{\partial \bar{u}_j}{\partial x_i}\right) \tag{6}$$

where μ is the dynamic viscosity.

The Reynolds-averaged Navier-Stokes (RANS) method is employed to solve the governing equations using the commercial CFD software STAR-CCM+. The flow variables are discretised in space using second-order schemes, and the convection term of the turbulence is used as a first-order upwind scheme. The shear stress transport (SST) k-ϖ turbulence model is applied to the complete RANS equations, as this combines the advantages of the k-ϖ and k-ε turbulence models. In this model, the k-ϖ formulation is applied to the inner part of the boundary layer, and the k-ε formulation to the free stream, which gives better predictions of the flow separation and adverse pressure gradients. To achieve reliable results, an appropriate choice of grids is crucial.

Physical modeling of the roughness geometry is not practical in CFD, due to its complexity. The wall-function approach is therefore applied to solve the flow equations near the wall, rather than using turbulence-model equations up to the wall.

PROPOSED ROUGHNESS FUNCTION

In general, roughness functions are obtained experimentally, since there is no universal roughness function model for all kinds of rough surfaces. It should be noted that the impact of roughness on ΔU^+ depends on the type and coverage of the roughness.

In this study, the roughness parameters measured by Schultz and Flack [29] are used to develop a new roughness function model. The proposed model is fitted to the roughness function values reported by Schultz and Flack [29]. One advantage of our roughness function model is that it can be applied to all types of fouled surfaces and typical antifouling coatings. The values of the sand grain roughness height and other relevant data are shown in Table 1 for a range of surface conditions.

Tab. 1. Representative coating and fouling conditions [23]

Description of condition	NSTM rating*	ks (μm)	R_{t50} (μm)
Hydraulically smooth surface	0.	0	0
Typical as applied AF coating	0	30	150
Deteriorated coating or light slime	10–20	100	300
Heavy slime	30	300	600
Small calcareous fouling or weed	40–60	1,000	1,000
Medium calcareous fouling	70–80	3,000	3,000
Heavy calcareous fouling	90–100	10,000	10,000
* NSTM (2002): Naval Ships' Technical Manual			

The proposed roughness function model is as follows:

$$\Delta U^+ = \begin{cases} 0 & k_s^+ \le 2.5 \\ \frac{1}{\kappa}\, ln\,(0.2667\, k_s^+)^{sin\left[\frac{\pi}{2}\frac{log(k_s^+/2.5)}{log\,(10)}\right]} & 2.5 < k_s^+ < 25 \\ \frac{1}{\kappa}\, ln\,(0.2667\, k_s^+) & k_s^+ \ge 25 \end{cases} \tag{7}$$

A brief explanation of the development of this roughness function model is presented in Appendix A.

Fig. 1 shows a schematic representation of the proposed roughness function model in Eq. (7), and compares it with the measurements of Schultz and Flack [29]. Good agreement is observed between the two.

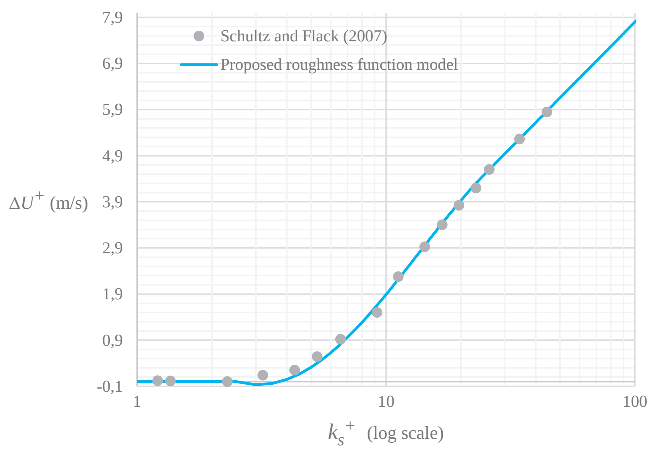

Fig. 1. Comparison of the proposed roughness function model with the values reported by Schultz and Flack [29]

The proposed roughness function model has a similar form to the built-in wall function of STAR-CCM+, and is employed as the wall function of STAR-CCM+. The proposed model is introduced to the CFD simulation setup via the coefficients $B = 0$, $C = 0.2667$, $R^{+}_{smooth} = 2.5$, and $R^{+}_{rough} = 25$ (Eq. (7)), to replace the STAR-CCM+ coefficients $B = 0$, $C = 0.253$, $R^{+}_{smooth} = 2.25$, and $R^{+}_{rough} = 90$. Hence, the mathematical formulation and flow calculations around the roughed propeller are the same as for the smooth propeller except for the roughness function model.

PROPELLER GEOMETRY

The VP1304 propeller has often been used for computational case studies, and was selected here for analysis. It is a five-blade right-handed propeller model with a diameter of 250 mm (Fig. 2). Specifications of the propeller are shown in Table 2 [30].

Tab. 2. Specifications of the VP1304 propeller

Parameter	Symbol	Value	Units
Number of blades	Z	5	-
Diameter	D	0.250	m
Area ratio	A_E/A_0	0.779	-
Pitch ratio at 0.7 R	$P_{0.7}/D$	1.635	-
Chord length at 0.7 R	$C_{0.7}$	0.104	m
Hub ratio	d_h/D	0.3	-
Rotation rate	n	15	rps
Advance coefficient	J	0.6–1.2	-
Inflow speed	V_A	adjust	m/s

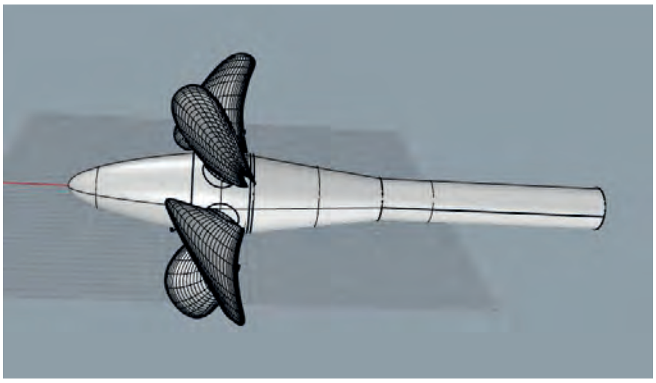

Fig. 2. Propeller geometry

COMPUTATIONAL DOMAIN AND BOUNDARY CONDITIONS

The computational domain is depicted in Fig. 3, where the length and diameter of the domain for the open-water simulations are 9D and 4D, respectively. The inlet is located at a distance 2D upstream, and the outlet is located at a distance 7D downstream, to avoid any reflections and to ensure a uniform inflow. The top and bottom boundary distances are 2D. The computational domain consists of two parts: the inner region, which rotates with the propeller, and the outer part, which is fixed.

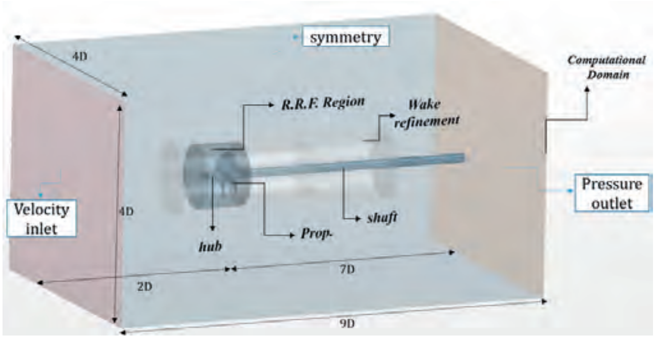

Fig. 3. Dimensions of the computational domain

Appropriate boundary conditions need to be applied to ensure accurate simulations. In this study, we set the velocity inflow for the inlet and the pressure boundary conditions for the outlet. The outer walls - are set to the slip wall condition, while a no-slip rough wall condition -is applied to the propeller, shaft, and hub, to represent rough surfaces. The water density and kinematic viscosity are 998.67 kg/m^3 and 1.070×10^{-6} m/s^2, respectively. The boundary conditions are summarised in Table 4 and Fig. 3.

Tab. 3. Boundary conditions

Region	Boundary	Type
Fixed parts	Inflow	Velocity inlet
	Outflow	Pressure outlet
	Shaft	No-slip condition
	Outer walls	Slip condition
Rotating parts	Hub	No-slip condition
	Blades	No-slip condition
	Interface	Nearest cell interpolation

GRID GENERATION

In order to achieve reliable results, the generation of appropriate grids is crucial. The rotating reference frame (RRF) method is adopted for the propeller simulations in this study. Since RRF does not require a complicated mesh motion and a steady-state solver can be used, it is simpler and computationally cheaper than unsteady approaches. In this approach, the domain remains stationary, with an assigned frame of reference rotating about an axis in the global coordinate system. Fig. 4 depicts the structured and unstructured grids, and Fig. 5 shows the propeller surface grids. The outer cylinder is meshed with coarse grids, and the inner cylinder with fine ones. The distance of the first cell from the wall, y^+, is given in Fig. 6.

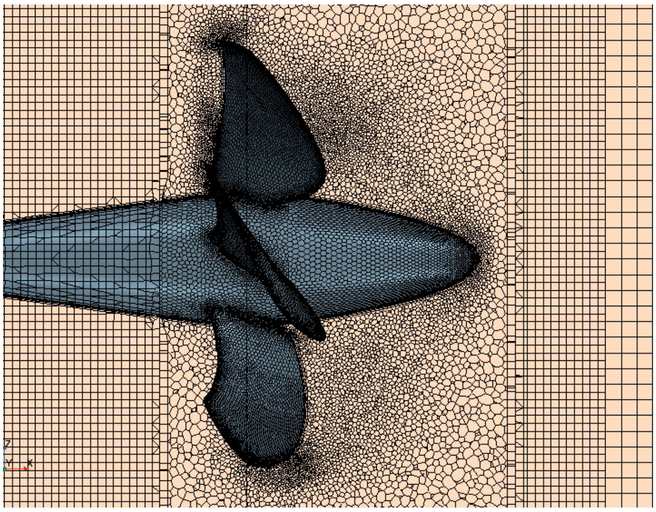

Fig. 4. Domain grids

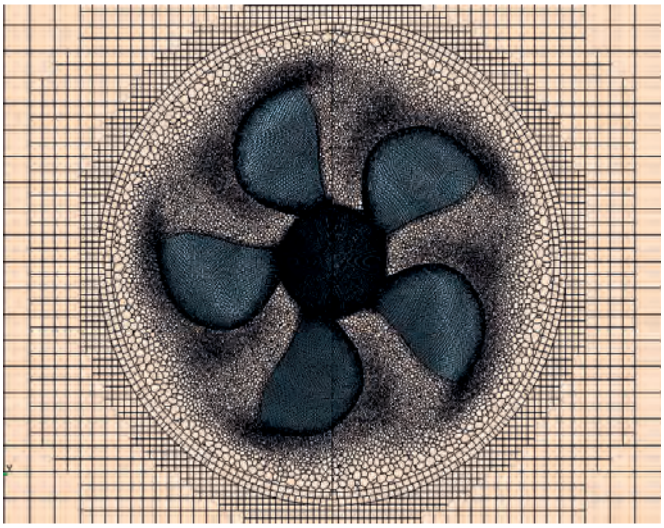

Fig. 5. Propeller surface grids

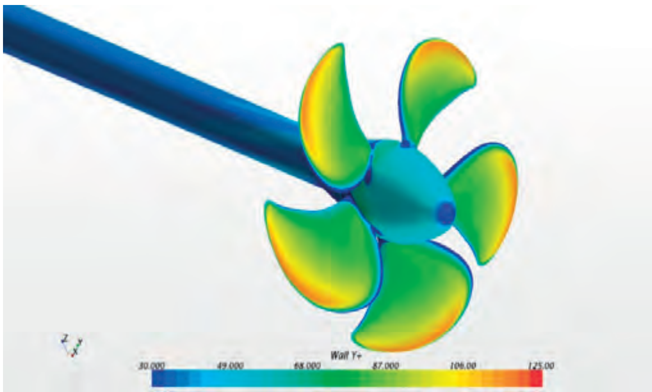

Fig. 6. Distance of the first cell from the wall, y^+

RESULTS

This section presents the CFD results for the propeller. The computational results are first compared with open-water experimental results for a smooth propeller, for validation purposes. The simulation procedure is then applied to a range of fouling conditions to investigate the effects of fouling roughness on the open-water performance. Finally, the required extra power is introduced and estimated in terms of the *specific sea margin, SSM*, for the power loss of the roughed propeller. Values of the *SSM* are obtained for roughed and painted propellers.

MESH SENSITIVITY AND VERIFICATION STUDY

A mesh sensitivity study is carried out to investigate the thrust coefficient for coarse to fine grids. Fig. 7 shows the uniform convergence of mesh sizes, and it can be seen that there are no signs of divergence or oscillation. The grid sensitivity is tested by estimating the numerical uncertainty. The grid convergence index (GCI) with the Richardson extrapolation [31] is employed to calculate the discretisation error, and a mesh refinement factor $r = \sqrt{2}$ of is chosen.

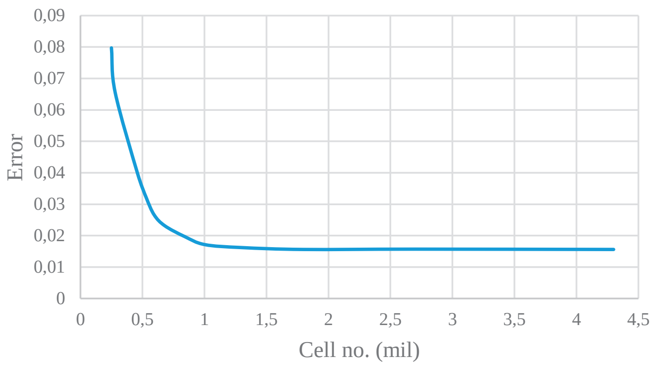

Fig. 7. Grid convergence results for K_T

he uncertainty is obtained using the following equations:

$$\varepsilon_{21} = \phi_2 - \phi_1$$
$$\varepsilon_{32} = \phi_3 - \phi_2 \qquad (8)$$

where the subscripts 1, 2, or 3 represent the numbers assigned to fine, medium, and coarse grids, respectively. is the function under consideration, which in this case is K_T or K_Q.

$$s = sign\left(\frac{\varepsilon_{32}}{\varepsilon_{21}}\right) \qquad (9)$$

$$p_a = \frac{1}{ln\,(r_{21})}\left|ln\left|\left(\frac{\varepsilon_{32}}{\varepsilon_{21}}\right)\right| + q(p_a)\right| \qquad (10)$$

$$q(p_a) = ln\left[\frac{r_{21}^{p_a} - s}{r_{21}^{p_a} - s}\right] \tag{11}$$

The extrapolated values are calculated as follows:

$$\phi_{ext}^{21} = \frac{(r_{21}^{p}\phi_1 - \phi_2)}{(r_{21}^{p} - 1)} \tag{12}$$

The approximate and extrapolated relative errors are obtained as:

$$e_a^{21} = \left|\frac{\phi_1 - \phi_2}{\phi_1}\right| \tag{13}$$

$$e_{ext}^{21} = \left|\frac{\phi_{ext}^{12} - \phi_1}{\phi_{ext}^{12}}\right| \tag{14}$$

The fine GCI is computed as:

$$GCI_{fine}^{21} = \frac{1.25e_a^{21}}{r_{21}^{p} - 1} \tag{15}$$

where s, p_a, $q(p_a)$, Φ_{ext}^{21}, ea^{21}, e_{ext}^{21} are intermediate parameters.

The GCI is also calculated for K_T and K_Q. Values for the numerical uncertainty of 2.81% and 2.40% are obtained for the discretisation errors of K_T and K_Q, respectively. The required data and details of the GCI are presented in Table 4.

Tab. 4. Uncertainty calculations for K_T and K_Q

	K_T	K_Q
r_{21}	$\sqrt{2}$	$\sqrt{2}$
r_{32}	$\sqrt{2}$	$\sqrt{2}$
ϕ_1	0.50560	0.11744
ϕ_2	0.50304	0.11718
ϕ_3	0.50095	0.11689
ε_{21}	−0.00256	−0.00026
ε_{32}	−0.00209	−0.00029
p_a	0.58528	0.31508
ϕ_{ext}^{21}	0.51698	0.11969
e_a^{21}	0.50%	0.22%
e_{ext}^{21}	2.20%	1.88%
GCI_{fine}^{21}	2.81%	2.39%

VALIDATION OF THE SIMULATIONS

The open-water simulation results are compared with the results of experiments performed by Barkmann et al. [32] at a speed n = 15 rps for the smooth propeller. The results for advance coefficients of J = 0.6–1.2 are shown in Table 5.

Tab. 5. Experimental and simulation results for the open-water smooth propeller

	Open-water test results [32]			Open-water CFD results		
J	K_T	K_Q	η_O	K_T	K_Q	η_O
0.6	0.6288	1.3964	0.4300	0.5961	1.3593	0.4188
0.8	0.5100	1.1780	0.5512	0.5056	1.1744	0.5481
1.0	0.3994	0.9749	0.6520	0.4008	0.9993	0.6383
1.2	0.2949	0.7760	0.7258	0.3007	0.7855	0.7311

Fig. 8 shows both the numerical and experimental results for the smooth propeller. In general, good agreement between numerical and experimental results is achieved; a 5% discrepancy in K_T is the largest error observed for advance coefficients in the range 0.6–1.2.

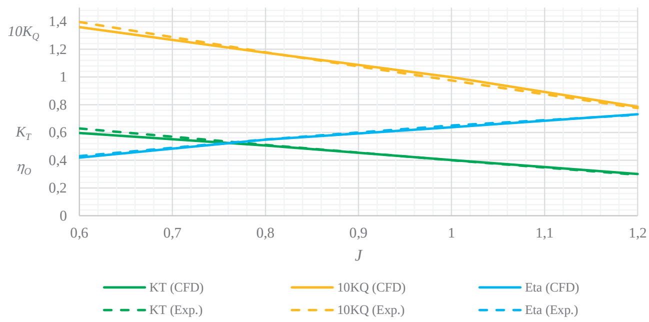

Fig. 8. Experimental [32] and CFD simulation results (current study) for a VP1304 propeller under smooth open-water conditions

The velocity contour at the surface of the propeller is shown in Fig. 9.

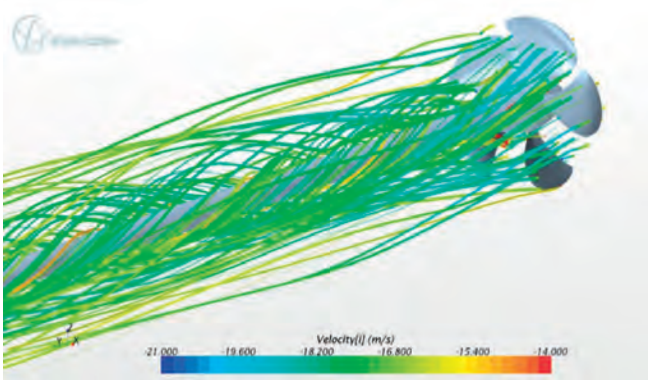

Fig. 9. Velocity contour

EFFECT OF FOULING ON THE OPEN-WATER PERFORMANCE OF THE PROPELLER

In the following, the sand-grain roughness heights are used to represent the fouling conditions (Table 1). The results for the propeller performance at a speed of n = 15 rps and values of J = 0.6–1.2 are presented for different fouling conditions in Table 6 and Fig. 10, and are compared with the results for the smooth propeller.

It can be seen that K_T and η_o gradually decrease with increasing fouling roughness, while K_Q increases. For a value of J = 1.2 for medium calcareous fouling, is reduced by about 26% and K_Q increases by about 7.0% with respect to the smooth propeller. Consequently, a 30.9% decrease in η_o is observed. The effects of medium and heavy calcareous fouling on the open-water performance of the considered propeller are almost the same. The reason for this may be related to the relative height of the roughnessand the sub-layer thickness.

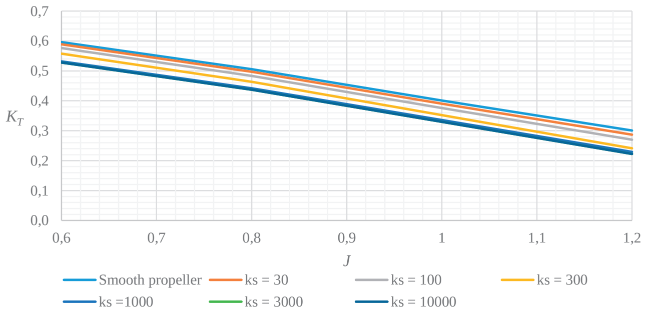

(a)

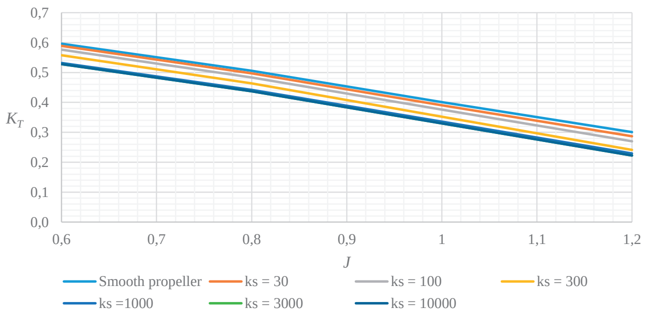

(b)

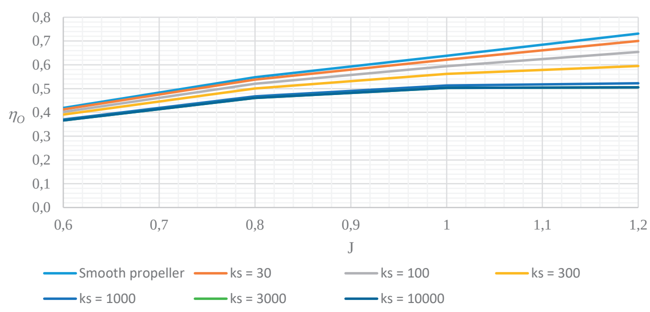

(c)

Fig. 10. Results for (a) the propeller thrust coefficient, (b) the torque coefficient, and (c) the efficiency for a range of surface conditions

To enable us to consider the roughness effect alone, Fig. 11(a) depicts K_T as a function of k_s. The slope of K_T versus k_s indicates that there is a large decline up to k_s = 500 μm over the whole range of J. It can be observed that K_T rapidly decreases as k_s increases up to k_s = 1000 μm; for k_s in the range 1000–3000 μm, a marginal decrease of K_T is observed, while K_T tends to a constant for k_s greater than 3000 μm.

When η_O is plotted as a function of k_s, it shows the same tendency as K_T, as discussed above (Fig. 11(c)).

Fig. 11(b) shows K_Q as a function of k_s. It can be seen that K_Q increases with k_s up to a value of k_s = 1000 μm. For k_s in the range 1000–3000 μm, a marginal increase in K_Q is observed, and K_Q is constant for k_s larger than 3000 μm.

The slopes for K_T, K_Q, and η_O versus k_s are larger at a value of J = 1.2 than J = 0.6. Fig. 11(c) shows that for a higher value of J, there is a more significant reduction in η_O. Figs. 10(c) and 11(c) also show that a slight increase in roughness leads to a large decrease in the value of η_O for the propeller. This is conclusive evidence that the initial roughness up to small calcareous fouling has crucial effect. This finding supports those of studies by Song et al. [25], Farkas et al. [28], and Owen et al. [23], among others. Therefore, the importance of the initial roughness on the propeller performance is emphasised, and propeller painting is recommended as a solution. In other words, the rate of required power will increase as the roughness increases. The propeller roughness arises from the accumulation of fouling as a function of the time operating at sea, meaning that a large drop in propeller performance is expected in the early stages of operation.

Tab. 6. Computed open-water characteristics under different fouling conditions

Propeller surface/fouling condition	J	K_T	ΔK_T(%)	$10K_Q$	ΔK_Q(%)	η_O	$\Delta\eta_O$(%)
Smooth propeller	0.6	0.5961	0	1.3593	0	0.4188	0
	0.8	0.5056	0	1.1744	0	0.5481	0
	1.0	0.4008	0	0.9993	0	0.6383	0
	1.2	0.3007	0	0.7855	0	0.7311	0
$k_s = 30\ \mu m$	0.6	0.5889	−1.21	1.3630	0.27	0.4126	−1.48
	0.8	0.4969	−1.71	1.1764	0.17	0.5378	−1.88
	1.0	0.3901	−2.66	0.9992	−0.01	0.6214	−2.65
	1.2	0.2868	−4.62	0.7822	−0.42	0.7003	−4.21
$k_s = 100\ \mu m$	0.6	0.5763	−3.33	1.3699	0.78	0.4017	−4.07
	0.8	0.4832	−4.42	1.1825	0.69	0.5203	−5.07
	1.0	0.3757	−6.27	1.0063	0.70	0.5942	−6.92
	1.2	0.2700	−10.20	0.7884	0.37	0.6541	−10.53
$k_s = 300\ \mu m$	0.6	0.5576	−6.47	1.3627	0.25	0.3907	−6.70
	0.8	0.4637	−8.28	1.1789	0.38	0.5008	−8.63
	1.0	0.3523	−12.10	0.9984	−0.10	0.5616	−12.01
	1.2	0.2412	−19.78	0.7742	−1.44	0.5951	−18.60
$k_s = 1{,}000\ \mu m$	0.6	0.5317	−10.81	1.3725	0.97	0.3699	−11.66
	0.8	0.4419	−12.60	1.2042	2.54	0.4672	−14.77
	1.0	0.3553	−16.33	1.0410	4.17	0.5127	−19.68
	1.2	0.2292	−23.77	0.8380	6.67	0.5224	−28.54
$k_s = 3{,}000\ \mu m$	0.6	0.5279	−11.44	1.3764	1.26	0.3663	−12.54
	0.8	0.4370	−13.57	1.2067	2.75	0.4611	−15.88
	1.0	0.3295	−17.80	1.0432	4.39	0.5026	−21.26
	1.2	0.2225	−26.02	0.8408	7.04	0.5053	−30.89
$k_s = 10{,}000\ \mu m$	0.6	0.5279	−11.44	1.3764	1.26	0.3663	−12.54
	0.8	0.4370	−13.57	1.2067	2.75	0.4611	−15.88
	1.0	0.3295	−17.80	1.0432	4.39	0.5026	−21.26
	1.2	0.2225	−26.02	0.8408	7.04	0.5053	−30.89

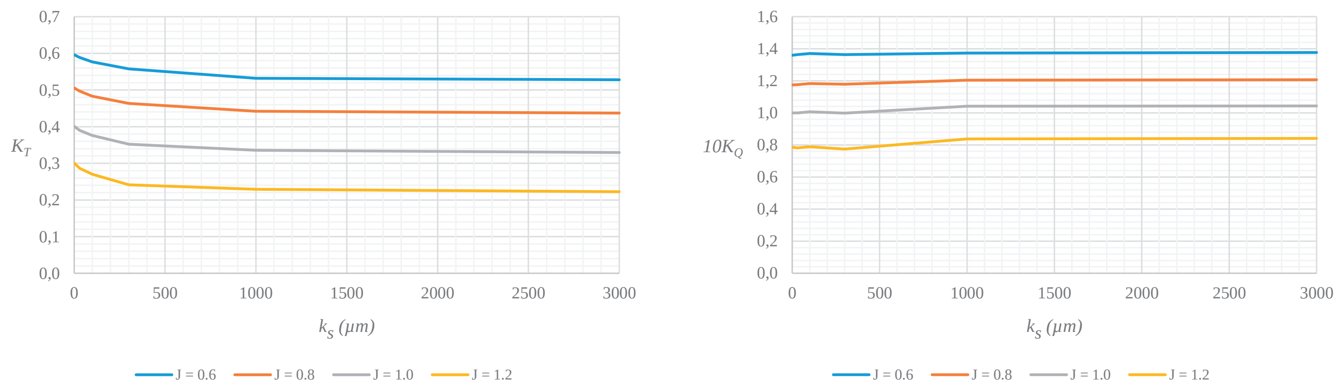

(a) *(b)*

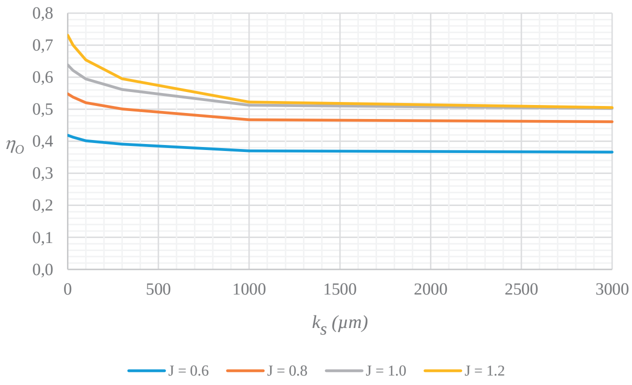

(c)

Fig. 11. Results for propeller performance: graphs of (a) thrust coefficient, (b) torque coefficient, and (c) efficiency versus roughness height

VALIDATION OF THE ROUGHED PROPELLER SIMULATIONS

The literature does not contain a description of a rough propeller and a corresponding smooth propeller as reference that would enable a validation study, and it is therefore not possible to run a validation study on the rough propeller. Although two papers have been published by Owen et al. [23] and Song et al. [25] that deal with rough and smooth propellers, with two different roughness function models, insufficient data are publicly available to repeat these simulations.

It can be seen that for the same roughness conditions, the results of both this study and prior works indicate a significant change in the hydrodynamic performance of the propeller. For example, Owen et al. [23] reported maximum changes in K_T, K_Q, and η_O of −25.5%, +6.9%, and −30.3% for k_s = 3,000 µm. The results of the current study predict changes in K_T, K_Q, and η_O of −26.0%, +7.0%, and −30.1% for k_s = 3,000 µm.

On this basis, it can be seen that the changes in propeller performance calculated in the current study are qualitatively similar to those of other research.

EFFECT OF PROPELLER PAINTING ON ENGINE BRAKE POWER

Our results indicate the importance of surface conditions on fuel consumption, and hence greenhouse gas emissions, which could be reduced by cleaning and appropriate propeller painting.

At the design stage, engine power is evaluated based on the assumption of smooth propeller conditions; however, a propeller will become rough, and the ship speed is consequently reduced. To maintain the speed calculated for the case of a clean propeller, one solution is to paint the propeller to keep its roughness below a certain level.

Roughness height for painted propellers

The roughness of a painted propeller over a period of operation can be considered as the summation of the roughness of the painted surface (k_{s1}) and the accumulation of fouling over a certain service time (k_{s2}).

A value of $k_{s1} = 0.17R_a$ can be used for painted propellers, according to Schultz [33] (Table 8). It should be noted that in this study, we use the roughness height of Schultz [33] but not the corresponding roughness function model.

Tab. 7. Annual roughness increments [34]

Coating type	Annual roughness increment Rt_{50} (µm/year)
Traditional AF coating	40–60
Self-polishing coating, SPC	10–30
Foul-release paints, FR	5–15

The final roughness of the painted propeller is shown in Table 8 for three types of paint after four years of service.

Tab. 8. Final roughness of a painted propeller after four years of service

	Paint roughness	Roughness due to fouling after four years based on Table 1		Final roughness
Paint type	k_{s1} (µm)	R_{t50} (µm)	k_{s2} (µm)	k_s (µm)
Traditional AF coating	k_s = 30	4×50=200	53	83
Self-polishing paints, SPC	$k_s = 0.17R_a = 3.4$	4×20=80	16	19.4
Foul-release paints, FR	$k_s = 0.17R_a = 2.4$	4×10=40	8	10.4
Note: In general, R_a is about 20 μm for SPC and about 14 μm for FR paints [33]				

Power estimation for fouled propellers

The ship hull is assumed to be clean, and only the propeller is fouled. Under these conditions, the power of the fouled propeller is derived based on the power for a clean propeller at the ship service speed, V_s. For a fouled propeller, the required torque, Q_f, increases for a given delivered power, P_D, which leads to a decrease in the propeller speed, n, and hence the ship speed, V_s. To maintain the ship speed calculated for the clean propeller condition, the engine power must be increased (referred to here as P_{Bf}). The clean propeller scenario is considered here as a benchmark to estimate the extra power for the fouled propeller that leads to an estimate of *SSM*. The value of P_B for a clean propeller is calculated as follows:

$$P_B = \frac{P_E}{\eta_O \eta_H \eta_R \eta_m} = \frac{R_T V_S}{\eta_O \eta_H \eta_R \eta_m} \tag{16}$$

where R_T is total hull resistance, and η_m is the mechanical efficiency.

Assuming the same hull efficiency, mechanical efficiency and relative rotative efficiency for the clean and fouled propellers, P_{Bf} for the fouled propeller can be estimated as follows:

$$P_{Bf} = \frac{P_E}{\eta_{Of}\eta_H\eta_R\eta_m} = \frac{R_T V_S}{\eta_{Of}\eta_H\eta_R\eta_m} \quad (17)$$

where η_O is the open-water efficiency of the fouled propeller.

For the fouled propeller, R_T and η_m, are the same as for the clean propeller. Based on the assumption that η_H and η_R are not significantly changed due to the propeller roughness, P_{Bf} is estimated as follows:

$$P_{Bf} = P_B \frac{\eta_O}{\eta_{of}} \quad (18)$$

Specific sea margin

Sea margin is defined as the extra power required due to the sea state in comparison with still water, as well as a roughed hull in comparison with smooth hull conditions. To define the propeller roughness effect on engine power, we define the 'specific sea margin' (*SSM*) as the extra power required to maintain the ship speed in the case of a roughed propeller compared to a smooth propeller.

The *SSM* is estimated as follows:

$$SSM = \frac{P_{Bf} - P_B}{P_B} \times 100 = (\frac{P_{Bf}}{P_B} - 1) \times 100 = (\frac{\eta_O}{\eta_{of}} - 1) \times 100 \quad (19)$$

The justification of this formula *SSM* is examined and compared with ΔP_s reported by Song et al. [25]. The concepts of SSM and ΔP_s are similar, which is why these two different methods show good agreement.

Specific sea margin for painted propellers

The performance of a propeller becomes worse with the fouling severity, as shown in Table 6. This table also shows that the performance of a propeller coated with antifouling paint is considerably better than that of a fouled propeller. The effects of fouled painted propellers are examined based on the propeller power, and SSM values for a propeller coated using three types of paint, after four years of service (becoming fouled), are considered. For the sake of simplicity, only the open-water efficiency is considered when predicting the extra power in terms of the SSM, and the effects of the other parameters such as η_H, η_R, etc. are disregarded.

The final roughness height, k_s, for each type of paint after four years of service is determined as shown in Table 8. The efficiency of a roughed propeller, η_{of}, is interpolated from Table 6 based on the final roughness height, and the *SSM* is calculated using Eq. (19). These data are presented in Table 9. It is worth mentioning that the first two cases represent fouled unpainted propellers, and the remainder are fouled painted propellers. At a given ship speed for a clean propeller, the SSM is calculated as 57.8%, 31.9%, 15.9%, 4.8%, and 2.7% for small calcareous fouling, heavy slime fouling, antifouling paint, self-polishing paint, and foul-release paint, respectively. It can be seen that the painting of the propeller is extremely effective; for instance, the difference between *SSM* values of 57.8% and 2.7% is huge in terms of fuel consumption and gas emissions. Painting of propellers is therefore strongly advised, using foul-release paint.

Tab. 9. Comparison of SSM values for fouled unpainted and fouled painted propellers

Case	Propeller surface condition	*ks* (μm)	η_{Of} *OR* η_O	*SSM* (%)
1	Small calcareous fouling or weed	1000	0.4634	57.8
2	Heavy slime	300	0.5544	31.9
3	AF paintings	83	0.6310	15.9
4	Self-polishing coatings, SPC	19.4	0.6974	4.8
5	Foul-release paints, FR	10.38	0.7116	2.7
	Clean propeller (J=1.2)	0	0.7311	0

CONCLUSION

The main goal of this study is to consider the effects of the roughness of a propeller on its performance using the CFD method. A five-blade propeller model is selected for the calculations, and a simulation of a clean propeller is verified. A new roughness function model is suggested based on existing measured roughness data. The simulations are extended to represent the same propeller under several roughness conditions, and the following conclusions could be drawn:

- A comparison of roughed and smooth propellers shows that K_T and ηo gradually decrease with increasing roughness up to k_s = 3,000 μm, while K_Q increases up to k_s = 3,000 μm. For instance, at J = 1.2 for medium calcareous fouling, K_T reduces by about 26%, K_Q increases by about 7.0%, and η_O decreases by 30.9%.
- The effects of medium and heavy calcareous fouling on the open-water performance of the propeller are found to be almost the same.
- Graphs of K_T, K_Q, and η_O versus k_s have larger slopes at J = 1.2 than J = 0.6. A higher value of J gives a more significant reduction in η_O.
- A slight increase in roughness leads to a large decrease in the value of η_o for the propeller. A large drop in propeller performance can therefore be expected in the early stages of its operation.
- The painting of a propeller is extremely effective. For instance, a propeller coated with foul-release paint had an *SSM* of 2.7%, while the unpainted propeller required 57.8% extra power with respect to the clean propeller for a period of four years in seawater. Propeller painting using foul-release paint is therefore strongly advised.

Our recommendations for future research work are as follows:

- The propeller model under roughed conditions could be tested in a towing tank.
- The even distribution of roughness considered here could be changed to a non-uniform real distribution, and both experiment and simulation could be conducted.
- A simulation of a full-scale fouled propeller could be a subject for future work, since the size of the roughness cannot be scaled up from a model to a full-scale propeller.
- The model of roughness accumulation is based on an annual roughness increment, whereas measurements at shorter intervals (such as six months) on a full-scale propeller would be very helpful if practically possible.

NOMENCLATURE

A	Roughness constant		U_τ	Friction velocity
B	Smooth wall log-law intercept		U^+	Non-dimensional velocity
C, C_s	Roughness constant		ΔU^+	Roughness function
D	Diameter of propeller		V_s	Speed of the ship
GCI	Grid convergence index		V_A	Propeller advance speed
J	Advance coefficient		w	Wake parameter
k_s	Equivalent sand-grain roughness height		y	Normal distance from the wall
k_s^+	Roughness Reynolds number based on ks		y^+	Non- dimensional distance from wall
K_T	Thrust coefficient		ρ	Fluid density
K_Q	Torque coefficient		ϕ_κ	K_T and K_Q on the k^{th} grid
n	Rotational speed of propeller		μ	Dynamic viscosity
P_B, P_{Bf}	Engine power (smooth, fouled)		κ	von Karman constant
P_D	Delivered power		$\overline{\tau_{ij}}$	Mean viscous stress tensor components
P_E	Effective power		η_D	Quasi-propulsive efficiency coefficient
Q, Q_f	Propeller torque (smooth, fouled)		η_H	Hull efficiency
R_a, R_{t50}	Roughness height parameters		η_m	Mechanical efficiency
R_T	Total hull resistance		η_O, η_{Of}	Open-water efficiency (smooth, fouled)
SSM	Specific sea margin		η_R	Relative rotative efficiency
t	Thrust deduction factor		ν	Kinematic viscosity
T	Propeller thrust		$\rho\overline{u_i'u_j'}$	Reynolds stresses
$\overline{u_i}$	Averaged Cartesian component velocity		U_τ	Friction velocity

REFERENCES

1. IMO, Second IMO GHG Study 2009. London, UK, 2009.
2. A. Banawan, M. Mosleh, and I. Seddiek, "Prediction of the fuel saving and emissions reduction by decreasing speed of a catamaran," J. Mar. Eng. Techno., (3), vol. 12, pp. 40-48, 2013.
3. M. H. Ghaemi and H. Zeraatgar, "Impact of propeller emergence on hull, propeller, engine, and fuel consumption performance in regular waves," Pol. Marit. Res. , (116), vol. 29, pp. 56-76, doi: 10.2478/pomr-2022-0044, 2022.
4. M. Burak Samsul, "Blade cup method for cavitation reduction in marine propellers," Pol. Marit. Res. , 2 (110), vol. 28, pp. 54-62, 10.2478/pomr-2021-0021, 2021.
5. P. Król, "Blade section profile array lifting surface design method for marine screw propeller blade," Pol. Marit. Res. , 4 (1040), vol. 26, pp. 134-141, doi: 10.2478/pomr-2019-0075, 2019.
6. A. Nadery and H. Ghassemi, "Numerical investigation of the hydrodynamic performance of the propeller behind the ship with and without WED," Pol. Marit. Res. , 4 (108), vol. 27, pp. 50-59, doi: 10.2478/pomr-2020-0065, 2020.
7. M. Perić, "Prediction of cavitation on ships," Brodogradnja, vol. 73, no. 3, pp. 39-58, 2022.
8. W. Tarełko, "The effect of hull biofouling on parameters characterizing ship propulsion system efficiency," Pol. Marit. Res. , 4(84), vol. 21, pp. 27-34X, 2014, doi: 10.2478/pomr-2014-0038.

9. L. Guangnian, Q. Chen, and Y. Liu, "Experimental study on dynamic structure of propeller tip vortex," Pol. Marit. Res. , 2 (106), vol. 27, pp. 11-18, 2020, doi: 10.2478/pomr-2020-0022.

10. Y. Zhang, X. Wu, M. Lai, G. Zhou, and J. Zhang, "Feasibility study of RANS in predicting propeller cavitation in behind-hull condition," Pol. Marit. Res. , 4 (108), vol. 27, pp. 26-35, 2020.

11. ITTC Virtual, The Resistance and Propulsion Committee, Final Report and Recommendations to the 29th ITTC, 13-18 June ITTC 2021 Virtual.

12. R. Townsin, and S. Dey, "The correlation of roughness drag with surface characteristics," Fluid Mechanics and Its Applications, vol 6. Springer, Dordrecht, doi.org/10.1007/978-94-011-3526-9_10, 1991.

13. Y. K. Demirel, "A CFD model for the frictional resistance prediction of antifouling coatings," Ocean Eng., vol. 89, pp. 21-31, 2014.

14. A. Vargas, and H. Shan, "Modeling of ship resistance as a function of biofouling type, coverage, and spatial variation," in 2nd Hull Performance & Insight Conference, pp. 264-281, Ulrichshusen, Germany, 2017.

15. C. Grigson, "Drag losses of new ships caused by hull finis," J. Ship Res., vol. 36, no. 02, pp. 182-196, 1992.

16. S. Song et al., "Investigating the effect of heterogeneous hull roughness on ship resistance using CFD," JMSE, vol. 9, no. 2, p. 1, 2021.

17. T. Cebeci and P. Bradshaw, "Momentum transfer in boundary layers," in Series in Thermal and Fluids Engineering, P. Bradshaw, Ed. Washington: Hemisphere Pub. Corp., 1977.

18. A. Farkas, N. Degiuli, and I. Martić, "Towards the prediction of the effect of biofilm on the ship resistance using CFD," Ocean Eng., vol. 167, pp. 169-186, 2018.

19. A. Farkas, N. Degiuli, L. Martic, and R. Dejhalla, "Impact of hard fouling on the ship performance of different ship forms," JMSE, vol. 8, p. 748, 2020.

20. A. Farkas, N. Degiuli, and I. Martić, "Impact of biofilm on the resistance characteristics and nominal wake," Proceedings of the Institution of Mechanical Engineers, Part M: Journal of Engineering for the Maritime Environment, vol. 234, no. 1, pp. 59-75, 2020.

21. A. Farkas, N. Degiuli, and I. Martić, "A novel method for the determination of frictional resistance coefficient for a plate with inhomogeneous roughness," Ocean Eng., vol. 237, p. 109628, 2021.

22. P. Kellett, K. Mizzi, K. Demirel, and O. Turan, "Investigation the roughness effect of biofouling on propeller performance," International Conference on Shipping in Changing Climates, SEMANTIC SCHOLAR, ID 55216316, 2015.

23. D. Owen, Y.K. Demirel, E. Oguz, T. Tezdoga, and A. Incecik, "Investigating the effect of biofouling on propeller characteristics using CFD," Ocean Eng., vol. 159, pp. 505-516, 2018.

24. S. Song, Y. Demirel, and M. Atlar, "An investigation into the effect of biofouling on full-scale propeller performance using CFD," in: Proceedings of the ASME 2019 38th International Conference on Ocean, Offshore & Arctic Engineering OMAE2019, June 9-14, 2019, Glasgow, Scotland, UK, 2019.

25. S. Song, Y. Demirel, and M. Atlar, "Propeller performance penalty of biofouling: CFD prediction," J. Offshore Mech. Arct. , vol. 142, no. 6, p. 0601901, 2020.

26. A. Farkas, N. Degiuli, and I. Martić, "The impact of biofouling on the propeller performance," Ocean Eng., vol. 219, p. 108376, 2021.

27. A. Farkas, N. Degiuli, and I. Martić, "Assessment of the effect of biofilm on the ship hydrodynamic performance by performance prediction method," International Journal of Naval Architecture and Ocean Eng., vol. 13, pp. 102-114, 2021.

28. A. Farkas, S. Song, N. Degiuli, I. Martić, and Y.K. Demirel, "Impact of biofilm on the ship propulsion characteristics and the speed reduction," Ocean Eng., vol. 199, p. 107033, 2020.

29. M. P. Schultz and K. A. Flack, "The rough-wall turbulent boundary layer from the hydraulically smooth to the fully rough regime," J. Fluid Mech., vol. 580, pp. 381-405, 2007.

30. SVA Hydrodynamic Solutions, "Potsdam Propeller Test Case (PPTC) Open Water Tests with the Model Propeller VP1304," 2011.

31. L. F. Richardson, and J. A. Gaunt, "The deferred approach to the limit," Philosophical Transactions of the Royal Society of London: Series A, vol. 226, pp. 299-361, 1927.

32. U. Barkmann, H. Heinke, and L. Lubke, "Potsdam propeller test case (PPTC) test case description," in: Second International Symposium on Marine Propulsors SMP'11, Hamburg, Germany, Workshop: Propeller Performance, 2011.

33. M. P. Schultz, “Frictional resistance of antifouling coating systems,” J. Fluids Eng., vol. 126, pp. 1039-1047, 2004.

34. J. Carlton, Marine Propellers and Propulsion. London: Butterworth Heinemann, 2010.

APPENDIX A

PROPOSED ROUGHNESS FUNCTION MODEL

In this study, the roughness parameters measured by Schultz and Flack [29] are utilised to develop a new roughness function model. The velocity profile on a rough flat plate can be expressed as follows:

$$U^+ = \frac{1}{\kappa} ln\, y^+ - \frac{1}{\kappa}\, ln\, k_s^+ + A \tag{A.1}$$

B is added and subtracted:

$$U^+ = \frac{1}{\kappa} ln\, y^+ + B - (\frac{1}{\kappa}\, ln\, k_s^+ + B - A) \tag{A.2}$$

By comparing Eqs. (2) and (A.2), ΔU^+ can be written as:

$$\Delta U^+ = \frac{1}{\kappa}\, ln\, k_s^+ + B - A \tag{A.3}$$

C_s is introduced as the sand-grain roughness constant, which is defined as follows:

$$\frac{1}{\kappa}\, ln\, C_s = B - A \tag{A.4}$$

Then, Eq. (A.3) can be reparametrized as follows:

$$\Delta U^+ = \frac{1}{\kappa}\, ln\, k_s^+ + \frac{1}{\kappa}\, ln\, C_s = \frac{1}{\kappa}\, ln\, C_s k_s^+ = \frac{1}{\kappa}\, ln\, C k_s^+ \tag{A.5}$$

where C, the roughness constant, is dependent on the type of roughness of the surface under consideration.

The experiments identified three flow regimes: a hydraulically smooth regime, a transitionally rough regime, and a fully rough regime.

In the rough regime, for a roughness different from the sand-grain, the roughness constant is different. Hence, Eq. (A.5) is applicable to any rough surface, while C is individually determined.

Schultz and Flack [17] introduced a relation between an engineering surface and an equivalent sand-grain roughness based on the root mean square of the roughness height, skewness, and flatness of the probability density function (pdf). The mean velocity profile is shown in Fig. A.1, and it can be seen that the flow is hydraulically smooth for $k_s^+ \leq 2.5$ ($\Delta U^+= 0$). For a higher flow velocity $k_s^+ \geq 25$, the flow regime becomes fully rough, and ΔU^+ will be a linear function of the logarithmic scale of k_s^+.

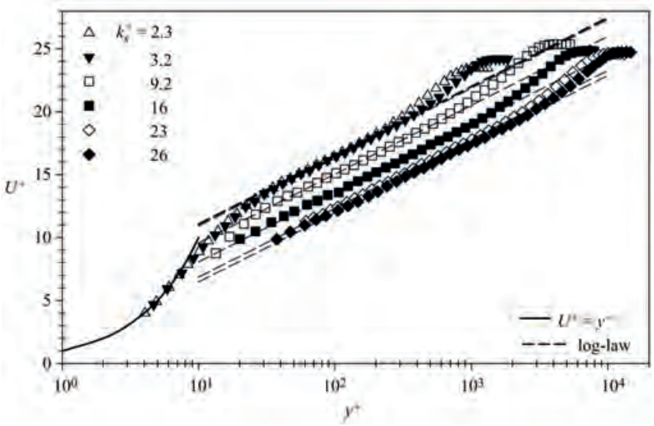

Fig. A.1. Rough wall mean velocity profiles [29].

The roughness constant C is determined by re-calling Eq. (A.5), as follows:

$$C = \frac{1}{k_s^+}\, e^{\kappa\, \Delta U^+} \tag{A.6}$$

Velocity profiles for different surface conditions are shown in Fig. A.1. The downward velocity shift due to roughness in the fully rough regime is 4.6 m/s ($k_s^+ = 26$, $\Delta U^+ = 4.6$, and $\kappa = 0.421$). Following Eq. (A.6), the roughness constant C becomes 0.2667.

The final roughness function model is presented in Eq. (7).

POLISH MARITIME RESEARCH 4 (120) 2023 Vol. 30; pp. 74-80
10.2478/pomr-2023-0060

TRANSFER FUNCTION FOR A CONTROLLABLE PITCH PROPELLER WITH ADDED WATER MASS

Volodimir Leshchev
Igor Maslov
Oleksandr Palagin
Andrii Naydyonov
Department of Ship Power Plants and Systems, Danube Institute of the National University „Odessa Maritime Academy", Ukraine

* Corresponding author: *v.leshchev@ukr.net (V. Leshchev)*

ABSTRACT

The relevance of this study lies in the fact that it presents a mathematical model of the dynamics of the propulsion system of a ship that takes into consideration the mass of water added to it. The influence of this phenomenon on the resonant frequencies of the propeller shaft is examined, and a transfer function for a controllable-pitch propeller is obtained for various operating modes. The purpose of the study is to improve the calculation of the dynamic operating modes of a controllable-pitch propeller by examining the features of a visual models. The VisSim software package is used in the study. A visual model is developed that considers the influence of the rotational speed on the value of the rotational inertia attached to the variable-pitch screw of the mass of water, and a special transfer function is proposed. The study shows that a transfer function of this type has a loop enabling negative feedback. An analysis of the operation of the propeller shaft at its resonant frequency is conducted based on the application of frequency characteristics using the transfer functions obtained. We show that in the low-frequency region, a consideration of the added rotational inertia using the proposed transfer function leads to a significant difference compared to the result obtained with the existing calculation method.

Keywords: propulsion system, torsional vibrations, shaft line, added water mass, transfer function, propeller screw

INTRODUCTION

When calculating the free oscillations that occur in the propeller shaft of a ship, the inertia moment of the controllable pitch propeller (CPP) is usually increased by 20–40% to obtain a match between the calculated results and the experimental ones. Such a solution is not always optimal, since there is a discrepancy between the specified calculated frequencies and the actual ones, especially at low angular speeds of rotation. This means that when calculating the dynamic modes of operation of the propulsion system of a ship, it is necessary to use techniques based on a simplification of the physical process, as reported in [1-5].

One of the existing ways to increase the accuracy of the calculated results compared to those obtained in practice is to search for a solution using a mathematical model based on the construction of a visual image. This issue has been widely covered in a great number of studies. For example, in [6-10], the problems associated with the hydrodynamic interaction between a propeller and water are investigated, and the authors explore how the unevenness of the water flow affects the results of the axial and tangential forces acting on the propeller. However, it is not shown how the resulting harmonic components of the moments of these forces affect the resonant phenomena in the propulsion complex. In [11-14], the interaction between the propeller and the elements of the ship's hull is investigated, and it is shown that modern computational fluid dynamics solvers can give correct calculation results when the rudder operates in the propeller flow, although these studies rarely consider the features of the dynamics of the propulsion system from the action of the displaced water mass.

The studies in [15-20] explore the dynamics of a ship's propeller when the water surface is agitated using a model that includes an increase in the rotational inertia of the propeller due to the simple addition of the water mass. The difficulty of this approach means that such studies are limited. Thus, despite abundant research in the field of dynamics on the propulsion system of ships, the issue of the features of stability and resonant frequency phenomena in the interaction of the propeller and the aquatic environment remains unresolved.

The purpose of this study is to improve the calculation of the dynamic operating modes of a controllable-pitch propeller by examining the features of a visual model.

MATERIALS AND METHODS

This study involves mathematical modelling of the process that occurs during the movement of the ship, that is, the interaction between a controllable-pitch propeller and the aquatic environment for a propulsion system represented in the form of a three-mass mechanical system (TMS) [21]. In this approach, three distinct masses represent integral components of the propulsion pathway. The first mass corresponds to the diesel engine, and includes its rotational inertia and the torque it produces. The intermediary mass represents the gearbox or reduction gear, and accounts for its rotational inertia and its role in moderating the engine speed for the propeller. The final mass represents the propeller and its shaft, and includes the propeller's rotational inertia and the resistance it faces due to water and other factors. The VisSim software package is used here to visualise the results of the study. VisSim is a visual-based block diagram programming language tailored for simulation and embedded system development. It has been extensively employed in the design of control systems and digital signal processing, and facilitates multi-domain design and simulation. The language offers blocks for arithmetic, Boolean, and transcendental operations, in addition to digital filters, transfer functions, numerical integration, and interactive graph plotting [22]. Figure 1 shows a model diagram of the TMS of a ship's propulsion system [17, 22], with a modified transmission function for the CPP in accordance with the one proposed in this study.

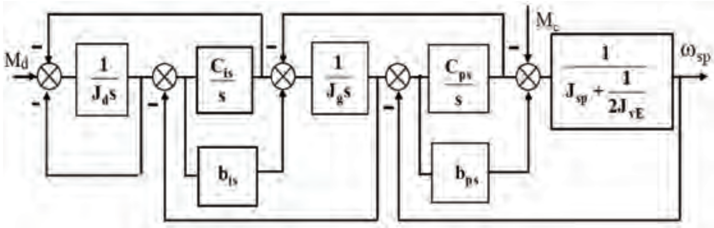

Figure 1. Model of the three-mass mechanical part of the propulsion system (M_d – torque produced by the diesel engine, M_c – resistance torque on the propeller shaft, J_d, J_g, J_{sp} – rotational inertia of the engine, gearbox, and propeller respectively, C_{is} – stiffness of the intermediate shaft, C_{ps} – stiffness of the propeller shaft, b_{is}, b_{ps} – viscous friction coefficients for the shafts, s – differentiation operator)

Table 1 shows the designations of the model elements used in the study and their given values. The angular velocities of the rotating elements of the propulsion system, after being connected to the motor shaft, are assumed to be equal:

$$\omega_d = \omega_{is} = \omega_{ps} = \omega_{sp} = 1 \quad (1)$$

All values of frequencies and angular velocities in the text and figures are given in rad·s^{-1} due to the limitations of the VisSim software product.

Table 1. Designations and technical parameters of the ship's propulsion system

Elements of the propulsion system of the ship	Symbol	Parameter values before casting	Parameter values after casting
Diesel rotational inertia	J_d	4.50·10^3 kg. m^2	4.50kg. m^2
Rotational inertia of the gearbox	J_r	2.40·10^3 kg. m^2	0.24kg. m^2
Estimated rotational inertia of the screw	J_{sp}	3.2·10^3 kg. m^2	0.32kg. m^2
Rotational inertia of the added water	$J_v=(0.2\text{-}0.4)J_{sp}$	(0.6-1.2)·10^3 kg. m^2	(0.6-0.12)kg. m^2
Stiffness of the intermediate shaft	C_{is}	0.64·10^6 N.m	0.64N.m
Stiffness of the propeller shaft	C_{ps}	0.24×10^6 N.m	0.024N.m
Gear ratio of the gearbox	i_g	3.19	3.19
Nominal angular rotation speed of the diesel engine	ω_{dn}	40.317rad·s^{-1}	1

Since the action of the dissipative forces of the viscous action is assumed to be equal to zero, the values of the resonant frequencies in the shaft line obtained from experiment are close to the calculated values [22]. The study was conducted using the VisSim experimental setup shown in Figure 2. In addition to the TMS, the model shown in Figure 2 also contains an exciting scanning signal generator (SSG) [17].

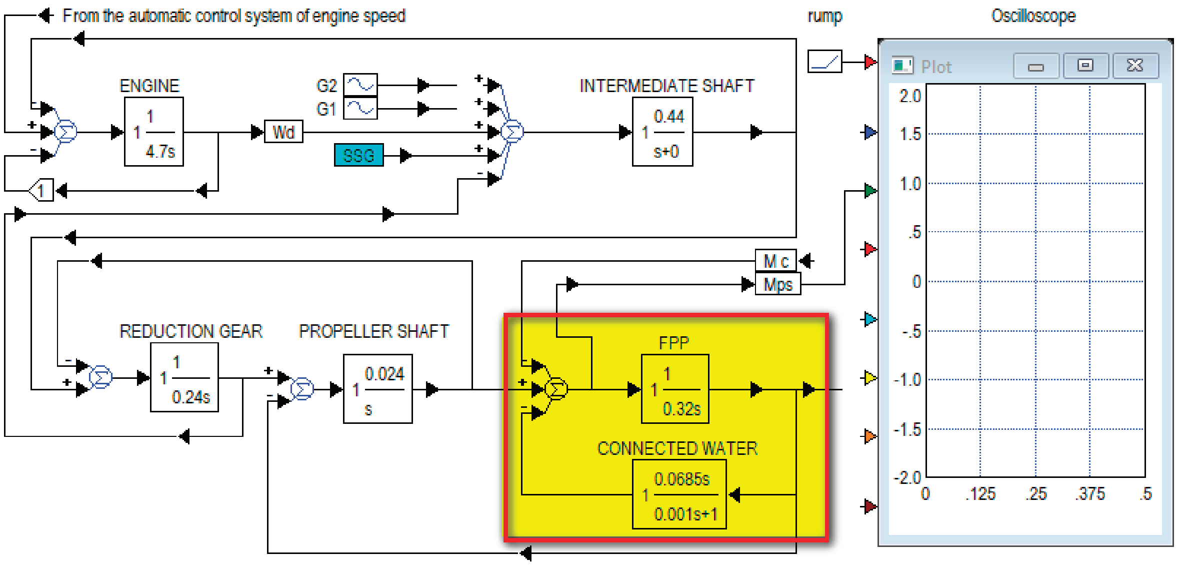

Figure 2. Diagram of the dynamic model of the three-mass mechanical part of the propulsion system of the ship

This generator supplies the diesel output with a sinusoidal signal with a constant amplitude and frequency, which varies in proportion to time with acceleration $\varepsilon_\omega = 0.001 \text{rad/s}^2$. This signal simulates the rotation of the diesel engine, which leads to resonant phenomena in the shaft line.

The operation of the model and the interaction of its parts are described in [22]. Fixed frequency generators G1 and G2 are designed to check and refine the values found during scanning of the critical frequencies Ω_{cr1} and Ω_{cr2}. The experimental equipment for the study was provided by the Danube Institute of the Odessa Maritime Academy.

RESULTS AND DISCUSSION

It is known that in a ship's propulsion system, a fixed-pitch propeller (FPP) under ideal conditions, taking into account the slippage of the propeller blades relative to the water, displaces and swirls a unit mass of attached water per one revolution:

$$m_{vE} = \pi\rho \frac{D_{sp}^2}{4}(1-\alpha)H_{sp}, \quad (2)$$

where m_{vE} is the unit mass of the added water formed from one turn of the screw; H_{sp} is the pitch of the propeller; D_{sp} is the diameter of the propeller; ρ is the density of water; and α is the coefficient of sliding.

When using the above units, the angular frequency of a rotation and the rotational speed are related by the expression:

$$n_{sp} = \frac{\omega_{sp}}{2\pi} \quad (3)$$

The mass of the added water jet m_v at the rotational speed of the propeller ω_{sp}(rad/s) can then be represented by the formula:

$$m_v = m_{vE} n_{sp} = \pi\rho \frac{D_{sp}^2}{4}(1-\alpha)H_{sp}\frac{\omega_{sp}}{2\pi} = \frac{1}{8}\rho D_{sp}^2(1-\alpha)H_{sp}\omega_{sp}, \quad (4)$$

where n is the speed of rotation of the propeller, and ω_{sp} is its rotational speed (rad/s).

If the rotating mass of water is a full-bodied cylinder with radius:

$$R_v = \frac{D_{sp}}{2}, \quad (5)$$

then, from Eq. (4), the following can be obtained:

$$J_v(t) = \frac{1}{2}\pi R_v^2 m_v(t) = \frac{1}{64}\pi\rho D_{sp}^4(1-\alpha)H_{sp}(t)\omega_{sp}(t). \quad (6)$$

In the existing method of dynamic calculation, the problem of finding the moment:

$$J_\Sigma = J_{sp} + J_v \quad (7)$$

is reduced to simply increasing it by 20–40% of the calculated value:

$$J_\Sigma = (1.2 - 1.4)J_{sp} \quad (8)$$

This allows for some coincidence between the results of the calculation of critical frequencies with their real values. However, it follows from Eq. (6) that the moment J_v is not constant, but changes over time depending on the changes of the variable components $\omega_{sp}(t)$ and $H_{sp}(t)$. The dynamics equation for the screw in this case takes the form:

$$M_{ps}(t) = \frac{d}{dt}\left[J_\Sigma\left(H_{sp}(t), \omega_{sp}(t)\right)\right]$$
$$= \frac{d}{dt}\left[J_{sp}\omega_{sp}(t) + \left(\frac{1}{64}(1-\alpha)\pi\rho D_{sp}^4\right)H_{sp}(t)\omega_{sp}^2(t)\right] =$$
$$= J_{sp}\frac{d\omega_{sp}}{dt} + \left(\frac{1}{64}(1-\alpha)\pi\rho D_{sp}^4\right)\frac{d}{dt}\left[H_{sp}(t)\omega_{sp}^2(t)\right] =$$
$$= J_{sp}\frac{d\omega_{sp}}{dt} + J_v\frac{d}{dt}\left[H_{sp}(t)\omega_{sp}^2(t)\right]. \quad (9)$$

The second part of Eq. (9) represents the torque of the displaced water mass M_v, which contains the differential of the product of the variables H(t) and $\omega_{sp}(t)$. This product is differentiated as follows:

$$\frac{d}{dt}\left(H_{sp}\omega_{sp}^2\right) = 2H_{sp}\omega_{sp}\frac{d\omega_{sp}}{dt} + \omega_{sp}^2\frac{dH_{sp}}{dt}. \quad (10)$$

If the expression in Eq. (10) is substituted into Eq. (9), then we have:

$$M_{ps} = J_{sp}\frac{d\omega_{sp}}{dt} + 2\left(\frac{1}{64}(1-\alpha)\pi\rho D_{sp}^4\right)H_{sp}\omega_{sp}\frac{d\omega_{sp}}{dt} + $$
$$+\left(\frac{1}{64}(1-\alpha)\pi\rho D_{sp}^4\right)\omega_{sp}^2\frac{dH_{sp}}{dt}. \quad (11)$$

The terms of this equation by derivatives after grouping are:

$$M_{ps} = \left[J_{sp} + 2\left(\frac{1}{64}(1-\alpha)\pi\rho D_{sp}^4\right)H_{sp}\omega_{sp}\right]\frac{d\omega_{sp}}{dt} +$$
$$+\left(\frac{1}{64}(1-\alpha)\pi\rho D_{sp}^4\right)\omega_{sp}^2\frac{dH_{sp}}{dt}. \quad (12)$$

This expression for the moment M_{ps} holds both for a unit with an FPP and for a unit with a CPP. It describes a single dynamic process that occurs when both accelerating or decelerating $\omega_{ps}(t)$, and when changing the step $H_{sp}(t)$ towards an increase or decrease. There is also a scenario where these two cases act simultaneously. In this study, we investigate the option in which the ship has FPP or a CPP that operates with a given fixed step H_{sp}. Eq. (12) then takes the form:

$$M_{ps} = \left[J_{sp} + 2\left(\frac{1}{64}(1-\alpha)\pi\rho D_{sp}^4\right)H_{sp}\omega_{sp}\right]\frac{d\omega_{sp}}{dt}, \quad (13)$$

where M_{ps} is the torque of the propeller shaft with the FPP.

Part of the second term in Eq. (13) can be interpreted as the rotational inertia of the added water for one revolution of the propeller, and is expressed by the formula:

$$J_{vE} = \left(\frac{1}{64}(1-\alpha)\pi\rho D_{sp}^4\right)H_{sp}. \quad (14)$$

Considering the damping effect of water, we can write Eq. (13) with respect to the rotational inertia of the propeller J_{sp} as follows:

$$M_{ps}(t) - 2J_{vE}\omega_{sp}\frac{d\omega_{sp}}{dt} = J_{sp}\frac{d\omega_{sp}}{dt} \quad (15)$$

Then, the equation for the propeller dynamics takes the form:

$$M_{ps}(t) - M_v(t) = J_{sp}\frac{d\omega_{sp}(t)}{dt}, \quad (16)$$

where $M_v(t) = 2J_{vE}\omega_{sp}(t)d\omega_{sp}(t)\frac{d\omega_{sp}(t)}{dt}$ is the torque from the water added to the propeller.

If we assume that the moment of the load $M_c(s) = 0$ then under zero initial conditions of the dynamic process, Eq. (16) in the operator form is:

$$M_{ps}(s) - 2J_{vE}\frac{1}{s^2}s = M_{ps}(s) - 2J_{vE}\frac{1}{s} =$$
$$= M_{ps}(s) - M_v(s) = J_{sp}s, \quad (17)$$

where s is the Laplace operator.

Since the propeller is affected by two torques, $M_{ps}(s)$ and $M_v(s)$, the mathematical model of this interaction takes the form shown in Figure 3.

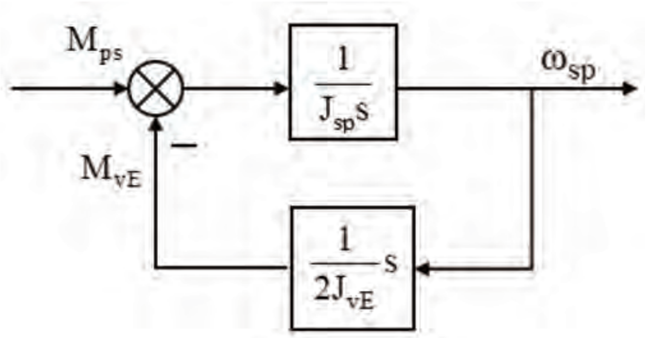

Figure 3. Diagram of the mathematical model of the dynamic interaction between torque and a unit moment

In the diagram of the propulsion system model in Figure 2, this node is highlighted in colour. It contains the values of the elements that correspond to numerical experiment. As can be seen from Figure 3, the moments J_{sp} and J_{vE} are combined into a loop containing negative feedback. The total transfer function of the FPP $W_{sp}^{\Sigma}(s)$ can be then presented in generalised form as:

$$W_{sp}^{\Sigma}(s) = \frac{W_{sp}(s)}{1+W_{sp}(s)W_{vo}(s)} = \frac{\frac{1}{J_{sp}s}}{1+\frac{1}{J_{sp}s}\frac{s}{2J_{vE}}} =$$
$$= \frac{1}{\left(J_{sp}+\frac{1}{2J_{vE}}\right)s}. \quad (18)$$

It follows from Eq. (18) that the model of the total transfer function of the propeller $W_{sp}^{\Sigma}(s)$ has the form shown in Figure 4.

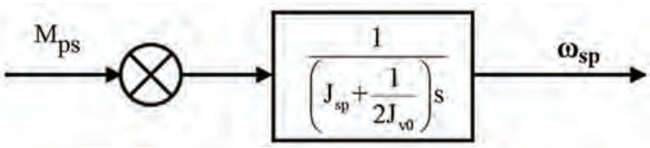

Figure 4. Model of the generalised transfer function of the CPP $W_{sp}^{\Sigma}(s)$ considering the added water mass

The transfer function of the FPP $W_{sp}^{\Sigma}(s)$ found here differs significantly from the one used today in practice, which is accepted as:

$$W_{sp} = \frac{1}{(1.2\text{-}1.4)J_{sp}}. \tag{19}$$

It can also be seen from Eq. (18) that the value J_{vE} is specific to each case, and is subject to calculation. The moment J_v is inversely proportional to the unit moment J_{vE}. It follows from this that with a decrease in the step ratio

$$\lambda_{sp} = \frac{H_{sp}}{D_{sp}}, \tag{20}$$

the critical frequency Ω_{cr1} shifts downwards. For a TMS propulsion system, this displacement mainly affects low rotational speeds, and may go beyond the range that corresponds to (1.2 - 1.4) J_{sp}. When calculating the dynamic modes, attention should be paid to this phenomenon. A numerical experiment is conducted with a dynamic model as shown in Figure 2, where the values of the elements of this model are shown in the diagram in accordance with Table 1. Descriptions of the interaction between the parts of the model are presented in [23-26]. For example, the propulsion system of the ship is taken as an FPP with the following technical characteristics: step ratio λ_{sp} = 1.045; coefficient of relative slip α = 0.14; screw diameter D_{sp} = 1.1 m; and engine 6NVD 48A-2U with rated power 852 kW (1158.4 hp), rated engine speed n_{dn} = 385 rpm, and rated speed of the propeller shaft n_{sp} = 118 rpm. A comparative analysis of the dynamics of the propulsion system is conducted for three scenarios. In the first, the FPP has an estimated rotational inertia of

$$J_{sp1} = 3.20 \text{ kg} \cdot m^2, \tag{21}$$

and in the second, the FPP has a rotational inertia that is increased by 40%:

$$J_{sp2} = 4.48 \text{ kg} \cdot \text{m}^2. \tag{22}$$

The third involves a screw with a rotational inertia determined using the method proposed in this study in accordance with Eq. (18). The unit moment J_{vE} is calculated by Eq. (2), where the screw pitch H_{sp} is replaced by a step ratio λ_{sp}. Then, for ω_{spn} = 1, Eq. (2) becomes:

$$J_{vE} = \frac{1}{64}\pi\rho D_{sp}^5(1-\alpha)\lambda_{sp}k_g, \tag{23}$$

where $k_g = \frac{1}{i^2}$ is the moment reduction coefficient.

By substituting the values of the circuit elements (Table 1) into Eq. (23), the following estimate can be obtained:

$$J_{vE} = \frac{1}{64}\pi \cdot 1.025 \cdot 1.1^5 \cdot (1-0.14) \cdot 1.045 \cdot 0.10 \simeq \\ \simeq 0.0073 \text{ t} \cdot m^2 = 7.30 \text{ kg} \cdot m^2 \tag{24}$$

The transfer function of the added moment W_v then takes the value:

$$W_v = \frac{1}{2J_{vE}}s = \frac{1}{2\cdot 7{,}30}s = 0.0685s. \tag{25}$$

The transfer function $W_v(s)$ is implemented as a typical differentiating link:

$$W_v(s) = \frac{T_1 s}{T_2 s+1} = \frac{0.0685s}{0.001s+1}. \tag{26}$$

The total value of the moment J_Σ in this case is equal to:

$$J_\Sigma = J_{sp} + \frac{1}{2J_{vE}} = 0.32 + 0.0685 = \\ = 0.3885\text{кг} \cdot m^2. \tag{27}$$

After modelling the dynamic process, the critical frequencies are found by scanning the model with the SSG variable signal generator for the three variants, and have the following values: $\Omega_{cr1\text{-}1}$ = 0.2081rad*s^{-1}, $\Omega_{cr1\text{-}2}$ = 0.22329rad*s^{-1}, $\Omega_{cr1\text{-}3}$ = 0.2603rad*s^{-1}, $\Omega_{cr2\text{-}1} = \Omega_{cr2\text{-}2} = \Omega_{cr2\text{-}3}$ = 1.4332rad*s^{-1}.

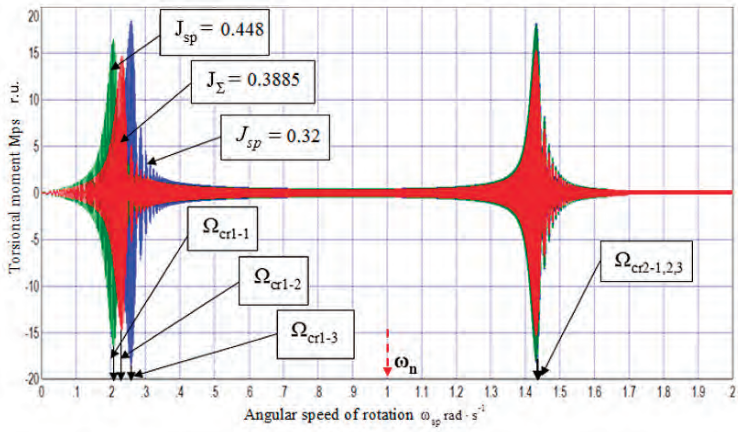

Figure 5. Critical frequencies of the torque $\Omega_{cr1\text{-}1}$, $\Omega_{cr1\text{-}2}$, and $\Omega_{cr1\text{-}3}$ for the TMS propulsion system for various values of the moment J_v

As can be observed from the oscillogram in Figure 5, the high critical frequencies of the torque , $\Omega_{cr2\text{-}1}$, $\Omega_{cr2\text{-}2}$ and $\Omega_{cr2\text{-}3}$ are almost the same. This allows us to conclude that the rotational inertia of displaced water J_v has little effect on critical frequencies that occur below the maximum engine speed [27-31].

CONCLUSION

Our results show that for the propulsion system considered here, the critical frequency $\Omega_{cr1\text{-}2}$ obtained using the propeller transfer function proposed in this study is within the existing range of changes in critical frequencies, which are typically estimated in practice by increasing the moment J_{sp} by 20–40%. It corresponds to a total moment J_{sp} = 0.3885 kg · m², which represents an increase of 21.9% and confirms the validity of its application. The proposed method for determining the rotational inertia of a screw with a displaced water mass allows us to calculate the ratio directly, without the need for approximate empirical formulae such as Kutuzov's formula, which does not consider the dependence of the moment J_v on the rotation frequency of the mass of the water jet.

A visual dynamic model was developed that considered the influence of the rotational speed on the value of the rotational inertia of water mass added to the CPP, and a special transfer function for the propeller was proposed. It was established that such a transfer function has a loop with negative feedback. The operation of the ship's shaft line when using the proposed transfer functions in the model of the propulsion system was explored. An analysis of the resonant modes based on the application of frequency characteristics using the transfer functions obtained in the study was conducted. It was found that when determining the critical oscillation frequencies of the shaft line in the lower part of the propeller operating range, considering the added moment leads to a significant difference compared to the results obtained from the existing method.

NOMENCLATURE

CPP	Controllable-pitch propeller
FPP	Fixed-pitch propeller
SSG	Scanning signal generator
TMS	Three-mass mechanical system

REFERENCES

1. MacPherson, D.M., Puleo, V.R., Packard, M.B. 2007. Estimation of entrained water added mass properties for vibration analysis. https://cutt.ly/8GVZdOe.

2. Faltinsen, O., Minsaas, K.J., Liapias, N., Skjørdal, S.O. 1981. Prediction of resistance and propulsion of a ship in a seaway. In: T. Inui (Ed.). Proceedings of 13th Symposium on Naval Hydrodynamics (pp. 1-19). Tokio: University of Trondheim.

3. Król, P. 2021. Hydrodynamic state of art review: Rotor – stator marine propulsor systems design. Polish Maritime Research, 28(1), 72-82. https://doi.org/10.2478/pomr-2021-0007

4. Koibakov, S.M., Umirkhanov, M.G. 2013. Model research of ice jams. World Applied Sciences Journal, 25(8), 1158-1160. https://doi.org/10.5829/idosi.wasj.2013.25.08.13382

5. Koibakov, S.M., Umirkhanov, M.G. 2013. Icebreaker unit. World Applied Sciences Journal, 25(8), 1251-1254. https://doi.org/10.5829/idosi.wasj.2013.25.08.13423

6. Gayen, D., Chakraborty, D., Tiwari, R. 2017. Whirl frequencies and critical speeds of a rotor-bearing system with a cracked functionally graded shaft – finite element analysis. European Journal of Mechanics – A/Solids, 61, 47-58.

7. Lou, B., Cui, H. 2021. Fluid–structure interaction vibration experiments and numerical verification of a real marine propeller. Polish Maritime Research, 28(3), 61-75. https://doi.org/10.2478/pomr-2021-0034

8. Prohl, M.A. 1945. A general method for calculating critical speeds of flexible rotors. Journal of Applied Mechanics, 12(3), 142-148.

9. Ostanin, V. 2022. Vadym Effects of repulsion and attraction between rotating cylinders in fluids. Scientific Herald of Uzhhorod University. Series "Physics", (51), 39-47. https://doi.org/10.54919/2415-8038.2022.51.39-47

10. Klendii, M., Logusch, I., Dragan, A., Tsvartazkii, I., Grabar, A. 2022. Justification and calculation of design and strength parameters of screw loaders. Machinery & Energetics, 13(4), 48-59. https://doi.org/10.31548/machenergy.13(4).2022.48-59

11. Yoon, M. 2016. A Transfer Function Model of Thrust Dynamics for Multi-Rotor Helicopters. International Journal of Engineering Research & Technology, 5(1), 15-18.

12. Boletis, E., de Lange, R., Bulten, N. 2015. Impact of propulsion system integration and controls on the vessel DP and maneuvering capability. IFAC-PapersOnLine, 48(16), 160-165.

13. Xiros, N.I. 2004. PID marine engine speed regulation under full load conditions for sensitivity H∞-norm specifications against propeller disturbance. Journal of Marine Engineering & Technology, 3(2), 3-11.

14. Smailova, G., Yussupova, S., Uderbaeva, A., Kurmangaliyeva, L., Balbayev, G., Zhauyt, A. 2018. Calculation and construction of the tolling roller table. Vibroengineering Procedia, 18, 14-19. https://doi.org/10.21595/vp.2018.19908

15. Koushan, K. 2006. Dynamics of ventilated propeller blade loading on thrusters. In: World Maritime Technology Conference (pp. 18-21). London: Macmillan Education.

16. Senjanović, I., Hadžić, N., Murawski, L., Vladimir, N. 2019. Analytical procedures for torsional vibration analysis of ship power transmission system. Engineering Structures, 178, 227-244.

17. Leschev, V.A. 2018. Marine diesel ACS with external feedback speed sensor. Modern Engineering and Innovative Technologies, 5, 11-17.

18. Kukhar, V., Vasylevskyi, O., Khliestova, O., Berestovoi, I., Balalayeva, E. 2022. Hydraulic Press Open Die Forging of 21CrMoV5-7 Steel CCM Roller with Flat Upper and Concave Semi-round Lower Cogging Dies. Lecture Notes in Mechanical Engineering, 489-498. https://doi.org/10.1007/978-3-030-91327-4_48

19. Aghbalyan, S., Simonyan, V. 2022. Study of hardening and structure of maraging powder steel grade PS-H18K9M5TR (18%Ni+9%Co+5%Mo+1%Ti+1%Re+66%Fe). Scientific Herald of Uzhhorod University. Series "Physics", (52), 46-55. https://doi.org/10.54919/2415-8038.2022.52.46-55

20. Nussupbek, Z.T., Bekenov, T.N., Sattinova, Z.K., Beisenbi, M.A., Tassybekov, Z.T. 2023. Substantiation of methods for calculation of traction forces redistribution indicators on modular front and rear wheels of the vehicle (4X4). Transportation Engineering, 13, 100193. https://doi.org/10.1016/j.treng.2023.100193

21. Gierusz, W. 2016. Modelling the dynamics of ships with different propulsion for control purpose. Polish Maritime Research, 89(23), 31-36.

22. Guimarães, D. A. 2009. Digital Transmission: A Simulation-Aided Introduction with VisSim/Comm. New York: Springer Verlag. https://doi.org/10.1007/978-3-642-01359-1

23. Leshchev, V.A., Naydyonov, A.I. 2021. Dynamic Method for Determining Resonant Frequencies of Torsional Vibrations of a Ship's Propeller Shaft. A Scientific Look into the Future, 1(21), 15-26.

24. Gorb, S., Popovskii, A., Budurov, M. 2023. Adjustment of speed governor for marine diesel generator engine. International Journal of GEOMATE, 25(109), 125-132. https://doi.org/10.21660/2023.109.m2312

25. Califano, A. 2010. Dynamic loads on marine propellers due to intermittent ventilation. Trondheim: NTNU.

26. Kaplun, V., Chuenko, R., Makarevych, S. 2022. Investigation of energy parameters of a compensated asynchronous motor in the mode of repeated short-term starts. Machinery & Energetics, 13(3), 25-33. https://doi.org/10.31548/machenergy.13(3).2022.25-33

27. Ghaemi, M.H., Zeraatgar, H. 2022. Impact of propeller emergence on hull, propeller, engine, and fuel consumption performance in regular head waves. Polish Maritime Research, 29(4), 56-76. https://doi.org/10.2478/pomr-2022-0044

28. Kluczyk, M., Grządziela, A., Batur, T. 2022. Design and operational diagnostics of marine propellers made of polymer materials. Polish Maritime Research, 29(4), 115-122. https://doi.org/10.2478/pomr-2022-0049

29. Xiang, L., Yang, S.X., Gan, C.B. 2012. Torsional vibration of a shafting system under electrical disturbances. Shock and Vibration, 19, 1-11.

30. Quang, P.K., Hung, P.V., Cong, N.C., Tung, T.X. 2022. Effects of rudder and blade pitch on hydrodynamic performance of marine propeller using CFD. Polish Maritime Research, 29(2), 55-63. https://doi.org/10.2478/pomr-2022-0017

31. Fleischer, K.P. 1973. Untersuchungen über das Zusammenwirken von Schiff und Propeller bei teilgetauchten Propellern. Forschungszentrum des Deutschen Schiffbaus Bericht, 130(73), 291-308. [in German].

POLISH MARITIME RESEARCH 4 (120) 2023 Vol. 30; pp. 81-91
10.2478/pomr-2023-0061

DIGITAL TWIN TEST-BENCH PERFORMANCE FOR MARINE DIESEL ENGINE APPLICATIONS

Dmytro Minchev [1]
Roman Varbanets [1]
Oleksandr Shumylo [1]
Vitalii Zalozh [2]
Nadiia Aleksandrovska [1]
Pavlo Bratchenko [1]
Thanh Hai Truong [3]
[1] Odesa National Maritime University, Odesa, Ukraine
[2] Danube Institute of the National University „Odesa Maritime Academy", Ukraine
[3] DPATET Research Group, Ho Chi Minh City University of Transport, Ho Chi Minh City, Viet Nam

* Corresponding author: *dmytro.minchev@nuos.edu.ua (D. Minchev)*

ABSTRACT

The application of Digital Twins is a promising solution for enhancing the efficiency of marine power plant operation, particularly their important components – marine internal combustion engines (ICE). This work presents the concept of applying a Performance Digital Twin for monitoring the technical condition and diagnosing malfunctions of marine ICE, along with its implementation on an experimental test-bench, based on a marine diesel-generator. The main principles of implementing this concept involve data transmission technologies, from the sensors installed on the engine to a server. The Digital Twin, also operating on the server, is used to automatically process the acquired experimental data, accumulate statistics, determine the current technical state of the engine, identify possible malfunctions, and make decisions regarding changes in operating programs. The core element of the Digital Twin is a mathematical model of the marine diesel engine's operating cycle. In its development, significant attention was devoted to refining the fuel combustion model, as the combustion processes significantly impact both the engine's fuel efficiency and the level of toxic emissions of exhaust gases. The enhanced model differs from the base model, by considering the variable value of the average droplets' diameter during fuel injection. This influence on fuel vapourisation, combustion, and the formation of toxic components is substantial, as shown. Using the example of calibrating the model to the test results of a diesel engine under 27 operating modes, it is demonstrated that the application of the improved combustion model allows better adjustment of the Digital Twin to experimental data, thus achieving a more accurate correspondence to a real engine.

Keywords: digital twin, combustion model, marine diesel engine, diagnostics

INTRODUCTION

Digital twin technology is a promising solution for current and future marine power plants. It could be used in various ways for various purposes: advanced control, monitoring and diagnostics, management and data analysis.

The idea of Digital Twin technology was originally developed for product lifecycle management issues, by M. Grieves in 2002, and subsequently refined by J. Vickers of NASA in 2010 [1]. It proved to be a very promising approach, as the global market for Digital Twin products was valued at USD $3.8 billion in 2019 and is expected to reach USD $35.8 billion by 2025 [2].

The concept of Digital Twins has been experiencing rapid development in recent years. Today, Digital Twins are classified as the following types: Digital Twin Instance (DTI), Digital Twin Prototype (DTP) and Performance Digital Twin (PDT) [3]. However, all types of Digital Twins have common characteristics: high-fidelity, dynamic, self-evolving, identifiable, multiscale, metaphysical, and hierarchical [4], [5].

According to some specialists, the Digital Twin could be described as having the highest possible bidirectional integration level between the physical object and virtual model. In contrast, the Digital Shadow only reflects the state of the physical object while the Digital Model has no automatic interactions with the physical object [4]. Major areas for the implementation of Digital Twins are: smart cities and urban centers, freight logistics, medicine, engineering and automotive technologies.

A major area of Digital Twins applications is fault diagnostics and continuous monitoring of an object's tecnnical state. By combining Digital Twins with the deep transfer learning approach, accurate machine fault diagnosis could be provided, even with insufficient measured fault condition data [6]. The Digital Twin is continuously updated to generate possible fault conditions close to the actual asset and constructs the training data in the source domain for transfer learning. Digital Twin technology also can provide the visualisation of the monitoring process for the object being monitored, including 3D-visualisation and augmented reality technologies [7]. The very promising predictive maintenance method, based on Digital Twin, could be applicable in many areas and presents three unique characteristics: real-time perception, a high fidelity model and high confidence simulation prediction [8].

For a marine power plant and its components, Digital Twin could serve various purposes, among which are: prototyping and design, technical state monitoring and diagnostics, control and efficiency analysis, lifecycle management. It could also be a solution for environmental impact monitoring from shipping, which is one of the IMO goals with high priority [9]. Various components of marine power plants require monitoring [10], [11], while diesel engines remain one of the most important.

In terms of marine diesel engines, the most challenging factors for the successful implementation of Performance Digital Twin are: accurate engine operation simulation and enabling fast calculations. Obviously, for engine control tasks, it is necessary to provide 'real-time' engine operating process calculations [12], [13]. The ultimate goal should be defined as: engine operating cycle synthesis time equal to the actual engine operating cycle time. It is always a trade-off between calculation time and accuracy, which should be considered at the decision making stage of choosing an appropriate mathematical model for the Digital Twin core.

Engine manufacturers can potentially adopt high-fidelity Digital Twins for real-time engine control issues, as they have all the complete information about engine sub-systems and components. The heuristic-type model could be applied in this case [14]. In contrast, the monitoring systems with Digital Twins provided by external independent developers should have the characteristic of flexible tuning and adaptation, even in the absence of data.

One of the most critical things for the sufficient operation of Digital Twins is the correct prediction of the heat release process in the engine cylinder due to the fuel burning. Simulation of fuel combustion represents the toughest challenge, in terms of the development of the Digital Twin mathematical model, as the processes of fuel injection, atomisation, evaporation, mixing with air and combustion are extremely complicated. Although some researchers reported the application of simplified combustion models, based on the Wiebe function [15], it has a huge limitation, in terms of predicting fuel timing and atomisation parameters for combustion processes.

This paper presents developments in the proven Razleitsev combustion model for marine diesel engines with Digital Twins and the research test-bench, based on the marine diesel-generator, which proves the concept. The research focuses on improvements in fuel evaporation and mixing prediction and its effect on further combustion and pollutant formation processes.

DIGITAL TWIN FOR ENGINE MONITORING AND CONTROL

A Digital Twin type of marine diesel engine serves the following purposes: monitoring of an engine's technical state, diagnostics of possible malfunctions, and control of the engine operating mode. For these purposes, the Digital Twin has to include the mathematical model of the engine operating cycle, which meets the requirements of accuracy and computational speed.

The diagram of the Digital Twin-based engine monitoring system is shown in Fig. 1. The engine is equipped with an array of sensors, allowing measurement of the engine's operating parameters. All of the sensors transfer the data to the set of controllers, which transmits the data to a Web Server via a Wi-Fi wireless connection.

The Web Server contains the Database, which stores the measured data, as well as the data generated by the Digital Twin. The Digital Twin autonomously takes data from the Database and runs the necessary calculations to compare the measured data with the predicted engine performance.

The visualisation of the actual engine operation and the predicted engine performance is provided in a pseudo real-time mode for educational and scientific purposes. Based on the comparison of the experimental and predicted engine performance, the Digital Twin provides diagnostic information related to the conditions of engine subsystems, such as: the turbocharging system, the fuel injection system and the gas distribution mechanism.

The Digital Twin also has to set up the user interface before it can be used in an actual engine.

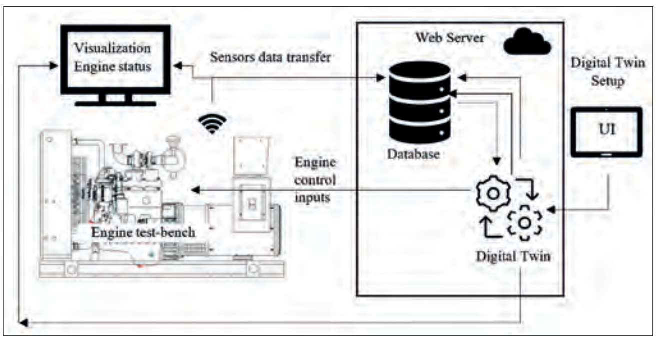

Fig. 1. Digital Twin application for engine control and monitoring issues.

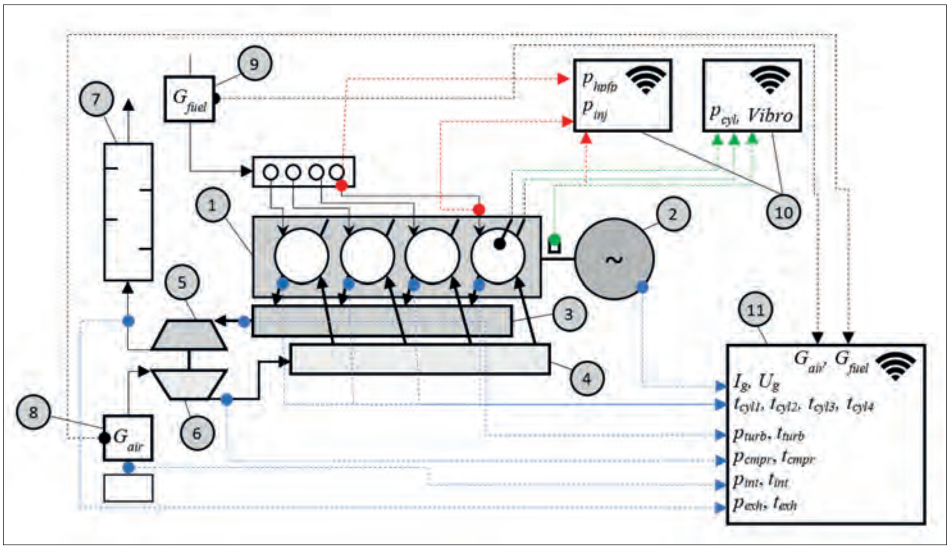

Fig. 2. Test-bench measuring points diagram:1 – engine; 2 – AC alternator; 3 – exhaust manifold; 4 – intake receiver; 5 – turbine; 6 – compressor; 7 – exhaust silencer; 8 – air mass flow meter; 9 – fuel mass flow meter; 10 – high-speed analogue-to-digital converters and transmitters; 11 – set of slow-speed analogueue-to-digital converters and transmitters.

We considered some detailed peculiarities of the concept using the actual test-bench as an example. The test-bench is based on the Weichai WP4C82-15 marine diesel-generator and was installed in the Odesa National Maritime University Laboratory.

The measuring device diagram is presented in Fig. 2 and it shows the measuring points and parameters. The measuring system can be considered as consisting of two sub-systems: 'static' and 'dynamic'. The former has low-speed parameters, which are measured as averages of the number of engine crankshaft revolutions, and the latter are high-speed parameters, which show the engine operating cycle as a function of the crank angle degree (the measuring step is 0.5-1.0 c.a.d.).

Static parameters include intake and exhaust system temperatures and pressures, engine power, air and fuel flow. The turbocharger speed is estimated by an acoustic method, as described in [16]. Dynamic parameters embrace in-cylinder pressure, pressures at the exit of the fuel injection pipe and before the fuel injector and the vibration sensor signal. The vibration sensor provides vibroacoustic data concerning fuel injection, and intake and exhaust valve timings [17], [18]. The obtained data is preprocessed using a special treatment for indicated diagrams analysis [19].

The database diagram, shown in Fig. 3, shows its basic structure and includes tables for both static and dynamic parameters.

The Digital Twin is based on the Blitz-PRO online service, providing simulations of both the static and transient operation of Internal Combustion Engines of various types [20]. The mathematical model of the engine's operating cycle is based on the two-zone quasi-steady approach for in-cylinder process synthesis, one-dimensional simulation of the intake and exhaust pipes processes, and advanced supercharger performance map treatment.

The important task of providing the closed-loop modelling of the operating process of a turbocharged engine is solved using the advanced characteristic maps of supercharging devices.

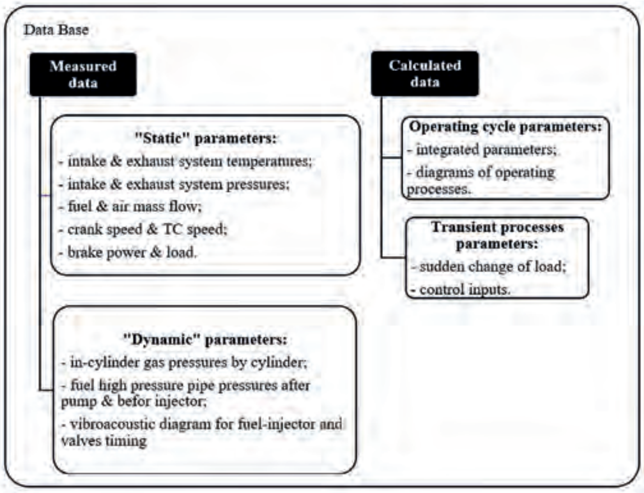

Fig. 3. Database structure.

Among other things, these maps allow for the consideration of phenomena such as compressor surge in a turbocharger [21].

The mathematical model of fuel combustion is based on the Razleitsev method for the equivalent fuel spray approach and the toxic emission estimation implements Zvonov's method of burned zone gas composition prediction. As the fuel combustion processes have a significant impact on the performance parameters of the engine and the level of toxic emmisions in the exhaust gases, as well as the fact that these processes have an inherently complex physicochemical nature, one of the most important components for the mathematical model of a Digital Twin is a precise fuel combustion model.

As the fuel combustion depends greatly on the movement of fuel spray, the injection rate diagrams, fuel atomisation and in-cylinder air motion, the application of a complex combustion model is challenging; this type of information is hardly achievable at engine operating conditions. From this point of view, the combustion model should be simple enough to set up and apply to practical power plants and accurate enough to correctly replicate engine performance.

IMPROVEMENTS IN FUEL COMBUSTION MODEL

The fuel combustion model for diesel engines was proposed for the equivalent spray approach by Razletsev in 1980 [22], and further developed in 1992 [23], to account for the peculiarities of fuel jet motion with a detailed mechanism of interaction between the fuel flame and the combustion chamber walls. Subsequently, Razletsev's model was slightly improved by Kuleshov [24] and implemented in commercial software tools for the calculation of engine operating processes.

Razletsev's method involves a sequential and interconnected consideration of the fuel injection, evaporation, mixture formation, and fuel combustion using fundamental laws of physics and chemical kinetics.

The characteristics of fuel injection are determined using experimental or statistical data. The basic Razletsev method assumes single injection events but it can be adopted for multiple injections, as we will show later. The movement of fuel sprays and their atomisation is determined using criteria equations proposed by Lyishevsky.

$$\begin{cases} l_a = 1.22 \cdot l_c \cdot \rho^{-0.5} Э_g^{-0.35} \cdot Э^{0.35} e^{-0.2\left(\frac{\tau}{\tau_c}\right)}; \\ l_b = \sqrt{d_{inj.holes} u_0 We^{0.21} M^{0.16} / (3\sqrt{2\bar{\rho}})\tau^{0.5}}; \\ l_c = 8.85 d_{inj.holes} We^{0.25} M^{0.4} \bar{\rho}^{-0.6}; \end{cases} \quad (1)$$

$$d_{32} = 10^6 E_c d_{inj.holes} \frac{M^{0.0733}}{(\bar{\rho} We)^{0.266}}; \quad (2)$$

$$M = \frac{\mu_{fuel}^2}{d_{inj.holes}\rho_{fuel}\sigma_{fuel}}; \quad \bar{\rho} = \frac{\rho_c}{\rho_{fuel}};$$

$$We = \frac{u_{inj}^2 d_{inj.holes}\rho_{fuel}}{\sigma_{fuel}}; \quad Э = \frac{\tau^2\sigma_{fuel}}{d_{inj.holes}^3\rho_{fuel}};$$

where l_a, l_b and l_c are the spray length development at the initial stage, the main stage of injection and at the end of the initial stage; τ and τ_c are time moments from injection start and from injection start to the end of the initial stage of injection; μ_{fuel}, ρ_{fuel}, and σ_{fuel} are the dynamic viscosity, specific gravity and surface tension of the fuel; E_c is a coefficient; and $d_{inj.holes}$ is the nozzle hole diameter.

Fuel atomisation is characterised with the Sauter diameter of fuel droplets d_{32}, which is the ratio of the total volume of fuel drops to their combined surface area. For simplification reasons **the value d_{32} was considered to be constant by Razletsev** and equal to the average for the injection period [22], [23].

To calculate the fuel evaporation, a modification of Sreznevsky law for the evaporation of an individual droplet is used. To determine the fraction of fuel evaporated at a given moment in time, integration is performed for all fuel portions injected up until that moment:

$$\frac{d\sigma_{ev}}{d\varphi} = \int_{\varphi_{inj.start}}^{\varphi} \frac{3}{2}\chi_{wall} b_{ev}\left(1 - \chi_{wall} b_{ev}\frac{\varphi - \varphi_{inj.start}}{6n}\right)^{0.5}\left[\frac{d\sigma}{d\varphi}\right] d\varphi, \quad (3)$$

where σev is the evaporated portion of the fuel; dσ/dφ is the relative injection rate; bev is the evaporation constant; and χ_{wall} is the reduction in the evaporation rate which occurs when fuel interacts with the walls.

It should be noted that Razletsev and his followers, instead of using the accurate solution mentioned above, used a simplified equation, **assuming a constant injection rate** over the injection process time and equal to the average value:

$$\frac{d\sigma_{ev}}{d\varphi} = \frac{1}{\varphi_{inj}}\chi\left([1 - b_{ev}(\varphi - \varphi_{inj})]^{3/2} - [1 - b_{ev}]^{3/2}\right). \quad (4)$$

The use of the simplified equation lead to a significant error in the calculation results, as shown in Fig. 4. For nonlinear injector rate profiles, the cumulative error of the evaporated fuel share could exceed 20% and so the application of the accurate solution is important.

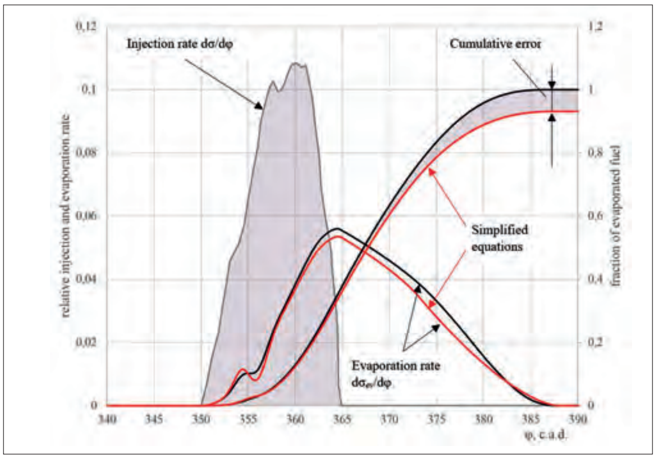

Fig. 4. Comparison of fuel injection rate diagrams calculated using simplified and accurate equations

The fuel evaporation constant is dependent on the average diameter of the fuel spray droplets d32 and can be calculated using the following expression:

$$b_{ev} = Y\frac{10^{12}}{d_{32}^2}\frac{1}{p_c}, \quad (5)$$

where Y is the correction factor; p_c is the end pressure of the compression process; and m_Y is the exponent of the evaporation function.

According to Razletsev's recommendations, the correction factor Y can be calculated using the following expression:

$$Y = \left(\frac{n_{crank}}{1000}\right)^{m_Y}, \quad (6)$$

where m_Y is the exponent of the evaporation correcting function.

Typically, m_Y is chosen within the range 0.65-1.00. However, if the crankshaft rotational speed of the engine is below 1000 rpm, the value of m_Y can be selected within the range 0.35-0.70. These values allow for appropriate adjustments in the evaporation function, to account for different engine operating conditions.

Kuleshov proposed a more complex expression for the function Y:

$$Y = 0.372 \cdot 10^{-9}(18 + y_s + y_{rpm}) y H_y^{0.35} d_{32}^{-1.5}, \quad (7)$$

where $y_S = f(S)$ is the scaling factor dependent on the piston stroke S; $y_{rpm} = f(n_{crank})$ is the correction coefficient dependent on the crankshaft rotational speed ncrank; Hy is the corrected swirl number; and y is an empirical coefficient ranging from 5-35.

This more comprehensive expression for the function Y considers additional factors, such as piston stroke, crankshaft rotational speed, and the corrected swirl number, to provide a more accurate estimation of the evaporation constant. From the given expression, we can conclude that the evaporation constant is variable during fuel injection and depends on the average diameter of the droplets.

The relative reduction in the evaporation rate when the fuel sprays come into contact with the combustion chamber walls, according to the original methodology [22], can be calculated using the following equation:

$$\chi_{wall} = 1 - \left(\frac{1-\chi_0}{0.485}\right) \cdot 0.707\left(\frac{\varphi-\varphi_{wall}}{\varphi_{fr}}\right) \cdot \frac{2}{\sqrt{\pi}} e^{-0.5\left(\frac{\varphi-\varphi_{wall}}{\varphi_{fr}}\right)^2};$$
$$\varphi_{fr} = A_{st} \cdot 2\varphi_{wall} \frac{\bar{\rho}^{0.5} We^{0.32}}{M^{0.07}}, \tag{8}$$

where φ_{wall} is the moment when the spray reaches the combustion chamber wall; χ_0 is the minimum value of the reduction coefficient of the evaporation rate; φ_{fr} is the duration of the interaction between the spray and the combustion chamber walls; and A_{st} is the coefficient in the formula for calculating the cone angle of the fuel spray.

To calculate the ignition delay period, a modified Tolstov equation is used:

$$\tau_i = B_0(1 - k_n n_{crank}) \sqrt{\frac{p_{cyl}^{in.j.start}}{T_{cyl}^{in.j.start}}}\, e^{\frac{E_a}{RT_{cyl}^{in.j.start}}} \frac{70}{25+CN}, \tag{9}$$

where B_0 and k_n are coefficients; $p_{cyl}^{in.j.start}$ and $T_{cyl}^{in.j.start}$ are the pressure and temperature at the beginning of compression; and E_a and CN are the activation energy and cetane number of the fuel.

In a further development, a more advanced model of the fuel spray was proposed, which includes the following seven characteristic zones [23]: dense axial core, dense front jet, rarefied jet envelopee, conical axial core of the boundary flow, boundary flow core on the piston surface (head, cylinder liner), and rarefied boundary flow envelope. For each of these characteristic zones, the fuel evaporation constant is calculated using individual equations.

The application of a more advanced model of fuel sprays complicates the combustion model tuning process and requires accurate information about the geometry of the combustion chamber and fuel injector, which is not always available.

During the calculation of heat release, the following processes are considered separately: combustion of the air-fuel mixture formed during the ignition delay period, diffusion combustion in the fuel supply region, and post-injection fuel burning after the end of injection. The transition between equations for each stage occurs at specific time points: when $x = \sigma_i$ from the equations for the first stage to the equations for the second stage, and when $\varphi = \varphi_{inj.end} + \Delta\varphi_{k.ext}$ from the equations for the second stage to the equations for the third stage. The continuation of using the equations for the second stage after the end of injection is possible for a period of $\Delta\varphi_{k.ext}$ by setting the parameters $\Delta\varphi_k$ and $\Delta\tau_k$.

Typically, for the external characteristic, $\Delta\varphi_k = 0$, reaching values of 5-12 in idle modes, while $\Delta\tau_k$ is recommended to be selected in the range of 0.3-0.8 for direct injection and 0.5-0.9 for split combustion chambers. The basic system of equations is as follows:

$$\frac{dx}{d\varphi} = \begin{cases} \frac{1}{6n}\left(\left(P_0 + 6n_{crank}\frac{d\sigma_{ev}}{d\varphi}\right)\Big/\left(1 + A_1\left(P_0 + 6n_{crank}\frac{d\sigma_{ev}}{d\varphi}\right)\right)\right)\Big|_{x=0}^{x=\sigma_i}; \\ \frac{1}{6n}\left(P_2 + 6n_{crank}\frac{d\sigma_{ev}}{d\varphi}\right)\Big/\left(1 + A_1 6n_{crank}\frac{d\sigma_{ev}}{d\varphi}\right)\Big|_{\sigma=\sigma_i}^{\varphi=\varphi_{inj.end}+\Delta\varphi_{k.ext}}; \\ \frac{1}{6n}A_3\frac{\xi_{a.c}\alpha}{x}(1 - \Delta_{U.F} - x)x)\Big|_{\varphi=\varphi_{inj.end}+\Delta\varphi_{k.ext}}^{\varphi=\varphi_{comb.end}}, \end{cases} \tag{10}$$

where σ_i is the fraction of fuel supplied during the ignition delay period; $\varphi_{inj.end}$ is the end of injection moment; $\Delta\varphi_k$.ext is the extended period of applying the second equation; $\Delta\varphi_{comb.end}$ is the end of the combustion process; $\xi_{a.c}$ is the air utilisation function; and $\Delta_{U.F}$ is the unburned fuel fraction.

Functions P_0, P_2, A_0, and A_2 are determined according to the equations:

$$\begin{cases} P_0 = \frac{A_0 q_{fuel}(\sigma_{ev} - x_0)}{V(\varphi_{comb.start})}(b_0\sigma_{ev} + x_0); \\ P_2 = \frac{A_2 q_{fuel}(\alpha - x)}{V_c}(\sigma_{ev} - x); \end{cases} \tag{11}$$

$$\begin{cases} A_0 = a_0 (n \cdot H)^{m_{comb}}; \\ A_1 = a_1 (n \cdot H)^{m_{comb}}; \\ A_2 = a_2 (n \cdot H)^{m_{comb}}, \end{cases} \tag{12}$$

where H is a swirl number; and a_0, a_1, a_2, b_0, and m_{comb} are adjustable coefficients.

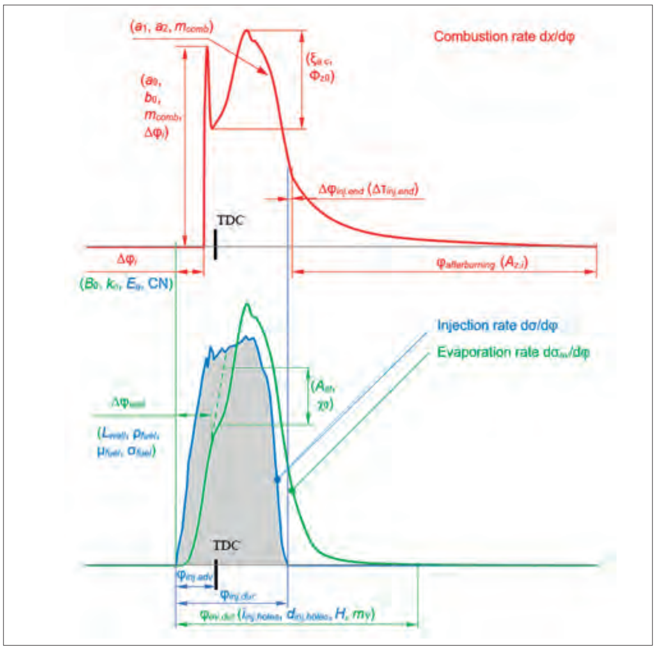

Fig. 5. The relationship between fuel injection, fuel vapourisation processes, and fuel combustion for the Razleytsev model, along with the model tuning parameters for a single injection case.

Tab. 1. Recommended values for fuel combustion model

Engine type	$a_0 \cdot 10^{-3}$	$a_1 \cdot 10^2$	a_2	b_0	m_{comb}	H	m_Y
n = 50…250 rpm, two-stroke	5…12	5…10	10…15	0.1…0.2	0.6…0.8	1.5…3	0.30…0.65
n = 400…750 rpm, four-stroke	8…15	4…9	8…13	0.05…0.15	0.5…0.7	1…1.1	0.45…0.7
n = 750…1500 rpm, two-stroke	10…40	3…7	4…8	0.05…0.1	0.5…0.7	1…1.2	0.5…0.75
n > 1500 rpm, two-stroke	15…30	3…6	3…7	0.04…0.08	0.6…0.8	1.2…2	0.5…0.9

As seen from the given system of equations, the first and second stages of the combustion process are significantly influenced by fuel vapourisation rate and mixture formation, while the fuel post-injection stage is determined by the air utilisation function in the engine cylinder $\zeta_{a.c}$:

$$\zeta_{a.c} = 1 - 1.46(1 - \zeta_{a.c0})\,\frac{\Phi_z}{\Phi_{z0}}\,\frac{2}{\sqrt{\pi}}\,e^{-0.5\left(\frac{\Phi_z}{\Phi_{z0}}\right)^2}, \tag{13}$$

where Φ_z is the relative combustion duration; and $\zeta_{a.c0}$ and Φ_{z0} are the coordinates of the minimum of the function $\zeta_{a.c} = \zeta_{a.c}(\Phi_{z0})$.

Table 1 provides typical values of the coefficients in the fuel combustion model equations for different types of engines, while Fig. 5 illustrates the influence of various tuning parameters on the characteristics of heat release.

CONSIDERING VARIABLE FUEL DROPLETS SIZE DURING INJECTION

As previously mentioned, Razleitsev used the average value of the fuel droplet diameter d_{32} to predict fuel evaporation and considered it to be constant during injection. In his latest studies, Kuleshov considered variable fuel droplet size for the ignition delay period [24], [25]. Obviously, this means that the fuel evaporation constant b_{ev}, as well as the correction factor Y, are also constant in the evaporation process. To examine the applicability of simplified equations, consider Fig. 6-8, which show the calculated fuel evaporation diagrams for two cases: assuming a variable fuel droplets size across the injection process and using the constant value of d_{32} averaged for the injection period (d_{32} = const). As shown, assuming the variable fuel droplets diameter makes a significant impact on fuel the evaporation diagrams, which causes a further influence on fuel combustion and in-cylinder pressure build-up.

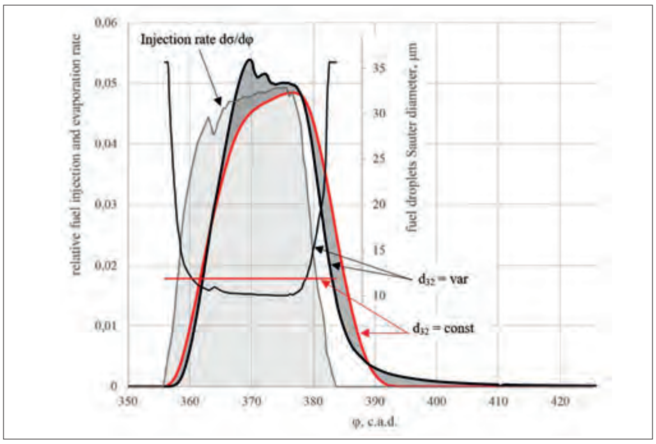

Fig. 6. Calculated diagrams of fuel evaporation rate. Medium-speed diesel engine, MCR.

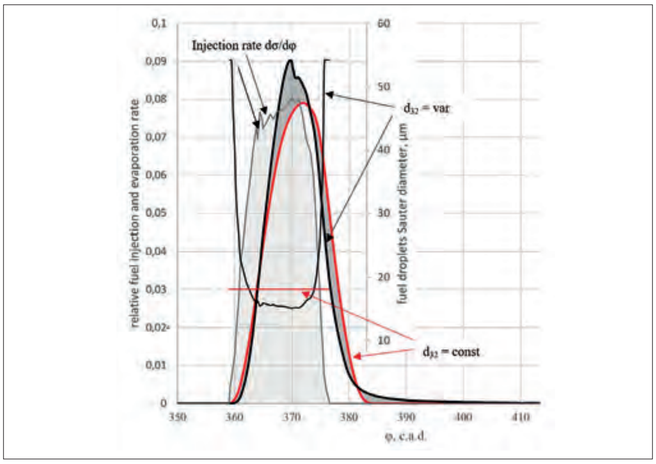

Fig. 7. Calculated diagrams of fuel evaporation rate. Medium-speed diesel engine, 40% of MCR.

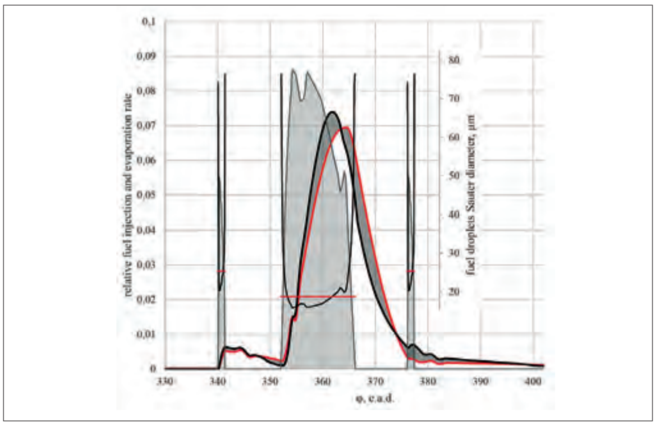

Fig. 8. Calculated diagrams of fuel evaporation rate. High-speed diesel engine, triple injection, part load.

Fuel combustion processes contribute to the emission of toxic compounds in the exhaust gases of marine diesel engines. These emissions primarily consist of CO, soot (and other particulate matter), SO_x, and NO_x. Accurate prediction of the buildup of toxic emissions is crucial for the application of engine Digital Twins.

CONSIDERING TOXIC EMISSION FORMATION IN THE COMBUSTION PROCESSES

In order to predict the gas composition in different zones, a two-zone combustion model is employed. This model separates the fresh charge zone from the burned gases zone. The composition of the burned gases is determined using Professor Zvonov's method, which assumes an 18-component mixture consisting of O, O_2, O_3, H, H_2, OH, H_2O, C, CO, CO_2, CH_4, N, N_2, NO, NO_2, NH_3, HNO_3, and HCN.

The calculation of NO_x concentration in the exhaust gas is based on the Zeldovich mechanism for 'thermal' nitric oxide (NO). This mechanism involves a series of three equations.

The first equation is the most important, in terms of total NO formation kinetics. The equation for NO kinetics can be expressed as:

$$\frac{d[\mathrm{NO}]}{d\tau} = K_{1p}[N_2][O] - K_{1r}[\mathrm{NO}][N] - K_{2r}[\mathrm{NO}][O] + K_{3p}[N][\mathrm{OH}] - K_{3r}[\mathrm{NO}][H],$$

where the square brackets '[ ]' express the volumetric concentration of the corresponding matter, and K_{1p}, K_{1r}, K_{2p}, K_{2r}, K_{3p}, and K_{3r} are constants for direct and reverse chemical reactions.

The NO formation kinetic equation incorporates the first and second equations, based on Zvonov's approach:

$$\frac{d[\mathrm{NO}]}{d\tau} = \frac{2K_{1p}[N_2][O]}{1+\frac{K_{1r}[\mathrm{NO}]}{K_{2p}[O_2]}}\left(1 - \frac{[\mathrm{NO}]^2}{K_4[O_2][N_2]}\right);\ K_4 = \frac{K_{1p}K_{2p}}{K_{1r}K_{2r}}; \tag{14}$$

It should be noted that $K_4[O_2][N_2] = [\mathrm{NO}]_{eq}$ is the equilibrium concentration of NO.

The conversion of the equation into volumetric fraction units gives:

$$\frac{d[\mathrm{NO}]}{d\tau} = \frac{p}{RT_{burned}}\frac{2K_{1p}[N_2][O]}{1+\frac{K_{1r}[\mathrm{NO}]}{K_{2p}[O_2]}}\left(1 - \left(\frac{[\mathrm{NO}]}{[\mathrm{NO}]_{\mathrm{eq}}}\right)^2\right), \tag{15}$$

where p is the pressure in the cylinder (bar); R = 8.3144 J/(mole·K) is the gas constant; and T_{burned} is the temperature of the burned gases.

The Arrhenius Law equations are used to calculate reaction rate constants:

$$K = AT^B\, exp\left(-\frac{E_a}{RT}\right), \tag{16}$$

where A and B are empirical coefficients; and E_a is the activation energy.

For high-speed engines, the final concentration of CO in exhaust gases is estimated as an equivalent concentration at the combustion finish point. For medium-speed and low-speed diesel engines, the following kinetic equation is used:

$$\frac{d[\mathrm{CO}]}{d\tau} = K_{1C}[\mathrm{CO}]\ [\mathrm{OH}]\ , \tag{17}$$

where $K_{1C} = 7.1 \cdot 10^{12} \cdot e^{-32200RT}$ is the reaction constant; and [CO] and [OH] are the corresponding CO and OH concentrations.

Calculation of the formation of particulate matter in diesel engines is performed using Razlejtsev's approach. The equation for the instantaneous volumetric soot concentration rate is as follows:

$$\frac{d[\mathrm{C}]}{d\tau} = \left(\frac{d[\mathrm{C}]}{d\tau}\right)_{kin} + \left(\frac{d[\mathrm{C}]}{d\tau}\right)_{pol} - \left(\frac{d[\mathrm{C}]}{d\tau}\right)_{burn} - \left(\frac{d[\mathrm{C}]}{d\tau}\right)_{vol}. \tag{18}$$

The components of this equation are:

– the kinetic soot formation rate (in the flame) $\left(\frac{d[\mathrm{C}]}{d\tau}\right)_{kin} = B_{1S}\frac{q_{fuel}}{V}\frac{dx}{dt}$;

– the core polymerisation of fuel droplets rate during fuel injection:

$$\left(\frac{d[\mathrm{C}]}{d\tau}\right)_{pol} = B'_{2s}\delta_d\frac{q_{fuel}}{V}\frac{1-exp\left(-\left(\frac{\sqrt{K_{ev}(\tau-\tau_{inj.start})}}{d_{32}}\right)^{n_{disp}}\right)}{\tau_{inj}},$$

and after fuel injection ends:

$$\left(\frac{d[\mathrm{C}]}{d\tau}\right)_{pol} = B''_{2s}\delta_d\left(1 - x_{inj.end}\right)\frac{n_{disp}q_{fuel}}{2V(\tau-\tau_{inj.end})}\left(\frac{\sqrt{K_{ev}(\tau-\tau_{inj.start})}}{d_{32}}\right)^{n_{disp}}\frac{1-e^{-\left(\frac{\sqrt{K_{ev}(\tau-\tau_{inj.start})}}{d_{32}}\right)^{n_{disp}}}}{\tau_{inj}};$$

– the soot particles burning rate: $\left(\frac{d[\mathrm{C}]}{d\tau}\right)_{burn} = B_{3S}k_{O_2}\sqrt{n}\cdot p\cdot[C]$;

– and the change in soot concentration rate due to cylinder volume change:

$$\left(\frac{d[\mathrm{C}]}{d\tau}\right)_{vol} = B_{4S}\frac{6n}{V}\frac{dV}{d\phi}.$$

In the above equations B_{1s}, B'_{2s}, B''_{2s}, B_{3s}, and B_{4s} are empiric coefficients; δ_d is the droplet core size; K_{ev} is the evaporation constant; $\tau_{inj.start}$ and $\tau_{inj.end}$ are moments of time for injection start and injection end; $x_{inj.end}$ is the burned fuel fraction for the moment of injection end; n_{disp} is the distibution constant to consider fuel injection uniformity; $k_{0_2}$is the oxidation coefficient; and $[C]$ is the volumetric soot concentration.

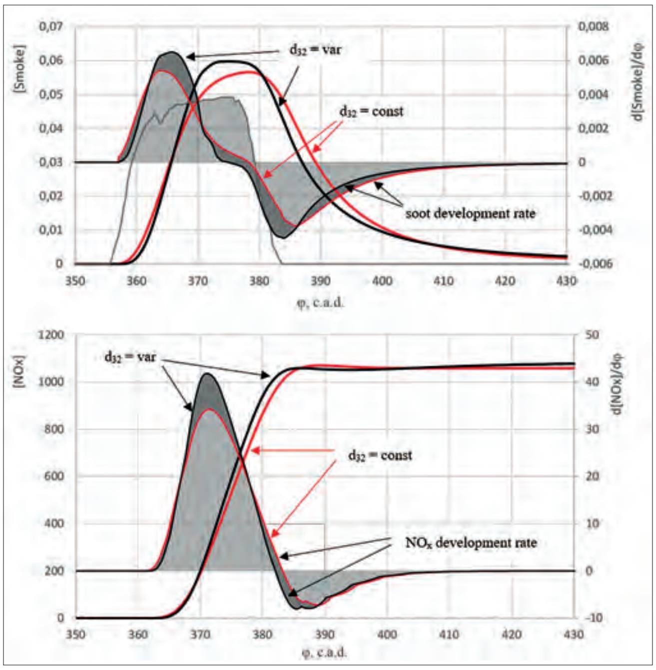

Fig. 9. Soot concentration and nitrogen oxide development in the cylinder. Medium-speed engine, MCR.

The oxidation coefficient is considered using following equation:

$$k_{O_2} = 1.8 \left(1-\left(1-(1-\alpha)\,\frac{L_0}{M_2}\right) x\right), \quad (19)$$

where L_0 is the stoichiometric amount of air (in kmole per 1 kg of fuel); and M_2 is the amount of combustion products (in kmole per 1 kg of fuel).

The influence of the variable diameter of fuel droplets, considering during the development of toxic emmissions, is illustrated in Fig. 9.

DISCUSSION

Therefore, it can be concluded that, the variable size of fuel droplets during injection is significant in the provided combustion model, as it not only substantially affects the processes of vapourisation, mixture formation, and combustion, but also the formation of toxic emissions, primarily nitrogen oxides and particulate matter. The proposed improvements in the mathematical model allow for a more accurate calibration with experimental data and, importantly for its Digital Twin application, do not lead to an increase in calculation time.

As an example, consider the calibration of a Digital Twin for a high-speed diesel engine with a cylinder diameter/stroke of 120/120 mm, using the results of its comprehensive testing under 27 operating modes, including the determination of emissions of key pollutants (nitrogen oxides) and smoke opacity of the exhaust gases.

Table 2 illustrates the values of relative errors in determining the specific indicated fuel consumption b_{ii}, concentrations of nitrogen oxides [NOx], and smoke opacity [Smoke]. Consideration of variable fuel droplet size during injection helped to obtain better cumulative accuracy, calculated with the equation:

$$\delta_\Sigma = \sqrt{\frac{\Sigma\delta_i^2}{N}}, \quad (20)$$

where $N = 27$ (the total number of measurements).

Table 2 shows that consideration of fuel droplet size variation helped to simultaneously increase the accuracy of the prediction of b_i – from $\delta_\Sigma = 5.7\%$ to $\delta_\Sigma = 5.1\%$, [NOx] – from $\delta_\Sigma = 6.2\%$ to $\delta_\Sigma = 3.2\%$ and [Smoke] from $\delta_\Sigma = 41.6\%$ to $\delta_\Sigma = 17.8\%$.

However, it is necessary to acknowledge that the proposed refinement of the combustion model, which is thoroughly grounded from a theoretical standpoint, presents certain pragmatic challenges. It becomes evident that, in order to optimally harness the enhanced capabilities of the model, the characteristics of the fuel injection (in the form of multi-parameter functions denoted as $d\sigma/d\varphi$ = f(rpm, bmep)) are required, at the very least. The procurement of such data necessitates the execution of intricate and dedicated experimental investigations, typically carried out on specialised test-benches.

It is essential to consider that the mere existence of such dependencies under actual operating conditions is insufficient, as these relationships are derived for the proper state of the fuel system: the high-pressure fuel pump, high-pressure pipes, and fuel injector.

Thus, it is necessary to be able to assess the characteristics of fuel injection during the engine's operation. To achieve this, use of the following data is proposed:

- In the case of a research engine, sensors for fuel pressure are installed after the high-pressure fuel pump and directly in front of the injector, as shown in Fig. 2. These sensors allow for obtaining pressure diagrams at the corresponding points, as well as a vibroacoustic sensor.
- For engines operating within a marine power plant, if the installation of pressure sensors is not provided for by the design, a vibroacoustic sensor is exclusively used, which enables the acquisition of the moments of the beginning and end of fuel injection [17].

The data obtained from the sensors allow for obtaining the necessary characteristics of fuel injection and, importantly, taking into account their changes due to wear or malfunctions of the fuel apparatus. A detailed review of the algorithms and results of similar data processing requires a separate publication and represents a prospect for further research.

Specifically indicated fuel consumption biNitrogen oxide content at exhaust [NOx]Particulate matter content at exhaust [Smoke]

CONCLUSIONS

Digital Twin technology represents a promising direction for enhancing the operational efficiency of marine internal combustion engines. The advanced systems for monitoring the technical conditions and diagnosing engine malfunctions can be developed, complying with the principles and requirements of the fourth industrial revolution for modern transportation systems. The performance-type Digital Twin, as the core element of these systems, uses the data from engine sensors to predict the virtual operating cycle, which gives additional information about engine parameters and helps to estimate the efficiency of the engine and detect possible malfunctions.

Technically, the monitoring system includes the server with the database for the engine operating parameters, transmitted from the set of sensors. The data include slow-speed 'static' and high-speed 'dynamic' parameters. The Digital Twin uses the database in autonomous mode and is also capable of providing the malfunctions alarm or control inputs.

When developing a Digital Twin for an internal combustion engine, it is important to reliably and accurately calculate the development of the fuel combustion processes, as they significantly impact both the engine's efficiency and the level of toxic emissions in exhaust gases. Considering the variation in fuel droplet diameter during the injection process, allows for a substantial improvement in the accuracy of engine modelling using the Digital Twin, as is shown for the set of 27 operational points of the high-speed diesel engine.

Tab. 2. Relative accuracy of Digital Twin predicted diesel engine parameters

Specifically indicated fuel consumption b_i

Crank speed	Ignition advance	d_{32} = const		δ_Σ=5.7%	d_{32} = var		δ_Σ=5.1%
		40% load	70% load	100% load	40% load	70% load	100% load
1000	10	14.1%	2.8%	−0.7%	11.8%	1.2%	−1.4%
	13	14.9%	8.6%	5.9%	13.3%	7.3%	6.0%
	18	7.7%	4.5%	3.6%	6.8%	3.9%	3.2%
1400	10	3.5%	1.2%	−0.1%	1.8%	−0.4%	−1.5%
	13	9.5%	6.6%	2.0%	7.9%	5.3%	1.1%
	18	2.7%	2.7%	3.6%	2.0%	2.1%	3.4%
2200	10	−2.8%	−3.3%	0.9%	−4.5%	−4.5%	−1.7%
	13	1.6%	−1.7%	−2.6%	0.4%	−2.4%	−3.0%
	18	−4.2%	−2.6%	−0.8%	4.7%	−2.8%	−2.3%

Nitrogen oxide content at exhaust [NO_x]

Crank speed	Ignition advance	d_{32} = const		δ_Σ=6.2%	d_{32} = var		δ_Σ=3.2%
1000	10	−3.6%	−1.6%	−1.9%	1.7%	1.5%	1.6%
	13	−2.6%	0.4%	0.5%	−0.8%	−1.3%	−0.8%
	18	2.3%	1.4%	10.9%	−0.8%	−2.5%	3.2%
1400	10	−6.6%	3.7%	2.1%	−6.1%	−1.3%	1.3%
	13	−2.2%	0.4%	−1.0%	1.3%	−0.2%	−1.0%
	18	−0.9%	0.8%	−6.1%	0.9%	−3.6%	−2.9%
2200	10	11.1%	21.2%	−7.6%	−10.0%	4.5%	−6.4%
	13	−3.1%	1.8%	−3.3%	−2.0%	−1.3%	−1.0%
	18	10.6%	−3.0%	−0.2%	3.6%	−0.4%	−0.3%

Particulate matter content at exhaust [Smoke]

Crank speed	Ignition advance	d_{32} = const		δ_Σ=41.6%	d_{32} = var		δ_Σ=17.8%
1000	10	−12.6%	−1.9%	−6.9%	−23.8%	−1.3%	−4.2%
	13	13.9%	0.0%	−2.3%	0.0%	−0.1%	0.9%
	18	33.7%	14.2%	41.8%	12.6%	15.7%	43.7%
1400	10	−12.4%	7.5%	3.4%	−24.4%	5.0%	7.9%
	13	−8.6%	23.4%	−15.2%	−21.2%	25.1%	−10.6%
	18	10.2%	17.2%	11.9%	0.1%	18.6%	15.6%
2200	10	−24.5%	0.7%	−4.4%	−33.7%	−7.9%	−4.7%
	13	−20.6%	−2.9%	3.8%	−31.6%	−11.0%	1.1%
	18	−16.1%	−11.6%	3.7%	−24.3%	−15.6%	1.1%

However, for the successful utilisation of the additional capabilities inherent to the fuel combustion model, it is necessary to have the ability to conduct an evaluation of fuel injection characteristics during engine operation. This is proposed to be accomplished through the use of vibroacoustic sensors and, where feasible, pressure sensors within the fuel system, and represents the direction of future research.

REFERENCES

1. M. Grieves and J. Vickers, "Digital twin: Mitigating unpredictable, undesirable emergent behavior in complex systems," Transdisciplinary perspectives on complex systems: New findings and approaches. 2017, pp. 85-113, https://www.researchgate.net/profile/Michael-Grieves/

publication/306223791_Digital_Twin_Mitigating_Unpredictable_Undesirable_Emergent_Behavior_in_Complex_Systems/links/5aa54e1ea6fdccd544bc386f/Digital-Twin-Mitigating-Unpredictable-Undesirable-Emerge.

2. S. Evans, C. Savian, A. Burns and C. Cooper, "Digital Twins for the Built Environment: An Introduction to the Opportunities," Built Environmental News. 2019, https://www.theiet.org/media/8762/digital-twins-for-the-built-environment.pdf.

3. D. Botín-Sanabria, A.-S. Mihaita, R. Peimbert-García, M. Ramírez-Moreno, R. Ramírez-Mendoza and J. Lozoya-Santos, "Digital Twin Technology Challenges and Applications: A Comprehensive Review," Remote Sensing. 2022, vol. 14(6), no. 1335, doi: 10.3390/rs14061335.

4. M. Singh, E. Fuenmayor, E. Hinchy, Y. Qiao, N. Murray and D. Devine, "Digital Twin: Origin to Future," Appl. Syst. Innov. 2021, vol. 4, no. 36, doi: 10.3390/asi4020036.

5. L. Li, S. Aslam, A. Wileman and S. Perinpanayagam, "Digital Twin in Aerospace Industry: A Gentle Introduction," IEEE Access. 2022, vol. 10, pp. 9543-9562, doi: 10.1109/ACCESS.2021.3136458.

6. M. Xia, H. Shao, D. Williams, S. Lu, L. Shu and C.W. de Silva, "Intelligent fault diagnosis of machinery using digital twin-assisted deep transfer learning," Reliability Engineering & System Safety. 2021, vol. 215, doi:10.1016/j.ress.2021.107938.

7. S. Choi, J. Woo, J. Kim and J. Lee, "Digital Twin-Based Integrated Monitoring System: Korean Application Cases," Sensors. 2022, vol. 22, no. 5450, doi: 10.3390/s22145450.

8. D. Zhong, Z. Xia, Y. Zhu and J. Duan, "Overview of predictive maintenance based on digital twin technology," Heliyon. 2023, vol. 9, no. 4, doi: 10.1016/j.heliyon.2023.e14534.

9. A.T. Hoang, A.M. Foley, S. Nižetić, Z. Huang, H.C. Ong, A.I. Ölçer, V.V. Pham and X.P. Nguyen, "Energy-related approach for reduction of CO2 emissions: A critical strategy on the port-to-ship pathway," Journal of Cleaner Production. 2022, vol. 355, doi:10.1016/j.jclepro.2022.131772.

10. O. Melnyk, O. Sagaydak, O. Shumylo and O. Lohinov, "Modern Aspects of Ship Ballast Water Management and Measures to Enhance the Ecological Safety of Shipping," in Systems, Decision and Control in Energy V. Studies in Systems, Decision and Control, Springer ed. 2023, vol. 481, Cham, doi: 10.1007/978-3-031-35088-7_39.

11. O. Onishchenko, A. Bukaros, O. Melnyk, V. Yarovenko, A. Voloshyn and O. Lohinov, "Ship Refrigeration System Operating Cycle Efficiency Assessment and Identification of Ways to Reduce Energy Consumption of Maritime Transport," in Systems, Decision and Control in Energy V. Studies in Systems, Decision and Control, 2023, vol 481. Springer, Cham., doi: 10.1007/978-3-031-35088-7_36.

12. S. Hautala, M. Mikulski, E. Söderäng, X. Storm and S. Niemi, "Toward a digital twin of a mid-speed marine engine: From detailed 1D engine model to real-time implementation on a target platform," International Journal of Engine Research. 2022, doi: 10.1177/14680874221106168.

13. S. Stoumpos, G. Theotokatos, C. Mavrelos and E. Boulougouris, "Towards Marine Dual Fuel Engines Digital Twins — Integrated Modelling of Thermodynamic Processes and Control System Functions," J. Mar. Sci. Eng. 2020, vol. 8, no. 3(200), doi: 10.3390/jmse8030200.

14. I. Asimakopoulos, L. Avendaño-Valencia, M. Lützen and N. Rytter, "Data-driven condition monitoring of two-stroke marine diesel engine piston rings with machine learning," Ships and Offshore Structures. 2023, doi: 10.1080/17445302.2023.2237302.

15. O. Bondarenko and T. Fukuda, "Development of a diesel engine's digital twin for predicting propulsion system dynamics," Energy. 2020, vol. 196, doi:10.1016/j.energy.2020.117126.

16. R. Varbanets, O. Fomin, V. Píštěk, V. Klymenko, D. Minchev, A. Khrulev, V. Zalozh and P. Kučera, "Acoustic method for estimation of marine low-speed engine turbocharger parameters," Journal of Marine Science and Engineering. 2021, vol. 3, no. 9, doi: 10.3390/jmse9030321.

17. R. Varbanets, O. Shumylo, A. Marchenko, D. Minchev, V. Kyrnats, V. Zalozh, N. Aleksandrovska, R. Brusnyk and K. Volovyk, "Concept of vibroacoustic diagnostics of the fuel injection and electronic cylinder lubrication systems of marine diesel engines," Polish Maritime Research. 2022, vol. 29, no. 4, pp. 88-96, doi: 10.2478/pomr-2022-0046.

18. S. Neumann, R. Varbanets, D. Minchev, V. Malchevsky and V. Zalozh, "Vibrodiagnostics of marine diesel engines in IMES GmbH systems," Ships and Offshore Structures. 2022, doi: 10.1080/17445302.2022.2128558.

19. O. Yeryganov and R. Varbanets, "Features of the fastest pressure growth point during compression stroke," Diagnostyka. 2018, vol. 19, no. 2, pp. 71-76, doi: 10.29354/diag/89729.

20. D. Minchev, R. Varbanets, N. Alexandrovskaya and L. Pisintsaly, "Marine diesel engines operating cycle simulation for diagnostics issues," Acta Polytechnica. 2021, vol. 61, no. 3, pp. 428-440, doi: 10.14311/ap.2021.61.0435.

21. D. Minchev, O. Gogorenko, R. Varbanets, Y. Moshentsev, V. Píštěk, P. Kučera, O. Shumylo and V. Kyrnats, "Prediction of centrifugal compressor instabilities for internal combustion engines operating cycle simulation," Proceedings of the Institution of Mechanical Engineers, Part D: Journal of

Automobile Engineering. 2023, vol. 237, no. 2-3, pp. 572-584, doi: 10.1177/09544070221075419.

22. Н. Ф. Разлейцев, Моделирование и оптимизация процесса сгорания в дизелях, Харьков: Вища школа, 1980, p. 169.

23. А. Ф. Шеховцов, Ф. И. Абрамчук and В. И. и. д. Крутов, Процессы в перспективных дизелях, Харьков: Основа, 1992, p. 352.

24. L. Grekhov, K. Mahkamov and A. Kuleshov, "Optimization of Mixture Formation and Combustion in Two-Stroke OP Engine Using Innovative Diesel Spray Combustion Model and Fuel System Simulation Software," SAE. 2015, 2015-01-1859, doi: 10.4271/2015-01-1859.

25. A. Kuleshov, K. Mahkamov, A. Kozlov and Y. Fadeev, "Simulation of dual-fuel diesel combustion with multi-zone fuel spray combustion model," Proceedings of the ASME 2014 Internal Combustion Engine Division Fall Technical Conference. 2014, pp. 1-13, doi: 10.1115/ICEF2014-5700.

POLISH MARITIME RESEARCH 4 (120) 2023 Vol. 30; pp. 92-101
10.2478/pomr-2023-0062

AN EXPERIMENTAL STUDY OF THE EFFECTS OF CYLINDER LUBRICATING OILS ON THE VIBRATION CHARACTERISTICS OF A TWO-STROKE LOW-SPEED MARINE DIESEL ENGINE

Gang Wu [1*]
Guodong Jiang [1]
Changsheng Chen [2]
Guohe Jiang [1]
Xigang Pu [1]
Biwen Chen [2]
[1] Merchant Marine College, Shanghai Maritime University, Shanghai, China
[2] Shanghai Marine Equipment Research Institute, Shanghai, China

* Corresponding author: *wugang@shmtu.edu.cn (Gang Wu)*

ABSTRACT

Two-stroke, low-speed diesel engines are widely used in large ships due to their good performance and fuel economy. However, there have been few studies of the effects of lubricating oils on the vibration of two-stroke, low-speed diesel engines. In this work, the effects of three different lubricating oils on the vibration characteristics of a low-speed engine are investigated, using the frequency domain, time-frequency domain, fast Fourier transform (FFT) and short-time Fourier transform (STFT) methods. The results show that non-invasive condition monitoring of the wear to a cylinder liner in a low-speed marine engine can be successfully achieved based on vibration signals. Both the FFT and STFT methods are capable of capturing information about combustion in the cylinder online in real time, and the STFT method also provides the ability to visualise the results with more comprehensive information. From the online condition monitoring of vibration signals, cylinder lubricants with medium viscosity and medium alkali content are found to have the best wear protection properties. This result is consistent with those of an elemental analysis of cylinder lubrication properties and an analysis of the data measured from a piston lifted from the cylinder after 300 h of engine operation.

Keywords: two-stroke; low-speed marine diesel engine; cylinder lubricating oils; vibration characteristic; condition monitoring

INTRODUCTION

The internal combustion (IC) engine is a classical rotating power machine that has been widely employed for transportation and power production [1]. In particular, the two-stroke low-speed diesel engine is a unique type of IC engine that has been used in many medium and large ships due to its advantages such as multi-fuel feasibility, fuel economy, large output power, and durability [2]. With the increasing emphasis on ship safety, more and more researchers are focusing on the hazards to reliability posed by engine vibration. Harmful engine vibration can have direct effects on the hull, machinery, crew, and passengers when it occurs in ships. The main source of engine vibration is an imbalance in the force and moment created by the inertial force of its moving parts, although another source is the side thrust and overturning moment generated by the in-cylinder pressure of fuel combustion. Further factors include the influence of lubricating oils [3, 4], fuels [5-8], and engine faults [9, 10], which can all affect engine vibration. The engine contains many internal components, such as the piston-cylinder assembly, which require a good lubricating oil to run; hence, the characteristics of the lubricating oil, and its quality and performance, will have a significant impact on the behaviour of the engine, especially for two-stroke low-speed marine diesel engines with complex structures and large dimensions.

In general, lubricating oil is an oil-like liquid that is applied between moving surfaces and can carry out the functions of reducing friction and wear. It also has the ability to eliminate shock loads, and can ensure cooling, sealing, etc. Thus, lubricating oil requires several properties, such as a suitable viscosity, flash point, and alkali value, which are related to the functions mentioned above. Prior research [11] has confirmed the importance of the properties of the lubricant, as it affects not only the engine itself but also attached components such as turbochargers, meaning that it is very important in terms of the transient response of the engine. The viscosity-temperature characteristics of lubricating oil reveal the relationship between viscosity and temperature, where the lower the temperature, the higher the viscosity. This relationship is strongly related to the performance of the engine, as a high viscosity for the lubricating oil will increase the friction loss of the engine, especially in a low-temperature environment. It is therefore important to develop suitable grades of engine lubricating oil with different viscosities. The American Society of Automotive Engineers (SAE) grading system is widely used internationally to represent the viscosity of lubricating oil.

Lubricating oil with different properties can produce different levels of friction and wear in an engine, which can lead to different vibration characteristics and different amounts of wear to metals from the lubricating oil used. In research conducted by Ahmad Taghizadeh-Alisaraei, it was found that the replacement of lubricating oil helps to reduce engine vibration, as it can reduce the friction between components such as bearings, piston cylinders, etc. [12]. One potential reason for this is that degradation of the lubricating oil and the presence of wear debris in the unreplaced lubricating oil lead to greater engine vibration. Recent studies have revealed further information on the effects of fuel type on the status of lubrication oil. Nantha Gopal et al. [13] studied the effects of biodiesel fuel on the surface wear to cylinder liners, and quantified the cylinder wear of the engine by comparing the surface roughness of the cylinder liner as well as the concentration of wear debris in the lubricant samples from the engine. The results revealed significant degradation of the lubricating oil in a biodiesel blended fuel engine. A further analysis of the oil revealed the presence of wear metals in the used oil, which were also considered to be related to degradation. Hence, the problem of degradation is critical for lubrication oil, as it can cause a significant reduction in the kinematic viscosity and the flash point of the lubricating oil.

For a two-stroke low-speed marine diesel engine, the type of lubrication required for the cylinder liner is unique. A larger cylinder bore and a longer cylinder stroke require a greater injection of lubricating oil to the cylinder. In addition, matching the sulphur level of heavy fuel oil (HFO) to the cylinder lubricating oil is a critical issue. This requires that the cylinder lubricating oil has an appropriate alkali value: if too little alkali is present, the acids in the combustion products will not be neutralised and will attack the piston liner, causing corrosive wear, whereas if too much alkali is present, inorganic calcium carbonate will form hard deposits that cannot be burned out, leading to abrasive wear. With the trend towards low-sulphur fuel, there is a lack of experience in terms how to address the issues of lubricity and cleanliness between the piston and cylinder liner. In addition, the traditional method of inspecting the piston and cylinder liner relies on manual disassembly of the piston-cylinder assembly, which is not efficient.

In recent years, vibration and noise signals have been shown to be useful for assessing the condition of engines, such as combustion processes, valve faults, and fuel injection behaviours, and can be used for fault detection in diesel engines. Researchers have already begun to investigate engine performance and optimal fuel selection based on engine vibration signals. Ahmad Taghizadeh-Alisaraei [12] designed a systematic experiment to evaluate the minimum engine vibration for seven engine speeds and nine biodiesel fuel blend ratios by calculating the root mean square (RMS) and comparing the amplitudes of the vibration signals. Ahmet Çalık [14] measured the vibration characteristics of an engine when hydrogen was added to biodiesel. The RMS was used to compare the vibrations of different fuel blends. Their results showed that biodiesel fuel could reduce engine vibration, and hydrogen could reduce the vibration further. Similarly, ethanol-diesel blended fuel has also been investigated for a diesel engine [15], and the RMS and kurtosis were used to scrutinise the performance of the engine.

In other studies, airborne acoustic signals have been used to assess the lubrication quality of the engine. Albarbar et al. [16] studied the effects of lubricating oil based on structure-borne acoustic signals, and found that the amplitude of the spectral components was proportional to the engine speed and load. The RMS values of the signals were found to be influenced by the lubricant conditions.

Some newly developed signal analysis and processing methods have also been used as effective tools for detecting piston scratching faults. In Ref. [15], the short-time Fourier transform (STFT) was developed to characterise various sources of engine vibration. Through an STFT analysis, the authors successfully identified engine knocking cycles when the ethanol concentration in diesel fuel exceeded 8%. Moosavian et al. [17] investigated the vibration signature of a diesel engine under healthy and fault operating conditions, using the fast Fourier transform (FFT) and continuous wavelet transform (CWT) methods to explore the approximate frequency band caused by a piston scratching fault. The results showed that the scratching fault excited the 3–4.7 kHz frequency band [17]. Omar et al. [18] carried out an experimental study in which FFT and STFT were used to compare the vibrations of a liquefied petroleum gas (LPG) dual-fuel engine and a base diesel engine. The results showed that the vibration of the LPG dual-fuel engine was lower than for the diesel engine.

Although the studies described above show that the use of vibration signal is promising in terms of monitoring the tribological behaviours of engine cylinders, there are few studies of the monitoring of two-stroke low-speed marine diesel engines fuelled by HFO, which are vital to prevent the gradual degradation of cylinder lubrication oil and to avoid any unnecessary wear and corrosion of the cylinder liner.

In this paper, we improve on the findings described above by using a more powerful analysis based on the RMS, FFT, and STFT methods to characterise the engine vibration signals acquired for cylinder lubricating oils with different SAE grades and base numbers, thereby establishing a more accurate and reliable indicator for monitoring the tribological behaviours of the piston ring and cylinder liner of a two-stroke low-speed marine diesel engine. To further verify the diagnostic performance of the vibration signal responses extracted using optimised FFT and STFT spectra, three formulas for cylinder lubricating oils were sampled for elemental analysis after 300 h of steady-state engine operation, and the carbon deposits on the surface of the pistons were compared before and after these 300 h of operation. The main objectives were to explore the effects of different cylinder lubricating oils on the wear to the engine cylinder, and to explore the vibration characteristics of a two-stroke low-speed marine diesel engine fuelled by HFO.

MATERIALS AND METHODS

EXPERIMENTAL SETUP AND DATA ACQUISITION

The experiments were performed on a two-stroke low-speed marine diesel engine, manufactured by MAN B&W corporation, which was installed in the laboratory of Shanghai Maritime University (SMU), China. This type of low-speed diesel engine is widely used in large ocean-going vessels, and is a typical example of such an engine. The engine was fuelled with low-sulphur-content heavy fuel oil (0.5% S) during the experiments. The main technical specifications of this low-speed engine are shown in Table 1.

Tab. 1. Technical specifications of the engine used in the experiments

Item/parameter	Details
Brand	MAN B&W
Model	6S35ME-B9
Engine type	6-cylinder, water-cooled, direct injection, crosshead type
Combustion order	1-5-3-4-2-6
Bore & stroke	350 × 1550 mm
Compression ratio	17:1
Displacement	894 L
Rated output power	3750 kW @ 142 rpm
Maximum indicated pressure	180 bar
Valve opening pressure	380 bar

Three different formulas of cylinder lubricating oil (recipes A, B, and C) were prepared and used. These three cylinder oils all contained the same percentages of additives to the base oil, which included compound ester, ester base, amide, phosphate ester, zinc compound additive, etc., but they had different SAE grades and total base numbers (TBNs). The SAE grade represents the viscosity of the oil. The detailed specifications of these lubricating oils are shown in Table 2. It is worth noting that although the viscosity of recipe B is as same as that of recipe C (both are SAE 40), they have different TBNs.

Tab. 2. Specifications of the lubricating oils used for testing

Lubricating oil	SAE grade	TBN
Recipe A	SAE100	TBN 70
Recipe B	SAE 40	TBN 40
Recipe C	SAE 40	TBN 25

Fig. 1 presents a schematic diagram of the experimental setup used for vibration testing, which shows the connections between the accelerometer, proximity sensor, power supply, data acquisition system, load control system, and a laptop computer with a measuring system. A dynamometer was employed to apply the load to the engine via a load control system. The accelerometer was mounted on the engine head, and a proximity sensor was coupled to the crankshaft to measure its angle. The signals from both transducers were transferred to a data acquisition system (INV3062-C2(L)), and the output data cable was connected to the data acquisition system and a laptop computer to transfer the data. Finally, the data were analysed by a measuring system in the laptop computer. The electricity for the data acquisition system was provided by a power supply.

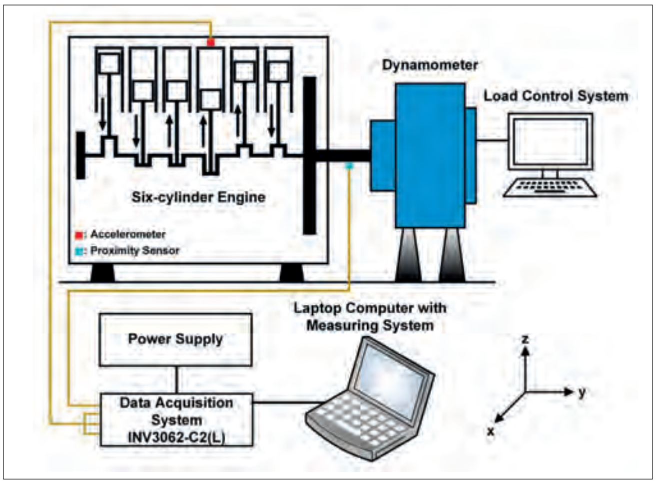

Fig. 1. Schematic diagram of the experimental setup.

The vibration signals were measured with a tri-axial vibration accelerometer (made by Coinv, China). Detailed specifications of the transducers are shown in Table 3. As can be seen from Fig. 1, the accelerometer was mounted on the engine cylinder cover, and the vibrations in three directions (x, y, z) were all acquired by the accelerometer simultaneously. The vibration signals were measured under the same engine load condition for each of the three cylinder lubricating oils. The angle of the engine crankshaft was recorded by the proximity sensor during the vibration measurements. The coordinate system used for both the accelerometer and the engine is shown to the lower right of Fig. 1.

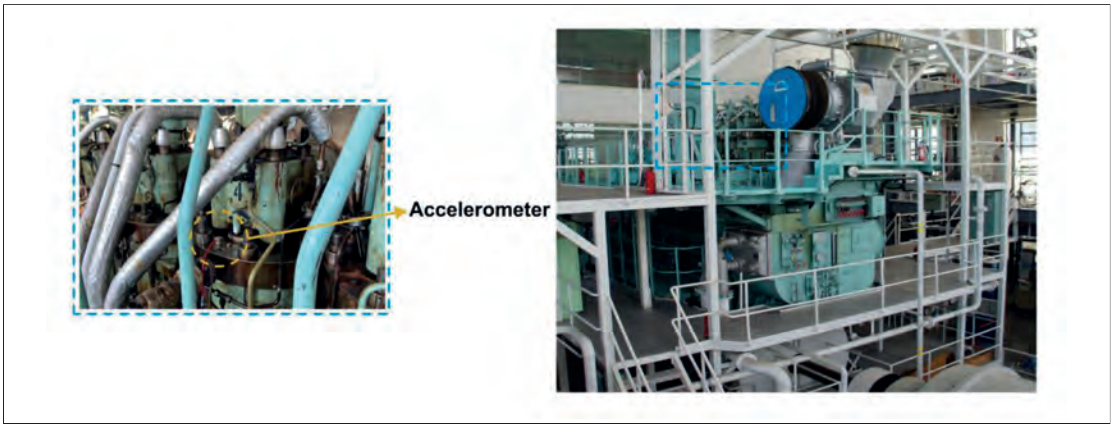

Fig. 2. Installation layout of the experimental equipment.

Tab. 3. Accelerometer specifications

Item/parameter	Details
Type	INV9832-50
Sensitivity	100 mV/g
Measuring range	0.4–12,000 Hz
Weight	12 g
Size	19×19×19 mm³
Temperature	–50 to 120 °C

The locations at which the vibration sensors were installed are shown in Fig. 2.

In order to approximate the engine operating conditions for the navigation of a real ship, the experiments included three different engine loads (25%, 40%, and 50%). Each sampling was performed after the engine speed had stabilised over 6 h. The data acquisition period was approximately 30 s, and the sampling frequency was 5 kHz for each record; these values of the sampling time and frequency allowed sufficient engine operating cycles to be recorded. The other parameters of the engine, such as its speed, output power, and torque, are shown in Table 4.

Tab. 4. Additional engine parameters

Engine load	Engine speed	Output power	Torque
25%	98 rpm	812.5 kW	91.64 kN·m
40%	105 rpm	1300 kW	116.13 kN·m
50%	113 rpm	1625 kW	136.40 kN·m

ANALYSIS METHODS

In order to compare the differences between the vibration signals in the time domain, the values of the RMS, kurtosis, mean, skewness, standard deviation, and squared deviation of the signals were considered.

For the frequency and time-frequency domain analyses, the FFT and STFT were used. These analyses were all performed using MATLAB (2019 b) and Origin software.

RMS of acceleration signal

The RMS represents the strength of the signal, and is also an expression of the average energy of the signal. The RMS along each axis for all experiments was calculated using Eq. (1) [9]:

$$x_{RMS} = \sqrt{\frac{1}{N}\sum_{i=1}^{N} x_i^2} \tag{1}$$

where x_{RMS} (m/s²) is the value of the RMS for the calculated signal.

To compare the total vibration for each cylinder, the values of RMS_{total} were calculated for three axes (x, y, and z) using Eq. (2) [15]:

$$RMS_{Total} = \sqrt{RMS_x^2 + RMS_y^2 + RMS_z^2} \tag{2}$$

where RMS_{Total} (m/s²) is the total vibration acceleration, and RMS_x, RMS_y and RMS_z are the RMS values for the accelerations along the x, y, and z axes, respectively.

Kurtosis of acceleration signal

The kurtosis is a parameter used to describe the sharpness of a signal distribution. In general, the sharper the signal centroid, the higher the kurtosis. The magnitude of its value can be regarded as the degree to which the signal is abnormal. To analyse the kurtosis, its value was calculated using Eq. (3) [9]:

$$x_{Kurtosis} = \frac{\sum_{i=1}^{N}(x_i - \bar{x})^4}{(N-1)\sigma^4} \tag{3}$$

To compare the total vibration in each cylinder based on the kurtosis, $Kurtosis_{total}$ was derived from the values for the x, y and z axes using Eq. (4) [15]:

$$Kurtosis_{Total} = \sqrt{Kurt_x^2 + Kurt_y^2 + Kurt_z^2} \tag{4}$$

where $Kurtosis_{Total}$ is the total vibration acceleration, and $Kurt_x$, $Kurt_y$ and $Kurt_z$ are the values of the kurtosis for accelerations along the x, y, and z axes, respectively.

Mean of acceleration signals

The mean is the sum of all the data in a set divided by the total number of data points. It is used to reflect the general overall level of data, and can be calculated using Eq. (5) [9]:

$$\bar{x} = \frac{1}{N}\sum_{i=1}^{N} x_i \tag{5}$$

Skewness of acceleration signals

The skewed direction and degree of the signals can be described by the skewness parameter. The skewness value determines whether the signal has a positive, negative, or zero skew (normal distribution), and is calculated by Eq. (6) [9]:

$$x_{Skewness} = \frac{\sum_{i=1}^{N}(x_i - \bar{x})^3}{(N-1)\sigma^3} \tag{6}$$

Standard deviation of acceleration signals

The standard deviation of the arithmetic square root of the squared deviation, which indicates the degree of dispersion between samples of vibration data, is defined by Eq. (7) [10]:

$$\sigma = \sqrt{\frac{\sum_{i=1}^{N}(x_i - \bar{x})^2}{N}} \tag{7}$$

Squared deviation of acceleration signals

The squared deviation of signals represents the degree of fluctuation of the signal around the mean; it can also be understood as the degree of vibration signal shock that exists. It is calculated using Eq. (8):

$$\delta = \frac{1}{N}\sum_{i=1}^{N}(x_i - \bar{x})^2 \tag{8}$$

Fast Fourier transform

The feature parameters mentioned above are quantitative assessments of the time domain of signals, whereas an analysis of the frequency domain of the signal is also required. The FFT can be used to convert a signal from the time domain to the frequency domain, so that the frequency-domain content of the signal can be obtained. The FFT is defined as shown in Eq. (9) [15]:

$$X(k) = \sum_{j=1}^{n} X(j)\, W_n^{(j-1)(k-1)} \tag{9}$$

where n is the length of signal X, and $W_n = e^{(-2\pi i)/n}$.

Short-time Fourier transform

In the STFT, a signal is split into multiple segments using a window function (in our analysis, the Hamming window function was used). The FFT is then applied to calculate each segment of the signal, and the spectrograms obtained from the FFT are arranged along the time axis, to obtain the time-frequency diagram. Hence, one of the advantages of the STFT over the FFT is that the time and frequency information can both be retained simultaneously, as the time information is lost when the FFT is used. Another advantage is that the STFT can be applied to non-stationary signals, which is not possible for the FFT. The formula for the STFT is given in Eq. (10) [17]:

$$STIF(\tau, f) = \int_{-\infty}^{+\infty} x(t)h(t-\tau)e^{-j2\pi ft} \tag{10}$$

where h is a window function. f and τ denote the frequency and time variables, respectively.

However, the STFT also has certain limitations, as the size of the window cannot change with frequency. Thus, the time and frequency resolution cannot be optimised at the same time in the STFT. The shorter the window, the more obvious the time-domain features become, and the frequency-domain features become more insignificant; conversely, the longer the window, the clearer the frequency-domain features and the more indistinct the time features.

RESULTS AND DISCUSSION

The objectives of this study were to compare the effects of three different lubricating oils on a two-stroke low-speed marine diesel engine, and to explore the vibration of the engine under low to medium load conditions. The results of the experimental study are therefore presented in four sections relating to the time domain, the frequency domain, a time-frequency domain analysis of the vibration signal, and an elemental spectra analysis.

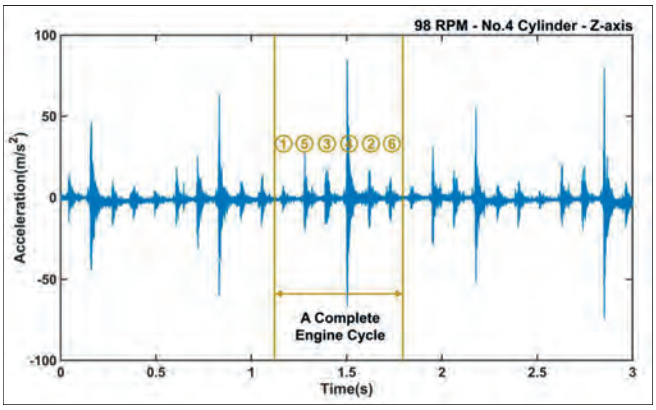

Fig. 3. A complete engine cycle in the time domain

TIME DOMAIN ANALYSIS OF VIBRATION SIGNALS

The lubricating oil not only provides lubrication and reduces friction between the cylinder and piston ring, but also participates in the combustion process. The vibration of an IC engine mainly arises from the gas force generated by the combustion in the cylinders, and a prior study [19] was conducted to explore the in-cylinder combustion process of a low-speed engine using the CFD method. The usage of different lubricating oils is also a crucial factor affecting the vibration in the engine. To investigate the detailed information for the time domain, we consider the z 3 s segment of the signal in Fig. 3, where a complete engine cycle is marked by red lines. This signal represents the conditions with lubricating oil recipe B, at an engine speed of 98 rpm under a load of 25%, along the z-axis. As shown in the figure, the firing order of the cylinders is 1-5-3-4-2-6. The acceleration of the vibration signal in cylinder 4 has the maximum value, while that of cylinder 1 shows the minimum. The reason for this is that the accelerometer was mounted on the head of cylinder 4, whereas cylinder 1 was farthest from the accelerometer. The acceleration values for the other cylinders decrease with increasing distance from cylinder 4. The recording period for the vibration signal was 30.1056 s, containing 150,528 samples. Hence, for an engine speed of 98 rpm, it can be calculated that the duration of a complete cycle under the 25% load condition is approximately 0.6122 s, containing 3,061 samples. Similarly, from the speeds in Table 4, we can calculate the time for a complete cycle under the 40% load condition as 0.5714 s, and that under the 50% load condition as 0.5310 s.

Before carrying out a frequency domain signal analysis, we calculated the time domain feature parameters (RMS, RMS_{Total}, kurtosis, $Kurtosis_{Total}$, mean, skewness, standard deviation, and squared deviation) for the vibration signals for the three recipes of lubricating oil for 15 complete engine cycles at loads of 25%, 40%, and 50%. Figs. 4 and 5 display scattergrams of the calculated results, showing 15 data points for each recipe under each load condition.

Firstly, the value of the RMS for each axis was calculated using Eq. (1) and the calculation results for the z-axis are shown in Fig. 4a. It can be clearly seen that the RMS values for recipe B are low for all three load conditions, and the data points for this recipe are relatively concentrated. This indicates that the marine diesel engine experiences low vibration along the z-axis under low to medium load when lubricated with lubricating oil based on recipe B. It also suggests that the medium-level TBN of cylinder oil is better matched to its low-sulphur property and gives better engine performance. Recipe A also gave low RMS values under the 25% and 40% load conditions, in a similar way to recipe B. However, under the 50% load condition, there was an increase in some of the RMS values compared to the previous low load conditions. For recipe C, the RMS values show fluctuations under each of the three loads, meaning that TBN values that are too high or too low are not conducive to stable engine vibration.

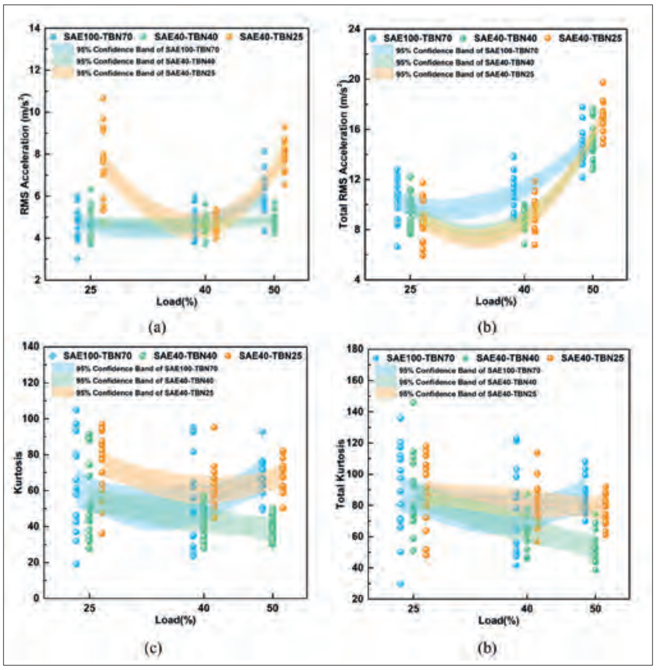

Fig. 4. Plots of feature parameter values for three engine loads for three recipes of lubricating oil: (a) RMS; (b) ; (c) kurtosis; (d) .

The RMS values for each recipe of lubricating oil are low under the 40% load condition. The reason for this is related to the characteristics of this diesel engine, as different lubricating oils have little effect on the intensity of engine vibrations under a 40% load. To enable a comparison of the total vibration of the diesel engine, the RMS_{Total} of the vibration signal was calculated for the *x*, *y*, and *z* vibrations using Eq. (2). There are clear similarities in Fig. 4(b) between the data for the RMS and RMS_{Total} for recipe *B* under the 25% and 40% load conditions. However, under a load of 50%, an increase in RMS_{Total} is observed for recipes *A*, *B* and *C* compared to the RMS. This suggests that the vibrations along the other two axes are increased under the 50% load condition due to the centrifugal inertia force.

Figs. 4(c) and 4(d) show a high degree of similarity between the data point distributions of the kurtosis and $Kurtosis_{Total}$. Under a 25% load, the data points are scattered, whereas when the load is increased, the data points become more concentrated. This indicates that the vibration signal for this marine diesel engine is comparatively sharp under low load conditions, but shows improvement as the load increases. We can also see that the data points for recipe *B* are concentrated at lower values compared to the other two recipes of lubricating oil. The results for the kurtosis showed a trend that was consistent with the results for the RMS. Thus, recipe *B* for the lubricating oil gives better vibration performance for this diesel engine.

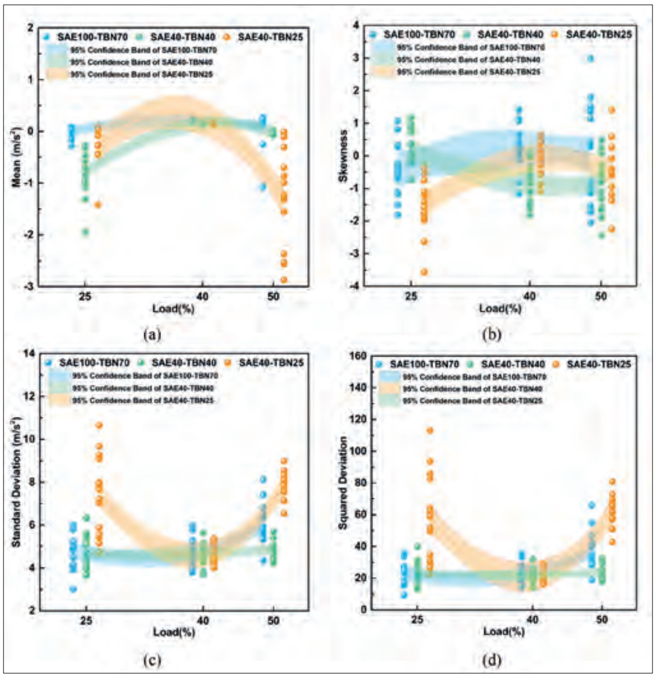

Fig. 5. Plots of feature parameter values for three engine loads for three recipes of lubricating oil: (a) mean; (b) skewness; (c) standard deviation; (d) squared deviation.

Fig. 5 shows the values of the mean, skewness, standard deviation, and squared deviation. For each of the three loads, the mean values for recipe *A* are almost all near zero, while the mean values for recipe *B* remain near zero only for the 40% and 50% load conditions. It is not hard to observe from Fig. 5(a) that the mean values of all three lubricating oils are relatively steady and remain near zero under the 40% load condition. Fig. 5(b) shows that under the 40% and 50% load conditions, recipe *B* has low values for the RMS, kurtosis, and mean, whereas its skewness values are almost all negative. In contrast, the data points for recipe *A* are uniformly distributed on both sides of zero, and do not vary greatly between the load conditions. Furthermore, it is clear that the data points are most concentrated under the 40% load condition for all three recipes of lubricating oil. In Figs. 5(c) and 5(d), the standard deviation data are fairly close to those of the RMS, and both have almost identical scatter distributions. Meanwhile, the scattergram distribution of the squared deviation is also in accordance with both of the above, despite the different values.

FREQUENCY AND TIME-FREQUENCY DOMAIN ANALYSES OF VIBRATION SIGNALS

In order to further analyse the effects of each oil recipe on the vibration of this two-stroke low-speed diesel engine, the vibration signals along the z-axis under three load conditions were transformed using FFT. Ten consecutive working cycles for each treatment condition were considered for the FFT analysis.

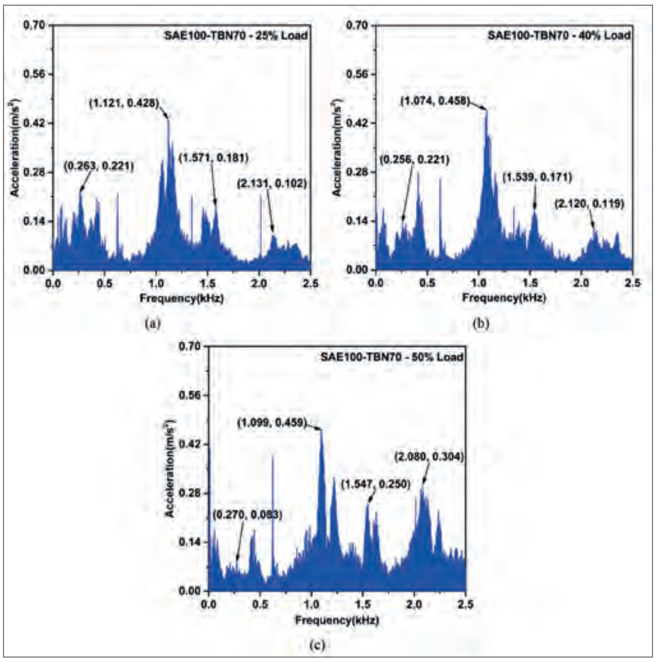

Fig. 6. FFT spectra for recipe A under three typical engine loads: (a) 25%, (b) 40%, (c) 50%.

Figs. 6–8 show FFT spectra for vibration signals under three different engine loads for the three recipes of lubricating oil. It can be observed that the vibration signatures of the diesel engine change when different cylinder lubricating oils are used, from Fig. 6 to Fig. 8. The changed frequency domain of 0–2.5 kHz can be divided into four subdomains: 0.12–0.38 kHz, 0.75–1.3 kHz, 1.3–1.75 kHz, and 1.9–2.5 kHz. In the range 0.12–0.38 kHz, which is the low-frequency region of engine vibration, the accelerations all decrease to varying extents for all three lubricating oils as the load increases, and especially their maximum values. Due to its high viscosity and alkaline nature, the decrease in the maximum value for recipe *A* at a higher load is greater than that for recipes *B* and C, with a decline of 60.2%. The maximum values for recipes *B* and *C* are fairly similar, as they have the same SAE 40 grade. It is known that the low-frequency components of vibration are the main contributors to noise and discomfort for human beings around an engine [18]. It can be seen from the results in Figs. 6–8 that the low-frequency vibration range of this engine shows a decreasing trend as the load increases, which is beneficial to the life of the engine and the comfort of the crew and passengers on board.

The range 0.75–1.3 kHz contains the dominant frequencies of the engine, which are induced by the shock generated by the combustion pressure. Our results show that there are no significant changes in the maximum value in this subdomain for recipes *A* and *C*. For example, the maximum values of recipe *C* in this range are close to 0.330 m/s^2. However, the maximum values of recipe B show a certain degree of reduction, with a decline of 27.7%. This finding indicates that although lowering the alkalinity to a moderate level facilitates lightening the intensity of the engine combustion, a TBN level that is too low does not significantly improve the vibration from engine combustion.

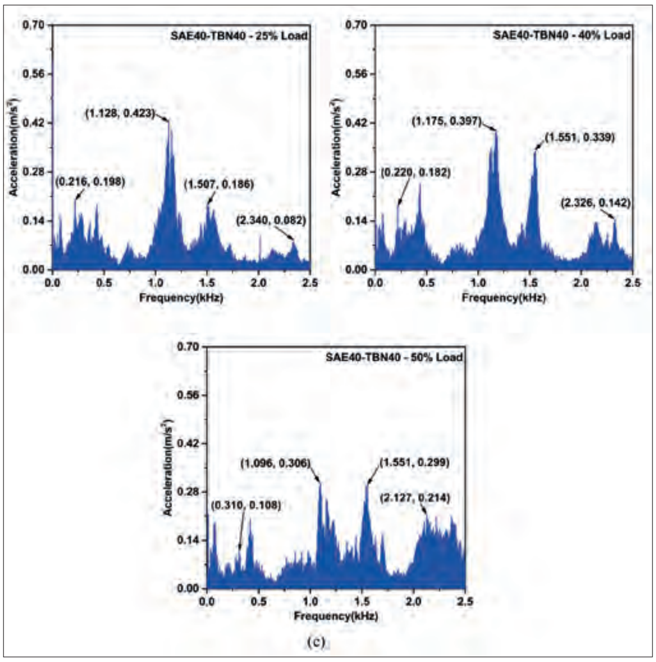

Fig. 7. FFT spectra for recipe B under three typical engine loads: (a) 25%, (b) 40%, (c) 50%.

In the range 1.3–1.75 kHz, all three recipes for the lubricating oil show different trends with increasing load. However, under the 50% load condition, their maximum values are all at a relatively low level of below 0.34 m/s^2. The changes in the maximum values for recipes A and B are similar in the high-frequency subdomain (1.9–2.5 kHz), as both increase with rising loads. The increase in the maximum value for recipe *A* is 198%, and for recipe *B* it is 161%. It is notable that the maximum value under 25% load is 0.426 m/s^2 for recipe *C*, which is higher than for its principal frequency domain. However, under the 40% load condition, the maximum value is only 0.1 m/s^2, while the value is 0.352 m/s^2 under the 50% load condition. We conclude that under low to medium loads, using lubricating oil with recipe *C* causes high-frequency vibration fluctuations in the engine. This also provides some evidence that a TBN level that is too low may affect the detergency between the piston and liner.

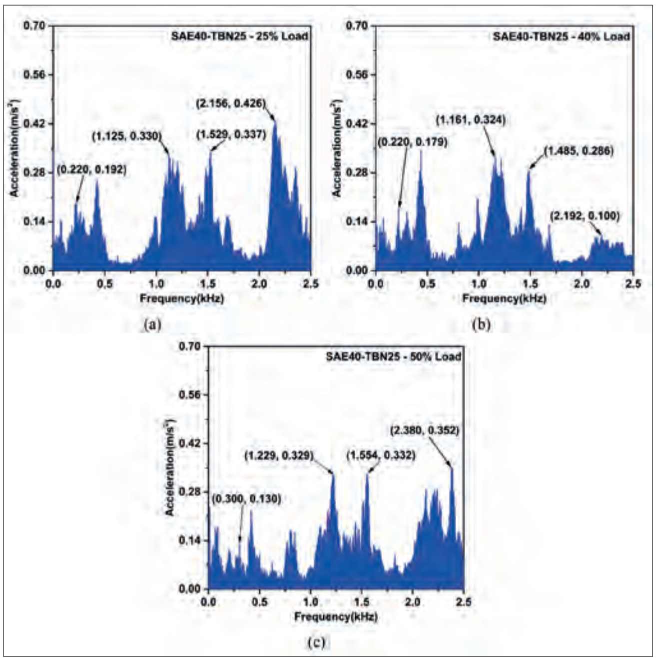

Fig. 8. FFT spectra for recipe C under three typical engine loads: (a) 25%, (b) 40%, (c) 50%.

Furthermore, from the time-domain parameters described above, it can be seen that the vibration data for this engine with these three lubricating oils are relatively centralised under a 40% load, which implies good stability of the engine. In order to further explore the effects of the three oil recipes on the engine vibration characteristics, the STFT method was applied to analyse only the vibration signals under the 40% load condition. Unlike the FFT method, the STFT method involves time information, meaning that the differences between various engine cycles can be observed in the STFT spectra. The signals analysed for each of the above segments all had a length of 5.714 s, and contained 10 consecutive engine cycles.

In Fig. 9, each STFT diagram contains 10 obvious spectrum peaks, representing the 10 engine cycles. In each cycle, several lower peaks can be seen, indicating the vibration of the remaining cylinders; the amplitude for the cylinder on which the tri-axis vibration sensor was mounted on is the largest, and the amplitudes for the other cylinders decrease towards both sides of the engine. The STFT method can be used to analyse engine vibration caused by combustion and friction. This approach is an excellent visualisation tool for monitoring the condition of diesel engines, and can easily provide information about engine vibration and combustion. Since combustion occurs inside the cylinder, it cannot be observed readily. Hence, the state of combustion which is non-visualized can be observed using the STFT method.

As can be seen from Fig. 9a, at 40% engine load, the maximum vibration amplitude of the low-speed marine engine is around 1.5 kHz for all three oils, where the vibration is mainly caused by combustion. Recipe *A* shows three consecutive periods of unusually high amplitude in the frequency band 1.3–1.75 kHz; there are also two continuous engine cycles where the amplitude is extremely low. In Fig. 9(c), the peak of each cycle in the 1.9–2.5 kHz range for recipe *C* is comparable to the values for recipes *A* and *B*, but the vibration of the other cylinders is much lower than for recipes *A* and *B*. What can be clearly seen in the 10 cycles for recipe *B* is better stability in all four subdomains. This further corroborates the findings for the time domain, and indicates that recipe *B* has the best vibration characteristics of the three lubricating oils under 40% load conditions.

LINER WEAR ANALYSIS

The carbon deposits on the surface of each piston were compared before and after 300 h of steady-state engine operation. These deposits covered the surface of each piston with a similar thickness, and were mainly composed of the combustion products from the HFO and cylinder lubricating oils as well as piston-cylinder frictional wear particles, of which the major elements were C, O, S, Fe, and Al.

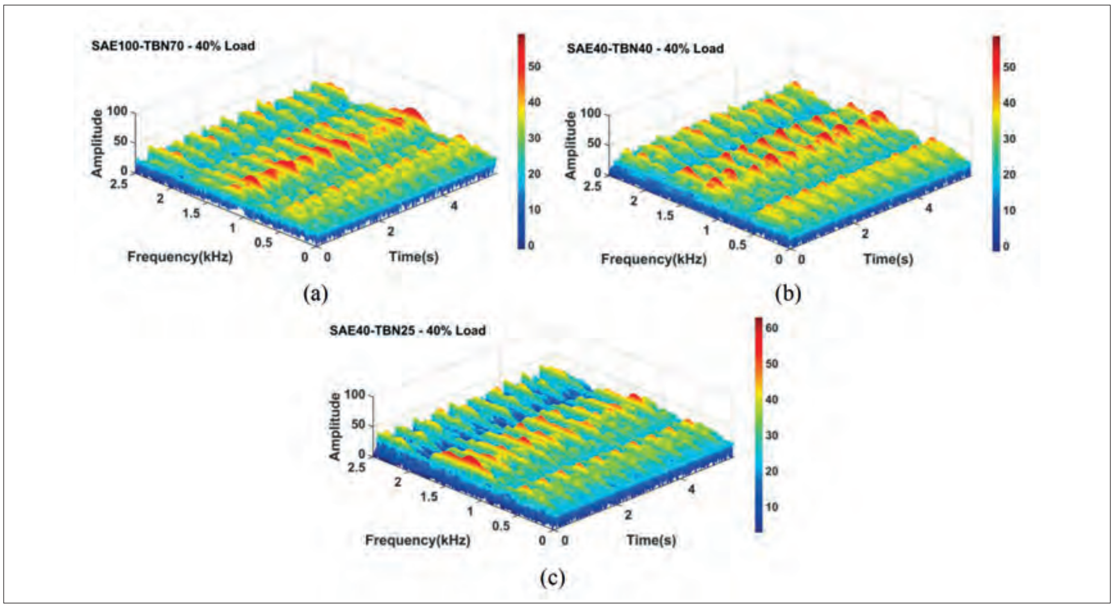

Fig. 9. STFT diagrams for lubricating oils under 40% load: (a) recipe A; (b) recipe B; (c) recipe C.

In order to study the main components of the frictional wear particles, the elements in the lubricating oil were measured through an oil analysis. Several typical elements were selected to compare their contents for evaluation. The cylinder of the marine diesel engine was mainly made of iron-carbon alloy, meaning that Fe was the main metallic element. Al and Si were the main components of the piston, while Mn, Cu, and Ni were also contained in the piston material. Since the three lubricating oils have the same additive ratio but different formulas, they varied in terms of the content of each metallic material before service. We therefore calculated the difference value (D-value) for each major element before and after service. From Fig. 10, it can be seen that the D-values of Fe are 75.2×10^{-6} for recipe B, 80×10^{-6} for recipe *A*, and 88.2×10^{-6} for recipe *C*, meaning that the D-value for recipe *B* is the lowest. For the other five elements, the D-values are also the lowest for recipe *B*, followed by recipe *A* and then recipe *C*. This indicates that recipe *B* has the best anti-wear performance of the three types of oil.

Recipe *C* has the same SAE grade as recipe *B* but a lower TBN value, meaning that its alkali level is too low to completely neutralise the acids of combustion; the un-neutralised acid will attack the piston liners, resulting in corrosive wear and more wear debris during the operation of the pistons. Thus, a cylinder lubricating oil with medium alkali values provides better anti-wear properties than one with a low alkali value. Recipe *A* has a somewhat higher D-value than recipe *B*. One reason for this is that its excess alkali is in the form of inorganic calcium carbonate that cannot be burned, causing hard deposits and three-body abrasive wear between the piston and cylinder. The high viscosity of recipe *A* will also increase the friction loss of the engine, and may increase the wear of the piston-cylinder assembly to a certain extent. In brief, a cylinder lubricating oil with a medium level of viscosity and a medium alkali value has the best anti-wear properties.

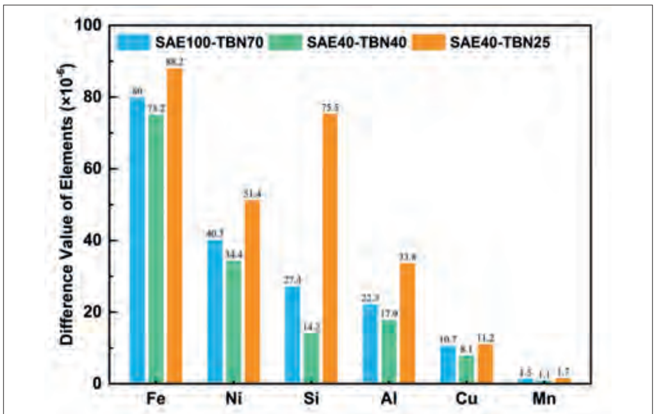

Fig. 10. Difference values for each major element before and after service.

CONCLUSION

In this experimental study, the vibration signals for three different cylinder lubricating oils were measured using a six-cylinder low-speed marine diesel engine (MAN B&W 6S35ME-B9). The main objectives were to analyse the effects of the lubricating oils on engine vibration, in order to select the optimum lubricating oil to reduce wear, and to investigate the vibration characteristics of the low-speed engine under typical load conditions. A triaxial vibration transducer was placed at planned locations. The vibration signals obtained in the experiments were analysed using various time domain characteristics, FFT and STFT. The metallic elements in the cylinder lubricating oils were also measured via an oil analysis before and after operation. The conclusions from the experiment can be summarised as follows.

The vibration characteristics of the two-stroke, low-speed marine diesel engine operating on heavy fuel oil were first investigated, and it was found that the characteristic time-domain parameters of the vibration signal were relatively stable at low engine loads, due to the reduced friction frequency. The alkalinity and viscosity characteristics of the cylinder lubricant had the least effect on the engine vibration under a 40% load. The influence of the cylinder lubricant on engine vibration gradually increased as the load increased.

Under typical ship propulsion loads, recipe *B* was found to have the most concentrated and stable data distributions for RMS, kurtosis, mean, skewness, standard deviation, and squared deviation of the three lubricating oils. This indicates that the medium level alkaline value and medium level viscosity of the cylinder oil are more suitable for low-sulphur heavy oil and cause less wear of cylinder liners and less vibration of the engine.

Real-time FFT and STFT methods were successfully used for non-invasive monitoring of the cylinder liner wear of a marine engine. The sub-ranges of the FFT graphs also show that moderately alkaline cylinder oils improve engine smoothness, while excessively low alkaline levels can worsen vibration in the engine combustion chamber. The STFT method was used as a new way to visually analyse the cylinder under its operating conditions in terms of time and frequency, and the results agreed well with those of a time domain analysis and offline elemental analysis.

This study has presented the results of a vibration data analysis of a two-stroke low-speed marine diesel engine in healthy condition under low to medium operating conditions, which can serve as a data reference for future fault monitoring. Fault diagnosis of a two-stroke low-speed marine diesel engine will be explored in our future work.

AUTHOR CONTRIBUTIONS

Gang Wu: Conceptualization, Methodology, Investigation, Writing - original draft & editing, Funding acquisition. Guodong Jiang: Investigation, Experimentation, Data curation, Writing - original draft & editing. Changsheng Chen: Conceptualization, Methodology. Guohe Jiang: Writing - review. Xigang Pu: Experimentation. Biwen Chen: Writing - review.

ACKNOWLEDGEMENT

The authors disclose receipt of the following financial support for the research, authorship, or publication of this article: This work was supported by the Science & Technology Commission of Shanghai Municipality and Shanghai Engineering Research Center of Ship Intelligent Maintenance and Energy Efficiency under Grant 20DZ2252300.

CONFLICTS OF INTEREST

The author(s) declare no potential conflicts of interest with respect to the research, authorship, and/or publication of this article.

REFERENCES

1. A. M. K. P. Taylor, „Science review of internal combustion engines," *Energ. Policy*, vol. 36, no. 12, pp. 4657-4667, 2008, https://doi.org/10.1016/j.enpol.2008.09.001.

2. M. Yang et al., „Matching method of electric turbo compound for two-stroke low-speed marine diesel engine," *Appl. Therm. Eng.*, vol. 158, 2019, https://doi.org/10.1016/j.applthermaleng.2019.113752.

3. J. Kałużny et al., „Reducing friction and engine vibrations with trace amounts of carbon nanotubes in the lubricating oil," *Tribol. Int.*, vol. 151, 2020, https://doi.org/10.1016/j.triboint.2020.106484.

4. W. Li, Y. Guo, X. Lu, X. Ma, T. He, and D. Zou, „Tribological effect of piston ring pack on the crankshaft torsional vibration of diesel engine," *Int. J. Engine Res.*, vol. 16, no. 7, pp. 908-921, 2014, https://doi.org/10.1177/1468087414556134.

5. Ö. Böyükdipi, G. Tüccar, and H. S. Soyhan, „Experimental investigation and artificial neural networks (ANNs) based prediction of engine vibration of a diesel engine fueled with sunflower biodiesel – NH3 mixtures," *Fuel*, vol. 304, 2021, https://doi.org/10.1016/j.fuel.2021.121462.

6. K. Çelebi, E. Uludamar, and M. Özcanlı, „Evaluation of fuel consumption and vibration characteristic of a compression ignition engine fuelled with high viscosity biodiesel and hydrogen addition," *Int. J. Hydrogen Energ.*, vol. 42, no. 36, pp. 23379-23388, 2017, https://doi.org/10.1016/j.ijhydene.2017.02.066.

7. K. Çelebi, E. Uludamar, E. Tosun, Ş. Yıldızhan, K. Aydın, and M. Özcanlı, „Experimental and artificial neural network approach of noise and vibration characteristic of an unmodified diesel engine fuelled with conventional diesel, and biodiesel blends with natural gas addition," *Fuel*, vol. 197, pp. 159-173, 2017, https://doi.org/10.1016/j.fuel.2017.01.113.

8. G. Chiatti, O. Chiavola, and F. Palmieri, „Vibration and acoustic characteristics of a city-car engine fueled with biodiesel blends," *Appl. Energ.*, vol. 185, pp. 664-670, 2017, https://doi.org/10.1016/j.apenergy.2016.10.119.

9. A. Moosavian, G. Najafi, B. Ghobadian, M. Mirsalim, S. M. Jafari, and P. Sharghi, „Piston scuffing fault and its identification in an IC engine by vibration analysis," *Appl. Acoust.*, vol. 102, pp. 40-48, 2016, https://doi.org/10.1016/j.apacoust.2015.09.002.

10. S. M. Ramteke, H. Chelladurai, and M. Amarnath, „Diagnosis and classification of diesel engine components faults using time–frequency and machine learning approach," *J. Vib. Eng. Technol.*, vol. 10, no. 1, pp. 175-192, 2021, https://doi.org/10.1007/s42417-021-00370-2.

11. E. G. Giakoumis, „Lubricating oil effects on the transient performance of a turbocharged diesel engine," *Energy*, vol. 35, no. 2, pp. 864-873, 2010, https://doi.org/10.1016/j.energy.2009.08.009.

12. A. Taghizadeh-Alisaraei, B. Ghobadian, T. Tavakoli-Hashjin, and S. S. Mohtasebi, „Vibration analysis of a diesel engine using biodiesel and petrodiesel fuel blends," *Fuel*, vol. 102, pp. 414-422, 2012, https://doi.org/10.1016/j.fuel.2012.06.109.

13. K. Nantha Gopal and R. Thundil Karuppa Raj, „Effect of pongamia oil methyl ester–diesel blend on lubricating oil degradation of di compression ignition engine," Fuel, vol. 165, pp. 105-114, 2016, https://doi.org/10.1016/j.fuel.2015.10.031.

14. A. Çalık, „Determination of vibration characteristics of a compression ignition engine operated by hydrogen enriched diesel and biodiesel fuels," *Fuel*, vol. 230, pp. 355-358, 2018, https://doi.org/10.1016/j.fuel.2018.05.053.

15. A. Taghizadeh-Alisaraei and A. Rezaei-Asl, „The effect of added ethanol to diesel fuel on performance, vibration, combustion and knocking of a CI engine," *Fuel*, vol. 185, pp. 718-733, 2016, https://doi.org/10.1016/j.fuel.2016.08.041.

16. A. Albarbar, F. Gu, A. Ball, and A. Starr, „Internal combustion engine lubricating oil condition monitoring based on vibro-acoustic measurements," *Insight*, vol. 49, no. 12, pp. 715-718, 2007, https://doi.org/10.1784/insi.2007.49.12.715.

17. A. Moosavian, G. Najafi, B. Ghobadian, and M. Mirsalim, „The effect of piston scratching fault on the vibration behavior of an IC engine," *Appl. Acoust.*, vol. 126, pp. 91-100, 2017, https://doi.org/10.1016/j.apacoust.2017.05.017.

18. F. K. Omar, M. Y. E. Selim, and S. A. Emam, „Time and frequency analyses of dual-fuel engine block vibration," *Fuel*, vol. 203, pp. 884-893, 2017, https://doi.org/10.1016/j.fuel.2017.05.034.

19. X. Zhou, T. Li, N. Wang, X. Wang, R. Chen, and S. Li, „Pilot diesel-ignited ammonia dual fuel low-speed marine engines: A comparative analysis of ammonia premixed and high-pressure spray combustion modes with CFD simulation," *Renew. Sust. Energ. Rev.*, vol. 173, 2023, https://doi.org/10.1016/j.rser.2022.113108.

POLISH MARITIME RESEARCH 4 (120) 2023 Vol. 30; pp. 102-109
10.2478/pomr-2023-0063

EXPLORATION OF A MODEL THERMOACOUSTIC TURBOGENERATOR WITH A BIDIRECTIONAL TURBINE

Volodymyr Korobko [1]
Serhiy Serbin [1 *]
Huu Cuong Le [2]
[1] Admiral Makarov National University of Shipbuilding, Mykolaiv, Ukraine
[2] Institute of Maritime, Ho Chi Minh City University of Transport, Viet Nam

* Corresponding author: *serbin1958@gmail.com (Serhiy Serbin)*

ABSTRACT

The utilisation of the thermal emissions of modern ship power plants requires the development and implementation of essentially new methods of using low-temperature waste heat. Thermoacoustic technologies are able to effectively use low-temperature and cryogenic heat resources with a potential difference of 500–111 K. Thermoacoustic heat machines (TAHMs) are characterised by high reliability, simplicity and environmental safety. The wide implementation of thermoacoustic energy-saving systems is hampered by the low specific power and the difficulties of directly producing mechanical work. An efficient approach to converting acoustic energy into mechanical work entails the utilisation of axial pulse bidirectional turbines within thermoacoustic heat engines. These thermoacoustic turbogenerators represent comprehensive systems that consist of thermoacoustic primary movers with an electric generator actuated by an axial-pulse bidirectional turbine. The development of such a thermoacoustic turbogenerator requires several fundamental issues to be solved. For this purpose, a suitable experimental setup and a 3D computational fluid dynamics (CFD) model of a thermoacoustic engine (TAE) with bidirectional turbines were created. The research program involved conducting physical experiments and the CFD modelling of processes in a TAE resonator with an installed bidirectional turbine. The boundary and initial conditions for CFD calculations were based on empirical data. The adequacy of the developed numerical model was substantiated by the results of physical experiments. The CFD results showed that the most significant energy losses in bidirectional turbines are manifested in the output grid of the turbine.

Keywords: waste heat recovery; ship power plant; thermoacoustics; thermoacoustic engine; bidirectional turbine

INTRODUCTION

Maritime transport is an important component of the global economy, as it provides the bulk of freight traffic. Marine heat engines consume carbon-based recoverable fuel, producing significant amounts of heat emissions of various potentials that harm the environment. These emissions include fuel combustion products, such as CO_2, SO_n, NO_x, volatile organic compounds (VOCs), carbon particles, etc.

The International Maritime Organization (IMO), in accordance with the provisions of the United Nations Sustainable Development Goal (SDG) 13 [1]–[3], introduced requirements that direct the general trend in shipping towards a significant limitation of the volume and composition of emissions from ship power plants, including diesel and gas turbine units [4]–[8].

The task of the decarbonisation of marine energy has become vital; it aims to minimise the consumption of carbon fuels, which is a key factor in reducing greenhouse gas (GHG) emissions. The result of these measures was the introduction of efficient dual-fuel engines that use new types of fuel, including cryogenic fuels. These measures led to a significant decrease in the temperature of thermal emissions (Table 1).

Under such conditions, traditional ship thermal emission utilisation schemes, based on the classic water Rankine cycle (WRC), become ineffective. It is these circumstances that lead to the use of other energy-saving technologies, such as the organic Rankine cycle (ORC) system [9]]–[11] and thermo-chemical conversion [12].

A promising method for the utilisation of the low-temperature thermal emissions of ship power plants (SPPs) may be the use of thermoacoustic technologies [13], [14].

There are two types of thermoacoustic machines: thermoacoustic engines (TAEs) and thermoacoustic refrigerators (TARs), or heat pumps. Thermoacoustic engines (movers) implement a direct process – converting thermal energy from external sources into an acoustic form. A TAR performs the opposite process – it consumes acoustic energy and converts it into the heat with different potential.

Tab. 1. Temperatures of waste heat carriers of modern SPPs

Heat carrier/source	2S ICE	4C ICE	PEM FC
	Temperature, K		
Waste gases of ICE	490–530	500–690	–
Air charger	400–490	380–470	–
Cooling system liquid	355–360	360–370	(LT PEM) 333–363 (HT PEM) 450–493
LNG fuel	111	111	111
NH_3 fuel	240	240	240

In ship power systems, TAEs can utilise high-potential heat sources with temperatures ranging from 330–550 K or higher, such as emissions from internal combustion engines (ICEs) or electrochemical generators like solid oxide fuel cells (SOFCs) and polymer electrolyte membrane fuel cells (PEMFCs). On the other hand, low-potential thermal sources might be the ambient environment or cryogenic fluids such as liquefied hydrogen (LH_2), natural gas (LNG) or ammonia (NH_3), with temperatures from 4–240 K [15]. The widespread application of thermoacoustic systems in practice is hindered by the complexity of the efficient conversion of acoustic energy into mechanical work, a low specific power density and the lack of practical experience. Issues related to the development of low-temperature thermoacoustic systems were considered in [16].

In terms of renewable energy, we are familiar with wave power plants that utilise oscillating water columns (OWCs), which incorporate bidirectional turbines like the Wells turbine and impulse bidirectional turbines [17]–[19]. The application of bidirectional turbines in thermoacoustic heat recovery systems has also been addressed in previous studies [19]–[23].

Bidirectional turbines are the most efficient transducers for ship thermoacoustic waste heat recovery systems (WHRSs) when it comes to generating mechanical work and driving electric generators. They are capable of transforming the energy of acoustic oscillation into the rotational motion of the turbine rotor. Therefore, it can be considered that such thermoacoustic turbine generators (TATGs) are the most rational solution for low-temperature ship WHRSs.

Obviously, the use of bidirectional turbines in thermoacoustic devices is an appropriate solution. However, it should be noted that OWC units differ significantly from TAE units in terms of the design and parameters of the working environment, and therefore the direct use of existing approaches in the design of such turbines is problematic. The existing problem is a complex task and requires a set of additional studies.

FUNCTIONING CONDITIONS OF BIDIRECTIONAL TURBINES

It is known that OWC plants are open systems that operate at atmospheric pressure ($P_m = P_{amb}$). In these systems, the working medium, air, undergoes oscillatory motion. In the flowing part of the OWC, the amplitude of these oscillations' motion can reach several metres, while the frequency of oscillations does not exceed 0.2 to 1 Hz:

$$\zeta = \frac{u_s}{\rho a} = \frac{(0.05\text{–}0.1)P_m}{2\pi f\rho\sqrt{\chi RT}}, \tag{1}$$

where ρ is the density of the medium in kg/m^3; χ is the adiabatic index; T is the temperature in K; and R is the universal gas constant.

TAEs are closed systems in which noble gases are the working fluid, the internal pressure P_m can reach 0.3–3.0 MPa and the frequency of the acoustic wave is f = 50–150 Hz.

Accordingly, in thermoacoustic devices, the amplitude of the oscillatory motion of the acoustic wave ζ_{TAE} is much smaller than ζ_{OWC}(Fig. 1).

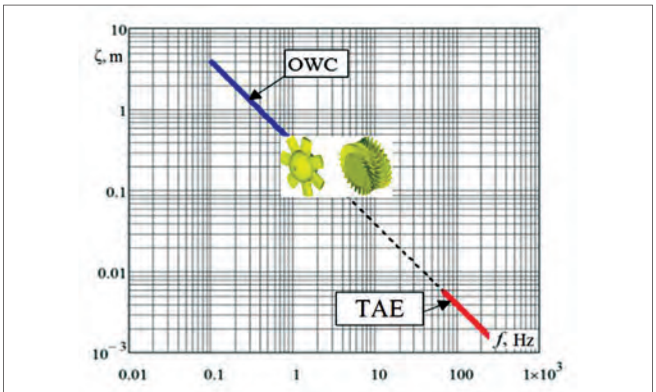

Fig. 1. Comparison of the amplitudes of the oscillatory motion of the medium in an OWC and a TAE

It is obvious that the hydrodynamic processes in the flow channels of OWC systems are significantly different from the processes in TAE resonators. In a thermoacoustic apparatus under high-frequency oscillations, the influence of inertial factors on the hydrodynamic parameters of the medium should increase significantly. In addition, there is a significant difference between the designs of the flow parts of these bidirectional turbines. In the case of an OWC, large-volume collectors are used. In thermoacoustic devices, the resonators have much

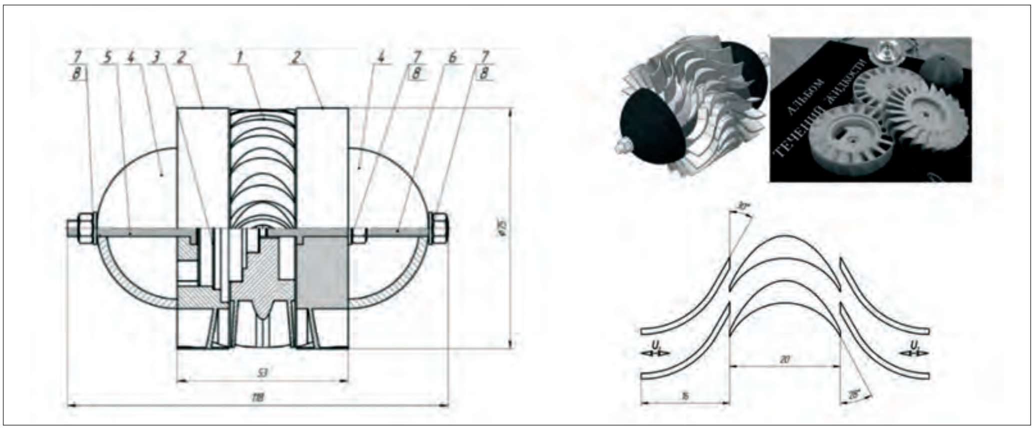

Fig. 2. Experimental turbine generator assembly: 1 – turbine rotor, 2 – stator, 3 – generator, 4 – fairing, 5 and 6 – turbine axes, 7 and 8 – fasteners

smaller dimensions. In this regard, it is possible to expect the formation of stable oscillating structures in the TATG resonator, which will introduce additional excitations and inhomogeneities at the input to the rectifier of the turbine. They will create a novel energy-consuming mechanism that should be confined on both sides of the bidirectional turbine. In view of these circumstances, it can be considered appropriate to conduct a complex of studies to obtain an in-depth understanding of these issues.

Purpose of research. Considering the disparities in the working processes between OWCs and TAEs, it is sensible to carry out research focused on understanding the peculiarities of hydrodynamic processes within the TATG resonator to identify the most rational design solutions. Research should involve both physical experiments and numerical calculations using computational fluid dynamics (CFD) procedures, which requires the creation of appropriate equipment and methods of research.

EXPERIMENTAL SETUP

The investigation was conducted utilising an experimental bidirectional turbine. This turbine was designed and manufactured in accordance with the guidelines outlined in [24]. A 3D model of an experimental bidirectional turbine was developed in the CAD software developed by SolidWorks. The turbine's components, including the rotor, guide grids and fairings, were produced using 3D printing techniques and plastic material, as depicted in Fig. 2. Detailed information about the dimensions of the elements of the experimental bidirectional turbine is provided in Table 2.

The rotor of the turbine was rigidly coupled to a three-phase brushless electric generator of the Sankyo F2JGL type. The output voltage from the generator was fed to a diode converter made of Schottky diodes, and a P517-M laboratory rheostat or a set of precision resistors was used as a load.

The rotation speed of the turbine was monitored by an SDS 1074CFL digital oscilloscope, which was connected to one of the windings of the generator.

Such a scheme made it possible to simultaneously control the speed of rotation of the turbine rotor, the root-mean-square (RMS) voltage of the generator V_{RMS} and the current in the electric grid. The characteristics of bidirectional turbines in a unidirectional flow were studied using the experimental installation, the scheme of which is shown in Fig. 3.

Tab. 2. Design parameters of bidirectional turbines

Element	Value
Internal diameter of TAE resonator, mm	46
Outer diameter of turbine stator, mm	76
Outer blade diameter of turbine, mm	75
Turbine rotor diameter, mm	50
Blade width of rotor, mm	20
Number of rotor blades	24
Width of stator blades, mm	16
Number of stator blades	18

Differential thermostabilised pressure sensors of MPXV NXP semiconductors were used to measure the pressure drop along the turbine and on the entrance lemniscate. The equipment of the experimental stands and the available microprocessor-based data acquisition system (DAS) provided multiple measurements of sensor readings in each of the modes, which reduced the random error.

The STM32F407VGT6 microcontroller, which has a 32-bit architecture and an operating frequency of 168 MHz, was used to measure and register signals from pressure sensors, current sensors, voltage sensors, etc.

The equipment of the test stands ensured multiple measurements of sensor readings in each of the modes, which reduced the random error.

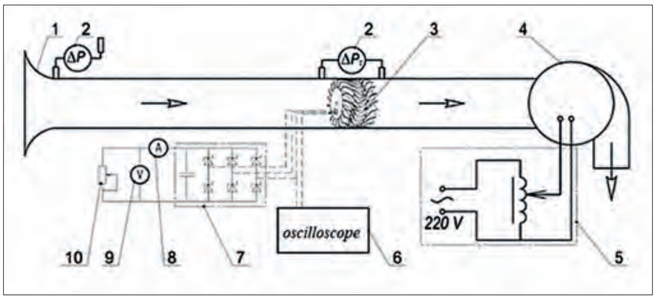

Fig. 3. Diagram of the experimental stand for the study of the hydraulic resistance of the bidirectional turbine: 1 – lemniscate; 2 – inclined differential pressure gauge; 3 – turbine; 4 – fan; 5 – LATR; 6 – DAS oscilloscope SDS 1074CFL; 7 – diode bridge; 8 – ammeter; 9 – voltmeter; 10 – resistors

The polling frequency of the pressure sensor controller by the STM32F407VGT6 controller was 10 kHz, and the bit rate was 32 bits.

A digital 4-channel oscilloscope, SDS 1074CFL, was used for the visual control of the operation of the TAE and the progression of the experiments, as a duplicating the measurement and registration of research information. Communication with the DAS and the oscilloscope was ensured using the USB interface. This microprocessor-based control and measurement system is discussed in more detail in [25].

An important task of the experimental research was to assess the operability of a model sample of a pulsed bidirectional turbine and its suitability for further experiments. All failings that were identified at the preparation stage were fixed.

Taking into account instrument errors and errors of approximation of expressions, the total measurement error does not exceed 2.5%. The error of determining the power of the generator, when using the existing DAS, does not exceed 2%.

EXPERIMENT RESULTS

At this stage of the experiments, the characteristics of the turbogenerator exclusively in the longitudinal flow at different air flows rates were studied. The results of the experiments, that is, the pressure drops of the bidirectional turbine, are shown in Fig. 4.

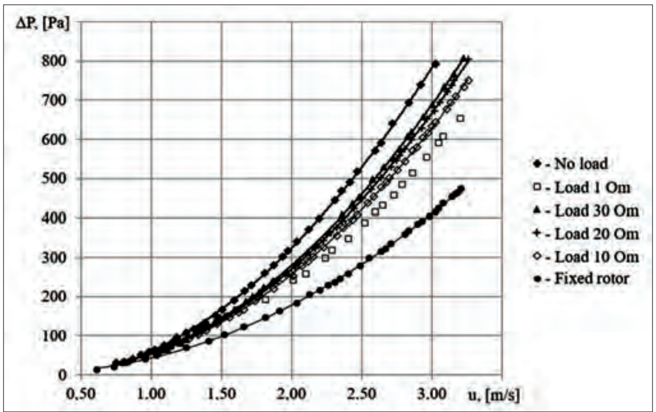

Fig. 4. Dependence of hydraulic resistance of bidirectional turbines on flow velocity under different loads

The load on the turbogenerator was changed using a set of precision resistors with different resistance values R_i. Data on the hydraulic resistance of a turbine with a fixed rotor were also obtained.

Research results have shown that a turbine with a fixed rotor has minimal flow resistance, which is quite natural. For a turbine with a free rotor, as the load decreases, the flow resistance increases. Furthermore, the data of these studies were used to verify the correctness of the results of the CFD modelling. The results of measuring the frequency of rotation of the turbine rotor depending on the speed of the oncoming flow are shown in Fig. 5. The main task of these experiments was to test the performance of the turbine in long-term operating modes and to assess the stability of external indicators.

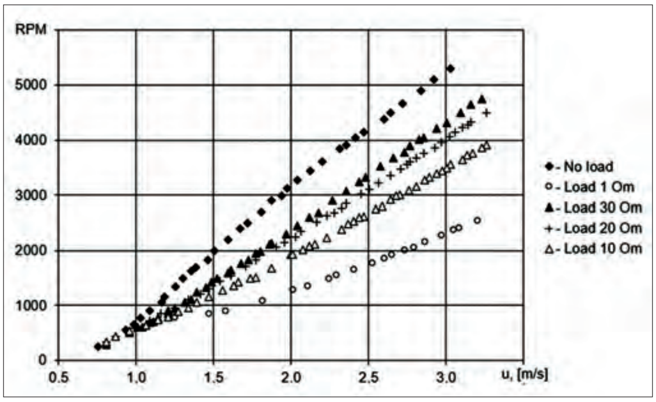

Fig. 5. Turbine rotor revolutions depending on the speed of the oncoming flow

It can be seen that the turbine rotation frequency also depends on the generator load. The maximum speed of rotation under the conditions of the experiment reached 5300 rpm. As can be expected, the maximum frequency of rotation of the turbine occurred when there was no load, in the idle regime. Additionally, during experimental studies, data were obtained that made it possible to determine its power depending on the speed of rotation. The results of these calculations are presented in Fig. 6.

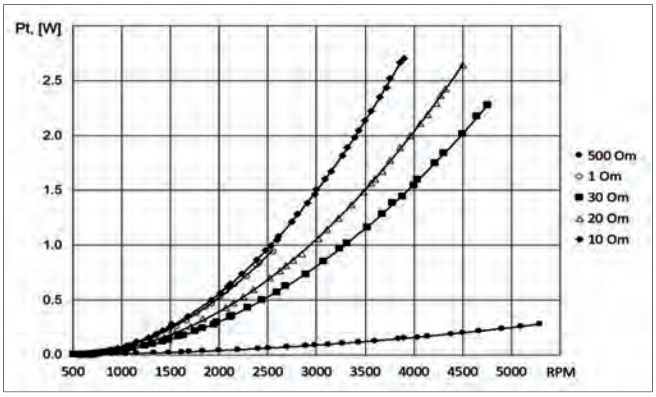

Fig. 6. The electrical power generated by the experimental turbine generator at various rotor speeds and loads

The minimum load mode of the generator was simulated using a resistor rated at 500 ohms. The results of the tests showed the suitability of the turbogenerator model for further research.

CFD SIMULATION RESULTS

For a detailed study of hydrodynamic processes in the TAE resonator, a series of computational experiments was carried out. These studies were carried out with the help of various software products, which made it possible to compare the results obtained and assess the adequacy of the modelling.

In the ANSYS package [26], the channel geometry was created using the ANSYS Design Modeler and Blade Modeler programs, and the mesh was created using the ANSYS Turbo Grid program (Fig. 7); the analysis of the results was carried out using the CFD-Post software module. The features of various mathematical models that can be used in the CFD approach are described in detail in [27]–[31].

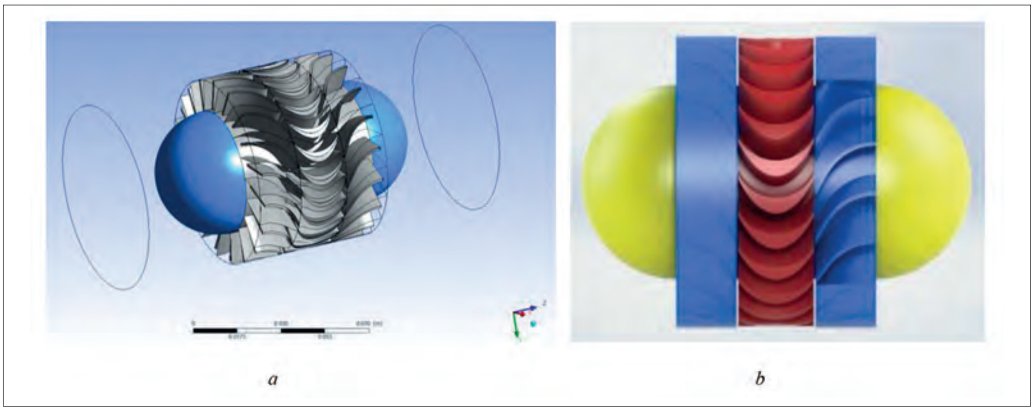

Fig. 7. Experimental sample of a bidirectional turbine and its CFD model: a) ANSYS Design Modeler, b) SolidWorks 3D model

In the first stage of research, in order to check the correctness of the construction of the CFD calculation models and create a time-efficient calculation scheme, test calculations were carried out. Considering the complexity of the task, the calculations were restricted to the fixed turbine rotor. In these experiments, the conditions of full-scale experiments to measure the resistance of a bidirectional turbine in a unidirectional flow were simulated.

The boundary conditions were set in accordance with the parameters of the physical experiment, and the standard k-e turbulence model was used. Fig. 8 shows the results of the CFD simulation of the hydraulic resistance of a resonator section with a bidirectional turbine.

It can be seen that the results of the CFD calculations and physical experiments coincide satisfactorily, since the difference between them does not exceed 10%. The existing deviations in the results can be explained by the difficulty of determining and taking into account the roughness of the surface of the bidirectional turbines and by some design deviations that were due to the capabilities of the existing 3D printer.

In further calculations, the hydrodynamic structure of the flow in the resonator with bidirectional turbines was studied. The calculations were made for the speed range of 3–25 m/s, which fully covers the range of amplitude values of the oscillating velocity that could be achieved during the experiments. The complexity of the hydrodynamic picture is shown in Figs. 9–11.

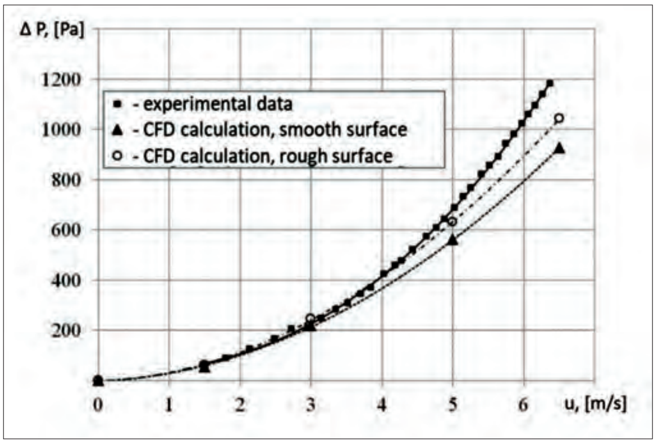

Fig. 8. Hydraulic resistance of IDT specimen: comparison of experimental data with CFD simulation results

The vortex structures in the flow behind the bidirectional turbines are more effectively visualised through the results presented in Figs. 12 and 13.

These figures demonstrate that within the resonator of the thermoacoustic generator, swirl flows developed, wherein the tangential velocity component equals nearly 60% of the longitudinal component. These persistent circulating vortex structures possess substantial energy accumulation capabilities and are rather stable.

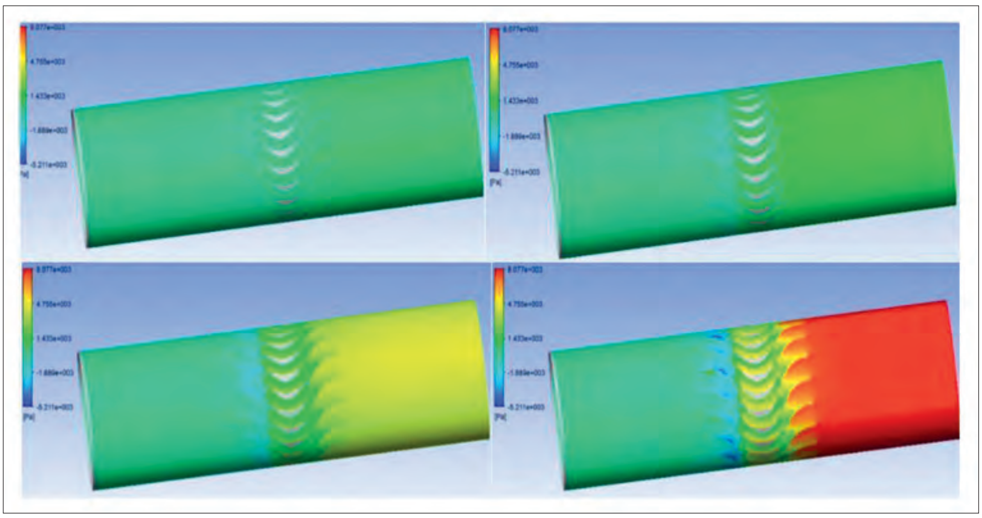

Fig. 9. Distribution of static pressure in the resonator channel with bidirectional turbines at different flow rates

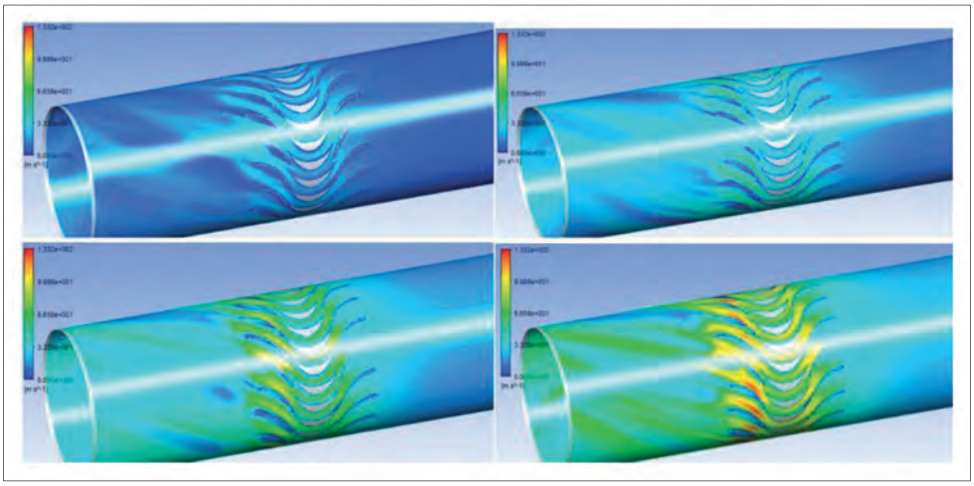

Fig. 10. Distribution of static pressure in the resonator channel with bidirectional turbines at different flow rates

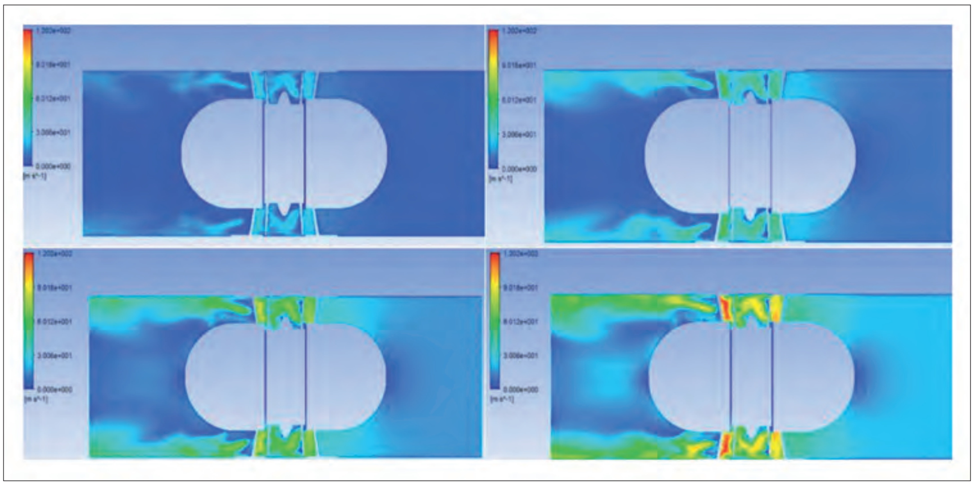

Fig. 11. Velocity distribution across the resonator cross-section

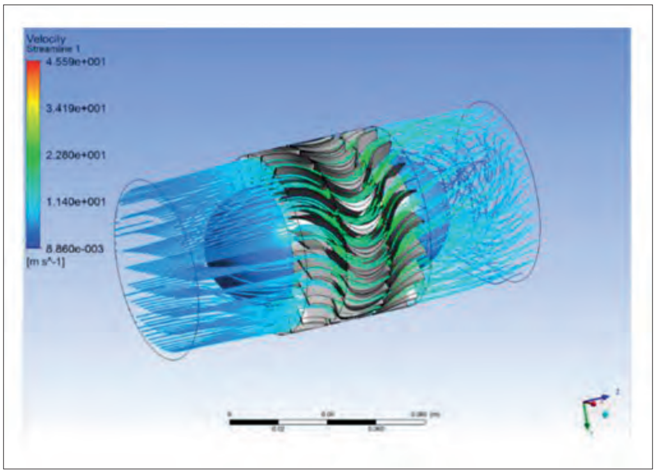

Fig. 12. Current lines in a resonator with an experimental turbine; the rotor is stationary

It can be argued that these phenomena in conditions of oscillating motion should lead to a non-uniform flow distribution in front of the straightening blades of bidirectional turbines, which is an undesirable factor. When designing such bidirectional turbines, measures should be taken to reduce these effects. In addition, the presence of tangential currents on the concave surface of the resonator will lead to the formation of secondary vortex structures of the Hertler-Taylor type, which also represent an energy-consuming mechanism.

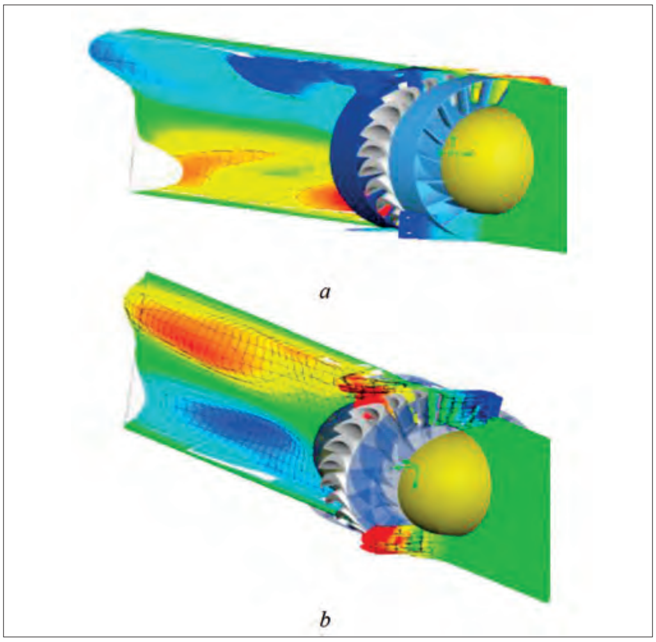

Fig. 13. Distribution of circumferential velocity along the length of the resonator with bidirectional turbines: a) velocity of 5 m/s; b) velocity of 10 m/s

CONCLUSIONS

To perform the research program, a suitable experimental setup was developed; it includes a test worktable and a microprocessor data acquisition and recording system. A prototype of a turbogenerator equipped with a pulsed bidirectional turbine was fabricated, and a numerical counterpart was established for CFD simulations.

First, experimental evaluations were conducted under straight-line medium movement conditions with varying generator loads. Hydraulic resistance measurements of the turbine model within the resonator were sourced empirically. The results demonstrated that peak pressure losses transpire during the idling phase at the generator's minimal load. Under such conditions, rotor rotational speeds reached up to 5500 rpm.

A CFD framework was constructed to represent the combination of a bidirectional turbine and a thermoacoustic engine resonator. This model facilitated the exploration of turbine characteristics both for a stationary rotor and during the rotor's rotation.

The hydraulic resistance computations for the stationary-rotor turbine aligned closely with empirical results, deviating by less than 10%. This concurrence validates the utility of the developed CFD model for subsequent investigations. Simulations, executed across various software packages, consistently yielded analogous outcomes.

Numerical analyses revealed the emergence of pronounced tangential and radial secondary currents immediately behind the bidirectional turbine within the resonator. These secondary vortex patterns introduce augmented energy expenditures and require minimisation. Given the derived results, optimising the design of the bidirectional turbine's guide apparatus, as well as refining the profiling of the shroud and the resonator, emerges as a reasonable solution.

In analysing the current results, it is very important to consider that the simulations were focused on a small two-way turbine with an output power of only a few watts. However, for shipboard thermoacoustic WHRSs, the turbine generators should provide power at levels of approximately 10^2 to 10^3 kW. For such significantly larger structures, the occurrence of so-called large-scale effects is likely. In addition, the question of the construction of TATG resonators and their overall aggregate location is open.

In future efforts, the priority should be the integration of innovative design solutions aimed at mitigating the appearance of secondary radial flows in the resonators of high-power thermoacoustic generators.

REFERENCES

1. N. Olmer, B. Comer, B. Roy, X. Mao, and D. Rutherford, "Greenhouse gas emissions from global shipping." [Online]. Available: https://theicct.org/wp-content/uploads/2021/06/Global-shipping-GHG-emissions-2013-2015_ICCT-Report_17102017_vF.pdf. [Accessed: Oct. 15, 2023].

2. International Maritime Organization, "Initial IMO GHG strategy." [Online]. Available: https://www.imo.org/en/MediaCentre/HotTopics/Pages/Reducing-greenhouse-gas-emissions-from-ships.aspx. [Accessed: Oct. 15, 2023].

3. International Maritime Organization, "Note by the International Maritime Organization to the UNFCCC Talanoa Dialogue." [Online]. Available: https://unfccc.int/sites/default/files/resource/250_ IMO%20submission_Talanoa%20Dialogue_April%202018.pdf. [Accessed: Oct. 15, 2023].

4. International Maritime Organization, "IMO. Low carbon shipping and air pollution control." [Online]. Available: http://www.imo.org/en/MediaCentre/HotTopics/GHG/Pages/default.aspx. [Accessed: Oct. 15, 2023].

5. International Maritime Organization, "Fourth IMO GHG study 2020 executive-summary." [Online]. Available: https://wwwcdn.imo.org/localresources/en/OurWork/Environment/Documents/ Fourth%20IMO%20GHG%20Study%20 2020%20Executive-Summary.pdf. [Accessed: Oct. 15, 2023].

6. Finnish Marine Industries, "Journey to a carbon-free world: Introducing the NYK SUPER ECO SHIP 2050." [Online]. Available: https://meriteollisuus.teknologiateollisuus.fi/en / ajankohtaista/news/journey-carbon-free-world-introducing-nyk-super-eco-ship-2050. [Accessed: Oct. 15, 2023].

7. H. Shi, Q. Zhang, M. Liu, K. Yang, and J. Yuan, "Numerical Study of the Ejection Cooling Mechanism of Ventilation for a Marine Gas Turbine Enclosure," *Polish Maritime Research*, Vol. 29, No. 3, pp. 119–127, 2022, doi: org/10.2478/pomr-2022-0032.

8. T. Niksa-Rynkiewicz, A. Witkowska, J. Głuch, and M. Adamowicz, "Monitoring the Gas Turbine Start-Up Phase on a Platform Using a Hierarchical Model Based on Multi-Layer Perceptron Networks," *Polish Maritime Research*, Vol. 29, No. 4, pp. 123–131, 2022, doi: 10.2478/pomr-2022-0050.

9. E.-L. Tsougranis and D. Wu, "A feasibility study of organic Rankine cycle (ORC) power generation using thermal and cryogenic waste energy on board an LNG passenger vessel," *International Journal of Energy Research*, Vol. 42, No. 9, pp. 3121–3142, July 2018, doi: 10.1002/er.4047.

10. M. E. Mondejar, J. G. Andreasen, L. Pierobon, U. Larsen, M. Thern, and F. Haglind, "A review of the use of organic Rankine cycle power systems for maritime applications," *Renewable and Sustainable Energy Reviews*, Vol. 91, pp. 126–151, 2018, doi: 10.1016/j.rser.2018.03.074.

11. T. Hoang, "Waste heat recovery from diesel engines based on Organic Rankine Cycle," *Applied Energy*, Vol. 231. 2018, doi: 10.1016/j.apenergy.2018.09.022.

12. O. Cherednichenko, S. Serbin, and M. Dzida, "Application of thermo-chemical technologies for conversion of associated gas in diesel-gas turbine installations for oil and gas floating units," *Polish Maritime Research*, Vol. 26, No. 3, pp. 181–187, Sep. 2019, doi: 10.2478/pomr-2019-0059.

13. G. W. Swift, "Thermoacoustic engines," *J. Acoust. Soc. Am.*, Vol. 84, No. 4, pp. 1145–1180, 1988.

14. G. W. Swift, "Thermoacoustics: A unifying perspective for some engines and refrigerators," *Acoust. Soc. Am.*, 2002. ISBN 0-7354-0065-2.

15. L. M. Qi, P. Lou, K. Wang, et al., "Characteristics of onset and damping in a standing-wave thermoacoustic engine driven by liquid nitrogen," *Chin. Sci. Bull.*, Vol. 58, pp. 1325-1330, 2013, doi: 10.1007/s11434-012-5214-z.

16. Z. Yang, V. Korobko, M. Radchenko, and R. Radchenko, "Improving thermoacoustic low-temperature heat recovery systems," *Sustainability (Switzerland)*, Vol. 14, No. 19, art. No. 12306, 2022, doi: 10.3390/su141912306.

17. T. K. Das, P. Halder, and A. Samad, "Optimal design of air turbines for oscillating water column wave energy systems: A review," *Int. J. Ocean Clim. Syst.*, Vol. 8, No. 1, pp. 37–49, 2017, doi: 10.1177/1759313117693639.

18. A. F. O. Falcao and J. C. C. Henriques, "Oscillating-water-column wave energy converters and air turbines: A review," Renewable Energy, 2015, doi: 10.1016/j.renene.2015.07.086.

19. A. Thakker and F. Hourigan, "Modeling and scaling of the impulse turbine for wave power applications," Renewable Energy, Vol. 29, No. 3, pp. 305–317, 2004, doi: 10.1016/S0960-1481(03)00253-2.

20. D. Liu, Y. Chen, W. Dai, et al., "Acoustic characteristics of bi-directional turbines for thermoacoustic generators," *Front. Energy*, Vol. 16, pp. 1027–1036, 2022, doi: 10.1007/s11708-020-0702-3.

21. M. A. Elhawary, A. H. Ibrahim, A. S. Sabry, and E. Abdel-Rahman, "Experimental study of a small scale bi-directional axial impulse turbine for acoustic-to-mechanical power conversion," *Renewable Energy*, 2020, doi: 10.1016/j.renene.2020.05.162.

22. C. Iniesta, J. L. Olazagoitia, J. Vinolas, and J. Aranceta, "Review of travelling-wave thermoacoustic electric-generator technology," in *Proceedings of the Institution of Mechanical Engineers, Part A: Journal of Power and Energy*, 2018, doi: 10.1177/0957650918760627.

23. Y. Kondratenko, S. Serbin, V. Korobko, and O. Korobko, "Optimisation of bi-directional pulse turbine for waste heat utilization plant based on green IT paradigm," *Studies in Systems, Decision and Control*, Vol. 171, pp. 469–485, 2019, doi: 10.1007/978-3-030-00253-4_20.

24. T. Kloprogge, "Turbine design for thermo-acoustic generator," Master's thesis, Aeronautical Engineering, Hogeschool. Holland Delft, 2012. Available: https://bioenergyforumfact.org/sites/default/files/2018-06/5.%20Turbine%20 Design %20for%20a%20Thermo-acoustic%20Generator.pdf. [Accessed: Oct. 15, 2023].

25. Y. Kondratenko, O. Korobko, and V. Korobko, "Microprocessor system for thermoacoustic plants efficiency analysis based on a two-sensor method," *Sensors & Transducers*, Vol. 24, Aug. 2013. Available: https://www.academia.edu/95466184/Microprocessor_System_for_Thermoacoustic_Plants_Efficiency_Analysis_Based_on_a_Two_Sensor_Method. [Accessed: Oct. 15, 2023].

26. ANSYS, Inc., ANSYS *Fluent Theory Guide*. ANSYS, Inc., 2013.

27. S. I. Serbin, I. B. Matveev, and G. B. Mostipanenko, "Plasma-assisted reforming of natural gas for GTL: Part II - Modeling of the methane-oxygen reformer," *IEEE Trans. Plasma Sci.*, Vol. 43, No. 12, pp. 3964–3968, 2015, doi: 10.1109/TPS.2015.2438174.

28. I. Matveev, S. Serbin, T. Butcher, and N. K. Tutu, "Flow structure investigations in a Tornado combustor," in *4th International Energy Conversion Engineering Conference, AIAA2006-4141*, Vol. 2, 2006, pp. 1001–1013, doi: 10.2514/6.2006-4141.

29. O. Cherednichenko, S. Serbin, and M. Dzida, "Investigation of the combustion processes in the gas turbine module of an FPSO operating on associated gas conversion products," *Polish Maritime Research*, Vol. 26, No. 4, pp. 149–156, 2020, doi: 10.2478/pomr-2019-0077.

30. S. Serbin, K. Burunsuz, M. Dzida, J. Kowalski, and D. Chen, "Investigation of ecological parameters of a gas turbine combustion chamber with steam injection for the floating production, storage, and offloading vessel," *International Journal of Energy and Environmental Engineering*, Vol. 13, No. 3, pp. 873–888, 2022, doi: 10.1007/s40095-021-00433-w.

31. I. B. Matveev, N. V. Washchilenko, and S.I. Serbin, "Plasma-Assisted Reforming of Natural Gas for GTL: Part III - Gas Turbine Integrated GTL," *IEEE Trans. Plasma Sci.*, Vol. 43, No. 12, pp. 3969–3973, 2015, doi: /10.1109/TPS.2015.2464236.

POLISH MARITIME RESEARCH 4 (120) 2023 Vol. 30; pp. 110-119
10.2478/pomr-2023-0064

QUANTUMNESS IN DIAGNOSTICS OF MARINE INTERNAL COMBUSTION ENGINES AND OTHER SHIP POWER PLANT MACHINES

Jerzy Girtler
Jacek Rudnicki *
Gdansk University of Technology, Institute of Naval Architecture, Gdansk, Poland

* Corresponding author: *jacekrud@pg.edu.pl (J.Rudnicki)*

ABSTRACT

The article provides proof that the diagnostics of marine internal combustion engines and other ship power plant machines should take into account the randomness and unpredictability of certain events, such as wear, damage, the variations of mechanical and thermal loads, etc., which take place during machine operation. In the article, the energy E, like the other forms (methods) that it can be converted into (heat and work), is considered the random variable E_t; at time t, this variable has the mean value $\overline{E}_t$, which is the observed value of the statistic $\overline{E}_{st}$ with an asymptotically normal distribution $N\left(E(E_t), \frac{\sigma_t}{\sqrt{n}}\right)$, irrespective of the functional form of the random variable E_t. A proof is given that shows that the expected value estimated in the above way, considering the time t of the performance of task Z by a marine internal combustion engine or other ship power plant machine, can be used to determine the machine's possible action (D_M). When compared to the required action (D_W) needed for task Z to be performed, this possible action makes it possible to formulate an operating diagnosis concerning whether the engine or machine of concern is able to perform task Z. It is assumed that an energy device of this type is able to perform a given task when the inequality $D_M \geq D_W$ holds. Otherwise, when $D_M < D_W$, the device cannot perform the task for which it was adopted in the design and manufacturing phase, which means that it is in the incapability state, although it still can be started and convert energy into the form of heat or work..

Keywords: diagnostics, stochastic process, internal combustion engine, random variable

INTRODUCTION

During the operation of any marine internal combustion engine or ship power plant machine, irrespective of the applied diagnosis system (*SDG*), collecting the information needed to formulate the diagnosis of the state of the engine or machine that is the diagnosed system (*SDN*) requires the initiation and continuation of the diagnostic process. This process [2], [6], [10], [11] is a two-dimensional stochastic process $\{D(t, \vartheta): t \geq 0, \vartheta \geq 0\}$. It consists of the process $\{B(t): t \geq 0\}$, which represents the *SDG* operation, and the process $\{C(\vartheta): \vartheta \geq 0\}$, which represents data collection by *SDG* and the formulation of a diagnosis about the state of *SDN*.

The process $\{B(t): t \geq 0\}$ is the process resulting from the use of *SDG* during the operation of the engine or machine performing a given task (*SDN*). This process is considered a long-term process, and it can but does not have to involve generating short-term diagnoses and/or formulating prognoses or geneses. The course of this process has a fundamental impact on the reliability of the diagnosis [12]–[14], [25], [38]. The process $\{C(\vartheta): \vartheta \geq 0\}$ is connected with performing measurements of the current values of diagnostic parameters (physical quantities such as temperatures, pressures, vibrations, etc.), with further diagnostic reasoning performed in the short term, i.e. the time interval of the *SDG* operation (work) in which the diagnosis is obtained.

The process $\{C(\vartheta): \vartheta \geq 0\}$ always consists of the following realisations: diagnostic testing and diagnostic reasoning (of the signal, measurement, symptom, structural, and operating type) [4]. The output of the process $\{C(\vartheta): \vartheta \geq 0\}$ is a diagnosis, the reliability of which is highest when, during the testing process, *SDG* works reliably and the disturbances resulting from environmental influences can be omitted due to the sufficient resistance of *SDG* to these influences.

In a general case, diagnostic reasoning is carried out using the following types of reasoning in the following order: the signal, measurement, symptom, structural, and operating reasoning types [4]. Each of the above types of reasoning is characterised by the diagnostic uncertainty, resulting from the fact that diagnostic reasoning can be (and, as a rule, is) burdened with errors. As a result, diagnostic reasoning can lead to one of two possible mistakes to be made by the user (diagnostician) of the engine or machine:

- a first-type mistake, which consists of diagnosing the engine or machine as being in the incapability state, although it is still able to perform the given task, i.e. it is in the state of capability;
- a second-type mistake, which consists of diagnosing the engine or machine as being in the state of capability, although it is already unable to perform the given task, i.e. it is in the incapability state.

The above interpretation of the process $\{C(\vartheta): \vartheta \geq 0\}$ shows that this process has values (states) that correspond to diagnostic tests and the above types of reasoning, and the durations of the diagnostic tests and the above types of reasoning are the execution times of these states. A characteristic feature of this process is that certain probabilities of occurrence can (and should) be attributed to its states, while the duration of each of these states is a random variable.

During each diagnostic test, the measurements are made with a certain accuracy, which depends on the applied measuring methods and devices, as well as on the measurement conditions and the experience and qualifications of the people performing the test; all of these factors are possible sources of inaccuracy in the measurement. This inaccuracy results from both the inaccuracy of the applied measuring methods and devices, and changes in the characteristics of the tested engine or machine that take place during the measurement. The main causes of inaccuracy include the limited resolution of the measuring devices (resulting from their sensitivity threshold and the randomness of the examined phenomena) and errors such as the quantisation error, aperture error, and sampling time error when a digital signal is used in the measurement [27]. Hence, the diagnostic testing of a marine engine or other ship power plant machine is burdened with a certain measurement inaccuracy. This inaccuracy should be recognised well enough to determine its main cause, i.e. whether it is mainly caused by [26], [27]

- errors in the applied measuring methods and devices, which are known to depend mainly on the accuracy and sensitivity of the measuring sensors and transducers, the inaccuracy of the measuring devices, given by their inaccuracy class, and the stability and reliability of the measuring devices; or
- changes in the characteristics of the tested engine or machine that take place during the measurement.

The correct identification of the causes of the inaccuracy of the performed measurement is necessary for the accurate evaluation of the current inaccuracy of the characteristics of the tested machine and that of the applied measuring devices, with the further correct selection of the proportions of these inaccuracies. The difficulty in evaluating the inaccuracy of a measurement related to the properties of the applied measuring method and devices and that related to the current characteristics of the diagnosed machine originates from the quantum nature of their changes, which leads to randomness and the unpredictability of events in the diagnostics of marine internal combustion engines and other ship power plant machines. Therefore, this issue needs to be thoroughly considered.

RANDOMNESS AND UNPREDICTABILITY OF EVENTS IN DIAGNOSTICS OF MARINE INTERNAL COMBUSTION ENGINES AND OTHER SHIP POWER PLANT MACHINES

In the diagnostics of not only marine internal combustion engines but also those used in cars, airplanes, etc., as well as other machines of all types, it is advisable to stop using the deterministic approach for the identification of the technical state of these machines and focus on the probabilistic aspects of their diagnostics [3], [6], [11], [17], [21], [24], [29], [30], [38]–[40]. The deterministic approach to the diagnostics of marine engines and machines, as well as those used in other branches of technology, results from the traditional perception of changes in their technical state, according to which it is believed that, in general, randomness and unpredictability can be omitted in technical diagnostics intended to assess the technical state of these types of devices. One of the main reasons for such an approach to the diagnostics of energy devices was the fact that until the 20th century, a deterministic theory of the description of phenomena, events, and processes was in force. This theory was developed by Pierre Simon de Laplace, who assumed that similar laws of physics exist in both the macroworld and microworld, and all changes take place according to these laws. They control the appearance and disappearance of each phenomenon, and the course of all events (facts) and processes. According to this theory, the entire universe is totally deterministic on both the microscale and macroscale. This vision of changes taking place in space and time was the basis for the development of science until the early 1920s – it was a basic methodological assumption made by physicists. This view led to the foundation of mechanics, which now is referred to as classical, or non-quantum, mechanics – in contrast to quantum mechanics, which was developed later. It also led to the conviction that all the laws of motion and any other changes can be expressed as differential equations that have unique solutions. This determinism can be found in the principles formulated by Isaac Newton to describe the laws of nature, in the partial differential equation proposed by Erwin Schrödinger (1926), the solution of which is the wave function determining the quantum state of a particle at an arbitrary time in a deterministic aspect, and in Albert Einstein's equations describing the photoelectric effect and the relationship between energy, mass, and velocity [36], [37]. All these equations are not only deterministic but also time-reversible [22], [34]. However, despite the efforts of many mathematicians, researchers have failed to prove the existence of unique solutions to differential equations, which was the inspiration for searching for a concept of the probabilistic interpretation of reality. An example of such an approach is the probabilistic interpretation of the wave function proposed as the solution to Schrödinger's wave equation by Max Born (in 1926), who could not accept the fact that this function represents a 'real' electron wave, even though other physicists accepted this equation as a tool for solving quantum mechanics problems. In Max Born's interpretation, the wave function Ψ is a product with complex numbers as values [5], [17], [19], such that $|\Psi|^2$ is the probability of finding a particle in a given area (point) in space. That means that there is no certainty about the exact position of an electron, but the probability that the electron is at a given point in space can be calculated, provided that the wave function Ψ is known. This interpretation corresponded to Niels Bohr's opinion; he accepted partial and wave theoretical models of the existence of particles. He also believed that we cannot predict an exact result of an empirical examination; in his opinion, we can only calculate the probability that the result of a given experiment will take a given value and not another value.

However, the final blow to the deterministic theory of Laplace came from the uncertainty principle formulated by Werner Heinsenberg (1926). Along with Max Planck's quantum hypothesis (1900), which explained the nature of electromagnetic radiation generated by hot bodies, the uncertainty principle became one of fundamental elements (achievements) of quantum mechanics. Today, this theory is the basis for contemporary science and technology. It was developed in the 1920s by Werner Heinsenberg, Erwin Schrödinger, and Paul Dirac, as well as by Wolfgang Pauli and Niels Bohr. Additionally, Albert Einstein and Richard Feynman contributed to the development of this theory (the latter being the creator of nanotechnology). Its principles explain, for instance, the functioning of transistors and integrated circuits, i.e. most important components of electronic devices, without which modern diagnostics (not just technical) could not exist. These principles also apply in modern chemistry (quantum chemistry) [23], cryophysics (quantum liquid), and biology (medical diagnostics). Among the physical sciences, only the theory of gravity and cosmology has not been fully aligned with quantum mechanics [20]. However, it may be expected that one day this will happen. The general theory of relativity describes observations well, due to the fact that gravitational fields existing in ordinary conditions are weak. However, according to the singularity theorems, the gravitational field is very strong in two situations, at least: in the areas of black holes, and during and directly after the Big Bang [20]. Evidently, quantum effects cannot be neglected in these fields [17], [20], [40]. We can expect that the classical theory of relativity should finally collapse because of the above space-time singularities. Currently, research is in progress to develop the quantum gravity theory. Classical (non-quantum) mechanics was questioned because it assumed that atoms should collapse to the state of infinite density. According to that theory, a hot body should emit electromagnetic waves with the same intensity at all wave frequencies, which means that the total energy emitted by this body is infinite. This conclusion is not true, and this was why Max Planck formulated a hypothesis that electromagnetic waves cannot be emitted at an arbitrary rate but only as strictly defined portions, which he called quanta (hence the name: quantum hypothesis).

It results from quantum mechanics that physical quantities such as energy or angular momentum can only change in steps. Moreover, the quantities referred to as complementary have an important property: the simultaneous and accurate measurement of their values is impossible. For instance, the more accurate the position measurement of a microparticle (subatomic particle) is, the less accurate the measurement of its momentum and, consequently, velocity will be. This is according to the Heisenberg's uncertainty principle, which defines the inaccuracy degree of the measurement of the above basic physical quantities (the position and momentum of a particle, as well as energy and time). This inaccuracy has nothing in common with the accuracy of the applied measuring methods and/or devices [5], [17], [19], [20]. The uncertainty principle says that in the microworld, we cannot predict exactly the future position of a particle smaller than an atom, which is important, for instance, in controlling the stream of neutrons in a kinescope. Therefore, it is understandable that the atom models proposed first by Joseph John Thompson and then by Ernest Rutherford and Bohr (although Bohr's model quite precisely described the structure of the hydrogen atom, as it is the simplest atom) were replaced by the quantum mechanical model of atom structure. In this model, the electrons in atoms do not move on specific orbits; instead, they move in so-called orbitals, which are space regions around the nucleus in which the probability of the existence of (finding) an electron at a given moment has a precisely defined value. Following the proposal of Richard Feynman, it was assumed that the particle does not move on one track but on all possible trajectories (permissible orbits) [1], [17], [20], [34]. These permissible orbits, called the orbitals of electrons in atoms, are understood as space regions around the nucleus in which the electron can appear at a given time with a certain probability [1], [19], [34].

Transferring these conclusions to the macroscale research area, we can say that, according to Heisenberg's uncertainty principle, we cannot expect the same result when repeating any empirical research, regardless of whether it is observational or an active experiment. Thus, the question of how different the obtained results can be arises. The answer is that the range of this difference depends on the adopted testing method, the accuracy of the measuring devices, the current measurement conditions and their repeatability, the experience of the person conducting the test, the number of measurements made, the duration time of the measurement, etc. All of this means that when an empirical test is repeated, in a particular experiment and in given conditions, different results are always to be expected. This also means that obtaining a specific test result is a random event, and the measured quantities should be considered random variables. Indeed, when the variability of the measurement results is small, it can be neglected, but in each case, this decision should be justified. Formulating a diagnosis first requires the diagnostic test to be performed, as it is the first link in the diagnosis chain. The diagnostic test consists of measurements made using a proper measuring device or the organoleptic identification of the values of diagnostic parameters [3], [4], [11], [17], [21], [24], [29], [30], [38]–[40]. The results of this test make it possible, using diagnostic reasoning, to formulate a relevant diagnosis (of the signal, measurement, symptom, structural, and operating type) [4]. At each stage of the diagnostic procedure, including diagnostic tests and the subsequent types of diagnostic reasoning, the obtained results are burdened with the above-mentioned uncertainty and with errors caused by various disturbances. Therefore, the randomness of a diagnosis, prognosis, or genesis should be considered an indispensable attribute.

The quantum mechanics based on Heisenberg's uncertainty principle introduce unavoidable randomness and unpredictability to science and engineering practice.

A more general uncertainty than that defined by Heisenberg's principle is introduced by the phenomenon known as deterministic chaos [35]. This phenomenon can be observed when the tested model is a system of differential equations, especially nonlinear equations of the 2nd, 3rd, and 4th order. It is a well-known fact that the solution to a deterministic system of differential equations can take the form of very complicated oscillations; the reason for this is not a large number of degrees of freedom, nor local disturbances, but the increasing instability depending on the precision with which the initial state is determined, which, in turn, depends on time-related initial conditions and time-dependent equation coefficients. Deterministic chaos is closely connected with the occurrence of so-called attractors, which usually have the form of aperiodic trajectories that attract other trajectories from their environment [1], [38]. The detection of attractors enables better prediction of the appearance of random events. Therefore, recognising the fact that a given empirical system develops chaotically may facilitate the study of its evolution. This means that chaos is not always a negative phenomenon. Adding noise with random parameters to the non-disturbed empirical system can lead to statistical stabilisation or the periodicity of the evolution of this system. This requires as new look at relations between deterministic diagnostic models and those representing statistical and probabilistic approaches.

Another source of chaos can be inaccuracy in determining the model parameters. This fact is connected with the phenomenon of bifurcation (splitting between the real and expected test results), which can be observed during the state identification of machines such as marine piston or turbine engines, as well as positive displacement or rotary compressors, pumps, fans, electric motors, generators, etc. This phenomenon is an obstacle to obtaining a credible diagnosis, prognosis, or genesis.

The discovery of the principle of ambiguous causality in science has led to the questioning of the earlier belief of unequivocal determinism (i.e. unequivocal effect resulting from each cause) and the adoption of ambiguous determinism, i.e. determinism resulting from the probabilistic laws of quantum mechanics, which accepts the existence of choice (as a known rule).

It results from the above considerations that when constructing and using the diagnostic model of a marine engine or machine to formulate a complete diagnosis (i.e. current diagnosis, genesis, and prognosis), the following laws (principles) should be taken into account:

- ambiguous causality, i.e. the existence of the randomness of events (including events such as machine state diagnosis), which indicates a need to accept at least ambiguous determinism,
- the uncertainty formulated by Heinsenberg,
- the existence of the general randomness of natural phenomena resulting from their infinite complexity,
- the existence of deterministic chaos resulting from the so-called sensitivity of models of empirical systems, in particular internal combustion engines but also other machines (not only those installed in ship's engine rooms), to their initial state,
- the limited, as a rule, accuracy of the measuring methods and devices, which leads to the limited accuracy of the measurements made using these methods and devices,
- the operating inaccuracy of the marine engine or ship power plant machine that is the diagnosed system (*SDN*),
- the unreliability of the diagnosing systems (*SDG*) adopted to identify the technical state of a marine engine or ship power plant machine.

The measurements are associated with certain diagnostic procedures, during which some mistakes can be made as a result of the following:

- performing a diagnostic test in highly disturbed conditions,
- using an incorrect course of measurements and incorrect error assessment (e.g. neglecting quantisation, aperture, and sampling time errors), as a result of the application of measuring devices with insufficient (inadequate) accuracy and/or the omission of some measurements,
- incorrectly recording the results of measurements that have been correctly performed and correctly signalled by the measuring devices,

- incorrectly interpreting the results of diagnostic tests both during the diagnostic test and in the further steps of diagnostic reasoning, which is the result of the inaccurate (incorrect) reading of the indicators of the measuring sensors (devices) and the application of inaccurate data processing algorithms,
- incorrectly identifying the state of the engine or machine that is the diagnosed system (*SDN*), despite correctly performing the measurements and obtaining correct results from the diagnostic tests.

All of this means that in empirical diagnostic testing, making use of certain measuring methods and devices, there is a problem of measurement inaccuracy that results from changes in the characteristics of the tested machine that take place during the measurement and errors associated with the use of certain measuring methods and devices [20], [21]. As a consequence, an indeterminacy appears that should be explained. In particular, the main cause of this indeterminacy should be recognised, i.e. it should be determined whether it results from

- a change in the characteristics of the engine or machine that is the object of diagnostic testing that took place during the measurement, or
- errors associated with the use of the given measuring methods and devices.

Therefore, it is of high importance in this type of testing to [28]

1. estimate the value of the operating uncertainty of the marine engine or other ship power plant machine that is the object of the diagnostic test,
2. estimate the value of the inaccuracy of the utilised measuring technique (measuring method and devices),
3. select adequate proportions between the accuracy of the applied measuring technique and the current inaccuracy of the tested object (a marine engine or machine).

It follows from the above that when using diagnostic methods to determine the technical state of an engine or machine that is the diagnosed system (*SDN*) via an appropriate diagnosis system (*SDG*), it is difficult to obtain sufficiently unambiguous answers to the following questions:

- What is the current structure of the tested machine (*SDN*) and its resulting technical state ?
- What were the causes that led to the present technical state of the machine ?
- What will the specific properties of the SDN state be during and after its future evolution ?

In this situation, formulating a specific diagnosis, especially an operational diagnosis, requires the application of mathematical statistics, probability calculus, and stochastic processes. Additionally, formulating the operational diagnosis requires knowledge on the consequences of making a given decision that belongs to the set of possible decisions. Nevertheless, a deterministic approach can be applied to determine the symptoms of the technical state of the machine; for instance, integral calculus can be used to calculate the value of the machine's operation. In this case, further considerations concerning the diagnostics of machines will focus on demonstrating the suitability of the generalised diagnostic system, which can be the operation of a given marine engine or other ship power plant machine, for determining the operational capability of these devices, i.e. their ability to perform a given task in a given amount of time and given operating conditions.

THE ISSUE OF OPERATION OF MARINE INTERNAL COMBUSTION ENGINES AND OTHER SHIP POWER PLANT MACHINES IN TERMS OF THEIR DIAGNOSTICS

The operation of an arbitrary marine internal combustion engine or ship power plant machine can be interpreted as of conversion of the energy E into the form of heat and/or work and its delivery to a receiver in a given time t (heat and work are forms, or – in other words – methods of energy conversion) [15], [16], [31]. In this interpretation, the operation of each ship power plant machine, including the marine internal combustion engine, can be described (in an evaluative approach) using a physical quantity with a given numerical value and a unit of measure called the *joule-second* [joule×second].

Consequently, the operation of any marine internal combustion engine or ship power plant machine can be quantitatively determined using the physical quantity *D* ($D = E \cdot t$). This quantity contains information on how long the energy *E* is or can be converted by a given engine or machine. If we limit the analysis of the conversion of the energy *E* to only the form of work (*L*), then, taking into account the time of this energy conversion, we can calculate the operation of the engine or machine as $D_L = L \cdot t$. This type of data on the operation of a given engine or machine contains information on how long the work *L* is or can be performed. This information is as important as that about the power (*N*) of a given marine internal propulsion engine or ship power plant machine, as it indicates how fast a given amount of work (*L*) can be done.

With time, the operation of each marine internal combustion engine and ship power plant machine is becoming worse. Therefore, the issue that may be of a certain interest is the analysis and assessment of the operation of these devices, taking into consideration the above aspect.

The evaluation presented here of the operation of an arbitrary marine internal combustion engine or ship power plant machine has the following advantage: the descriptive evaluation of its operation (the operation of the engine or machine is good, acceptable, not very good, incorrect, bad, etc.) is replaced by an evaluation resulting from comparing the operation of a given engine or machine with another that is used as a reference.

The meaning of such an interpretation of the operation of a marine internal propulsion engine or ship power plant machine can be justified by the following reasoning: the operation D ($D = E \cdot t$) of an engine or machine (due to its technical state) is better if more energy is delivered to the receiver in a given amount of time (t). When the energy transfer has the form of work (L), the operation ($D_L = L \cdot t$) of the machine (due to its technical state) is better if more work (L) is done by this machine in a given amount of time (t).

It is noteworthy that when the energy E is converted into the combined form (method) of work L and heat Q, then, in the evaluative approach, the following equivalence holds:

$$E \equiv L + Q, \tag{1}$$

which means that in this case, the value W_E of the energy E is equal to the sum of the value W_L of the work L and the value W_Q of the heat Q, i.e. $W_E = W_L + W_Q$.

In the case when the energy E is solely used to perform the work L (converted into the form of the work L), then, in the evaluative approach, the following equivalence occurs:

$$E \equiv L, \tag{2}$$

which means that in this case, the value W_E of the energy E is equal to the value W_L of the work L, i.e. $W_E = W_L$.

Similarly, when the energy E is solely used for generating the heat Q, then, in the evaluative approach, the following equivalence occurs:

$$E \equiv Q, \tag{3}$$

which means that in this case, the value W_E of the energy E is equal to the value W_Q of the heat Q, i.e. $W_E = W_Q$.

The operation of a marine internal propulsion engine or other ship power plant machine can be considered using the following terms: required operation (D_W) and possible operation (D_M) [16]. We can conclude that each engine or machine is in the capability state, i.e. it can perform a given task, when

$$D_M \geq D_W. \tag{4}$$

Otherwise, when $D_M < D_W$, we can conclude than the engine or machine is in the incapability state or partial incapability state [15], [16], [32]. The capability of an engine or machine can be assessed after comparing the area of required operation (D_W) with that of possible operation (D_M). This issue is discussed in [16].

In a deterministic approach, the operation of a given marine engine or other ship power plant machine can be described using a general functional relationship describing the change in the energy E at an arbitrary time t of machine operation. The operation of the marine engine or other ship power plant machine analysed for $E(t) = f(t)$ in a given time interval, e.g. $[t_1, t_2]$, is shown as the area in Fig. 1.

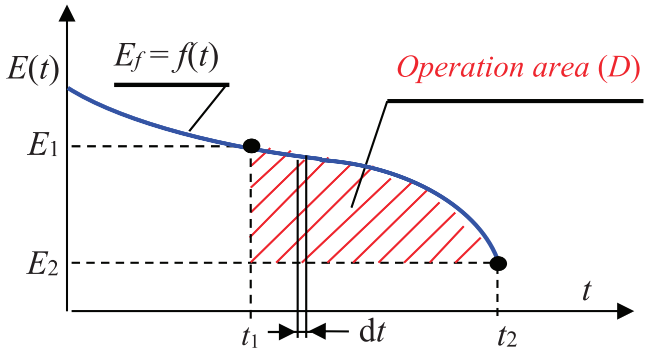

Fig. 1. Machine operation diagram: E – energy, E_1 – energy attributed to time t_1, E_2 – energy attributed to time t_2, t – time

When this energy is converted in the time interval $[t_1, t_2]$, the operation of the engine or machine can be interpreted in general terms as follows [15], [16], [33]:

$$D = \int_{t_1}^{t_2} E(t)\mathrm{d}t\,, \tag{5}$$

where $E(t) = f(t) - E_2$, D is the engine (machine) operation; E is the converted (obtained) energy that allows the realisation of the task in the time interval $[t_1, t_2]$, and t is the time of conversion of the energy E.

Therefore, if we assume that $E(t) = f(t) - E_2$, then formula (5) can be written as (Fig. 1)

$$D = \int_{t_1}^{t_2} f(t)\mathrm{d}t - E_2(t_2 - t_1)\,. \tag{6}$$

The use of formula (5) or formula (6) requires the geometric application of a definite integral, and the following inequalities must be taken into account during the integration:

$$E_1 \leq E \leq E_2.$$

The integral given by formula (6) is the Riemann definite integral [7], with the integration interval defined in this case as equal to $[t_1, t_2]$ and the integrand $E(t) = f(t) - E_2$. This function is integrable in the Riemann sense in the above time interval according to the following formula:

$$D = \int_{t_1}^{t_2} f(t)\mathrm{d}t - \int_{t_1}^{t_2} E_2\mathrm{d}t = D(t)\Big|_{t_1}^{t_2} - E_2(t_2 - t_1)\,. \tag{7}$$

Hence, if we can determine the functional relation between the energy (E) and time (t) that characterises the operation of an engine or machine, i.e. the function $E = f(t)$, and this function is continuous, for instance, in a given time interval $[t_1, t_2]$, then, according to the second fundamental theorem of calculus (Newton-Leibniz theorem), we can write

$$\int_{t_1}^{t_2} E(t)\mathrm{d}t = D(t_2) - D(t_1)\,. \tag{8}$$

The application of the Newton-Leibniz theorem is necessary here because it enables the effective calculation of a definite integral of any continuous function if an antiderivative of this function is known.

In general, the functional relationship $E = f(t)$ is not simple. It is also possible that the antiderivative of the integrand describing the relation between energy and time cannot be defined by elementary functions. In that case, calculating the definite integral using the Newton-Leibniz formula is troublesome, and sometimes even impossible. The trouble in this case is that determining the antiderivative requires difficult transformations to be performed. In these cases, similarly to the situation in which the integrand is given in a tabular form, an approximate value of the operation of an engine or machine can be determined as the value of the definite integral calculated using the trapezoidal rule or the Simpson method – the latter is considered more accurate.

Taking into consideration the randomness and unpredictability of events that exists in operating practice and, as a consequence, in the diagnostics of marine internal combustion engines and other ship power plant machines, their operation can also be considered in the way described above. However, in that case, the analysis and the resulting evaluation of machine operation should be presented using a probabilistic approach, making use of the theory of stochastic processes. A stochastic process is a random function with time as a parameter. This approach to the evaluation of the operation of marine engines and other ship power plant machines results from the need to obtain information on the machine operation in the time interval between two arbitrary moments, e.g. $[t_0, t_n]$, where time is the parameter of this process and not a random variable. In this case, to each time t within the given time interval $[t_0, t_n)]$, we can assign the state called the current state of the process, which is the random variable E_t; this variable has an expected value $\mathrm{E}(E_t)$ and a variance $\mathrm{D}^2(E_t)$ that depend on the current value of t. It is not just the energy (E) that can be the variable in these considerations; its conversion forms, i.e. work (L) or heat (Q), can also be variables. Therefore, the stochastic process is a set of random variables E_t for $t \in [t_0, t_n]$, i.e. for $t_0 \le t \le t_n$. It is worth mentioning here that the expected value $\mathrm{E}(E_t)$ and variance $\mathrm{D}^2(E_t)$ of the random function $\{E(t): t \in [t_0, t_n]\}$ depend on t, i.e. the values of $\mathrm{E}(E_t)$ and $\mathrm{D}^2(E_t)$ can be different for different t values. They are not random functions of E(t), because $\mathrm{E}(E_t)$ and $\mathrm{D}^2(E_t)$ are not random variables, but they are constant for a given value of t and a given set of realisations of the random variable E_t [8], [10].

Examples of the dependence of $\mathrm{E}[E(t)]$, $\mathrm{E}[E(t)] + \sigma[E(t)]$, and $\mathrm{E}[E(t)] - \sigma[E(t)]$ on the time t are shown in Fig. 2 [17]. In this figure, $\sigma[E(t)]$ is the standard deviation of the random variable E, which is calculated as the square root of the variance $\mathrm{D}^2[E(t)]$.

Evaluating the expected value of $\mathrm{E}(E_t)$ for each time t requires the use of statistical inference, which consists of the use of point or interval estimation.

It is known that the mean value $\overline{E}_t$ can be calculated from the following formula [8], [10]:

$$\overline{E}_t = \frac{1}{n}\sum_{i=1}^{n} E_{ti} \; . \tag{9}$$

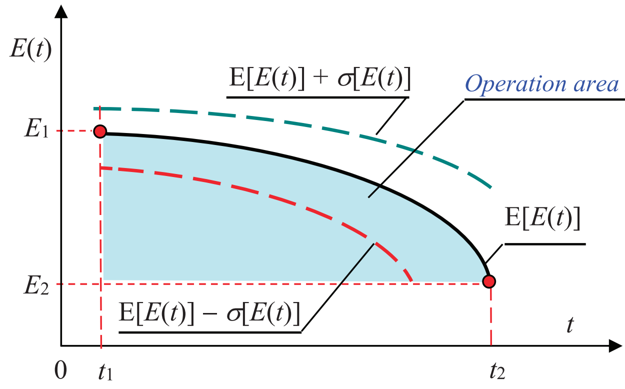

Fig. 2. Example of a stochastic process illustrating the relation E(t), where E is a random variable: E – energy, E_1 – energy assigned to time t_1, E_2 – energy assigned to time t_2, t – time as the process parameter, E[E(t)] – expected value of E, σ[E(t)] – standard deviation of E

The estimation of the expected value of $\mathrm{E}(E_t)$, which consists of its evaluation in the form of the arithmetic mean $\overline{E}_t$, is a point estimation. However, this estimation method does not provide opportunities for evaluating the accuracy of the evaluation (estimation) of $\mathrm{E}(E_t)$. Such an opportunity is provided by interval estimation, which provides the confidence interval [6], [8], [26].

The confidence interval of an unknown quantity $\mathrm{E}(E_t)$ is defined as the interval (E_d, E_g) with random ends; it contains the unknown value of $\mathrm{E}(E_t)$ with a predetermined probability β (the so-called confidence level) [8], [26].

It is well known that the average $\overline{E}_t$ calculated from formula (9) is the observed value of the statistic $\overline{E}_{st}$ with an asymptotically normal distribution $\mathrm{N}\left(\mathrm{E}(E_t), \frac{\sigma_t}{\sqrt{n}}\right)$, irrespective of the functional form of the random variable E_t [6]. The quantities $\mathrm{E}(E_t)$ and σ_t represent, respectively, the expected (average) value and the standard (mean) deviation of the energy E, which is a random variable at time t.

If the value of σ_t, is known, then, making use of the distribution $\mathrm{N}\left(\mathrm{E}(E_t), \frac{\sigma_t}{\sqrt{n}}\right)$ of the statistic $\overline{E}_{st}$, we can calculate the confidence interval for an unknown expected value $\mathrm{E}(E_t)$ from the following formula [8], [26]:

$$P\left\{\overline{E}_t - y_\alpha \frac{\sigma_t}{\sqrt{n}} \le \mathrm{E}(E_t) \le \overline{E}_t + y_\alpha \frac{\sigma_t}{\sqrt{n}}\right\} = \beta \, , \tag{10}$$

where y_α is the standardised variable of the normal distribution corresponding to the confidence interval $\beta = 1 - \alpha$.

However, the value of σ_t is usually unknown and should be estimated based on the obtained results of tests from the following formula:

$$\sigma_t^* = \sqrt{\frac{1}{n-1}\sum_{i=1}^{n}\left(E_{ti} - \overline{E}_t^{\,2}\right)} . \tag{11}$$

Then, assuming that the random variable E_t has a normal distribution $\mathrm{N}(\mathrm{E}(E_t), \sigma_t)$, we can make use of the fact that the random variable $\frac{\overline{E_t} - \mathrm{E}(E_t)}{\sigma_t^*}\sqrt{n-1}$ has the t-Student distribution with $k = n - 1$ degrees of freedom. The assumption about the normal distribution $\mathrm{N}(\mathrm{E}(E_t), \sigma_t)$ of the random variable E_t imposes no limitations in practice, as the statistic $\overline{E_{st}}$ always has an asymptotically normal distribution $\mathrm{N}\left(\mathrm{E}(E_t), \frac{\sigma_t}{\sqrt{n}}\right)$ and the convergence of this distribution to the normal distribution is very fast. This statistic can be used for values $n \geq 4$, i.e. always in practice [8].

Hence, the confidence interval can be calculated from the following formula [8], [26]:

$$P\left\{\overline{E_t} - t_{\alpha,n-1}\frac{\sigma_t^*}{\sqrt{n-1}} \leq \mathrm{E}(E_t) \leq \overline{E_t} + t_{\alpha,n-1}\frac{\sigma_t^*}{\sqrt{n-1}}\right\} = \beta, \tag{12}$$

where $t_{\alpha,n-1}$ is the coefficient of the t-Student distribution, the values of which are such that $P\{|t| \geq t_\alpha\} = \alpha$.

In the proposed evaluation approach, studying the operation of a marine internal combustion engine or other ship power plant machine (pump, compressor) as a diagnostic symptom of the technical state of this type of energy device requires the collection of relevant statistics, which will make it possible to determine the expected values of the energy converted in these devices and further to attribute these values to the individual times of operation of a given machine. Due to the quantum nature of the measurement resulting from the basic postulate of metrology, which is the assumption that the sensitivity threshold $2\varepsilon > 0$ [27], a sufficiently large number of diagnostic tests repeated over a relatively long period of time during the operation of engines or machines can deliver measurement results that will enable the description of the energy in the form of the realisation of the process $\{E(t)\colon \geq 0\}$, which is discrete in states and continuous in time. When studying the accumulation of the dissipated energy E_r or a decrease in the useful energy E_u for a given engine or machine due to its wear, we can obtain the realisation of this process, which is similar to that shown in Fig. 3.

After collecting a sufficient number of such realisations (Fig. 3), we can calculate the characteristic parameters of the stochastic process describing the relation *E(t)* shown in Fig. 2.

Another option is to use the model of the changes in the operation of an internal combustion engine or other ship power plant machine in the form of a homogeneous Poisson process. This model enables the description of the decrease in the converted energy *E* in time t by an elementary portion (quantum) *e*, which can be recorded by a measuring device with a constant intensity $\lambda > 0$ (λ = idem).

Then, the course of the decrease in the energy *E* can be expressed as follows [2], [9], [15]–[17]:

$$E(t) = \begin{cases} E_{\max} & for \quad t = 0 \\ E_{\max} - e\lambda t \pm e\sqrt{\lambda t} & for \quad t > 0 \end{cases}. \tag{13}$$

A graphical interpretation of relation (13) is given in Fig. 4 for E_i (i = 1, …, 6). It shows that this process is discrete in states and continuous in time.

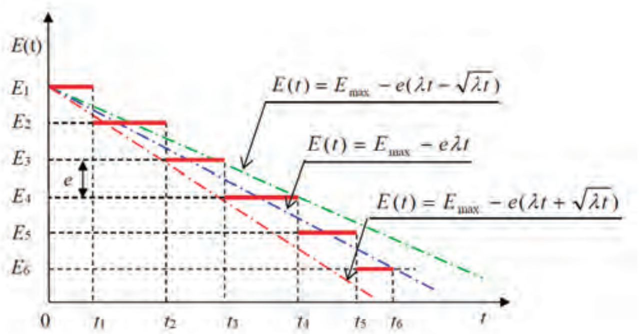

Fig. 4. Graphical interpretation of a sample realisation of the energy decrease of an engine or machine: E – energy, e – energy quantum by which the energy E is decreased, which can be recorded by a measuring device, λ – intensity of the appearance of quanta (e) by which the energy E is decreased, as recorded by the measuring device, t – time, $E_1 = E_{max}$, $E_6 = E_{min}$ *[16], [17]*

Another possible description of the decrease in the energy delivered by an engine or machine to the receiver, and the resulting worsening of its operation, can have the form of a semi-Markov process, applied as a model of the operation of

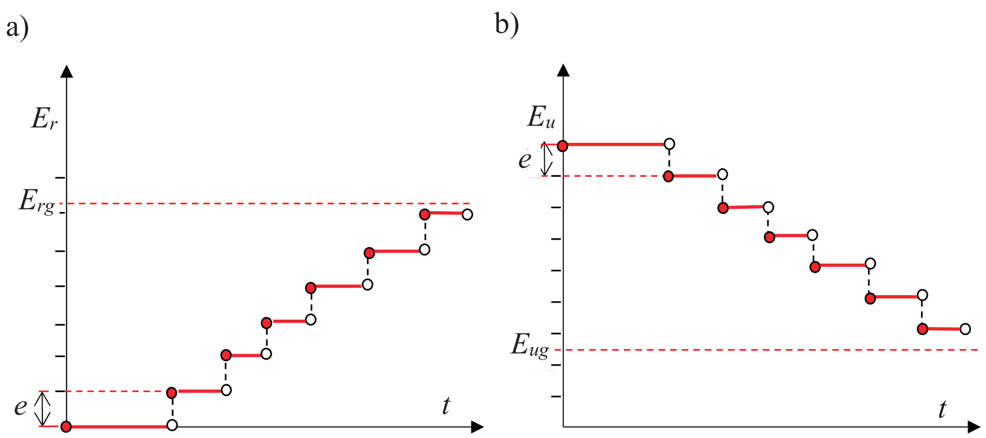

Fig. 3. Interpretation of a) the accumulation of dissipated energy E_r *and b) the resulting decrease in the useful energy* E_u *of an internal combustion engine or other ship power plant machine: e – portion (quantum) of energy by which the energies* E_r *and* E_u *change,* E_{rg} *– dissipated energy limit,* E_{ug} *– useful energy limit [17]*

this type of device [16]–[18].

SUMMARY – REMARKS AND CONCLUSIONS

The diagnostics of marine internal combustion engines and other ship power plant machines should take into account the randomness and unpredictability of the events that occur during their operation. Due to the operational practice of power devices of this type and quantum mechanics, when any empirical research is repeated, regardless of whether it is an observation or active experiment, we cannot expect the same results, but we can expect the same frequency of occurrence of an individual result. This means that obtaining a specific research result is a random event.

When performing diagnostic tests of marine internal combustion engines or other ship power plant machines, the principle of ambiguous causality should be taken into account, which means that there is a need to accept ambiguous determinism, i.e. the determinism resulting from the probabilistic laws of quantum mechanics, which accepts the existence of choice (as a known rule).

Taking into account the results of tests performed in the phase of operation of marine internal combustion engines or other ship power plant machines, a generalised diagnostic symptom has been proposed in the form of the operation of any of the above-mentioned energy devices, assuming that their energy values are becoming worse due to quantum energy dissipation.

The operation of an arbitrary marine internal combustion engine or other ship power plant machine is understood as the conversion of the energy E in a given amount of time t by these devices. This conversion process was compared to a physical quantity that can be expressed with a numerical value and a unit of measure called the *joule-second* [joule×second]. The operation understood in the above way becomes worse with time due to the increase in the wear of the engine or machine. This means that the value of this operation in a given amount of time will decrease due to the decrease in the energy generated by the engine or machine. A suggestion was made that in the case of the application of the theory of stochastic processes to analysing changes in the machine operation understood in the above way, integral calculus can be used to calculate machine operation parameters. A stochastic model of the decrease in the useful energy generated by the engine or machine in the form of a homogeneous Poisson process was proposed to describe the range of the worsening of the operation of the machine. A suggestion was also made to use for this purpose a model in the form of semi-Markov process, which is discrete in states and continuous in time.

When interpreted in the above way, the operation of an arbitrary marine internal propulsion engine or ship power plant machine depends on its technical state and is jointly characterised by the energy converted by this device and the time of its conversion.

In the version presented in this article, the operation of a marine internal propulsion engine or ship power plant machine can be examined by measuring the energy and the time of this energy's conversion; these results can then be presented

- as a number with a unit of measure called the *joule-second* (formulas (5)–(8));
- in a graphic form, as the area of operation (Figs. 1 and 2).

Despite the fact that it was formulated for marine internal propulsion engines and ship power plant machines, the interpretation of machine operation presented in this article can also be used to study the operation of other energy devices.

REFERENCES

1. A. D. Aczel, Probability 1. Zysk i S-ka. Poznań 1997 (in Polish).

2. J. R. Benjamin and C. A. Cornell, Probability, Statistics, and Decision for Civil Engineers. WNT. Warsaw 1977 (in Polish).

3. W. Batko, Z. Dąbrowski, Z. Engel, J. Kiciński, and S. Weyna, Modern Methods of Studying Vibroacoustic Processes. Radom Institute for Sustainable Technologies. Radom 2005 (in Polish).

4. L. Będkowski, Elements of Technical Diagnostics. Military University of Technology. Warsaw 1992 (in Polish).

5. I. Białynicki-Birula, M. Cieplak, and J. Kamiński, Quantum Theory. Wave Mechanics. PWN. Warsaw 2001.

6. W. Cholewa and J. Kiciński, 'Technical Diagnostics. Inverse Diagnostic Models'. Gliwice, Silesian University of Technology, 1977. (in Polish).

7. K. M. Delventhal, A. Kissner, and M. Kulicki, Mathematics. Compendium. Świat Książki, Warsaw 2005 (in Polish).

8. S. Firkowicz, Statistical Evaluation of the Quality and Reliability of Electron Lamps. WNT. Warsaw 1963 (in Polish).

9. J. B. Gercbach and Ch. B. Kordonski, Reliability Models of Technical Objects. WNT, Warsaw 1968 (in Polish).

10. J. Girtler, 'Controlling the Operation Process of Marine Internal Combustion Engines on the Basis of a Diagnostic Decision Model. Monograph', Gdynia, Notebook of Polish Naval Academy, 1989 (in Polish).

11. J. Girtler, 'Diagnostics as a condition for control of operation of marine internal combustion engines', Studia, vol. 28, Maritime School of Higher Education, Szczecin1997 (in Polish).

12. J. Girtler, "Probabilistic measures of a diagnosis likelihood about the technical state of transport means', Archives of Transport, vol. 11, no. 3–4, pp. 33–42, 1999 (in Polish).

13. J. Girtler, "Application of diagnostic reliability to decision-making in the process of equipment operation', 5th National Conference DIAG'2003 'Technical Diagnostics of Devices and Systems', Warsaw – Ustroń 2003 (in Polish).

14. J. Girtler, 'Probabilistic measures of the reliability of diagnosis about the technical condition of machinery and other equipment', XXXI National Symposium 'Machinery Diagnostics', Węgierska Górka 2006 (in Polish).

15. J. Girtler, 'Conception of valuation of combustion engine operation", Journal of KONES. Powertrain and Transport, pp. 89–96, 2008.

16. J. Girtler, 'Energy aspect of machinery diagnostics', Diagnostyka, vol. 1, no. 45, pp. 149–156, 2008 (in Polish).

17. J. Girtler, 'Aspects of quantum machine diagnosis,' XXXII National Symposium 'Machinery Diagnostics', Węgierska Górka 2012 (in Polish).

18. F. Grabski, 'Theory of semi-Markov processes of operation of technical objects', Science Notebook of Naval College, vol. 75A, Gdynia 1982 (in Polish).

19. J. Gribbin, In Search of Schrödinger's Cat. Zysk i S-ka. Poznań 1997 (in Polish).

20. S. W. Hawking, A Brief History of Time. From the Big Bang to Black Holes. ALFA Publisher, Warsaw 1990 (in Polish).

21. R. Michalski, Diagnostics of Working Machinery. Radom. Institute for Sustainable Technologies 2004 (in Polish).

22. M. Moskowits, Is science good. CiS Publisher. Warsaw 1997 (in Polish).

23. R.F. Nalewajski, Fundamentals and Methods of Quantum Chemistry. PWN. Warsaw 2001 (in Polish).

24. S. Niziński, Elements of Diagnosis of Technical Objects. University of Warmia and Mazury, Olsztyn 2001 (in Polish).

25. S. Pabis, Methodology and Methods of Empirical Sciences. PWN. Warsaw 1985 (in Polish).

26. Z. Pawłowski, Mathematical Statistics. PWN. Warsaw 1976 (in Polish).

27. J. Piotrowski, Fundamentals of Metrology. WNT. Warsaw 2002 (in Polish).

28. Z. Polański, Planning Experiments in Technology. PWN. Warsaw 1984 (in Polish).

29. P. Puzdrowska, "Diagnostic Information Analysis of Quickly Changing Temperature of Exhaust Gas from Marine Diesel Engine Part I Single Factor Analysis" Polish Maritime Research, vol.28, no.4, 2021, pp.97-106, https://doi.org/10.2478/pomr-2021-0052

30. S. Radkowski, Vibroacoustic Diagnosis of Low-Energy Damage. Institute for Sustainable Technologies. Warsaw-Radom 2002 (in Polish).

31. J. Rudnicki, 'Energy-time method for assessment of main diesel engine operation,' Journal of KONES Powertrain and Transport, vol. 14, no. 3, 2007.

32. J. Rudnicki, 'Assessment of operation of energy system of serial reliability structure on the example of ship main propulsion system,' Journal of Polish CIMAC, vol. 3, no. 2, 2008.

33. J. Rudnicki, 'Quantitative assessment of operation of ship main diesel engine,'IV International Conference on Computational Methods in Marine Engineering, Lisbon 2011.

34. B. F. Schutz, An introduction to general relativity theory. PWN. Warsaw 2002 (in Polish).

35. M. Tempczyk, Chaos Theory for the Brave. PWN. Warsaw 2002 (in Polish).

36. M. White and J. Gribbin, Einstein. A Life in Science. WNT. Warsaw 1995 (in Polish).

37. C. M. Wynn and A. W. Wiggins, The Five Biggest ideals in Science. Prószyński S-ka. Warsaw 1998 (in Polish).

38. B. Żółtowski, Fundamentals of Machine Diagnostics. University of Technology and Agriculture. Bydgoszcz 1996 (in Polish).

39. B. Żółtowski and C. Cempel, Eds., Engineering of Machine Diagnostics. The Polish Association of Technical Diagnostics. Radom Institute for Sustainable Technologies. Warsaw, Bydgoszcz 2004 (in Polish).

40. J. Kiciński, Ed., Modeling and Diagnostics of Mechanical, Aerodynamic and Magnetic in Power Turbine Units. Institute of Fluid-Flow Machinery Polish Academy of Sciences. Gdańsk 2005 (in Polish).

POLISH MARITIME RESEARCH 1 (117) 2023 Vol. 30; pp. 120-128
10.2478/pomr-2023-0065

HUMAN RESOURCE MANAGEMENT DIGITALISATION IN MULTIDISCIPLINARY SHIP DESIGN COMPANIES

Piotr Bilon
Wojciech Litwin
Gdansk University of Technology, Institute of Naval Architecture, Gdansk, Poland

* Corresponding author: *pb@wayman.software (Piotr Bilon)*

ABSTRACT

The digitalisation in the ship design sector is currently applied to the design process itself and is well defined, partially standardised and practically implemented by both independent design companies and the design departments of shipyards. The situation is similar in other sectors of engineering. However, the requirements for the digitalisation of other processes in design and engineering companies have not previously been studied, and the limited financial resources of ship design companies mean that there is a need for research on the digitalisation needs of multidisciplinary ship design companies. The implementation of building information modelling (BIM) solutions is costly for design companies and generates benefits mainly for shipyards and shipowners. The lack of benefits for design companies leads to the hesitation of managers whenever digitalisation is considered; the scope and scale of the digitalisation, as well as the selected software and BIM level, are defined by the shipyard requirements. The participation and support of management in the digitalisation process is one of the key success factors; the expected benefits caused by digitalisation for the organisation will increase the motivation of managers to invest limited resources in digitalisation. There are no data that indicate the processes with a high potential for digitalisation and the scale of expected improvements in ship design companies; therefore, research in this area was performed with a group of project managers from design and engineering companies. The research focused on collecting the opinions and experiences of the managers related to the manual management of resources and comparing the poll results with the conclusions from the enterprise resource planning (ERP) system data analyses. The paper analyses if the digital automation of the resource management process can lead to the substantial improvement of the operations of multi-project, multidisciplinary engineering ship design companies.

Keywords: Ship design human resource management, digital automation, project portfolio, multidisciplinary engineering, ship design, marine engineering

INTRODUCTION

All sectors of engineering are experiencing an intensive digitalisation process [1]; this applies to the marine [2], infrastructure, industrial, plant design, architecture engineering construction (AEC) and mechanical sectors [3]. The implementation of software solutions for design and engineering companies brings numerous benefits [4], and in most cases it leads to substantial efficiency improvements [5]; however, it generates a number of risks [6], especially when the organisation is not ready for implementation [7]. The impact of digitalisation is clearly visible in the design system area and the design of data management systems [8]. Change itself, for engineers, is an integral part of the iteration design process, which is usually turbulent due to the constant modifications [9]. Considering a business point of view, there should be a justification for a change, and usually there are good economic reasons to make a change [10].

The direct costs of the software, implementation, training and changes are covered by the design and engineering companies, which can be the reason that in the short term, digitalisation can be considered an unfavourable change. Another challenge for the design and engineering sector is the globalisation of services and distributed design networks. There is the possibility of easy cooperation with designers from different time zones and countries with lower cost levels, which is not always is beneficial in terms of quality [11].

The subject of project planning and execution is strongly connected with resource management [12], and for companies facing aggressive competitors from low-cost countries, the possibility of increasing the effectiveness of the organisation and simultaneously reducing management costs by lowering the amount of time required by the management process, which often involves highly experienced and expensive experts [13], [14], might be an interesting area to explore. It is interesting from the scientific point of view to understand the current solutions used by design and engineering companies to manage resources and how much of the project budget, in terms of time and financial resources, is utilised for management [15]. Data-driven analyses could provide answers that could be compared with the managers' individual opinions, which can be collected using a poll.

The conducted review of scholarly publications revealed a lack of studies specifically targeting human resource management processes in marine design firms; however, a prevalent recommendation among researchers in the domain of project portfolio management and its human resource management sub-process is to conduct inquiries within distinct engineering sectors, thereby catalysing research endeavours within the marine design firm sector. A good example of both multidisciplinary and diversified engineering activity is the ship design sector. Based on the matrix organisation structure, design and engineering companies are simultaneously performing several projects, facing a large number of changes [16]. In these circumstances, design and engineering resource management becomes a crucial foundation of competitiveness and the key to business and technical success [17]. High-level digitisation results in an increase in the design process' economic efficiency by improving internal procedures and eliminating manual activities [18]. The implementation of available software solutions allows the top management of engineering design companies to focus on the decision-making process [19]. In Fig. 1, a graphical representation of the scope of the multidisciplinary exhaust gas system conversion project developed by one of the Wayman software users is shown.

Fig. 1. Visualisation of the BIM model of the exhaust gas system of the cargo vessel

The greater the scale of the disturbances generated by changes, the more justified it will be to develop and implement digital solutions that support the process of continuous management [20]. The scale of the problem and the potential for improvement need to be determined [21]. The reduction of the management time and a faster decision-making process can generate benefits in the organisation and leverage the efficiency of the engineering departments. In examining the need for innovative solutions in human resource management for engineering and design projects, especially under conditions of change and uncertainty, the work by Litwin, Piątek, Leśniewski and Marszałkowski on the design and implementation of a hybrid propulsion system in a 50' sail catamaran provides a relevant example [22]. Their approach in effectively balancing multiple design criteria and navigating through complex engineering challenges underlines the importance of adaptive and forward-thinking strategies in project management. This aligns closely with our discussion on the necessity of rapid and flexible planning in human resource allocation, where the goal is to efficiently manage resources in the face of evolving project requirements, much like the multi-dimensional optimization challenges tackled in their yacht design project. Also the innovative approach detailed by Branowski, Zabłocki, Kruczewki and Walczak in their study on the universal design of yachts for people with disabilities demonstrates the necessity of adaptable design solutions that cater to diverse user needs, mirroring our discussion on the need for flexible and responsive human resource planning in engineering projects, where diverse and changing requirements must be met efficiently and effectively [23].The expected improvements might be a good justification for investments and the implementation of new solutions, and the solution selection process is an interesting subject in itself [24]. Current global trends in design and engineering companies lead to the conclusion that an increase in the subsidiary processes in the organisation and IT tool integration should lead to an increase in efficiency and collaboration; digitalisation is an obvious next step for the construction and shipbuilding industry [20]. As the implementation of the core business-related building information modelling (BIM) software generates the majority of profits for the end customer, the construction company [25], the management personnel of the independent design and engineering companies strive to cut the costs and time consumed by their own work [26]. Fig. 2 shows a visualisation of the complex multidisciplinary scope of the Ro-Pax vessel exhaust gas system developed by one of the Wayman users using the BIM software.

Fig. 2. Visualisation of the scope of a complex multidisciplinary exhaust gas modification for a Ro-Pax vessel

Among the subsidiaries of the core business process, those that require higher time and resource levels should be prioritised, and the available resources should be allocated to the implementation of the most promising solutions from a business point of view [17]. In order to be able to properly define the priorities and the scale of the potential positive impact on the organisation, it is necessary to understand the current state of the art and the resource management activity level [27]. This article describes results from the first iteration of research related to the changes initiated by the continuous resource management process in design and engineering companies. The goal of the enterprise resource planning (ERP) system database analysis, performed in parallel to the questionnaire research, was to collect and analyse the data registered in the ERP used by the design and engineering companies in order to understand how time and resources are consumed in the resource management process. It is expected that project management activities in ship design companies consume around 20% of the project budget, and 70 to 80% of the management budget is consumed by human resource management activities. Moreover, the poll made it possible to understand managers' opinions on the resource management process and the tools used among the various design and engineering sectors.

METHODS

The thesis, which boils down to the statement that the management of design and engineering resources is one of the key areas that needs to be digitised, leading to the need to eliminate manual management activities, has been verified in a selected community of medium-level managers of selected design and engineering companies in Poland. As part of the research, using anonymous questionnaires, information was collected from 1283 design and engineering company employees on how the problem of resource management is perceived, and the content of the databases containing information on the labour intensity of manual management activities was analysed. The analysed databases were not prepared for research and were taken directly from the production IT structure of the 20 engineering companies operating in the ship design, infrastructure, offshore, infrastructure and oil and gas sectors. The environment was not prepared in order to precisely collect data related to manual management.

Due to the standardisation of the nomenclature, the numbering of the activities performed and the possibility of importing data from various software systems, it was achievable to combine data from various design companies operating in various engineering sectors in order to compare and analyse the results. The first research step was to build an anonymous questionnaire that made it possible to obtain information relevant to the analysis of the problem. The link to the research was sent to managers of design companies using one of the most popular ERP systems in Poland used for managing multi-sector engineering companies. Courtesy of the software vendor of our own developed-in-house ERP software, a customer communication channel was used to promote and deliver a request to complete the questionnaire. Due to the need to protect the identities of users, the surveys were anonymous. The accessibility of a large number of design company managers and the serious approach to the research supported by the software vendor, which distributed the survey through official software vendor communication channels, justify the selection of the questionnaires as a research method. The survey research duration was 14 months.

The first group of questions in the survey was used to determine the characteristics of the enterprise in which the surveyed person is employed. Information was collected on the scale of the company, the engineering sector, the types of industries, the applied solutions supporting management and the share of the labour intensity devoted to manual management in the budget for project management and in the overall budget of the project. It is important to underline that budgets were examined in both hourly and financial terms.

In order to initially verify the validity of the thesis, the opinions of the respondents were examined to confirm the problem of a lack of digital resource management and to determine its significance and the possible impact of eliminating manual management. As part of the parallel study, the databases of ERP system users were downloaded and analysed in a way that allowed the results obtained by processing the data reported to the ERP system to be compared with the responses provided by the respondents. The ERP system dedicated to engineering made it possible to define task dictionaries, use a unified numbering of tasks for all projects and assign tasks to appropriate groups, as well as to use any attributes to group and process data and information. Such attributes can distinguish to some extent the hours allocated to manual management activities and other management activities.

The ERP systems used in the design and engineering companies require employees to be assigned to precisely defined roles. Based on this feature, it is possible to identify the users responsible for resource management activities. Typically, management tasks are performed by middle-level management experts (department managers, project managers, discipline leaders, leading engineers) who can be generally classified as the employees who are permanently or temporarily responsible for teams of designers or for tasks performed by a group of people. It is a common practice that each employee is obliged to record the amount of time spent on certain tasks. This makes it possible to collect information about who is doing what, compare the plan and the reality and easily calculate the cost of the work. In spite of the fact that there are local, national and corporation-wide standards for defining the tasks, there is no universal task-defining policy. Therefore, it is important to verify to which object in each analysed database the time consumed by resource management is registered.

RESULTS

Descriptive analyses of the survey results were used for the analysis of the questionnaire responses. Four hundred and thirty (430/1283) of the questionnaire respondents are employed in the ship design sector. Ship design sector representatives are the largest group of respondents in the research, and 1187 respondents confirmed that they are employed by design and engineering companies. This high conversion rate was achieved through cooperation with a dedicated ERP software vendor for the design and engineering sector. In the group mentioned above, 70% (893/1283) of the respondents declared that resource management is performed manually using spreadsheets, and the remaining managers also use the resource load matrix, which is available in popular project planning and management programs. Considering the impact of manual resource management on the consumption of the hourly budget dedicated to management activities, over 86% of respondents (1105/1283) believe that manual management activities consume 75% or more of the available time. According to the respondents, the cost of manual resource management also remains high; 79% of survey participants (1010/1283) believe that on average, more than 75% of the costs allocated to project management go to manual management. This is a value slightly lower (1010 vs 1105) than the number of hours spent on the manual management of the hourly budget, but due to the fact that some activities related to manual management can be delegated to staff with lower competencies, the values declared by the respondents seem to be consistent. The analysis of the results of the study in terms of the impact of manual resource management on the budget of the entire project, in terms of both the hourly and financial budgets, indicates that the majority of respondents define the share of activities related to manual resource management to be at the level of at least 10%, in both hourly and financial terms.

In the case of one company, it was possible to identify the date when the resource planning procedures were migrated from manual management using spreadsheets to a resource matrix in the planning/project management software. The organisation was performing, at the same time, a large amount of exhaust gas conversion multidisciplinary projects that, according to the company's management, were similar in terms of the scope and level of design process disturbances. Before the implementation of the planning procedure, the consumption was 2834 hours (2398 on design and 436 on management); the scope of the work of the referenced project is presented in Fig. 1. After the implementation of the planning procedure, the consumption on a similar project was 2140 hours (1820 for design and 320 on management); the graphical representation of the scope of the work of this project is presented in Fig. 2. The results are shown in Fig. 3.

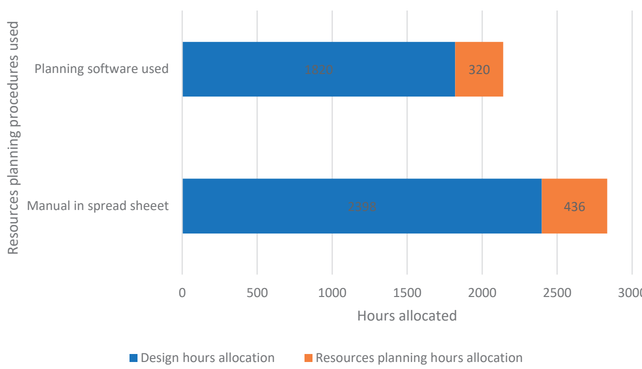

Fig. 3. Comparison of the time consumption (in hours) before and after the implementation of the planning procedure

Most of the respondents (1242/1283, or 93%) define the elimination of manual resource management as an important aspect of improving the efficiency of a design company and state that they develop several variants of future plans as part of manual management, while 75% of all respondents (957/1283) state their interest in a software solution that supports the preparation of future variants to support the resource management process in a design and engineering company. The combined results are presented in Table 1.

Tab 1. ERP software user questionnaire results

1. Can you describe your company as a design and engineering multidisciplinary corporation?			
No.	Answer	Res.	%
1.1.	Yes	1187	93%
1.2.	No	96	7%
2. Please indicate your sector of engineering			
2.1.	Marine (ship design)	430	34%
2.2.	Infrastructure	356	28%
2.3.	AEC	120	9%
2.4.	Plant design	257	20%
2.5.	Airspace	7	1%
2.6.	Energy	113	9%
3. Please indicate the methodology of resources management in your organization			
3.1.	Manual in spreadsheet	893	70%
3.2.	In resources matrix in planning/project management software	387	30%
3.3.	In dedicated automated resources management software	0	0%
3.4.	Other	3	0%
4. How big is the % of the hourly budget for project management consumed on resources management?			
No	Answer	Res.	%
4.1.	<25%	0	0%
4.2.	<50%	178	14%
4.3.	<75%	673	52%
4.4.	Other	432	34%
5. How big is the % of the financial budget for project management consumed on resources management?			
5.1.	<25%	0	0%
5.2.	<50%	273	21%
5.3.	<75%	437	34%
5.4.	Other	573	45%
6. How big is the % of the project hourly budget consumed on resources management?			
6.1.	<5%	767	60%
6.2.	<10%	389	30%
6.3.	<15%	124	10%
6.4.	Other	3	0%
7. How is the % of the project management financial budget consumed on resources management?			
7.1.	<5%	17	1%
7.2.	<10%	697	54%
7.3.	<15%	565	44%
7.4.	Other	4	0%
8. How big is the impact of resources manual management elimination on the efficiency of engineering company?			
8.1.	Critical	671	52%
8.2.	Significant	571	45%
8.3.	Minor	32	2%
8.4.	No impact at all	9	1%
9. Do you prepare several variants of resources management projection?			
9.1.	Always	25	2%
9.2.	When requested and when I feel it is needed	654	51%
9.3.	When requested	595	48%
9.4.	No, never, it is useless	9	1%
10. Would you be willing to use the software tool for automated resources management even if it creates only variants for consideration?			
10.1.	Yes	957	75%
10.2.	No	258	20%
10.3.	I do not know	68	5%

For some companies, manual management is just a part of general department management; it might be registered as a general management task, just like periodical project meetings and even quality control activities. This means that in this first iteration of the research, the assignment of tasks to the appropriate category may be imprecise, due to the fact that the users of the ERP system did not use attributes that clearly define tasks for managers for tasks related to manual management. This caused the need to manually review each stage of the selected projects and each task in order to manually assign the tasks and the hours allocated to each task to the proper group. On the other hand, an unambiguous result is that 18–27% of the financial budget and 22–28% of the hourly budget were used for activities related to the management of project work and resources; this is applicable to virtually all engineering sectors. Considering these numbers in the context of the average margins on design and engineering services should focus the attention of employees responsible for business efficiency on this particular area of the company's operations.

DISCUSSION

The subject of project portfolio selection and management is of scientific interest, and it is gaining momentum when it comes to the number of publications on the topic. Currently, researchers are exploring the area of decision support systems, and the trend is to develop more management-oriented solutions, as the usefulness of elegant and sophisticated mathematical methods is often questioned [28]. Within the area of ship design and engineering management activities, including engineering resource management, real-life managers, who face a limited amount of available time and an urgent need to make decisions, always prefer the tools that reduce the time required by a decision-making process over the complex methods that require the participation of an expert in order to be useful in real-life cases. The ship design sector tends to migrate from the area where activities are balanced among art, science and handcrafted approaches [29] to less creative approaches, where designers use computational methods and computer-based models.

The same research shows, in its onion model, that currently, research related to project portfolio management is focused on coping with change and uncertainty [28]. Considering the frequency of change in project portfolios, the ability to predict the future is urgently required [30]. In terms of human resource allocation in engineering, predicting the future is naturally impossible, but the concept behind the research presented in this article is the real need for a quickly available list of variants of future human resource allocation created on the basis of parameters that are easy to define for managers. The goal in this respect is not to create the optimal solution as it would lead to the infinitive number of Pareto optimal solutions, but to provide input data for decision maker to make a rational decision about the future plan of resources allocation. In addressing the complexities of human resource allocation in engineering, particularly under the constraints of unpredictability and the need for rapid adaptation, the principles outlined in Pawlusik, Szłapczyński, and Karczewski's study on optimizing rig design for sailing yachts using an evolutionary multi-objective algorithm [31] offer valuable insights. Their approach in handling multiple, often conflicting objectives through multi-objective optimization and multi-criteria decision making provides a pertinent framework for our discussion on managing dynamic project portfolios and resource allocation in engineering firms. Their methodology underscores the importance of balancing various factors, a concept that is integral to our analysis of efficient and flexible human resource planning in the face of change and uncertainty.

The current state of the art related to project portfolio resource management is presented by Hollister and Watkins [32]. They specified seven causes of the resource overload problem: impact blindness, multiplayer effects, political logrolling, unfunded mandates, band-aid initiatives, cost myopia and finally initiative inertia. In the same article, the authors provide a recipe for practically solving the project portfolio resource overload problem, and they share an interesting result of the research related to the scale of the involvement of managers in initiatives that are non-productive and not directly related to business, which reached 30% of the overall time. In the described example, the company implemented a process for the manual review of plans and selected the variant that allowed them to complete the top-priority projects and allocate more time and resources to business-related activities. The organisation described by Hollister and Watkins was a retail company that faced resource overload and the incorrect allocation of resources. For the design and engineering sector, the scale of project portfolio-related turbulence is much higher and turbulence occurs much more frequently compared to the example of the retail company. The available data and the ability to create variants of the future with various assumptions and priorities are obtainable but time-consuming. The scale of the difficulty and the involvement of managers in the resource management process in design and engineering companies has not previously been a subject of research; therefore, our research had the goal of verifying the scale of the involvement based on the available data and the opinions of the managers.

In this study, the results of research from two sources, databases and the subjective opinions of the surveyed managers of design and engineering companies, were compared. Currently, there is no data available from the wider design and engineering sector that could be compared to the results achieved. At the time that this research began, there was no synthetic information in the analysed customer databases that would allow one to determine the actual workload for activities related to manual resource management; however, it was possible to determine the total costs of project management based on hard data, registered working hours and the hourly rates of the reporting persons.

At the same time, the subjective assessments of managers regarding the share of activities related to manual resource management of the overall budget for project management, which oscillated around 70% of the budget, indicate that resource management is an area of interest and probably has the potential for both direct and indirect cost reductions. Considering the justification for this research and the actions leading to the digitalisation of human resource management in maritime engineering design firms, it is vital to focus not just on the benefits generated for the organisation itself, which stem from the anticipated reduction in the amount of time dedicated to human resource management tasks. It is equally crucial to emphasise the broader advantages, which will include enhanced quality, more efficient budget utilisation, the swifter development of value-driven projects and a more effective execution of engineering services.

As the database content does not allow the comparison of data at the same level of detail, it is worth focusing on the results obtained from the surveyed managers. It is remarkable that in design and engineering companies, according to the majority of respondents, 70% of management work is still done manually. This result is naturally surprising, especially when the number of changes and modifications that affect project implementation plans in shipbuilding, and also in other sectors of engineering, is considered. Reducing the amount of time spent on manual management decreases the direct costs of management, and most importantly, assuming that a faster transfer of guidelines to the project team results from the reduced management execution time, increases efficiency by shortening the circulation time of the decision loop.

CONCLUSIONS

The analysis of the results leads to the conclusion that the development of solutions that support the management of human resources in engineering and design companies may address the essential needs of managers and increase the efficiency of a company's work. Shortening the reaction time to changes can lead to the reduction of numerous risk elements, which can increase the company's competitiveness and the efficiency of engineers' work. The effort to minimize the time needed for preparing new project in shipbuilding is widely visible in the actions taken in other areas of ship design and shipbuilding for example application of reverse engineering in part design [33]

The responses of the respondents show the importance of the management topic and the perceived need to spend a large amount of time on management, with a simultaneous careful approach to the topic of preparing many variants of future projections, especially in terms of possible management variants. The great interest of managers in the application for the preparation of management variants also shows that the topic is worth further exploration and is one of the areas of operation of an engineering design company that is probably difficult to learn using classic manual methods.

The results of the research conducted lead to the conclusion that the analysed area has the potential to be improved; the activities related to the management of resources can be classified as problematic for managers, while the currently used methods involve numerous risks and are ineffective.

The opinions of a selected group of managers indicate that further exploration of data collected in ERP systems is justified and may lead to a more reliable and transparent picture of the situation, provided that the collected data are properly prepared. Users should be properly motivated to increase the amount of detail in their reporting to allow a precise understanding of the time spent on management and the preparation of future variants. The binary data that have been analysed so far have not been prepared in a way that allows the proper identification of resource planning-related activities and the separation of the planning budget from other management activities; therefore, in the future, an effort must be made to organise the database structure in order to make it possible to report resource planning hours for separate objects.

The short-term prospect can lead to the wrong conclusions, but competitiveness, or even remaining active on the engineering market, is not possible without modern design tools. Therefore, digitalisation for design and engineering companies is a part of reality that managers have to cope with, face and cover the costs of.

The objective of the research described in this article has been partially achieved. Over a 14-month period of survey research, 1283 responses were obtained; based on the content analysis of databases from ship design companies, these responses confirmed that over 20% of a project's hourly budget is allocated to management-related activities. The survey research further revealed that 86% of the surveyed project company managers believe that 75% of the time dedicated to project management activities is spent on human resource management tasks. However, it was not possible to reliably confirm these assertions, due to the lack of the precise definition of activities belonging to the set of tasks related to human resource management. This implies that in the future, there is a need to assign clear attributes to tasks associated with human resource management. Another significant conclusion is the confirmation of both a reduction in the hourly budget for project work and the budget allocated for project management after the introduction of a system that supported management. This suggests that potential further benefits in this area could be achieved through automation and the use of AI algorithms for human resource management in maritime engineering design firms.

REFERENCES

1. A. Ghosh, D. J. Edwards, and M. R. Hosseini, "Patterns and trends in Internet of Things (IoT) research: future applications in the construction industry," *Engineering, Construction and Architectural Management*, vol. 28, no. 2. 2021. doi: 10.1108/ECAM-04-2020-0271.

2. R. Iwańkowicz, "A Multi-Case-Based Assembly Management Method for the Shipbuilding Industry," *Polish Maritime Research*, vol. 28, no. 2. 2021. doi: 10.2478/pomr-2021-0018.

3. V. Koscheyev, V. Rapgof, and V. Vinogradova, "Digital transformation of construction organizations," in *IOP Conference Series: Materials Science and Engineering*, 2019. doi: 10.1088/1757-899X/497/1/012010.

4. J. Berlak, S. Hafner, and V. G. Kuppelwieser, "Digitalization's impacts on productivity: a model-based approach and evaluation in Germany's building construction industry," *Production Planning and Control*, vol. 32, no. 4, 2021, doi: 10.1080/09537287.2020.1740815.

5. Q. K. Jahanger, J. Louis, C. Pestana, and D. Trejo, "Potential positive impacts of digitalization of construction-phase information management for project owners," *Journal of Information Technology in Construction*, vol. 26, 2021, doi: 10.36680/j.itcon.2021.001.

6. B. R. K. Mantha and B. García de Soto, "Assessment of the cybersecurity vulnerability of construction networks," *Engineering, Construction and Architectural Management*, vol. 28, no. 10, 2021, doi: 10.1108/ECAM-06-2020-0400.

7. S. Demirkesen and A. Tezel, "Investigating major challenges for industry 4.0 adoption among construction companies," *Engineering, Construction and Architectural Management*, vol. 29, no. 3, 2022, doi: 10.1108/ECAM-12-2020-1059.

8. Jan Koeleman, Maria João Ribeirinho, David Rockhill, Erik Sjödin, and Gernot Strube, "Decoding digital transformation in construction," *McKinsey & Company*, no. August, 2019.

9. Z. Wang and J. Liu, "A Seven-Dimensional Building Information Model for the Improvement of Construction Efficiency," *Advances in Civil Engineering*, vol. 2020, 2020, doi: 10.1155/2020/8842475.

10. S. Parusheva, "Digitalization and Digital Transformation in Construction – Benefits and Challenges," *Proceedings of the International Conference dedicated to the 50th anniversary of the Department of Informatics, University of Economics, Varna*, 2019.

11. L. Zheng, W. Lu, K. Chen, K. W. Chau, and Y. Niu, "Benefit sharing for BIM implementation: Tackling the moral hazard dilemma in inter-firm cooperation," *International Journal of Project Management*, vol. 35, no. 3, 2017, doi: 10.1016/j.ijproman.2017.01.006.

12. M. Rauf, Z. Guan, L. Yue, Z. Guo, J. Mumtaz, and S. Ullah, "Integrated Planning and Scheduling of Multiple Manufacturing Projects under Resource Constraints Using Raccoon Family Optimization Algorithm," *IEEE Access*, vol. 8, pp. 151279–151295, 2020, doi: 10.1109/ACCESS.2020.2971650.

13. R. Moser, G. Narayanamurthy, K. Kusaba, and G. Kaiser, "Performance of low-cost country sourcing projects – Conceptual model & empirical analysis," *Int J Prod Econ*, vol. 204, pp. 30–43, Oct. 2018, doi: 10.1016/j.ijpe.2018.07.011.

14. H. Abbasianjahromi and S. Hosseini, "A risk-cost optimization model for selecting human resources in construction projects," *SN Appl Sci*, vol. 1, no. 11, 2019, doi: 10.1007/s42452-019-1570-5.

15. B. Ashuri and M. Tavakolan, "Shuffled Frog-Leaping Model for Solving Time-Cost-Resource Optimization Problems in Construction Project Planning," *Journal of Computing in Civil Engineering*, vol. 29, no. 1, Jan. 2015, doi: 10.1061/(asce)cp.1943-5487.0000315.

16. E. Acar, G. Bayrak, Y. Jung, I. Lee, P. Ramu, and S. S. Ravichandran, "Modeling, analysis, and optimization under uncertainties: a review," *Structural and Multidisciplinary Optimization*, vol. 64, no. 5. 2021. doi: 10.1007/s00158-021-03026-7.

17. S. Saeed, M. A. Khan, and R. Ahmad, *Business strategies and approaches for effective engineering management*. 2013. doi: 10.4018/978-1-4666-3658-3.

18. M. Fusko, Ľ. Dulina, P. Bubeník, M. Bučková, M. Kasajová, and R. Svitek, "THE IMPORTANCE OF DIGITIZATION AND INNOVATIONS FOR SMALL AND MEDIUM-SIZED ENTERPRISES," *Proceedings of CBU in Economics and Business*, vol. 2, 2021, doi: 10.12955/peb.v2.252.

19. M. Winfield, "Construction 4.0 and ISO 19650: A panacea for the digital revolution?," *Proceedings of Institution of Civil Engineers: Management, Procurement and Law*, vol. 173, no. 4, 2020, doi: 10.1680/jmapl.19.00051.

20. M. Eigner, "Engineering 4.0—Foundations of the Digitalization of Engineering," in *System Lifecycle Management*, 2021. doi: 10.1007/978-3-658-33874-9_3.

21. M. Müller and L. Jedličková, "Several Notes on the Existential Hermeneutic Phenomenology for Project Management and Possibilities of Its Extension by Other Existential Concepts: Case Study From the Research Project Team," *Project Management Journal*, vol. 51, no. 4, pp. 452–463, Aug. 2020, doi: 10.1177/8756972820910280.

22. W. Litwin, D. Piątek, W. Leśniewski, and K. Marszałkowski, "50' Sail Catamaran with Hybrid Propulsion, Design, Theoretical and Experimental Studies," *Polish Maritime Research*, vol. 29, no. 2, 2022, doi: 10.2478/pomr-2022-0012.

23. B. Branowski, M. Zabłocki, P. Kurczewski, and A. Walczak, "Selected Issues in Universal Design of Yachts for People with Disabilities," *Polish Maritime Research*, vol. 28, no. 3, 2021, doi: 10.2478/pomr-2021-0030.

24. L. Venz, A. Pundt, and S. Sonnentag, "What matters for work engagement? A diary study on resources and the benefits of selective optimization with compensation for state work engagement," *J Organ Behav*, vol. 39, no. 1, 2018, doi: 10.1002/job.2207.

25. J. Bin Yang and H. Y. Chou, "Subjective benefit evaluation model for immature BIM-enabled stakeholders," *Autom Constr*, vol. 106, 2019, doi: 10.1016/j.autcon.2019.102908.

26. L. Rihar, T. Žužek, and J. Kušar, "How to successfully introduce concurrent engineering into new product development?," *Concurr Eng Res Appl*, vol. 29, no. 2, pp. 87–101, Jun. 2021, doi: 10.1177/1063293X20967929.

27. N. Bibi, Z. Anwar, and A. Ahsan, "Comparison of search-based software engineering algorithms for resource allocation optimization," *Journal of Intelligent Systems*, vol. 2015, pp. 629–642, 2015, doi: 10.1515/jisys-2015-0016.

28. L. K. Hansen and P. Svejvig, "Seven Decades of Project Portfolio Management Research (1950–2019) and Perspectives for the Future," *Project Management Journal*, vol. 53, no. 3, pp. 277–294, 2022, doi: 10.1177/87569728221089537.

29. A. Karczewski and J. Kozak, "A Generative Approach to Hull Design for a Small Watercraft," *Polish Maritime Research*, vol. 30, no. 1, pp. 4–12, 2023, doi: 10.2478/pomr-2023-0001.

30. P. F. Drucker, E. Dyson, C. Handy, P. Saffo, and P. M. Senge, "Looking ahead: implications of the present.," in *Harvard business review*, 1997.

31. M. Pawłusik, R. Szłapczyński, and A. Karczewski, "Optimising Rig Design for Sailing Yachts with Evolutionary Multi-Objective Algorithm," *Polish Maritime Research*, vol. 27, no. 4, 2020, doi: 10.2478/pomr-2020-0064.

32. R. Hollister and M. D. Watkins, "Too many projects," *Harvard Business Review*, vol. 2018, no. September-October. 2018.

33. M. Deja, M. Dobrzyński, and M. Rymkiewicz, "Application of Reverse Engineering Technology in Part Design for Shipbuilding Industry," *Polish Maritime Research*, vol. 26, no. 2, 2019, doi: 10.2478/pomr-2019-0032.

POLISH MARITIME RESEARCH 1 (117) 2023 Vol. 30; pp. 129-147
10.2478/pomr-2023-0066

STRATEGIES FOR DEVELOPING LOGISTICS CENTRES: TECHNOLOGICAL TRENDS AND POLICY IMPLICATIONS

Minh Duc Nguyen
Faculty of Economics, Vietnam Maritime University, Haiphong, Viet Nam
Ko Tae Yeon
Heesung Electronics Vietnam Limited Company, Viet Nam
Vietnam Maritime University, Haiphong, Viet Nam
Krzysztof Rudzki
Gdynia Maritime University, Faculty of Marine Engineering, Gdynia, Poland
Hoang Phuong Nguyen
Academy of Politics Region II, Ho Chi Minh city, Viet Nam
Nguyen Dang Khoa Pham*
PATET Research Group, Ho Chi Minh City University of Transport, Ho Chi Minh city, Viet Nam

* Corresponding author: *khoapnd@ut.edu.vn (Nguyen Dang Khoa Pham)*

ABSTRACT

Logistics centres are currently performing a key function in the development of countries through their ability to regulate goods, markets, and transport. This is shown by the infrastructure, cost, goods flow, and quality of logistical services provided by these centres. Nevertheless, in developing nations or regions with antiquated logistics infrastructure, conventional logistics centres seem to struggle to manage the volume of commodities passing through them, resulting in persistent congestion and an unsteady flow of goods inside these facilities. This issue poses a challenge to the progress of any nation. The emergence of new technology offers a potential avenue to solve the problems inherent in traditional logistics centres. Most prominently, four technologies (the Internet of Things (IoT), Blockchain, Big Data and Cloud computing) are widely applied in traditional logistics centres. This work has conducted a thorough analysis and evaluation of these new technologies in relation to their respective functions and roles inside a logistics centre. Furthermore, this work proposes difficulties in applying new technologies to logistics centres related to issues such as science, energy, cost, or staff qualifications. Finally, future development directions, related to expanding policies in technological applications, or combining each country's policies for the logistics industry, are carefully discussed.

Keywords: Logistics centers, logistics infrastructure, logistical services, smart technologies

INTRODUCTION

An important topic for the growth of the world's economy and contemporary society is digitalisation. Continual expansion and long-term welfare are cited as essential drivers of successful digitalisation efforts. Therefore, government programmes that seek to develop innovation capacity, increase productivity, decrease costs, increase revenues, improve preparation for the digital era, and strengthen competitive advantages are regularly used to promote digitalisation goals within businesses. The term 'Industry 4.0' frequently refers to a wide range of digitalisation methods, approaches, and technologies because it largely focuses on applications in the industrial environment. Because of this, the application sectors range from enhancing material flows to buildings, manufacturing, and product development. These programmes should help industrial organisations achieve their objectives, including higher competitiveness based on open processes, more agility, improved adaption, and increased flexibility.

The initial commercial practices and academic studies on disruptive technologies are still very much relevant in today's society. Disruptive technologies were also the foundation of modern business models like Amazon and Flipkart, since they outperform incumbent technologies, in terms of productivity, efficiency, and convenience [1]. The Internet of Things (IoT), for instance, completely replaced warehouse and inventory management through a precise combination of supply hubs, transportation, and customer handling system, which was a boost for e-commerce industries. As a result, IoT could offer more individualised, responsive, and novel or unconventional customer service, in addition to decreased operational costs [2]. The Internet of Things is anticipated to play a significant role in the logistics sector in the near future. It is also evident that many objects and items have already begun to carry or tag bar codes, RFID tags, and sensors, bringing geospatial data and allowing tracking of a variety of goods and merchandise through a single supply chain from any location [3]. Primarily, there are three schools of thought with respect to the IoT [4]: (i) Things oriented, which aims to improve things like object traceability and the ability to understand their current location or status; (ii) Internet-oriented, which seeks to improve network protocols like the Internet Protocol, which is seen as the network technology to connect smart objects all over the world; and (iii) Semantic oriented, which centres on issues of meaning and context [5]. In addition to IoT, other new technologies have also begun to become more prominent during this period, such as Big Data, Blockchain, AI, etc. Each technology has different functions that are combined in an industry, thereby helping the industry develop strongly in all respects [6][7]. The logistics industry is no exception to this development; hence, the use of 4.0 technologies has transformed logistics into a strategic tool for gaining a competitive edge, shifting its perception from a simple financial burden to a valuable asset [8]. Table 1 presents a comprehensive compilation of definitions of Industry 4.0 technologies that have been specifically implemented in industrial environments.

Tab. 1. Definition of outstanding 4.0 technologies [9]

4.0 Technology	Definition	Ref
Internet of Things (IoT)	The implementation of sensors and devices that are networked through wireless networks and Internet-based interaction with the objective of enhancing the value of products and processes.	[10][11][12][13]
Blockchain	The digital platform facilitates the safe storage and distribution of information across a collective of users via the creation of time-stamped, tamper-proof, and indefinitely lasting records. The system comprises decentralised ledgers that store transactions as data blocks, which are interconnected by a cryptographic pointer. The aforementioned system exhibits attributes such as distributed consensus, enhanced security measures, traceability, verification, and transparency of information.	[14][15][16]
Cloud Computing	The online service provides users with the ability to do rapid and streamlined calculations, without the need for establishing a tangible infrastructure. This technology facilitates the provision of computer resources, including networks, servers, storage, applications, and services, with the ability to access a network that is readily available, easily accessible, and beneficial. The outcome is a more economically efficient and expeditious resolution with regard to operational platforms, software, and infrastructures.	[17][18][10]
Big Data	The effective facilitation of decision-making processes is achieved via the management of a substantial amount of data, defined by its high volume, rapid velocity, and diversity. This is accomplished by using cutting-edge analytic approaches that are creative in nature.	[19][20][5]

The logistics industry is showing an increasing dependence on new technologies. Therefore, in order to fully capitalise on the potential of this industry, it is imperative to develop the 'Logistics 4.0' initiative, which aims to maximise the utilisation of cutting-edge technologies and implement innovative advancements in the logistics field [21]. Governments should aggressively push its 'Logistics Centre 4.0' strategy, starting with the logistics centre, which serves as the beating heart of logistics systems. As a result, the whole manufacturing sector, including its logistics, is transitioning to a paradigm that is more adaptable and agile, making room for Industry 4.0. According to Khatib et al. [22], the heart of Industry 4.0 consists of four primary enabling technologies that will increase the adaptability of manufacturing and distribution processes: robotics, Big Data, wireless networking, and inexpensive sensors. The interdependencies between the various 4.0 technologies are depicted in Fig. 1.

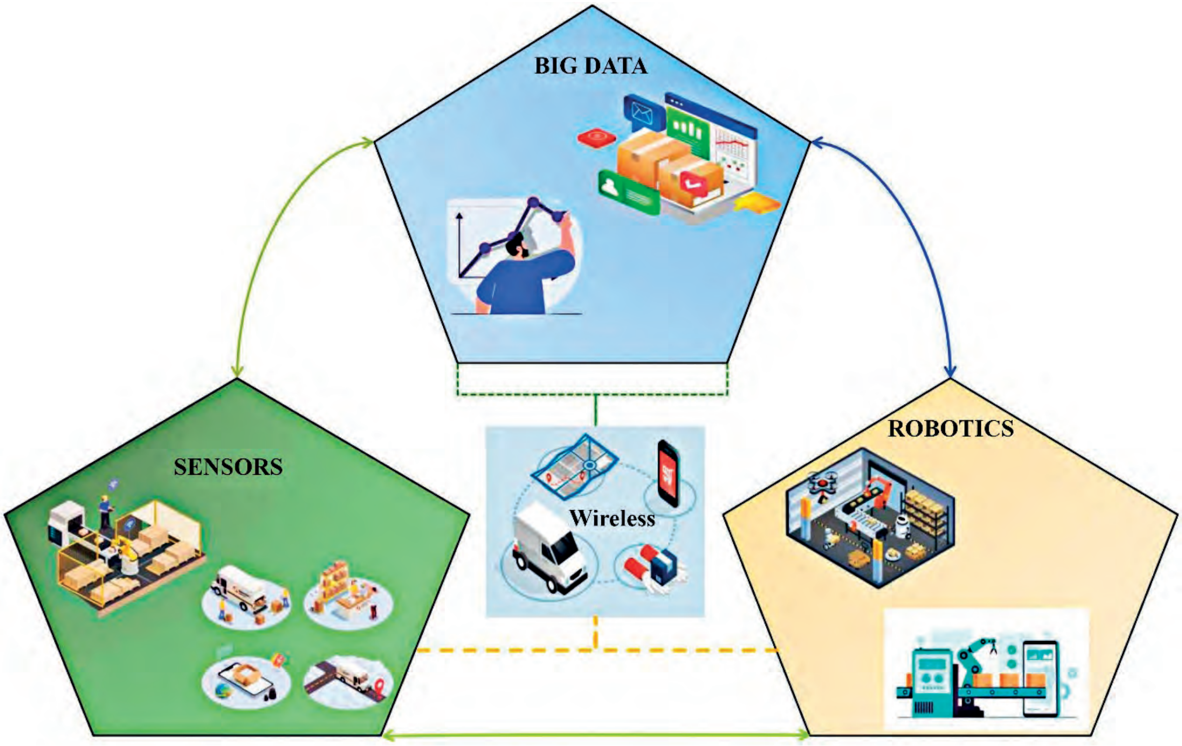

Fig. 1. Dependency between 4.0 technologies [22]

In the technologies mentioned above, IoT was acknowledged as one of the most significant fields of future technology and it is one of the key information and communication technologies (ICT). The IoT is quickly gaining ground in the context of contemporary wireless telecommunications, particularly with the rapid development of wireless communication technologies [23][24][25]. From an initial emphasis on machine-to-machine communication and applications in the 'ubiquitous aggregation' of data, the concept of IoT is continually changing. In other words, the IoT has generated vast amounts of data and various mathematical analytic methods can be used to continuously investigate the intricate links between the transactions represented by this data. Without a doubt, IoT would be crucial to the deployment of smart logistics [26][27], which would fundamentally alter the design of the logistics system and the logistical operation mode. These changes are very important in determining a company's competitiveness because logistics costs are seen as a significant component of overall production costs. Numerous businesses are thinking about how to operate their warehouses more cost-effectively and efficiently, especially in light of recent advancements in supply chain and logistics technology but there are also many businesses that are hesitant about applying smart technologies to a previously traditional infrastructure [28]. According to the public and academic literature, logistics centre management is a crucial component of the supply chain that has received increased attention, with the aim of meeting the rising freight demand and the increasingly high standards for logistics services [29]. In the last few decades, the warehouse and logistics centre business has experienced a remarkable development in major trading cities. Planners and social scientists have expressed concerns over the social and environmental impacts associated with this increase. Researchers have shown that transport infrastructure and links to supply chain partners are two of the most important factors in luring developers to an area [30][31]. Although the advantages of the effects and the role of digitalisation in logistics are still not properly recognised, it cannot be denied that digitalisation will be an essential step in the field of logistics [32][33]; this is reflected in transportation and warehouse activities [34]. As a typical example, in the past, real-time tracking of vehicles was performed using GPS systems. Then, with the advent of 4.0 technology and blockchain, real-time goods tracking systems using blockchain technology have been applied by many companies. From there, digital transformation frameworks are continuously being updated, based on emerging logistics activities. The research by Junge et al. [35] presented a framework for digital transformation in logistics, as demonstrated in **Fig. 2**.

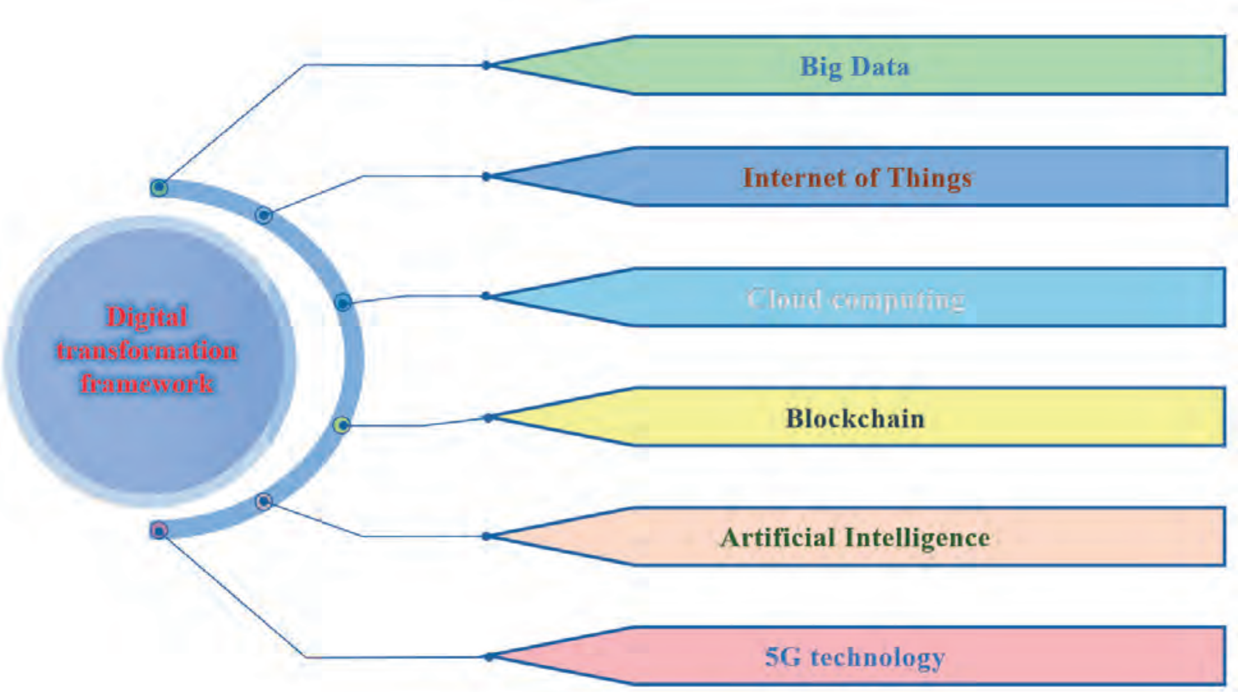

Fig. 2. The Logistics Digital Transformation Framework [35]

The next problem for the necessary development of 4.0 technologies is the e-commerce industry. The quantity of products that need to be handled in a logistics centre has grown over the past ten years, to meet the development of the e-commerce industry, making warehouse operations more complex. As a result, older manual methods are no longer sufficient or practicable to handle this enormous amount of activity [36]-[37]. From there, freight and logistics firms may encounter large delays between arrival and departure, as a result of poor management of the logistics centre [38]. Extra fees (fines for late transportation and additional expenditure for keeping the tractor-trailer driver on overtime) and orders being delivered late are the direct result of this [39]. Long lines of idle vehicles contribute to pollution [40]-[41], thus it is best to set up transport and storage facilities with standardised loading and warehousing efficiency. The primary objective of transportation and logistics centres is to minimise the overall costs associated with product transportation, while simultaneously increasing storage capacity through the implementation of short-term strategies and the use of technology. These elements play a crucial role in the efficient delivery of goods and enhancing transportation and logistics systems [42]-[43]. Moreover, the absence of cohesion in the managerial procedures within logistics centres leads to frequent instances of time wastage and mistakes in the tasks performed by personnel teams. Additionally, one company's barcode system will differ from their suppliers', leading to inconsistencies in the preservation of information about the items' features. This has long been a problem in conventional logistics centres, where it slows down the arrival of transporting vehicles and drives up waiting times and other expenses [44]. Because of this, the cost of logistics is consistently high in underdeveloped nations. Precisely for this reason, the Warehouse Management System was born to resolve the backlog of manual operations at warehouses and logistics centres. Warehouse Management Systems (WMS) evolved as a result of the emergence of increasingly complex tools and algorithms to run warehouses effectively in the 2000s [45]. A WMS has an information system that combines software programmes to keep track of, regulate, control, and manage inventory levels, and optimise warehousing choices. Order processing, order release, and master data are the three main WMS functions. In addition to the above functions, the additional capabilities of WMS include receiving (inbound), putting things away, and warehouse control [46]. However, WMS stopped meeting the needs of traditional logistics centres. For the e-commerce industry, specific characteristics related to the volume and quantity of goods still make it difficult for WMS to operate processing and storage.

By recognising the importance of technologies in applying the management of logistics centres to a smart environment, this work analyses and makes judgements of Industry 4.0 applications in the intelligent management of flogistics centres. Applications that reduce the number of pointless procedures can lighten the load in a logistics centre. Efficiency and operational productivity are then improved. These applications also pave the way for future studies in the field of smart logistics, where systems are combined with cutting-edge technology. However, there will be some notable obstacles, such as the cost of deploying the technology, the way in which the location of the logistics centre affects the environment, and the policies for applying these technologies; these will be of interest in future research.

LITERATURE REVIEW

LOGISTICS CENTRE DEFINITION

According to the European Economic Interest Group [47], a logistics centre is "the hub of a given area where all activities connected to transport, logistics, and products distribution both for national and international transit are carried out, on a commercial basis, by multiple operators". Facilities for storage, managing, clearing, reassembling, disassembling, inspecting quality, offering lodging, and providing social services are all found in logistics centres. Logistical activities are moving from urban to rural areas and using environmentally friendly modes of transportation, like electric vehicles. In the maritime field, the development of green solutions for ships and ports or green logistic centres is being considered as a priority, aiming to reduce carbon emissions and mitigate climate change [48]–[50]. In industrialised nations, logistics centres are crucial for sustainability and competitiveness, but they are also helpful for regional development in poor nations [51].

On the other hand, Uyanik et al. [52] asserted that an essential component of development strategy was the use of logistics centres, which were initially developed in Europe in the 1960s and were first observed in the US during the industrial revolution [53]. If such a centre was established in conjunction with combined and intermodal transport types, there would be innumerable advantages to doing so, including lower prices, reduced traffic congestion, lower environmental pollution levels, etc. However, the term 'logistics centre' was never defined in the literature. According to Higgins et al. [54] and Rimienė et al. [55], a number of terms implied a logistics centre, including distribution centre, freight village, dry port, inland port, load centre, logistics node, gateway, central warehouse, freight/transport terminal, transport node, logistics platform, logistics depot, and distribution park. Furthermore, Erkayman et al. [56] also published a concept for a logistics centre. National and international locations, known as logistics centres, are where various operators conduct all logistics-related activities on a for-profit basis, including shipping and forwarding, product distribution, material handling, storage, and other related transactions (such as banking and insurance). To carry out the aforementioned tasks, a logistics centre must be furnished with the necessary public amenities. These centres must be located near connections to highways, railways, airports, and seaports, as well as being located outside residential areas. Lastly, it has to be run by a single public or private organisation [46][57].

From the perspective of multimodal transport, according to Smail et al. [58], a logistics centre is a type of output point structure of the supply chain that includes stages like warehousing, distribution, and the provision of value-added services, and storage. According to Kaynak et al. [59], the logistics centre is a hub that combines various modes of transportation, almost performing like a multimodal transportation terminal, it is a crucial link in the multimodal transportation chain, and is a structure that serves as a hub for transportation activities among various modes of transportation. With the birth and evolution of the phrase 'supply chain management', the logistics centre concept has also altered and developed, much like the concept of logistics itself [60][61]. Nonetheless, it is most apparent that a logistics centre needs to have two main functions: shipping and warehousing. These are regarded as the two most crucial elements in setting up a basic logistics centre.

SMART LOGISTICS CENTRE

All facets of social life are being significantly impacted by the Industrial Revolution 4.0. Whether they want it or not, people are impacted by the revolution every single day. Automation, labour-saving production, lightning-fast product speed, and consistent quality are at the core of the fourth industrial revolution. One of the primary concerns is the use of automation as a means to effectively adapt to the strategic change that affects the national economy [62]. For logistics centres, the 4.0 revolution is bringing a lot of technology to support smarter and more flexible operations. New technologies are seen as a great support to meet the automation needs of logistics centres. Applying technology to logistics centres will help effectively manage the quantity, status, and flow of goods, in terms of time and cost.

The concept of 'smart logistics' has emerged in recent times, whereby advanced information technology serves as the fundamental basis for its implementation [63]-[64]. By processing information from all facets of logistics in real-time and thoroughly evaluating it, contemporary integrated logistics systems can be intelligently implemented. End-to-end visibility, improved transportation, warehousing, distribution processing, information services, and other aspects of smart logistics could all result in time and money savings. Additionally, it might be able to lessen the environmental damage that logistics causes. However, there are still difficult problems that must be solved before smart logistics can be implemented. One of the outstanding issues is the application of technology and connected activities in a logistics centre into a complete chain of activities, to overcome additional time and cost. In order to fulfil the needs of product storage, surveillance, safety, fire and explosion detection, and more, a smart logistics centre needs IoT equipment, such as IoT stacking shelves and an IoT inspection, as well as a monitoring system. The same degree of automation and network connectivity needs to be applied to machines and tools. It is obvious that IoT will play a pivotal role in the success of these modern logistics centres. These applications of IoT allow for the construction of a network-based cyber-logistics system that can be managed by humans. The incorporation of intelligence, automation, and automated choices of technology (IoT), elements of the supply chain, and logistics 4.0 are other important topics to explore in the Fourth Industrial Revolution [65][66]. A modern smart logistics centre, with intelligent goods arrangement and inventory management systems, is shown in **Fig. 3**. This is the result of the combination of many Industry 4.0 and Logistics 4.0 ideas, including driverless cars, digital connections, and information security, with the core functions of a logistics centre.

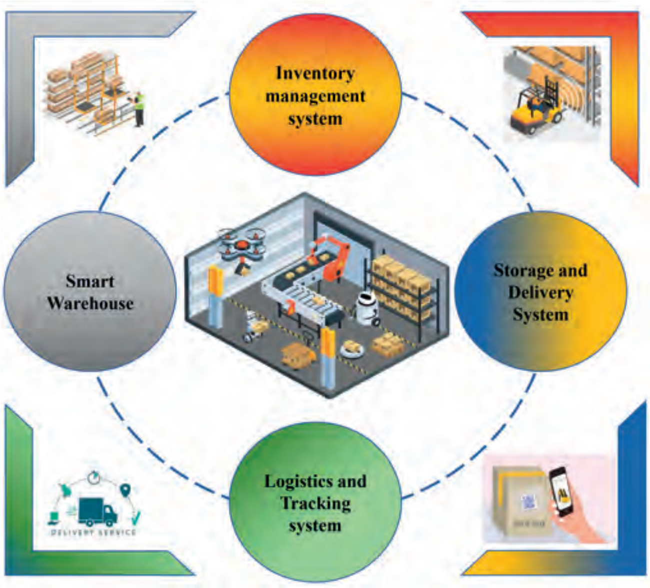

Fig. 3. Operations of a smart Logistics Centre [67]

To meet the needs related to the intelligence of a logistics centre, the study by Yavas et al. [68] focused their research on the transformation of logistics centres in industrial revolution 4.0 and identified key criteria for logistics centres in the new industrial era. The strategy was to look at the interactions between the operations of traditional logistics centres and then suggest a new framework for them. The four primary operations of logistics centres (handling management, information management, transport management, and warehouse management) were the basis for the twelve criteria for logistics centre 4.0 presented in this work. These criteria were acknowledged as the operational criteria at the logistics centre stated above and were linked to the four traditional criteria in the proposed framework [69], as illustrated in **Fig. 4**.

The operation of a smart logistics centre is based on the use of the latest technology, such as Big Data and IoT, to increase its operational efficiency. Through a decision support function based on logistics data, it also aids in the development of a managerial logistics operation plan. According to Cho [70], Logistics Centre 4.0 is based on IoT technologies. The data is collected and analysed using Big Data technology, the product is stored and transported based on the knowledge obtained through Artificial Intelligence, and a smart logistics centre system performs tasks automatically using robots. As the variety of items that need to be processed in a warehouse has grown over the past decade, conventional and manual techniques for warehouse management have proved to be unable to manage them.

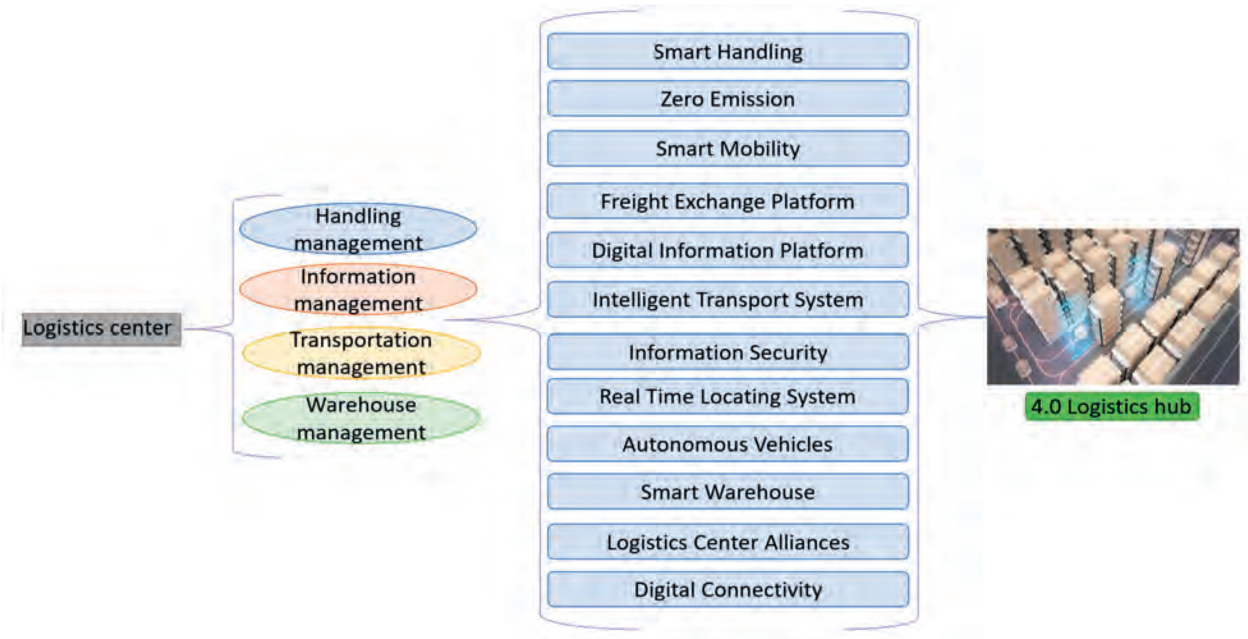

Fig. 4. A conceptual architecture for the 4.0 logistics hub [68]

This has resulted in a rise in the use of information technology to facilitate warehouse operations. The WMS has evolved as more sophisticated tools and algorithms for managing warehouses have been made available since the turn of the 2000s [45][71]. With the advancement of both technology and the marketplace, however, the manufacturing of products has shifted from make-to-stock (MTS) to make-to-order (MTO), leading to a dramatic rise in the number of commodities. As a result, new forms of warehouse technology are being integrated with existing warehouse management systems. In this article, a smart logistics centre is defined as having four 4.0 technologies: IoT, Blockchain, Big Data, and Cloud Computing. These technologies are applied for solving problems in logistics centres. In the next section, we analyse and review some applications that have been, and are being, applied at smart logistics centres. In addition, applicable policies, development possibilities, and future research directions will also be mentioned in this work.

APPLICATION OF 4.0 TECHNOLOGIES IN LOGISTICS CENTRES

The secret to creating a smart logistics centre is to use cutting-edge technologies to their fullest potential. Of these, IoT technology has emerged as a technology with outstanding data collection potential, helping managers to have a more holistic view of a logistics centre [72]-[73]. To facilitate data communication, exchange, and control among objects using distinct identifiers, a range of information sensing technologies are employed. These technologies encompass RFID, wireless sensor networks (WSN), and machine-to-machine systems. Additionally, embedded systems are also utilised, in conjunction with network communication technology, to achieve these objectives [26][74][75]. A sensor is apparatus that identifies and reacts to a certain kind of stimulus originating from the surrounding physical milieu. The input might include a range of environmental phenomena, such as heat, light, motion, moisture, pressure, or other factors. Alternatively, the data might be communicated by electronic means over a network, enabling remote access for reading or further processing [76]. The classification of sensor types is presented in **Table 2**.

Connecting and collecting massive amounts of data from sensor systems in logistics hubs is made possible by Internet of Things applications. This data can come from many different sources, such as product volume, temperature, humidity, shelf location, etc. According to Uckelmann et al. [85], the IoT is dedicated to connecting the physical world to the virtual internet and its primary drivers of development are object self-identification, information sharing, and interactive processing. Machine-to-machine and human-to-machine interactions are made possible by IoT applications [86]. The technological components of the IoT have been extensively discussed in Miorandi et al. [87], Mishra et al. [88], Ng et al. [89], Whitmore et al. [90], and Li et al. [91]. Despite the fact that several types of smart logistics exist due to different priorities, all of them rely on the use of ICTs. A new working concept of smart logistics is centred on the movement of goods, based on cutting-edge technology and intelligent management. Fig. 5 shows the concept map of a smart logistics centre with four technologies in the current industry 4.0 era: IoT, Big Data, Blockchain, and Cloud computing [92].

Tab. 2. Classification of sensors [77]

Type of sensor	Function	Ref
GPS sensors	The objective of this sensor is to determine the location of various components and to accurately detect and communicate the operational duration of equipment in the logistics centre.	[78][79][80]
Strain sensors	Quantify the instantaneous deformation experienced by structural components in a timely manner.	[81]
Accelerometer sensors	This particular sensor is capable of detecting changes in gravitational acceleration, enabling the measurement of tilt, vibration, and acceleration.	[78][79]
Barometric sensors	Barometric pressure sensors have been employed in many electronic devices such as smartphones, smart watches, and drones, to monitor air pressure readings and changes in altitude.	[78][79][82]
Wind-sensor, rain-sensor	The objective is to observe and measure the velocity of wind, as well as the amount of precipitation.	[83]
Fibre optic sensor	The automation of operations might be achieved by the activation of the reader for RFID and GPS detectors.	[84]
Laser sensor	The objective is to ascertain the duration required for the production process of the equipment.	[78]

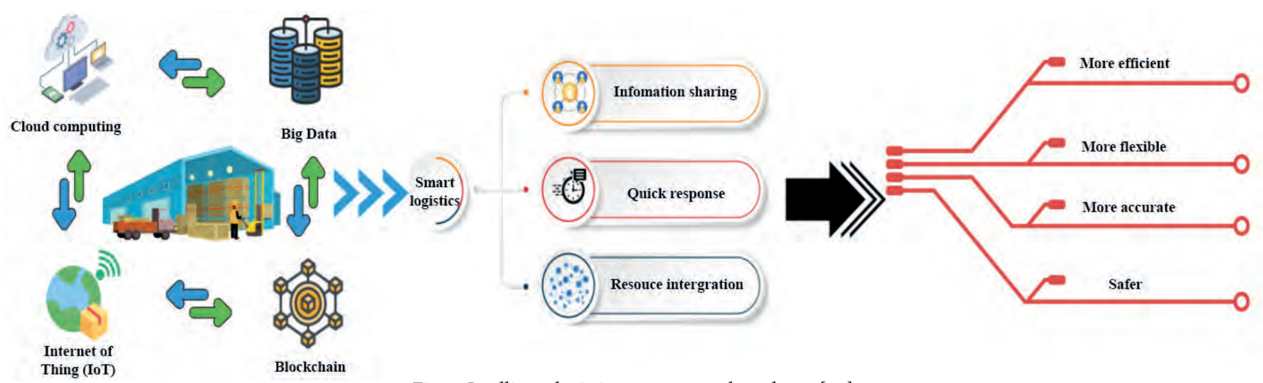

Fig. 5. Intelligent logistics: a conceptual roadmap [92]

INTERNET OF THINGS (IOT)

One potentially useful technology that might be included in a standard logistics system is the Internet of Things (IoT). Utilising Auto-ID methods, such as Barcode and Radio Frequency Identification (RFID), the IoT can accurately identify a wide range of things. The IoT would gather and record data in real-time from a wide variety of things, allowing for real-time visibility and traceability [93]. Data collected in real-time might be used for complex tasks like logistics route planning. The logistics sector has recently looked at wearable gadgets that combine IoT technology [94]. Logistics platforms have included state-of-the-art technology to allow for automated tracking of commodities and improved capabilities for logistics personnel [95]-[96]. With the help of IoT technology, a traditional logistics centre has the ability to connect devices and units, and manage those units within a network. **Fig. 6** shows the connectivity and management capabilities of IoT in a logistics centre.

Öner et al. [100] took a case study into account, for the application of RFID technology in the wool yarn sector. RFID is intended for the handling process, including receiving, picking, and shipping of semi-finished goods, as well as tracking work-in-progress, inventories, and stock levels. In order to accomplish this, an architectural framework for an RFID-based information system for the wool yarn sector was created and a cost-benefit analysis was carried out to determine whether the new system was cost-effective or not. Additionally, a risk analysis for RFID investments was performed. In the same study direction, a WMS was created by Tejesh et al. [101], based on RFID wireless communication technology. The IoT-based warehouse inventory management system is designed to track the products that are linked to tags and provide product information and their associated time stamps for additional verification. A server called Raspberry Pi would monitor and update all data. The entire system provides an archetype to match the material and information flow. The website is designed for ease of use and an interface for the user to track the products in mind. Comparing the developed system to the already-used warehouse inventory management systems, it was significantly more affordable and operated dynamically.

Fig. 6. IoT application in logistics centre management [97]

In order to promote intelligent logistics for Industry 4.0, Lee et al. [98] suggested an IoT-based warehouse management system with an enhanced data analysis methodology, based on computational intelligence approaches. Data acquired from a case firm demonstrated that the suggested IoT-based WMS might increase warehouse productivity, picking accuracy, and efficiency, while also being resilient to order unpredictability. The authors also discovered that employing RFID might increase efficiency in order picking by warehouses, pickup time, and inventory accuracy. A smart WMS framework was announced by Hamdy and colleagues [99]. The warehouse manager could perform more real-time management and monitoring of the activities because of this solution. The adoption of WMS and IoT in warehouses was reviewed. The building components and levels of the IoT were also shown, carefully.

A logistics centre's facilities were connected to a cloud centre, gateways, fog devices, edge devices, and sensors in Lin et al.'s [102] investigation of the deployment of an intelligent computing system. This work established an integer programming model for deploying gateways, fog devices, and edge devices in their respective potential sites, so that the total installation cost was minimised under constraints of maximal demand capacity, maximal latency time, coverage, and maximal capacity of devices. The locations of the cloud centres and sensors were determined based on the factory layout. The system's deployment was simulated using a mathematical programming model, which chose the locations of the gateways, fog devices, and edge devices in the logistics centre, to minimise the overall installation cost while maintaining the system's maximum capacity for demand, latency, coverage, and device capacity. Two new paths in the study of the vehicle routing problem (VRP) in transportation management (under the umbrella of smart logistics) have emerged, because of intelligent technologies like IoT and ICT. First, studies on VRP began to focus on multi-objective models and enhanced intelligent algorithms for handling dynamic optimisation problems. Data-driven models and dynamic models with various objectives have drawn more attention from academics, in terms of model types, because they address real-time data updating and coordination amongst numerous transportation agents. Second, some researchers have shown that the use of Big Data and geospatial positioning technology enables smart logistics to perform activities like visualisation, prediction, control, and decision-making in VRPs [103].

For the purpose of organising fresh integrations of intelligent food logistics systems, Li et al. [104] presented a linear approach. The costs of overall production, inventory, and transportation were minimised, while average food quality was increased. Then, a fresh approach was created to resolve it by fusing the fuzzy logic method with constraint-based two-stage heuristics. One case study and 185 randomly generated cases, with up to 100 stores and 12 periods, were used to evaluate the methodology. The case study's calculation results showed that the suggested model and method could resolve a real situation involving 40 merchants and 7 periods. The authors' method could give decision-makers a selection of Pareto solutions and assist them in selecting a preferred alternative. Moreover, Zhang [105] suggested a path decision approach based on an intelligent algorithm, merging the Cyber-Physical System's characteristics with the existing logistical system. The equipment layer's connectivity architecture and data processing utilised the IoT and cloud platform data storage technologies, which were based on the Cyber-Physical System's logistics path decision model. The impacts of using ant colony, simulated annealing, and genetic algorithms on logistic path optimisation were thoroughly examined. It was determined that the ant colony algorithm had the best path optimisation impact in solving the logistics path decision, by comparing the shortest transport route and convergence rate under the three algorithm decisions.

BIG DATA

Data obtained from the market, such as consumer preferences and the experiences of logistics users, can be processed and analysed with the use of big data gathering technologies, allowing logistics firms to improve the quality of their services in response to client needs. Additionally, logistics firms can improve their overall competitiveness by collecting data about their target markets, such as logistical costs, basic pricing, and marketplace assets [106][107]. In order to improve supply chain management and logistics centre efficiency, Big Data analytics sparked a revolution in inventory monitoring, forecasting, and management. By analysing massive amounts of data, Big Data provided insights that would otherwise be impossible to reach, driving the warehouse closer to its full potential. In the study by Xie et al. [108], the researchers conducted a survey of companies, looking at how Big Data is being used in the management of logistics, and used logistics hubs as a case study for using time series models to predict cargo load capacity. The results showed how smart logistics built on Big Data may improve logistics in many ways, including efficiency, cost, and user experience. The authors also concluded that the leadership and making of decisions, customer relationship maintenance, and resource allocation of logistics firms would all greatly benefit from the judicious use of Big Data technologies. Wang et al. [109] also conducted research on the topic of locating logistics facilities through Big Data analysis. This issue was stated in the form of a nonlinear mixed-integer programme. The simulation analysed the effect of varying demand, distribution centre operating costs, international shipping, and client count on the optimal placement of distribution centres produced in random, massive datasets. The experimental data showed that the model provided was practical and stable. This case study demonstrated the practical use of Big Data in designing a distribution network by evaluating different potential network layouts.

Big data could be especially useful in inventory management, as mentioned in the study by Wang et al. [110], where it could aid the development of cutting-edge inventory optimisation systems, the forecasting of future inventory requirements, the meeting of fluctuating customer demands, the cutting of inventory costs, the attainment of a more complete picture of stock levels, the improvement of inventory flow and storage, and the reduction of safety stock. Big Data provided additional information about the logistics hubs that support certain industries. An advanced data mining strategy was presented by Vieira et al. [111], for an automobile sector firm based on their analysis of proof of concept Big Data in a logistics centre. Due to the dearth of pre-existing methods, the most cutting-edge one was employed. To better identify relevant data to assist decision-making, the suggested strategy focused on goals that were user-driven. Another shared objective was to facilitate communication and consensus during decision-making. In order to ensure that the proper replacement parts were available for the right equipment at the right time and in the right amount, Zheng et al. [112] proposed an intelligent system for managing inventory that makes use of cutting-edge technologies, such as the IoT and Big Data Analytics. The Singapore Economic Development Board anticipated that this approach would benefit the whole of the Singapore semiconductor sector in the future. The interactions between providers and consumers should be investigated further to find ways to improve openness, adaptability, and satisfaction.

Furthermore, Wahab et al. [113] set out to learn what variables in Malaysia's warehousing industry were slowing down the use of Big Data analytics. The theoretical underpinning was the TOE model (technology-organisation-environment). Partial least squares structural equation modelling was used to evaluate survey responses from 110 logistics firms. The empirical findings indicated that the level of adoption of Big Data analytics was influenced by relative advantage, technical infrastructure, absorptive capacity, and government backing, but that industry rivalry had little impact on noticeable gains. The results of this research should make it easier for warehouses to use Big Data analytics in the most effective ways possible. Big Data analytics are more likely to be adopted by warehouses that place an emphasis on operational excellence, ICT infrastructure, and the integration of new technologies.

The inclusion of Big Data in data collection in the warehouse is a very feasible option, making data reception more passive. In addition, the combination of Big Data and IoT is also a good technological solution for helping the logistics centre become automated. This was also a premise for conducting transport flow management outside the logistics centre. The combination of managing the flow of goods and motor vehicles in and out of a logistics centre would greatly help in reducing transportation costs, warehousing costs, and waiting costs.

BLOCKCHAIN

For IoT or Big Data, the application of these technologies in logistics centres mean exploiting and processing information to achieve optimal goals, as well as reducing costs. However, the major drawback of the above applications is their transparency, as well as the ability to protect data, and this is what blockchain can do. By using examples and frameworks, Ahmad and colleagues [114] explored how blockchain technology might revolutionise port logistics and operations. In addition, researchers designed permissioned architectures to draw attention to the numerous elements, participants, and deployment options of port logistics services, in order to automate these processes. The results showed that blockchain technology could render it impossible for theft to happen, with documents linked to data management and storage, fleet management, trade paperwork, as-set and crew approval, and tracking shipments. This made transactions go more smoothly and built trust between authorities, organisations, and other players in the logistics centre transportation environment. With RFID tags, the supply chain process was described from the raw materials to the consumer. Each step was recorded in the blockchain to improve transparency, in which the activities at the logistics centre would be recorded, see **Fig. 7**.

A paradigm for the combination of blockchain with the IoT was presented for a logistics centre by Aleksieva et al. [116]. This technology, which made use of smart contacts on the blockchain, might be used for the logistics of cross-docking warehouses and shipping. The model showed the ability to operate effectively when it was possible to classify items in a logistics centre very well, thereby increasing operational efficiency and reducing waiting times. Blockchain logistics 'apps' for the optimum placement of intelligent transport logistics centres were created by Chen et al. [117], to make use of the blockchain system's simplicity and IoT input devices. This strategy was used to monitor where goods were in the supply chain at any given time. Based on the results of the experiments, it was clear that the optimum location technique is superior to conventional approaches, in terms of the amount of computing required, the precision of the locations it produces, the total cost, and the ease with which warehouse locations might be determined. Applying an intelligent logistics system built on the IoT and blockchain technology helps businesses get a clearer picture of their stock levels and shipping progress in real-time. Thereby, it ensures the assets and capital turnover of the enterprise.

It is impossible not to mention the traceability of blockchain technology as, with this ability, many applications have been launched, e.g. product traceability. In order to reliably record airplane parts and improve traceability data (with organisation-wide consensus and verification), Ho and colleagues [118] suggested a blockchain-based approach that was constructed using Hyperledger Composer and Hyperledger Fabric. Blockchain was also used to keep track of inventories at distribution facilities, cutting down on inefficiencies in both time and money. Kurdi et al. [119] analysed data from a sample size of 303 respondents, using regression and hypothesis testing with ANOVA, to apply a descriptive, exploratory, causal, and analytical design. One particularly noteworthy finding was the effect that blockchain and smart inventory systems had on the efficiency of supply chains and logistics hubs. Future studies should expand on the number of sectors and building types studied by using the same amount of organised research. On the other hand, Lakshmi et al. [120] used QR codes and blockchain technology to create a system for trustworthy distribution and open

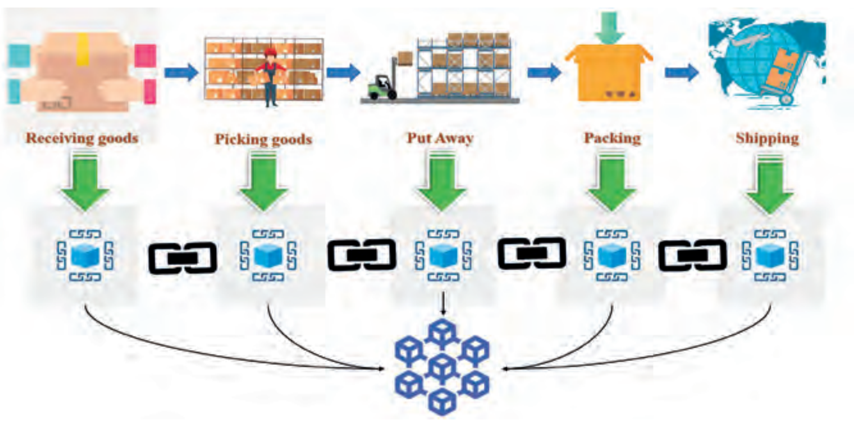

Fig. 7. The use of blockchain technology inside a supply chain framework [115]

inventory management. Distributors, retailers, suppliers, and manufacturers might all be linked via blockchain technology, with every transaction between them being permanently recorded. The use of QR codes helps the efficient management of this stock. Faster feedback loops mean fewer mistakes in inventory records and more reliable data for making well-informed decisions at review intervals.

CLOUD COMPUTING

The term 'cloud computing' refers to the delivery of computing resources and functions through the internet. The key features of cloud computing include on-demand service delivery, widespread network access, shared resource pooling, scalability, and use monitoring and control. Since a large number of users might share identical assets, cloud-based platforms automatically monitor and measure the usage of resources for each user [121]. This allows users to make as little or as much use of the system's capabilities as they see fit [122]. The most-mentioned advantages of cloud computing is that it reduces risks in the supply chain and limits the generation of waste. Supply chain risk might be mitigated and robustness improved in the same manner as cloud computing in logistics increases agility (by boosting speed, scalability, and visibility). In a poll by Accenture [123], 52% of supply chain executives claimed that cloud computing has helped them improve resilience. The executives also claimed a 26% improvement in the precision of demand projections as a result of using cloud computing. The effectiveness of supply networks in reducing waste and their long-term viability are under increasing examination. This was a major topic of discussion during COP26, held in Glasgow in 2021. Overall, 48% of supply chain executives polled by Accenture in 2021 [123] said that they had reduced waste because of cloud computing. Companies might use cloud computing to highlight waste and inefficiency in the supply chain and save costs, allowing them to make adjustments to reduce their waste. The cloud might assist businesses in reorganising their supply chains to improve efficiency, refine logistics and transport routes, and maximise resource use, all of which contribute to a smaller carbon footprint [124]. The application of cloud computing to each stage in the supply chain was an inevitable trend of businesses moving towards smart logistics. In the research by Jiang [125], the researcher took advantage of cloud computing to provide a strategy for determining the best geographical and transitable parameters for an international e-commerce logistics distribution hub. When micro-influences were taken into account, this model performed well. Transportation distances were stated to be reasonable, ranging from 3.5-7.5 km, when using this approach. Based on this technology, Zhang [126] also presented a two-layer unloading system for a railway logistics centre using cloud-edge communication technology. The simulation findings demonstrated that the discharging technique described in this research reduced the total time cost of unloading by as much as 40%. This technology's use also has the potential to expedite inter-device communication and enhance the efficacy of railway data transfer. Sharma et al. [127] illustrated research on how to leverage cloud computing to improve retail warehouse distribution and supply chain management through Microsoft Azure technology. Microsoft Azure is utilised in retailing, shipping, and warehousing, as well as supply chain management. The utilisation of this technology helps cost savings and eases administration, with more adaptability and better oversight. These are just some of the benefits of using this kind of technology in retail centre logistics. Gupta et al. [128] also confirmed that a suitable application created by cloud computing may greatly facilitate the simplification and automation of logistics centre management. Sivakumar et al. [129] investigated the storage facilities at Chennai Harbour. The warehouse management system for the Chennai Port Trust is hosted in the cloud, so that numerous people may use it from off-site locations. According to the findings of this study, warehouse operations benefit from cloud computing, which increases productivity and streamlines the workflow. Furthermore, Barreto et al. [130] noted that electronic contacts with customers, trade partners, and carriers may be handled by integrating warehouse administration and transportation administration using cloud computing technologies.

POLICY IMPLICATION FOR LOGISTICS CENTRE DEVELOPMENT

Smart logistics centres powered by the IoT, Big Data, Blockchain, and Cloud Computing would be safer, more accurate, and more efficient. Additionally, the warehousing procedure would be expedited, and resources would be utilised to their full potential. In a centralised warehouse management system, decentralised decision-making was possible using IoT. The hurdles for IoT-based smart warehousing still lie in the selection of a storage allocation strategy and the optimisation of indoor routing. The technical limitations of RFID, the IoT's limited technological capability, IoT standardisation issues, IoT data acquisition and processing issues, and IoT security and privacy concerns, are all obstacles to IoT-based smart logistics. IoT is unsuitable for sophisticated applications in logistics due to its constrained computing power and data processing capabilities. In transportation, IoT has a limited impact on cargo load optimisation and vehicle selection. IoT technology is unable to easily tackle the complicated problems of storage allocation and container/truck loading [131]. IoT could not be used to achieve the agile WMS [132]. Without the aid of an intelligent algorithm, IoT technology could not provide decision-making in truck route optimisation for the delivery of perishable goods [133]. IoT technology could gather large amounts of information about delivery resources and requirements [134][135], but it could not address how to improve the scheduling and use of delivery resources [20]. It is not sufficient to address the issues of resource waste and excessive cost in last-mile delivery.

Logistics become more difficult during the handling, palletising, and transporting of custom or limited-edition products [136]. The occurrence of eventualities modifies the demand for specific products quickly and calls for adjustments to the warehouse floor plan. Transportation scheduling changes at short notice also presents another difficulty for traditional logistics. In light of the transit stock being transported along the supply chain (and its scarcity, needs, and trends), the issues in current logistics centre on these factors [137][138], including spikes in the demand for otherwise stable products [139]. The desire to deploy Industry 4.0, according to Pereira et al. [140], involves a variety of technological hurdles with significant effects on many aspects of today's manufacturing industry. Therefore, before implementation begins, it is crucial to define a plan for all the actors engaged in the entire value chain and to come to an agreement on security-related concerns, as well as the appropriate architecture. Furthermore, a lot of scholars claim that putting Industry 4.0 into practice is a difficult task that would probably take ten or more years to complete. Adopting this new manufacturing method involves several factors and presents a variety of obstacles and challenges, including social, political, and economic issues, in addition to technical, economic, scientific, and energy hurdles. The gathering, processing, and presentation of manufacturing process data were three new, demanding activities that they should be able to test out using specialised Industry 4.0 technology [141]. Industry 4.0 has the potential to bring about significant changes in a number of areas that extend beyond the industrial sector and enable the development of new business models. With so much rivalry in today's market, businesses must constantly adapt to be competitive in terms of cost, quality, and turnaround time [142]. Due to global competition, businesses need to be quick to adopt new technologies and provide new items to the market [143]. Designing productive, efficient, and adaptable techniques is necessary to ensure process competitiveness throughout the value chain [142]. The integration of new technologies into manufacturing processes, goods, and machinery is crucial to facilitating rapid response to changes in the marketplace [144]. One of the main obstacles faced by different countries is the lack of policies that allow technology to be applied to the logistics sector. **Fig. 8** illustrates the relationship between logistics policy and governmental policies. It should be noted that logistics policy does not have a superior attitude toward other policies; rather, it implements some of these (such as security and transportation policies) and cooperates with others (e.g. industrial and maritime policies). Nonetheless, it should be considered in each area of its functioning, including in macroeconomic and detailed policies and (crucially) it should not be 'closed'. This phenomenon is closely related to the processes of globalisation and aims to create a 'no barriers' relationship between regions, states, and continents, in terms of logistics [145].

Fig. 8. Links between logistics strategy and other industries [145]

The use of 4.0 technology also requires ties with other fields and sectors within a nation. Furthermore, only a small portion of 4.0 technology is used in logistics centre management. Here, the focus is on building a nation's digital infrastructure and smart infrastructure. Although there are many questions about 4.0 technology's ability to safeguard information, its practical applicability, and the expense of doing so, this is thought to be one of its most risky. Theft, or the disclosure of user-data kept in databases, might compromise user privacy and impact the customer service of the logistics centre [146]. However, ensuring data privacy is just one of the obstacles to overcome; lowering operational expenses is also crucial [147][148]RFID (radio-frequency identification. Many questions have been raised about whether the application of these technologies in logistics centres would really cut or increase costs. As an added argument, applying technologies in a uniform way, or prioritising each technology applied in logistics centres, would also be a topic for future research. Therefore, in addition to the priority policies aimed at macro-development for countries, research directions for technology application should also be explored in future studies of logistics centres. Developing an acceptable application policy is a problem that requires further research.

CONCLUSIONS AND FUTURE PROSPECTS

Exponential growth in the number of products that are available has led to the persistent challenge of overload within logistics centres and freight operations in the logistics sector. Moreover, these activities not only result in the inefficient use of time and resources but also have detrimental effects on the environment. Hence, the use of novel technology arises as a viable approach to effectively address these issues in their entirety. The integration of advanced technologies, such as Big Data, Blockchain, Internet of Things, and Cloud Computing (commonly referred to as 4.0 technologies), has been extensively studied and applied in various domains. Through previous research and applications, this work has demonstrated the significant potential of these 4.0 technologies in enhancing the operational capabilities and efficiency of logistics centres, particularly in managing and controlling the movement of goods.

The primary uses of each technology are as follows: The Internet of Things (IoT) facilitates the collection of a substantial volume of data by using RFID tags affixed to individual packages and sensors installed throughout the whole of the logistics centre. The use of Big Data facilitates the processing of vast amounts of data in order to provide assistance for managerial decision-making. Blockchain technology in the logistics centre provides transparency across the whole of the workflow, including the arrival and departure of items. Cloud Computing facilitates the sharing of information while maintaining control, leading to continuous productivity improvements in logistics centres. The use of these technologies has the potential to enhance the intelligence and advancement of a logistics centre. In addition, it is recommended that future research is directed toward the development of a technologically advanced logistics centre that conforms to established environmental criteria. Hence, it can be inferred that the adoption of a green-smart logistics centre model will become an unavoidable trajectory in the future. This model would enable the systematic regulation of goods transportation to effectively cater to the substantial demand for commodities. Furthermore, these logistics hubs have the potential to function as seamless extensions of seaports, therefore mitigating congestion issues in port cities. Transportation operations within the logistics business are well acknowledged as being a significant contributor to environmental degradation. The escalation of congestion and prolonged waiting times at conventional logistics hubs and seaports has led to a significant rise in pollution levels, hence posing a substantial urban challenge. The use of 4.0 technologies enables the expeditious regulation of products inside centres, resulting in reduced waiting times and, subsequently, contributing to the mitigation of vehicle emissions. Hence, the establishment of a green and intelligent logistics centre emerges as a prominent research direction aimed at mitigating environmental pollution. Simultaneously, this development aligns with the evolving requirements of smart cities, which are experiencing rapid global growth.

REFERENCES

1. L. Atzori, A. Iera, and G. Morabito, "The internet of things: A survey," *Comput. networks*, vol. 54, no. 15, pp. 2787–2805, 2010.

2. D. Bandyopadhyay and J. Sen, "Internet of Things: Applications and Challenges in Technology and Standardization," *Wirel. Pers. Commun.*, vol. 58, no. 1, pp. 49–69, May 2011, doi: 10.1007/s11277-011-0288-5.

3. C. Bardaki, P. Kourouthanassis, and K. Pramatari, "Deploying RFID-Enabled Services in the Retail Supply Chain: Lessons Learned toward the Internet of Things," *Inf. Syst. Manag.*, vol. 29, no. 3, pp. 233–245, Jun. 2012, doi: 10.1080/10580530.2012.687317.

4. Hao Wang, O. L. Osen, Guoyuan Li, Wei Li, Hong-Ning Dai, and Wei Zeng, "Big data and industrial Internet of Things for the maritime industry in Northwestern Norway," in *TENCON 2015 - 2015 IEEE Region 10 Conference*, Nov. 2015, pp. 1–5. doi: 10.1109/TENCON.2015.7372918.

5. V. D. Bui and H. P. Nguyen, "A Comprehensive Review on Big Data-Based Potential Applications in Marine Shipping Management," *Int. J. Adv. Sci. Eng. Inf. Technol.*, vol. 11, no. 3, pp. 1067–1077, Jun. 2021, doi: 10.18517/ijaseit.11.3.15350.

6. S. Altendorfer-Kaiser, "The Influence of Big Data on Production and Logistics," 2017, pp. 221–227. doi: 10.1007/978-3-319-66923-6_26.

7. H. P. Nguyen, P. Q. P. Nguyen, and V. D. Bui, "Applications of Big Data Analytics in Traffic Management in Intelligent Transportation Systems," *JOIV Int. J. Informatics Vis.*, vol. 6, no. 1–2, pp. 177–187, May 2022, doi: 10.30630/joiv.6.1-2.882.

8. C. S. Tang and L. P. Veelenturf, "The strategic role of logistics in the industry 4.0 era," *Transp. Res. Part E Logist. Transp. Rev.*, vol. 129, pp. 1–11, Sep. 2019, doi: 10.1016/j.tre.2019.06.004.

9. A. Ferrari, G. Mangano, A. C. Cagliano, and A. De Marco, "4.0 Technologies in City Logistics: an Empirical Investigation of Contextual Factors," *Oper. Manag. Res.*, vol. 16, no. 1, pp. 345–362, 2023, doi: 10.1007/s12063-022-00304-5.

10. H. Golpîra, S. A. R. Khan, and S. Safaeipour, "A review of logistics Internet-of-Things: Current trends and scope for future research," *J. Ind. Inf. Integr.*, vol. 22, p. 100194, Jun. 2021, doi: 10.1016/j.jii.2020.100194.

11. D. Peraković, M. Periša, and P. Zorić, "Challenges and Issues of ICT in Industry 4.0," 2020, pp. 259–269. doi: 10.1007/978-3-030-22365-6_26.

12. K. Witkowski, "Internet of Things, Big Data, Industry 4.0 – Innovative Solutions in Logistics and Supply Chains Management," *Procedia Eng.*, vol. 182, pp. 763–769, 2017, doi: 10.1016/j.proeng.2017.03.197.

13. H. P. Nguyen, P. Q. P. Nguyen, D. K. P. Nguyen, V. D. Bui, and D. T. Nguyen, "Application of IoT Technologies in Seaport Management," *JOIV Int. J. Informatics Vis.*, vol. 7, no. 1, p. 228, Mar. 2023, doi: 10.30630/joiv.7.1.1697.

14. A. Bekrar, A. Ait El Cadi, R. Todosijevic, and J. Sarkis, "Digitalizing the Closing-of-the-Loop for Supply Chains: A Transportation and Blockchain Perspective,"

Sustainability, vol. 13, no. 5, p. 2895, Mar. 2021, doi: 10.3390/su13052895.

15. M. Kouhizadeh, S. Saberi, and J. Sarkis, "Blockchain technology and the sustainable supply chain: Theoretically exploring adoption barriers," *Int. J. Prod. Econ.*, vol. 231, p. 107831, Jan. 2021, doi: 10.1016/j.ijpe.2020.107831.

16. A. A. Mukherjee, R. K. Singh, R. Mishra, and S. Bag, "Application of blockchain technology for sustainability development in agricultural supply chain: justification framework," *Oper. Manag. Res.*, vol. 15, no. 1–2, pp. 46–61, Jun. 2022, doi: 10.1007/s12063-021-00180-5.

17. M. A. Ahad, S. Paiva, G. Tripathi, and N. Feroz, "Enabling technologies and sustainable smart cities," *Sustain. Cities Soc.*, vol. 61, p. 102301, Oct. 2020, doi: 10.1016/j.scs.2020.102301.

18. S. Bhardwaj, L. Jain, and S. Jain, "Cloud computing: A study of infrastructure as a service (IAAS)," *Int. J. Eng. Inf. Technol.*, vol. 2, no. 1, pp. 60–63, 2010.

19. T.-M. Choi, S. W. Wallace, and Y. Wang, "Big Data Analytics in Operations Management," *Prod. Oper. Manag.*, vol. 27, no. 10, pp. 1868–1883, Oct. 2018, doi: 10.1111/poms.12838.

20. D. Zhu, "IOT and big data based cooperative logistical delivery scheduling method and cloud robot system," *Futur. Gener. Comput. Syst.*, vol. 86, pp. 709–715, Sep. 2018, doi: 10.1016/j.future.2018.04.081.

21. T. T. Le *et al.*, "Management strategy for seaports aspiring to green logistical goals of IMO: Technology and policy solutions," *Polish Marit. Res.*, vol. 30, no. 2, pp. 165–187, 2023, doi: 10.2478/pomr-2023-0031.

22. E. J. Khatib and R. Barco, "Optimization of 5G Networks for Smart Logistics," *Energies*, vol. 14, no. 6, p. 1758, Mar. 2021, doi: 10.3390/en14061758.

23. J.-Q. Li, F. R. Yu, G. Deng, C. Luo, Z. Ming, and Q. Yan, "Industrial Internet: A Survey on the Enabling Technologies, Applications, and Challenges," *IEEE Commun. Surv. Tutorials*, vol. 19, no. 3, pp. 1504–1526, 2017, doi: 10.1109/COMST.2017.2691349.

24. M. Liu, F. R. Yu, Y. Teng, V. C. M. Leung, and M. Song, "Performance Optimization for Blockchain-Enabled Industrial Internet of Things (IIoT) Systems: A Deep Reinforcement Learning Approach," *IEEE Trans. Ind. Informatics*, vol. 15, no. 6, pp. 3559–3570, Jun. 2019, doi: 10.1109/TII.2019.2897805.

25. C. Qiu, F. R. Yu, H. Yao, C. Jiang, F. Xu, and C. Zhao, "Blockchain-Based Software-Defined Industrial Internet of Things: A Dueling Deep ${Q}$ -Learning Approach," *IEEE Internet Things J.*, vol. 6, no. 3, pp. 4627–4639, Jun. 2019, doi: 10.1109/JIOT.2018.2871394.

26. K. Ashton, "That 'internet of things' thing," *RFID J.*, vol. 22, no. 7, pp. 97–114, 2009.

27. K. Witkowski, "Internet of Things, Big Data, Industry 4.0 - Innovative Solutions in Logistics and Supply Chains Management," *Procedia Eng.*, vol. 182, pp. 763–769, 2017, doi: 10.1016/j.proeng.2017.03.197.

28. "Discussion: Will Warehouse Robots Completely Replace Traditional Logistics Industry Model?," *Geekplus*, 2018.

29. R. Bergqvist, "Transport and logistics facilities expansion and social sustainability: A critical discussion and findings from the City of Gothenburg, Swe-den." Gothenburg: Tesis Doctoral, 2016.

30. J. T. Bowen, "Moving places: the geography of warehousing in the US," *J. Transp. Geogr.*, vol. 16, no. 6, pp. 379–387, Nov. 2008, doi: 10.1016/j.jtrangeo.2008.03.001.

31. A. McKinnon, "The present and future land requirements of logistical activities," *Land use policy*, vol. 26, pp. S293–S301, Dec. 2009, doi: 10.1016/j.landusepol.2009.08.014.

32. Q. Yuan, "Environmental Justice in Warehousing Location," *J. Plan. Lit.*, vol. 33, no. 3, pp. 287–298, Aug. 2018, doi: 10.1177/0885412217753841.

33. Q. Yuan, "Location of Warehouses and Environmental Justice," *J. Plan. Educ. Res.*, vol. 41, no. 3, pp. 282–293, Sep. 2021, doi: 10.1177/0739456X18786392.

34. Q. Yuan and J. Zhu, "Logistics sprawl in Chinese metropolises: Evidence from Wuhan," *J. Transp. Geogr.*, vol. 74, pp. 242–252, Jan. 2019, doi: 10.1016/j.jtrangeo.2018.11.019.

35. F. Straube, A. L. Junge, P. Verhoeven, J. Reipert, and M. Mansfeld, *Pathway of digital transformation in logistics : best practice concepts and future developments*, no. July. 2019. doi: 10.14279/depositonce-8502.

36. R. Narasimhan and S. W. Kim, "INFORMATION SYSTEM UTILIZATION STRATEGY FOR SUPPLY CHAIN INTEGRATION," *J. Bus. Logist.*, vol. 22, no. 2, pp. 51–75, Sep. 2001, doi: 10.1002/j.2158-1592.2001.tb00003.x.

37. S. Kot, I. Goldbach, and B. Ślusarczyk, "Supply chain management in SMEs – Polish and Romanian approach," *Econ. Sociol.*, vol. 11, no. 4, pp. 142–156, Dec. 2018, doi: 10.14254/2071-789X.2018/11-4/9.

38. M. Levinson, *The box: how the shipping container made the world smaller and the world economy bigger*. Princeton University Press, 2016.

39. V. D. Bui and H. P. Nguyen, "The role of the inland container depot system in developing a sustainable transport system," *Int. J. Knowledge-Based Dev.*, vol. 12, no. 3/4, pp. 424–443, 2022, doi: 10.1504/IJKBD.2022.128914.

40. V. Aulin, A. Hrynkiv, S. Lysenko, A. Dykha, T. Zamota, and V. Dzyura, "Exploring a possibility to control the stressedstrained state of cylinder liners in diesel engines by the tribotechnology of alignment," *Eastern-European J. Enterp. Technol.*, vol. 3, no. 12 (99), pp. 6–16, Jun. 2019, doi: 10.15587/1729-4061.2019.171619.

41. V. Aulin, A. Hrinkiv, A. Dykha, M. Chernovol, O. Lyashuk, and S. Lysenko, "Substantiation of diagnostic parameters for determining the technical condition of transmission assemblies in trucks," *Eastern-European J. Enterp. Technol.*, vol. 2, no. 1 (92), pp. 4–13, Mar. 2018, doi: 10.15587/1729-4061.2018.125349.

42. J.-P. Rodrigue, *The Geography of Transport Systems*. Fifth edition. | Abingdon, Oxon ; New York, NY : Routledge, 2020.: Routledge, 2020. doi: 10.4324/9780429346323.

43. F. Weidinger, N. Boysen, and M. Schneider, "Picker routing in the mixed-shelves warehouses of e-commerce retailers," *Eur. J. Oper. Res.*, vol. 274, no. 2, pp. 501–515, Apr. 2019, doi: 10.1016/j.ejor.2018.10.021.

44. V. Aulin *et al.*, "Increasing the Functioning Efficiency of the Working Warehouse of the 'UVK Ukraine' Company Transport and Logistics Center," *Commun. - Sci. Lett. Univ. Zilina*, vol. 22, no. 2, pp. 3–14, Apr. 2020, doi: 10.26552/com.C.2020.2.3-14.

45. F. H. Staudt, G. Alpan, M. Di Mascolo, and C. M. T. Rodriguez, "Warehouse performance measurement: a literature review," *Int. J. Prod. Res.*, vol. 53, no. 18, pp. 5524–5544, Sep. 2015, doi: 10.1080/00207543.2015.1030466.

46. A. Nettsträter, T. Geißen, M. Witthaut, D. Ebel, and J. Schoneboom, "Logistics Software Systems and Functions: An Overview of ERP, WMS, TMS and SCM Systems," 2015, pp. 1–11. doi: 10.1007/978-3-319-13404-8_1.

47. "Logistics Centers Directions For Use," *EUROPLATFORMS EEIG*, 2004.

48. A. T. Hoang *et al.*, "Technological solutions for boosting hydrogen role in decarbonization strategies and net-zero goals of world shipping: Challenges and perspectives," *Renew. Sustain. Energy Rev.*, vol. 188, p. 113790, Dec. 2023, doi: 10.1016/j.rser.2023.113790.

49. A. T. Hoang *et al.*, "Energy-related approach for reduction of CO2 emissions: A critical strategy on the port-to-ship pathway," *J. Clean. Prod.*, vol. 355, p. 131772, Jun. 2022, doi: 10.1016/j.jclepro.2022.131772.

50. S. Vakili, A. I. Ölçer, A. Schönborn, F. Ballini, and A. T. Hoang, "Energy-related clean and green framework for shipbuilding community towards zero-emissions: A strategic analysis from concept to case study," *Int. J. Energy Res.*, vol. 46, no. 14, pp. 20624–20649, Nov. 2022, doi: 10.1002/er.7649.

51. C. Altuntaş and O. Tuna, "Greening Logistics Centers: The Evolution of Industrial Buying Criteria Towards Green," *Asian J. Shipp. Logist.*, vol. 29, no. 1, pp. 59–80, Apr. 2013, doi: 10.1016/j.ajsl.2013.05.004.

52. C. Uyanık, G. Tuzkaya, S. Oguztimur, C. Uyanik, and S. Oğuzti̇mur, "A Literature Survey On Logistics Centers' Location Selection Problem," *Sigma J. Eng. Nat. Sci.*, vol. 36, no. 1, pp. 141–160, 2018.

53. B. Koldemir, M. Çanci, and E. Gönüler, "Büyük ölçekli kent planlamasında lojistik köyler," *İzmir Ulaşım Sempozyumu*, pp. 8–9, 2009.

54. C. D. Higgins and M. R. Ferguson, "An Exploration of the Freight Village Concept and its Applicability to Ontario," 2011.

55. K. Rimienė and D. Grundey, "Logistics centre concept through evolution and definition," *Eng. Econ.*, vol. 54, no. 4, pp. 87–95, 2007.

56. B. Erkayman, E. Gundogar, G. Akkaya, and M. Ipek, "A Fuzzy Topsis Approach For Logistics Center Location Selection," *J. Bus. Case Stud.*, vol. 7, no. 3, pp. 49–54, Apr. 2011, doi: 10.19030/jbcs.v7i3.4263.

57. H. P. Nguyen, P. Q. P. Nguyen, and T. P. Nguyen, "Green Port Strategies in Developed Coastal Countries as Useful Lessons for the Path of Sustainable Development: A case study in Vietnam," *Int. J. Renew. Energy Dev.*, vol. 11, no. 4, pp. 950–962, Nov. 2022, doi: 10.14710/ijred.2022.46539.

58. İ. ÖNDEN, F. Eldemir, and M. Canci, "Logistics center concept and location decision criteria," *Sigma J. Eng. Nat. Sci.*, vol. 33, no. 3, pp. 325–340, 2015.

59. R. Kaynak, İ. Koçoğlu, and A. E. Akgün, "The Role of Reverse Logistics in the Concept of Logistics Centers," *Procedia - Soc. Behav. Sci.*, vol. 109, pp. 438–442, Jan. 2014, doi: 10.1016/j.sbspro.2013.12.487.

60. H. P. Nguyen, "Blockchain-an indispensable development trend of logistics industry in Vietnam: Current situation

and recommended solutions," *Int. J. e-Navigation Marit. Econ.*, vol. 13, pp. 14–22, 2019.

61. V. D. Bui and H. P. Nguyen, "A Systematized Review on Rationale and Experience to Develop Advanced Logistics Center System in Vietnam," *Webology*, vol. 18, pp. 89–101, 2021.

62. H. Makino, K. Tamada, K. Sakai, and S. Kamijo, "Solutions for urban traffic issues by ITS technologies," *IATSS Res.*, vol. 42, no. 2, pp. 49–60, Jul. 2018, doi: 10.1016/j.iatssr.2018.05.003.

63. S. Lee, Y. Kang, and V. V. Prabhu, "Smart logistics: distributed control of green crowdsourced parcel services," *Int. J. Prod. Res.*, vol. 54, no. 23, pp. 6956–6968, Dec. 2016, doi: 10.1080/00207543.2015.1132856.

64. A. Kawa, "SMART Logistics Chain," in *Intelligent Information and Database Systems*, 2012, pp. 432–438. doi: 10.1007/978-3-642-28487-8_45.

65. H. P. Nguyen, "Sustainable development of logistics in Vietnam in the period 2020-2025," *Int. J. Innov. Creat. Chang.*, vol. 11, no. 3, pp. 665–682, 2020.

66. J. Mehmann and F. Teuteberg, "Process reengineering by using the 4PL approach," *Bus. Process Manag. J.*, vol. 22, no. 4, pp. 879–902, Jul. 2016, doi: 10.1108/BPMJ-12-2014-0119.

67. Y. M. Tang, G. T. S. Ho, Y. Y. Lau, and S. Y. Tsui, "Integrated Smart Warehouse and Manufacturing Management with Demand Forecasting in Small-Scale Cyclical Industries," *Machines*, vol. 10, no. 6, 2022.

68. V. Yavas and Y. D. Ozkan-Ozen, "Logistics centers in the new industrial era: A proposed framework for logistics center 4.0," *Transp. Res. Part E Logist. Transp. Rev.*, vol. 135, p. 101864, Mar. 2020, doi: 10.1016/j.tre.2020.101864.

69. S. Winkelhaus and E. H. Grosse, "Logistics 4.0: a systematic review towards a new logistics system," *Int. J. Prod. Res.*, vol. 58, no. 1, pp. 18–43, Jan. 2020, doi: 10.1080/00207543.2019.1612964.

70. G. S. Cho, "A Study on Establishment of Smart Logistics Center based on Logistics 4.0," *J. Multimed. Inf. Syst.*, vol. 5, no. 4, pp. 265-272., 2018, doi: http://dx.doi.org/10.9717/JMIS.2018.5.4.265.

71. W. Hamdy, N. Mostafa, and H. Elawady, "Towards a smart warehouse management system," *Proc. Int. Conf. Ind. Eng. Oper. Manag.*, vol. 2018, no. SEP, pp. 2555–2563, 2018.

72. H. CHOW, K. CHOY, W. LEE, and K. LAU, "Design of a RFID case-based resource management system for warehouse operations," *Expert Syst. Appl.*, vol. 30, no. 4, pp. 561–576, May 2006, doi: 10.1016/j.eswa.2005.07.023.

73. V. Sharma, I. You, G. Pau, M. Collotta, J. Lim, and J. Kim, "LoRaWAN-Based Energy-Efficient Surveillance by Drones for Intelligent Transportation Systems," *Energies*, vol. 11, no. 3, p. 573, Mar. 2018, doi: 10.3390/en11030573.

74. R. H. Weber and R. Weber, "Governance of the Internet of Things," in *Internet of Things*, Berlin, Heidelberg: Springer Berlin Heidelberg, 2010, pp. 69–100. doi: 10.1007/978-3-642-11710-7_4.

75. X. Feng, L. T. Yang, L. Wang, and A. Vinel, "Internet of things," *Int. J. Commun. Syst.*, vol. 25, no. 9, pp. 1101–1102, 2012.

76. Robert Sheldon, "Definition Sensor," 2022.

77. M. Wang, C. C. Wang, S. Sepasgozar, and S. Zlatanova, "A Systematic Review of Digital Technology Adoption in Off-Site Construction: Current Status and Future Direction towards Industry 4.0," *Buildings*, vol. 10, no. 11, p. 204, Nov. 2020, doi: 10.3390/buildings10110204.

78. C. Mao, X. Tao, H. Yang, R. Chen, and G. Liu, "Real-time carbon emissions monitoring tool for prefabricated construction: An iot-based system framework," in *International Conference on Construction and Real Estate Management 2018*, 2018, pp. 121–127.

79. G. Liu *et al.*, "Cyber-physical system-based real-time monitoring and visualization of greenhouse gas emissions of prefabricated construction," *J. Clean. Prod.*, vol. 246, p. 119059, Feb. 2020, doi: 10.1016/j.jclepro.2019.119059.

80. Y. Zhai *et al.*, "An Internet of Things-enabled BIM platform for modular integrated construction: A case study in Hong Kong," *Adv. Eng. Informatics*, vol. 42, p. 100997, Oct. 2019, doi: 10.1016/j.aei.2019.100997.

81. M. Valinejadshoubi, A. Bagchi, and O. Moselhi, "Development of a BIM-Based Data Management System for Structural Health Monitoring with Application to Modular Buildings: Case Study," *J. Comput. Civ. Eng.*, vol. 33, no. 3, May 2019, doi: 10.1061/(ASCE)CP.1943-5487.0000826.

82. my Murata, "Barometric Pressure Sensor Basics."

83. X. Li, H. Chi, P. Wu, and G. Q. Shen, "Smart work packaging-enabled constraint-free path re-planning for tower crane in prefabricated products assembly process," *Adv. Eng. Informatics*, vol. 43, p. 101008, Jan. 2020, doi: 10.1016/j.aei.2019.101008.

84. Z. Wang, H. Hu, and W. Zhou, "RFID Enabled Knowledge-Based Precast Construction Supply Chain," *Comput. Civ. Infrastruct. Eng.*, vol. 32, no. 6, pp. 499–514, Jun. 2017, doi: 10.1111/mice.12254.

85. D. Uckelmann, M. Harrison, and F. Michahelles, "An Architectural Approach Towards the Future Internet of Things," in *Architecting the Internet of Things*, Berlin, Heidelberg: Springer Berlin Heidelberg, 2011, pp. 1–24. doi: 10.1007/978-3-642-19157-2_1.

86. R. K. Chahal, N. Kumar, and S. Batra, "Trust management in social Internet of Things: A taxonomy, open issues, and challenges," *Comput. Commun.*, vol. 150, pp. 13–46, Jan. 2020, doi: 10.1016/j.comcom.2019.10.034.

87. D. Miorandi, S. Sicari, F. De Pellegrini, and I. Chlamtac, "Internet of things: Vision, applications and research challenges," *Ad Hoc Networks*, vol. 10, no. 7, pp. 1497–1516, Sep. 2012, doi: 10.1016/j.adhoc.2012.02.016.

88. D. Mishra, A. Gunasekaran, S. J. Childe, T. Papadopoulos, R. Dubey, and S. Wamba, "Vision, applications and future challenges of Internet of Things," *Ind. Manag. Data Syst.*, vol. 116, no. 7, pp. 1331–1355, Aug. 2016, doi: 10.1108/IMDS-11-2015-0478.

89. I. C. L. Ng and S. Y. L. Wakenshaw, "The Internet-of-Things: Review and research directions," *Int. J. Res. Mark.*, vol. 34, no. 1, pp. 3–21, Mar. 2017, doi: 10.1016/j.ijresmar.2016.11.003.

90. A. Whitmore, A. Agarwal, and L. Da Xu, "The Internet of Things—A survey of topics and trends," *Inf. Syst. Front.*, 2015, doi: 10.1007/s10796-014-9489-2.

91. L. Da Xu, W. He, and S. Li, "Internet of Things in Industries: A Survey," *IEEE Trans. Ind. Informatics*, vol. 10, no. 4, pp. 2233–2243, Nov. 2014, doi: 10.1109/TII.2014.2300753.

92. Y. Ding, M. Jin, S. Li, and D. Feng, "Smart logistics based on the internet of things technology: an overview," *Int. J. Logist. Res. Appl.*, vol. 24, no. 4, pp. 323–345, Jul. 2021, doi: 10.1080/13675567.2020.1757053.

93. R. Y. Zhong, Q. Y. Dai, T. Qu, G. J. Hu, and G. Q. Huang, "RFID-enabled real-time manufacturing execution system for mass-customization production," *Robot. Comput. Integr. Manuf.*, vol. 29, no. 2, pp. 283–292, Apr. 2013, doi: 10.1016/j.rcim.2012.08.001.

94. X. T. R. Kong, X. Yang, G. Q. Huang, and H. Luo, "The impact of industrial wearable system on industry 4.0," in *2018 IEEE 15th International Conference on Networking, Sensing and Control (ICNSC)*, Mar. 2018, pp. 1–6. doi: 10.1109/ICNSC.2018.8361266.

95. G.-S. Cho, "A study on establishment of smart logistics center based on logistics 4.0," *J. Multimed. Inf. Syst.*, vol. 5, no. 4, pp. 265–272, 2018.

96. W. Wu, C. Cheung, S. Y. Lo, R. Y. Zhong, and G. Q. Huang, "An IoT-enabled Real-time Logistics System for A Third Party Company: A Case Study," *Procedia Manuf.*, vol. 49, pp. 16–23, 2020, doi: 10.1016/j.promfg.2020.06.005.

97. Oleksii Kholodenko, "IOT IN WAREHOUSE MANAGEMENT — EXTENSIVE GUIDE," 2022.

98. C. K. M. Lee, Y. Lv, K. K. H. Ng, W. Ho, and K. L. Choy, "Design and application of Internet of things-based warehouse management system for smart logistics," *Int. J. Prod. Res.*, vol. 56, no. 8, pp. 2753–2768, Apr. 2018, doi: 10.1080/00207543.2017.1394592.

99. W. Hamdy, N. Mostafa, and H. Elawady, "Towards a smart warehouse management system," in *Proceedings of the International Conference on Industrial Engineering and Operations Management*, 2018, pp. 2555–2563.

100. M. Oner, A. Budak, and A. Ustundag, "RFID-based warehouse management system in wool yarn industry," *Int. J. RF Technol.*, vol. 8, no. 4, pp. 165–189, Feb. 2018, doi: 10.3233/RFT-171655.

101. B. S. S. Tejesh and S. Neeraja, "Warehouse inventory management system using IoT and open source framework," *Alexandria Eng. J.*, vol. 57, no. 4, pp. 3817–3823, Dec. 2018, doi: 10.1016/j.aej.2018.02.003.

102. C.-C. Lin and J.-W. Yang, "Cost-Efficient Deployment of Fog Computing Systems at Logistics Centers in Industry 4.0," *IEEE Trans. Ind. Informatics*, vol. 14, no. 10, pp. 4603–4611, Oct. 2018, doi: 10.1109/TII.2018.2827920.

103. B. Feng and Q. Ye, "Operations management of smart logistics: A literature review and future research," *Front. Eng. Manag.*, vol. 8, no. 3, pp. 344–355, Sep. 2021, doi: 10.1007/s42524-021-0156-2.

104. Y. Li, F. Chu, C. Feng, C. Chu, and M. Zhou, "Integrated Production Inventory Routing Planning for Intelligent Food Logistics Systems," *IEEE Trans. Intell. Transp. Syst.*, vol. 20, no. 3, pp. 867–878, Mar. 2019, doi: 10.1109/TITS.2018.2835145.

105. N. Zhang, "Smart Logistics Path for Cyber-Physical Systems With Internet of Things," *IEEE Access*, vol. 6, pp. 70808–70819, 2018, doi: 10.1109/ACCESS.2018.2879966.

106. S. Jagtap, F. Bader, G. Garcia-Garcia, H. Trollman, T. Fadiji, and K. Salonitis, "Food Logistics 4.0: Opportunities and Challenges," *Logistics*, vol. 5, no. 1, p. 2, Dec. 2020, doi: 10.3390/logistics5010002.

107. Q. Zhang, L. Shi, and S. Sun, "Optimization of Intelligent Logistics System Based on Big Data Collection Techniques," 2023, pp. 378–387. doi: 10.1007/978-3-031-31860-3_40.

108. M. E. Xie and Q. Ou, "Explore the Application of Big Data Technology in Modern Enterprise Logistics Management," 2023, pp. 150–161. doi: 10.1007/978-3-031-24468-1_14.

109. G. Wang, A. Gunasekaran, and E. W. T. Ngai, "Distribution network design with big data: model and analysis," *Ann. Oper. Res.*, vol. 270, no. 1–2, pp. 539–551, Nov. 2018, doi: 10.1007/s10479-016-2263-8.

110. G. Wang, A. Gunasekaran, E. W. T. Ngai, and T. Papadopoulos, "Big data analytics in logistics and supply chain management: Certain investigations for research and applications," *Int. J. Prod. Econ.*, vol. 176, pp. 98–110, Jun. 2016, doi: 10.1016/j.ijpe.2016.03.014.

111. A. A. C. Vieira, L. Pedro, M. Y. Santos, J. M. Fernandes, and L. S. Dias, "Data Requirements Elicitation in Big Data Warehousing," 2019, pp. 106–113. doi: 10.1007/978-3-030-11395-7_10.

112. M. Zheng and K. Wu, "Smart spare parts management systems in semiconductor manufacturing," *Ind. Manag. Data Syst.*, vol. 117, no. 4, pp. 754–763, May 2017, doi: 10.1108/IMDS-06-2016-0242.

113. S. N. Wahab, M. I. Hamzah, N. M. Sayuti, W. C. Lee, and S. Y. Tan, "Big data analytics adoption: an empirical study in the Malaysian warehousing sector," *Int. J. Logist. Syst. Manag.*, vol. 40, no. 1, p. 121, 2021, doi: 10.1504/IJLSM.2021.117703.

114. R. W. Ahmad, H. Hasan, R. Jayaraman, K. Salah, and M. Omar, "Blockchain applications and architectures for port operations and logistics management," *Res. Transp. Bus. Manag.*, vol. 41, p. 100620, Dec. 2021, doi: 10.1016/j.rtbm.2021.100620.

115. S. Johar, N. Ahmad, W. Asher, H. Cruickshank, and A. Durrani, "Research and Applied Perspective to Blockchain Technology: A Comprehensive Survey," *Appl. Sci.*, vol. 11, no. 14, p. 6252, Jul. 2021, doi: 10.3390/app11146252.

116. V. Aleksieva, H. Valchanov, A. Haka, and D. Dinev, "Logistics Model Based on Smart Contracts on Blockchain and IoT," in *EEPES'23*, Jul. 2023, p. 8. doi: 10.3390/engproc2023041008.

117. J. Chen, S. Xu, K. Liu, S. Yao, X. Luo, and H. Wu, "Intelligent Transportation Logistics Optimal Warehouse Location Method Based on Internet of Things and Blockchain Technology," *Sensors*, vol. 22, no. 4, p. 1544, Feb. 2022, doi: 10.3390/s22041544.

118. G. T. S. Ho, Y. M. Tang, K. Y. Tsang, V. Tang, and K. Y. Chau, "A blockchain-based system to enhance aircraft parts traceability and trackability for inventory management," *Expert Syst. Appl.*, vol. 179, p. 115101, Oct. 2021, doi: 10.1016/j.eswa.2021.115101.

119. B. Al Kurdi, H. M. Alzoubi, I. Akour, and M. T. Alshurideh, "The effect of blockchain and smart inventory system on supply chain performance: Empirical evidence from retail industry," *Uncertain Supply Chain Manag.*, vol. 10, no. 4, pp. 1111–1116, 2022, doi: 10.5267/j.uscm.2022.9.001.

120. G. V. Lakshmi, S. Gogulamudi, B. Nagaeswari, and S. Reehana, "BlockChain Based Inventory Management by QR Code Using Open CV," in *2021 International Conference on Computer Communication and Informatics (ICCCI)*, Jan. 2021, pp. 1–6. doi: 10.1109/ICCCI50826.2021.9402666.

121. T. Mladenović, "Cloud Computing in logistics," University of Belgrade, 2018.

122. G. R and L. M, "The Concept of Logistics 4.0," *4th Logist. Int. Conf.*, pp. 283–293, 2019.

123. Accenture, "The state of of supply The state supply chain and the cloud chain and the cloud," 2022.

124. Maersk, "How cloud computing is shaping the future of logistics," 2023.

125. Y. Jiang, "Location and Path Planning of Cross-Border E-Commerce Logistics Distribution Center in Cloud Computing Environment," 2021, pp. 30–40. doi: 10.1007/978-3-030-67871-5_4.

126. X. Zhang, "Optimization design of railway logistics center layout based on mobile cloud edge computing," *PeerJ Comput. Sci.*, vol. 9, p. e1298, Apr. 2023, doi: 10.7717/peerj-cs.1298.

127. P. Sharma and S. Panda, "Cloud Computing for Supply Chain Management and Warehouse Automation: A Case Study of Azure Cloud," *Int. J. Smart Sens. Adhoc Network.*, pp. 19–29, Jan. 2023, doi: 10.47893/IJSSAN.2023.1227.

128. B. Gupta, A. Gupta, and A. Nagpal, "Implementation of Warehouse Management Through Cloud Computing," *IJIRST-International J. Innov. Res. Sci. Technol.*, vol. 3, no. 10, pp. 189–192, 2017.

129. V. Sivakumar, R. Ruthramathi, and S. Leelapriyadharsini, "Challenges of Cloud Computing in Warehousing Operations with Respect to Chennai Port Trust," in *Proceedings of the 2020 the 3rd International Conference on Computers in Management and Business*, Jan. 2020, pp. 162–165. doi: 10.1145/3383845.3383895.

130. L. Barreto, A. Amaral, and T. Pereira, "Industry 4.0 implications in logistics: an overview," *Procedia Manuf.*, vol. 13, pp. 1245–1252, 2017, doi: 10.1016/j.promfg.2017.09.045.

131. M. Vanderroost, P. Ragaert, J. Verwaeren, B. De Meulenaer, B. De Baets, and F. Devlieghere, "The digitization of a food package's life cycle: Existing and emerging computer systems in the pre-logistics phase," *Comput. Ind.*, vol. 87, pp. 1–14, May 2017, doi: 10.1016/j.compind.2017.02.002.

132. J. Yan *et al.*, "Intelligent Supply Chain Integration and Management Based on Cloud of Things," *Int. J. Distrib. Sens. Networks*, vol. 10, no. 3, p. 624839, Mar. 2014, doi: 10.1155/2014/624839.

133. Y. P. Tsang, K. L. Choy, C.-H. Wu, G. T. S. Ho, H. Y. Lam, and V. Tang, "An intelligent model for assuring food quality in managing a multi-temperature food distribution centre," *Food Control*, vol. 90, pp. 81–97, Aug. 2018, doi: 10.1016/j.foodcont.2018.02.030.

134. P. J. B. Sanchez *et al.*, "Use of UIoT for Offshore Surveys Through Autonomous Vehicles," *Polish Marit. Res.*, vol. 28, no. 3, pp. 175–189, Sep. 2021, doi: 10.2478/pomr-2021-0044.

135. M. Drzewiecki and J. Guziński, "Design of an Autonomous IoT Node Powered by a Perovskite-Based Wave Energy Converter," *Polish Marit. Res.*, vol. 30, no. 3, pp. 142–152, Sep. 2023, doi: 10.2478/pomr-2023-0047.

136. N. D. K. Pham, G. H. Dinh, H. T. Pham, J. Kozak, and H. P. Nguyen, "Role of Green Logistics in the Construction of Sustainable Supply Chains," *Polish Marit. Res.*, vol. 30, no. 3, pp. 191–211, Sep. 2023, doi: 10.2478/pomr-2023-0052.

137. A. Oke and M. Gopalakrishnan, "Managing disruptions in supply chains: A case study of a retail supply chain," *Int. J. Prod. Econ.*, vol. 118, no. 1, pp. 168–174, Mar. 2009, doi: 10.1016/j.ijpe.2008.08.045.

138. T. K. Dasaklis, C. P. Pappis, and N. P. Rachaniotis, "Epidemics control and logistics operations: A review," *Int. J. Prod. Econ.*, vol. 139, no. 2, pp. 393–410, Oct. 2012, doi: 10.1016/j.ijpe.2012.05.023.

139. S. Columbus, "Honesty-Humility, Beliefs, and Prosocial Behaviour: A Test on Stockpiling During the COVID-19 Pandemic," *Collabra Psychol.*, vol. 7, no. 1, Feb. 2021, doi: 10.1525/collabra.19028.

140. A. C. Pereira and F. Romero, "A review of the meanings and the implications of the Industry 4.0 concept," *Procedia Manuf.*, vol. 13, pp. 1206–1214, 2017, doi: 10.1016/j.promfg.2017.09.032.

141. H. Unger, F. Börner, and E. Müller, "Context Related Information Provision in Industry 4.0 Environments," *Procedia Manuf.*, vol. 11, pp. 796–805, 2017, doi: 10.1016/j.promfg.2017.07.181.

142. U. Dombrowski, T. Richter, and P. Krenkel, "Interdependencies of Industrie 4.0 & Lean Production Systems: A Use Cases Analysis," *Procedia Manuf.*, vol. 11, pp. 1061–1068, 2017, doi: 10.1016/j.promfg.2017.07.217.

143. F. Hecklau, M. Galeitzke, S. Flachs, and H. Kohl, "Holistic Approach for Human Resource Management in Industry 4.0," *Procedia CIRP*, vol. 54, pp. 1–6, 2016, doi: 10.1016/j.procir.2016.05.102.

144. A. G. Pereira*, T. M. Lima, and F. Charrua-Santos, "Industry 4.0 and Society 5.0: Opportunities and Threats," *Int. J. Recent Technol. Eng.*, vol. 8, no. 5, pp. 3305–3308, Jan. 2020, doi: 10.35940/ijrte.D8764.018520.

145. J. Korczak and K. Kijewska, "Smart Logistics in the development of Smart Cities," *Transp. Res. Procedia*, vol. 39, pp. 201–211, 2019, doi: 10.1016/j.trpro.2019.06.022.

146. D. S. Terzi, R. Terzi, and S. Sagiroglu, "A survey on security and privacy issues in big data," in *2015 10th International Conference for Internet Technology and Secured Transactions (ICITST)*, Dec. 2015, pp. 202–207. doi: 10.1109/ICITST.2015.7412089.

147. V. N. Inukollu, S. Arsi, and S. Rao Ravuri, "Security Issues Associated with Big Data in Cloud Computing," *Int. J. Netw. Secur. Its Appl.*, vol. 6, no. 3, pp. 45–56, May 2014, doi: 10.5121/ijnsa.2014.6304.

148. K. Buntak, M. Kovačić, and M. Mutavdžija, "Internet of things and smart warehouses as the future of logistics," *Teh. Glas.*, vol. 13, no. 3, pp. 248–253, Sep. 2019, doi: 10.31803/tg-20190215200430.